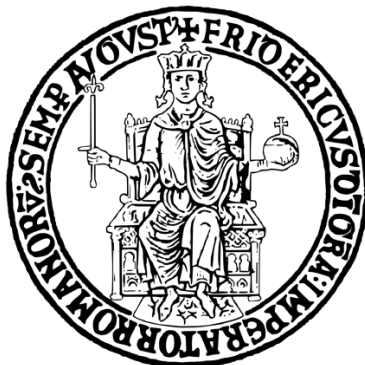


UNIVERSITY OF NAPLES FEDERICO II



SCHOOL POLYTECHNIC AND OF BASIC SCIENCES

Ph.D. in Chemical Sciences

**Structural and dynamic study of the molecular
mechanism of superspreading: towards the rational use
of new eco-friendly wetting agents**

Ph.D. Student

Rodolfo Esposito

Tutor

Prof. Gerardino D'Errico

Examiner

Prof. Roberta Marchetti

XXXV Cycle 2019/2022

Coordinator Prof.ssa Angela Lombardi

Structural and dynamic study of the molecular mechanism of superspreading: towards the rational use of new eco-friendly wetting agents

Index

Introduction	1
Reference	4
Chapter I	
1. Spreading and wetting agents	10
1.1. Basic theoretical principles of spreading phenomena	10
1.2. Technological applications of spreading	15
1.3. Wetting agents	16
1.3.1. Surfactants	16
1.3.2. Critical packing parameter	18
1.3.3. Hydrophilic-Lipophilic Balance	21
1.4. Micellization	22
1.4.1. Mixed micellization	25
1.4.2. Thermodynamics of mixed micellization	26
References	29
Chapter II	
2. Green chemistry principles in chemical formulations	34
2.1. Eco-friendly Surfactants	36
2.1.1. Bioinspired and bioderived synthetic surfactants	36
2.2. Biosurfactants	38
2.3. Rhamnolipids	41

2.3.1. Natural origin, biological functions, and molecular structure	41
2.3.2. Physico-chemical properties	44
2.3.3. Technological application	48
References	50

Chapter III

3. Molecular structure of glycosurfactants interfacial layers	59
3.1 Materials and samples preparation	60
3.2. Measurements	63
3.2.1. Pseudo-Phase diagram determination	63
3.2.2 Conductometric measurements	63
3.2.3. Electron Paramagnetic Resonance characterization	63
3.3 Results and discussions	64
3.3.1 Pseudo-Phase diagram and specific conductometry	64
3.3.2 Electron Paramagnetic Resonance results	67
3.4 Conclusions	72
Reference	75

Chapter IV

4. Rhamnolipids and their mixtures with conventional surfactants	79
4.1. Rhamnolipid and sodium lauryl ether sulfate	80
4.1.1. Materials and samples preparation	81
4.1.2. Measurements	82
4.1.2.1. Tensiometry	82
4.1.2.2. Dynamic Light Scattering	83
4.1.2.3. Electron Paramagnetic Resonance	83

4.1.2.4 Emulsification Index and foaming test	84
4.1.2.5. Contact angle	84
4.1.2.6. Ecotoxicity tests	85
4.1.3. Results and discussions	86
4.1.3.1. Rha-SLES mixed micellization: surface tension and DLS data	86
4.1.3.2 Microstructure and local dynamics in Rha-SLES mixed micelles: EPR data	88
4.1.3.3 Rha-SLES mixed micellization: models and molecular interactions	91
4.1.3.4 Rha-SLES aqueous mixtures: functional behavior	96
4.1.3.5. Ecotoxicity assay	99
4.2 monorhamnolipid and -CTAC	100
4.2.1 Materials and samples preparation	102
4.2.2. Measurements	103
4.2.2.1 Small Angle Neutron Scattering (SANS)	103
4.2.3 Results and discussions	104
4.2.3.1. mRha-CTAC mixed micellization: surface tension	104
4.2.3.2 mRha-CTAC mixed micellization: thermodynamic models	105
4.2.3.3 mRha-CTAC mixed micellization: specific conductometry	106
4.2.3.4 mRha-CTAC mixed micellization: Dynamic Light Scattering	108
4.2.3.3 mRha-CTAC mixed micellization: SANS	109
4.2.3.4 mRha-CTAC mixed micellization: contact angle	110
4.3 Conclusions	112
Reference	115
Chapter V	
5. Micellization of rhamnolipids in water/bioglycerol co-solvent mixtures	129

5.1. Bio-Glycerol	129
5.1.1. Glycerol in formulations and its effect on surfactant micellization	130
5.2. Materials and samples preparation	133
5.3. Measurements	133
5.3.1. Tensiometry	133
5.3.2. Dynamic light scattering	133
5.4. Results and discussion	134
5.4.1. water-Rha-Gly micellization: surface tension	134
5.4.2. water-Rha-Gly micellization: DLS	137
5.5. Conclusion	140
References	143
Conclusions	145
Experimental techniques	
1. Surface tension	147
1.2. The Gibbs isotherm	149
2. Electron Paramagnetic Resonance	154
2.1. Basic theoretical principles	155
2.2. Electron Paramagnetic Resonance instrument	158
3. Dynamic Light Scattering	160
3.1. Basic theoretical principles	160
3.2. Dynamic Light Scattering instrument	164
4. Contact angle	166
4.1. Contact angle instrument	167
5. Derivation of thermodynamics equations	168
Reference	172

Introduction

In the contemporary era the general wellness and the improving lifestyle of the population are driving a steady increase of the consumption of chemical products. In this stream, fine chemical industry is booming, based on the production of specialties such as intermediates, actives, additives, elastomers, flavors, fragrances, lubricants, catalysts, just to report a few examples. This is essential for the manufacturing of chemical formulations, including pharmaceuticals, cosmetics, detergents, inks and paints, agrochemicals, which allow, in turn, the technological progress of e.g., drug delivery, surface coating, oil recovery, and herbicide applications [1]. In all these categories, scientific and technological knowledge steers to design and production of chemicals and chemical formulation with enhanced effectiveness.

The ability of a chemical substance or complex formulation to wet and cover a surface, the so-called spreading phenomenon, is a key factor in most of the fields listed above [2]. Specifically, the capability to promote a rapid and spontaneous spreading on surfaces with low energy is called 'superwetting' or 'superspreading' and is maximally appealing for a variety of applications [3]. Despite the earliest reports of superspreading dating back to over 50 years ago, the precise physico-chemical mechanisms and the molecular determinants underlying this phenomenon remain unclear [4]. As regards aqueous solutions, an enhanced spreading is commonly obtained by the use of specialties named wetting agents. Surfactants are the most common wetting agents, which field a large variety of applications [5,6] spanning from detergent formulations (household [7], personal care [8], industrial processes [9-15]), agriculture [16], oil recovery [11] and remediation processes [17]; food [18], cosmetic [19] and pharmacological fields [19-24]. The large use of surfactants explain their production of about 17 million tons per year [25]. The great part of surfactants are produced from non-renewable resources with a sequential increasing of environmental pollution during the industrial processes [26-28]. Surfactants accumulate in the different environmental spheres increasing their pollution. About 60 wt% of produced surfactants, at the end of their lifecycle, enter the aquatic environment [29,30]. Surfactants or their by-products are also present in sediment and soils [31]. Because of their scarce biodegradability and toxicity, synthetic surfactants constitute an environmental issue worldwide [29,32]. Indeed, the social concern on the environmental issue has increased in recent years. This has an effect on the global market and, as consequence, on the scientific and technological research too. The study towards the discovery and development of new sustainable molecules characterized by high biocompatibility and biodegradability is prompted by the need to protect environmental and public health. It is proved that they can show some toxic effect to different

organisms [25,33-35] when dispersed in the environment, furthermore they can cause allergic reactions and skin irritation [36-38].

For these reasons, the research on environmentally friendly surfactants with a low toxicity and good biodegradability is an expanding sector [39]. Some interesting and promising alternative to commercial synthetic used surfactants is represented by eco-friendly surfactant and biosurfactants: [19,26,40-45] the first is a class of new surfactants designed in order to mimic natural amphiphilic and the second is a class naturally produced by plants, fungi and microorganisms, such as bacteria and yeasts [19,26,28,42,46-49].

In this framework, the present PhD thesis focuses on the physico-chemical characterization of sustainable eco-friendly surfactants and their use as spreading agents with the aim to exploit the acquired scientific and technological expertise for the rational design of eco-friendly wetting formulations.

The first part of the thesis summarizes the consolidated knowledge about the spreading phenomenon (Chapter 1) and eco-friendly surfactants (Chapter 2). Special attention is paid to a complete literature survey of the physico-chemical characterization of rhamnolipids, which are biosurfactants already available on the market on a large scale, thus being suitable candidates for applicative purposes. This literature review has been published (Paper I, [50]).

The original research carried out during the PhD project is reported in structured in three main topics which are discussed in Chapter 3, Chapter 4, Chapter 5, respectively.

At first, we explored the ability of two bio-inspired surfactants, the glycosurfactants Tween80 and Span80, to effectively stabilize W/O and O/W emulsions, as detailed in Chapter 3. This part of the work was performed in collaboration with the partner company Soltar s.r.l., in the framework of the Industrial PhD Program financed by the European Union (FSE, POC Ricerca e Innovazione 2014–2020, Azione I.1 “Dottorati Innovativi con caratterizzazione Industriale”). During various periods spent at the Company site (from September 2020 to September 2021, not continuously, for a total of six months) the relationship between the emulsion stability and the glycosurfactant supramolecular organization at the oil-water interface was analyzed. The results of this study were published in Paper II, [51].

Chapter 4 reports the results of a deep and wide characterization of the micellization process of rhamnolipids, in aqueous solution in presence of conventional synthetic surfactants (SLES or CTAC). The surfactant mixture behavior at the interface and in bulk solution is analyzed based on the

surfactant molecular features and intermolecular interactions. Part of this investigation was carried out from October 2021 to April 2022 at Institut Laue-Langevin (ILL) Grenoble, France, in the partnership for Soft Condensed Matter (PSCM) laboratories. The first part of the results of this study were published in Paper III, [52].

In Chapter 5, rhamnolipid micellization in the presence of a “green” co-solvent, bioglycerol (obtained as a side-product of biodiesel production), was investigated. This activity was carried out in collaboration with the NICL (Naples Industrial Chemistry Laboratory) group of the University Federico II.

The scientific strategy of the entire research relies on a physico-chemical approach in which surface tension measurements are used to investigate the concentration at which surfactant aggregation occurs, dynamic light scattering (DLS) measurements to estimate the size and distribution of the aggregates, electron paramagnetic resonance (EPR) measurements to analyze their microstructure and contact angle measurements to quantify the spreading ability. The theoretical principles for surface tension, DLS, EPR and contact angle measurements are described in the Appendix.

Overall, the present PhD research clearly points to bio-derived surfactants, and specifically to rhamnolipids, as suitable components of eco-sustainable surfactant formulations. The knowledge of their physico-chemical properties will constitute a reliable basis for the rational design of chemical formulations easily optimizable for each specific task.

References

- [1] Smiley R. A., Harold L. J., *Chemistry and the Chemical Industry: A Practical Guide for Non-Chemists*, CRC Press, Boca Raton, 2002, 1st ed.
- [2] Theodorakis P. E.; Müller E. A.; Craster R. V.; Matar O. K., Superspreading: mechanisms and molecular design, *Langmuir*, 2015, 31, 2304–2309.
- [3] Hill R. M., Superspreading. *Curr. Opin. Colloid Interface Sci*, 1998, 3, 247–254.
- [4] Matar O. K.; Craster R. V., Dynamics of surfactant-assisted spreading, *Soft Matter*, 2009, 5, 3801–3809.
- [5] Hargreaves A. E., *Chemical Formulation: An Overview of Surfactant Based Chemical Preparations Used in Everyday Life*, Royal Society of Chemistry, 2007.
- [6] Falbe, J. *Surfactants in Consumer Products: Theory, Technology and Application*; Springer Berlin, Heidelberg, 2012, 1st ed.
- [7] Scheibel J. J., The Evolution of Anionic Surfactant Technology to Meet the Requirements of the Laundry Detergent Industry. *J Surfactants Deterg*, 2004, 7, 319–328. <https://doi.org/10.1007/s11743-004-0317-7>.
- [8] Cornwell P. A., A Review of Shampoo Surfactant Technology: Consumer Benefits, Raw Materials and Recent Developments. *Int. J. Cosmet. Sci*, 2018, 40, 16–30. <https://doi.org/10.1111/ics.12439>.
- [9] Tadros, T. F. *Applied Surfactants: Principles and Applications*; John Wiley & Sons, 2006.
- [10] Farn, R. J. *Chemistry and Technology of Surfactants*; John Wiley & Sons, 2008.
- [11] Chowdhury S.; Shrivastava S.; Kakati A.; Sangwai J. S., Comprehensive Review on the Role of Surfactants in the Chemical Enhanced Oil Recovery Process. *Ind. Eng. Chem. Res*, 2022, 61, 21–64. <https://doi.org/10.1021/acs.iecr.1c03301>.
- [12] Pradip; Rai B., Design of Tailor-Made Surfactants for Industrial Applications Using a Molecular Modelling Approach. *Colloids Surf. A: Physicochem. Eng. Asp*, 2002, 205, 139–148. [https://doi.org/10.1016/S0927-7757\(01\)01153-0](https://doi.org/10.1016/S0927-7757(01)01153-0).

- [13] Kumar N.; Tyagi R., Industrial Applications of Dimeric Surfactants: A Review. *J Dispers Sci Technol*, 2014, 35, 205–214. <https://doi.org/10.1080/01932691.2013.780243>.
- [14] Tadros, T. F. *Polymeric Surfactants: Dispersion Stability and Industrial Applications*; Walter de Gruyter GmbH & Co KG, 2017.
- [15] Rosen, M. J.; Kunjappu, J. T. *Surfactants and Interfacial Phenomena*; John Wiley & Sons, 2012.
- [16] Castro, M.J.L., Ojeda, C., Cirelli, A.F. (2013). Surfactants in Agriculture. In: Lichtfouse, E., Schwarzbauer, J., Robert, D. (eds) *Green Materials for Energy, Products and Depollution. Environmental Chemistry for a Sustainable World*, vol 3. Springer, Dordrecht. https://doi.org/10.1007/978-94-007-6836-9_7
- [17] Rasheed T.; Shafi S.; Bilal M.; Hussain T.; Sher F.; Rizwan K.; Surfactants-Based Remediation as an Effective Approach for Removal of Environmental Pollutants—A Review. *J. Mol. Liq*, 2020, 318, 113960. <https://doi.org/10.1016/j.molliq.2020.113960>.
- [18] Kralova I.; Sjöblom J.; Surfactants Used in Food Industry: A Review. *J Dispers Sci Technol*, 2009, 30, 1363–1383. <https://doi.org/10.1080/01932690902735561>.
- [19] Moldes A. B.; Rodríguez-López L.; Rincón-Fontán M.; López-Prieto A.; Vecino X.; Cruz J. M.; Synthetic and Bio-Derived Surfactants Versus Microbial Biosurfactants in the Cosmetic Industry: An Overview. *Int J Mol Sci*, 2021, 22, 2371. <https://doi.org/10.3390/ijms22052371>.
- [20] Salager J.-L., Antón R.; Bullón J.; Forgiarini A.; Marquez R., How to Use the Normalized Hydrophilic-Lipophilic Deviation (HLDN) Concept for the Formulation of Equilibrated and Emulsified Surfactant-Oil-Water Systems for Cosmetics and Pharmaceutical Products. *Cosmetics*, 2020, 7, 57. <https://doi.org/10.3390/cosmetics7030057>.
- [21] Chen S.; Hanning S.; Falconer J.; Locke M.; Wen J., Recent Advances in Non-Ionic Surfactant Vesicles (Niosomes): Fabrication, Characterization, Pharmaceutical and Cosmetic Applications. *Eur. J. Pharm. Biopharm*, 2019, 144, 18–39. <https://doi.org/10.1016/j.ejpb.2019.08.015>.
- [22] Fait M. E.; Bakas L.; Garrote G. L.; Morcelle S. R.; Saparrat M. C. N., Cationic Surfactants as Antifungal Agents. *Appl Microbiol Biotechnol*, 2019, 103, 97–112. <https://doi.org/10.1007/s00253-018-9467-6>.
- [23] Colomer A.; Pinazo A.; Manresa M. A.; Vinardell M. P.; Mitjans M.; Infante M. R.; Pérez L.; Cationic Surfactants Derived from Lysine: Effects of Their Structure and Charge Type on

Antimicrobial and Hemolytic Activities. *J. Med. Chem.*, 2011, 54, 989–1002. <https://doi.org/10.1021/jm101315k>.

[24] Zakharova L. Y.; Pashirova T. N.; Doktorovova S.; Fernandes A. R.; Sanchez-Lopez E.; Silva A. M.; Souto S. B.; Souto E. B., Cationic Surfactants: Self-Assembly, Structure-Activity Correlation and Their Biological Applications. *Int. J. Mol. Sci.*, 2019, 20, 5534. <https://doi.org/10.3390/ijms20225534>.

[25] Freeling F.; Alygizakis N. A.; von der Ohe P. C.; Slobodnik J.; Oswald P.; Aalizadeh R.; Cirka L.; Thomaidis N. S.; Scheurer M., Occurrence and Potential Environmental Risk of Surfactants and Their Transformation Products Discharged by Wastewater Treatment Plants. *Sci. Total Environ.*, 2019, 681, 475–487. <https://doi.org/10.1016/j.scitotenv.2019.04.445>.

[26] Jimoh A. A.; Lin J. Biosurfactant: A New Frontier for Greener Technology and Environmental Sustainability. *Ecotoxicol. Environ. Saf.*, 2019, 184, 109607. <https://doi.org/10.1016/j.ecoenv.2019.109607>.

[27] Foley P.; Pour A. K.; Beach E. S.; Zimmerman J. B. Derivation and Synthesis of Renewable Surfactants. *Chem. Soc. Rev.*, 2012, 41, 1499–1518. <https://doi.org/10.1039/C1CS15217C>.

[28] Pardhi D. S.; Panchal R. R.; Raval V. H.; Joshi R. G.; Poczai P.; Almalki W. H.; Rajput K. N. Microbial Surfactants: A Journey from Fundamentals to Recent Advances. *Frontiers in Microbiology* 2022, 13.

[29] Johnson P.; Trybala A.; Starov V.; Pinfield V. J., Effect of synthetic surfactants on the environment and the potential for substitution by biosurfactants, *Adv. Colloid Interface Sci.*, 2021, 288, 102340. <https://doi.org/10.1016/j.cis.2020.102340>

[30] Jackson M.; Eadsforth C.; Schowanek D.; Delfosse T.; Riddle A.; Budgen N., Comprehensive review of several surfactants in marine environments: fate and ecotoxicity, *Environ. Toxicol. Chem.*, 2016, 35, 1077-1086 <https://doi.org/10.1002/etc.3297>

[31] Ivanković T.; Hrenović J., Surfactants in the environment, *Arh. Hig. Rada Toksikol.*, 2010, 95-110. <https://doi.org/10.2478/10004-1254-61-2010-1943>

[32] Villarreal-Reyes C.; de León-Martínez L. D.; Flores-Ramírez R.; González-Lara F.; Villarreal-Lucio S.; Vargas-Berrones K. X., Ecotoxicological impacts caused by high demand surfactants in Latin America and a technological and innovative perspective for their substitution, *Sci. Total Environ.*, 2021, 816, 151661. <https://doi.org/10.1016/j.scitotenv.2021.151661>

- [33] Han J.-H.; Jung S. K., Toxicity Evaluation of Household Detergents and Surfactants Using Zebrafish. *Biotechnol Bioproc E*, 2021, 26, 156–164. <https://doi.org/10.1007/s12257-020-0109-3>.
- [34] Olkowska E.; Ruman M.; Polkowska Ż., Occurrence of Surface Active Agents in the Environment. *J Anal Methods Chem.*, 2014, 2014. <https://doi.org/10.1155/2014/769708>.
- [35] Belanger S. E.; Boeijs G.; Federle T. W.; McAvoy D. C.; Morrall S. W.; Eckhoff W. S.; Dunphy J. C.; Itrich N. R.; Price B. B.; Matthijs E.; Wind T.; Toy R.; Cano M. L.; Eadsforth C. V.; Van Compennolle R.; Dorn P. B.; Stephenson R. J.; Sherren A. J.; Selby M.; Evans A.; Marshall S. J.; Gumbel H.; Zeller D., Special Issue on the Environmental Risk Assessment of Alcohol Ethoxylate Nonionic Surfactant. *Ecotoxicol. Environ. Saf*, 2006, 64, 1–2. <https://doi.org/10.1016/j.ecoenv.2006.01.009>.
- [36] Seweryn A., Interactions between Surfactants and the Skin – Theory and Practice. *Adv. Colloid Interface Sci.*, 2018, 256, 242–255. <https://doi.org/10.1016/j.cis.2018.04.002>.
- [37] Presley C. L.; Militello M.; Barber C.; Ladd R.; Laughter M.; Ferguson H.; Dewey J.; Pulsipher K. J.; Rundle C. W.; Dunnick C. A., The History of Surfactants and Review of Their Allergic and Irritant Properties. *Dermatitis®*, 2021, 32, 289. <https://doi.org/10.1097/DER.0000000000000730>.
- [38] Weinhammer A. P.; Scheman A.; Reeder M. J., Prevalence of Surfactant in the Contact Allergen Management Program. *Dermatitis®*, 2019, 30, 358. <https://doi.org/10.1097/DER.0000000000000511>.
- [39] Rebello S.; Anoopkumar A. N.; Sindhu R.; Binod P.; Pandey A.; Aneesh E. M., 23 - Comparative Life-Cycle Analysis of Synthetic Detergents and Biosurfactants—an Overview. In *Refining Biomass Residues for Sustainable Energy and Bioproducts*; Kumar, R. P., Gnansounou, E., Raman, J. K., Baskar, G., Eds.; Academic Press, 2020; pp 511–521. <https://doi.org/10.1016/B978-0-12-818996-2.00023-5>.
- [40] Otzen D. E., Biosurfactants and Surfactants Interacting with Membranes and Proteins: Same but Different? *Biochim Biophys Acta Biomembr*, 2017, 1859, 639–649. <https://doi.org/10.1016/j.bbamem.2016.09.024>.
- [41] Sarubbo L. A.; Silva M. da G. C.; Durval I. J. B.; Bezerra K. G. O.; Ribeiro B. G.; Silva I. A.; Twigg M. S.; Banat I. M., Biosurfactants: Production, Properties, Applications, Trends, and General Perspectives. *Biochem. Eng. J.*, 2022, 181, 108377. <https://doi.org/10.1016/j.bej.2022.108377>.

- [42] Baccile N.; Seyrig C.; Poirier A.; Alsondo-de Castro S.; Roelants S. L. K. W., Abel S., Self-Assembly, Interfacial Properties, Interactions with Macromolecules and Molecular Modelling and Simulation of Microbial Bio-Based Amphiphiles (Biosurfactants). A Tutorial Review. *Green Chemistry*, 2021, 23, 3842–3944. <https://doi.org/10.1039/D1GC00097G>
- [43] Bognolo G., Biosurfactants as Emulsifying Agents for Hydrocarbons. *Colloids Surf. A Physicochem. Eng. Asp*, 1999, 152, 41–52. [https://doi.org/10.1016/S0927-7757\(98\)00684-0](https://doi.org/10.1016/S0927-7757(98)00684-0).
- [44] Makkar R. S.; Rockne K. J., Comparison of Synthetic Surfactants and Biosurfactants in Enhancing Biodegradation of Polycyclic Aromatic Hydrocarbons. *Environ. Toxicol. Chem.* 2003, 22, 2280–2292. <https://doi.org/10.1897/02-472>.
- [45] Johnson P.; Trybala A.; Starov V.; Pinfield V. J., Effect of Synthetic Surfactants on the Environment and the Potential for Substitution by Biosurfactants. *Adv. Colloid Interface Sci.*, 2021, 288, 102340. <https://doi.org/10.1016/j.cis.2020.102340>.
- [46] De S.; Malik S.; Ghosh A.; Saha R.; Saha B., A Review on Natural Surfactants. *RSC Advances*, 2015, 5, 65757–65767. <https://doi.org/10.1039/C5RA11101C>.
- [47] Gayathiri E.; Prakash P.; Karmegam N.; Varjani S.; Awasthi M. K.; Ravindran B., Biosurfactants: Potential and Eco-Friendly Material for Sustainable Agriculture and Environmental Safety—A Review., *Agronomy*, 2022, 12, 662. <https://doi.org/10.3390/agronomy12030662>.
- [48] Rodrigues L. R.; Microbial Surfactants: Fundamentals and Applicability in the Formulation of Nano-Sized Drug Delivery Vectors., *J. Colloid Interface Sci*, 2015, 449, 304–316. <https://doi.org/10.1016/j.jcis.2015.01.022>.
- [49] Infante M. R.; Pérez L., Pinazo A.; Clapés P.; Morán M. C.; Angelet M.; García M. T.; Vinardell M. P., Amino acid-based surfactants, *C. R. Chim*, 2004, 7, 583-592. <https://doi.org/10.1016/j.crci.2004.02.009>
- [50] Esposito R.; Speciale I.; De Castro C.; D’Errico G.; Russo Krauss I.; Rhamnolipid self-aggregation in aqueous media: a long journey toward the definition of structure-property relationships, *Int. J. Mol. Sci*, 2023, submitted.
- [51] Esposito R.; Cavasso D.; Niccoli M.; D’Errico G., Phase Inversion and Interfacial Layer Microstructure in Emulsions Stabilized by Glycosurfactant Mixtures, *Nanomaterials*, 2021, 11, 331. <https://doi.org/10.3390/nano11020331>.

[52] Esposito R.; Ingenito L.; Cavasso D.; Siciliano A.; Alfieri M.L.; Chiappisi L.; Fragneto G.; Ottaviani M.F.; Guida M.; Paduano L.; D’Errico G., Rhamnolipid–SLES aqueous mixtures: From the molecular self-aggregation to the functional and ecotoxicological properties, *J. Mol. Liq*, 2022, 367, 120547. <https://doi.org/10.1016/j.molliq.2022.120547>

Chapter I

1. Spreading and wetting agents

The spreading phenomenon is the ability of a liquid to wet a solid surface. Depending on the properties of the spreading liquid and the covered surface, the phenomenon can be more or less efficient. In order to enhance this process, specific molecules are used in formulations. Wetting agents are surface-active compounds able to reduce the surface tension of a liquid, commonly water. They are applied in several fields such as detergency, [1], cosmetics [2], agrochemicals [3], pharmaceuticals [4], foods [5] and many others. The main purpose of a spreader is to enhance the area of a liquid film on a solid surface by reducing interfacial tension. Particularly, many problems occur in industrial processes involving water-based formulations, given the high value of water surface tension (72.8 mN/m at 20 °C); these problems mainly arise from the inability of these formulations to wet the surface onto which they are applied. For this reason, spreading or wetting agents are largely used. As an example, in the coating industry they help the fluid phase to spread pigment particles during the wetting process [6]. In pesticide application, wetting agents increase the efficiency of the formulation spreading them on the leaf surface [3]. Spreading agents continuously find new fields of application, and the current scientific and technological research is studying new and more effective types of agents and developing new technologies for their exploitation.

1.1. Basic theoretical principles of spreading phenomena

Spreading is a ubiquitous phenomenon in nature, which is also exploited in the industry field [7,8]. It consists of the coverage of a solid substrate exposed to the environment by a layer of liquid or fluid material. Different situations are possible by considering the nature of the surface forces involved for wetting behavior. Indeed, one can modify the properties of the solid surface with a plasma treatment [9] or silanization process [10] which reflect on a different contact energy of the surface. In this case, the interactions are on the molecular scale, so one can refer to them as “short-ranged interactions”. On the other hand, van der Waals forces and electrostatic forces also have to be taken in consideration; since they act on a distance larger than the single molecule, one can call them “long-ranged interactions” [11]. The surface science plays a key role in industry, and is a field where chemistry,

physics and engineering converge. Below, the theoretical principles of the spreading phenomenon are summarized, and the main factors which affect it are analyzed.

The spreading process is generally treated in thermodynamics as a wetting phenomenon. It fundamentally depends on the interfacial tension between contacting phases. The exact differential of the Gibbs free energy, G , of a two-phase system composed by k components is:

$$dG = Vdp - SdT + \sum_k \mu_k dn_k + \gamma dA \quad \text{Equation 1}$$

Where V is the volume, p is the pressure, S is the entropy, T the temperature, μ_k the chemical potential of component k , n the amount of substance (in mol), γ the interfacial tension and A the area of the interface between the two phases. The interfacial tension is defined as the work needed to increase the size of the interface between two adjacent phases. For a closed system at constant temperature, volume and amount of substance, the interfacial energy is the partial derivative of the Gibbs free energy with the respect of the interfacial area:

$$\gamma = \left(\frac{\partial G}{\partial A} \right)_{P,T,n} \quad \text{Equation 2}$$

We can distinguish various types of wetting, involving two or three phases at equilibrium. In all cases, each contact interface involves only two phases, and can be considered separately from the other interfaces in the system. The balance between the interface tension values of all the interfaces present in a given system determines its behavior.

The **immersional wetting** is the process in which a solid b , in contact with a gas or vacuum phase d , comes in contact with a liquid a with no change of the interface area; thus, the solid-gas interface is replaced by a solid-liquid interface of the same area. The work of immersional wetting per unit area for a reversible process is given by:

$$w_{iw}^{\alpha\beta\delta} = \gamma^{\beta\delta} - \gamma^{\alpha\beta} \quad \text{Equation 3}$$

where $\gamma^{\beta\delta}$ and $\gamma^{\alpha\beta}$ are the values of interfacial tension between the β and δ phases and the α and β phases, respectively.

The **adhesional wetting** is the process in which two initial interfaces, *e.g.*, the solid-gas and liquid-gas interfaces, are replaced by a single one, *e.g.*, the solid-liquid interface. The work required by a system in which two condensed phases *a* and *b* form reversibly a unit area substituting $\alpha\delta$ and $\beta\delta$ interfaces, is given by:

$$w_{aw}^{\alpha\beta\delta} = \gamma^{\alpha\delta} + \gamma^{\beta\delta} - \gamma^{\alpha\beta} \quad \text{Equation 4}$$

where $\gamma^{\alpha\delta}$ is the interfacial tension between the α and δ phases.

It is worth mentioning here that the work of cohesion per unit area for a condensed phase α (either solid or liquid) is defined as the work exerted on a system when a column of that phase, whose cross section has a unit area, is reversibly split in two, with creation of two surfaces, which are in equilibrium with the gas phase δ .

$$w_c^{\alpha\delta} = 2\gamma^{\alpha\delta} \quad \text{Equation 5}$$

The **spreading wetting** is a process in which a drop of liquid α at equilibrium with the gas phase δ , spreads over a solid β or another liquid substrate α in equilibrium with the gas phase. A liquid droplet, when placed onto a solid surface, spreads on it if the value of the spreading tension or the work of spreading per unit area, $\sigma^{\alpha\beta\delta}$, given by:

$$\sigma^{\alpha\beta\delta} = \gamma^{\beta\delta} - \gamma^{\alpha\delta} - \gamma^{\alpha\beta} \quad \text{Equation 6}$$

is positive. The equilibrium usually is not reached instantly, so we can distinguish between an initial and a final spread tension, $\sigma_i^{\alpha\beta\delta}$ and $\sigma_f^{\alpha\beta\delta}$. This is important, because if $\sigma_i^{\alpha\beta\delta}$ is positive and $\sigma_f^{\alpha\beta\delta}$ is negative, the system shows autophobicity, which means that no spreading is observed over time.

In general, if a liquid does not spread on a solid ($\sigma_f^{\alpha\beta\delta}$ is negative) a contact angle, θ , is observed; it is defined as the angle between two solid-liquid and liquid-gas interfaces. If a liquid spontaneously spreads on a solid the contact angle is zero.

When a spreading substance is poured onto a liquid substrate, with the covered and uncovered surface portions separated by a sliding mechanical barrier, the force exerted by the covered surface on the barrier is the surface pressure, $\pi\sigma$, which can be calculated as:

$$\pi^s = \gamma^0 - \gamma$$

Equation 7

Where γ is the surface tension of the covered surface and γ^0 is the surface tension of the clean surface.

Finally, the **condensational wetting** is a process similar to spreading wetting, where in the first case the liquid phase is formed by vapour condensation and in the second case by a drop spreading. During the condensation, a solid surface is covered by a vapour until the formation of a continuous liquid film. Thus, the solid-liquid and solid-vapour interfaces replace the solid-vacuum interface.

Summarizing, independently of the type of wetting phenomena, the main thermodynamic properties involved are the different energies per wetted area, i.e., the interfacial tension between the fluids as well as between each fluid and the solid, and the three-phase contact angle θ . In a three-phase system, three different interfacial energies exist from the pairwise combination between the phases (Fig. 1):

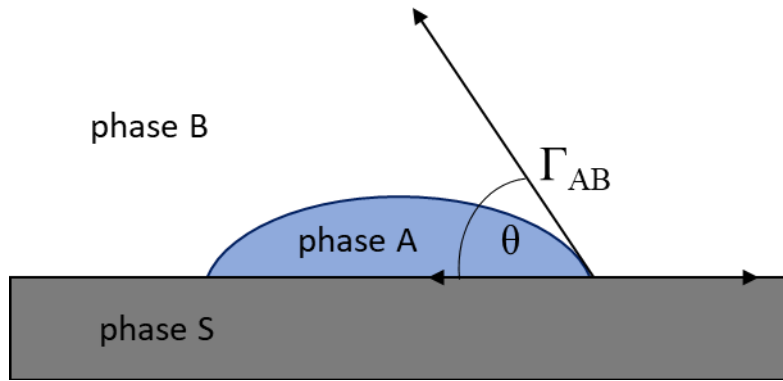


Figure 1. Schematic drawing of a solid-liquid-liquid arrangement of a droplet of a secondary fluid “A” residing on a flat surface of the solid “S” surrounded by a bulk liquid “B”.

The contact angle θ is determined from these quantities by the Young equation (Eq. 8):

$$\gamma_{SB} - \gamma_{SA} - \gamma_{AB} \cos \theta_Y = 0$$

Equation 8

Converting this balance leads to:

$$\cos \theta_Y = \frac{\gamma_{SB} - \gamma_{SA}}{\gamma_{AB}}$$

Equation 9

The Young equation is only valid for an ideal solid surface that is defined as rigid, smooth, chemically homogenous, insoluble and non-reactive [12]; if this is the case, the contact angle θ_Y is observed. For a rough solid surface, a correction to the Young equation must be applied. Wenzel’s model takes

account of the actual surface A_{actual} , that is increased compared to its projection (*i.e.*, the ideal flat surface A_{flat}). In this case, the contact angles became (Eq.10):

$$\cos \theta_W = \frac{A_{actual}}{A_{flat}} \cos \theta_Y \quad \text{Equation 10}$$

where Wenzel contact angle θ_w is the apparent contact angle that forms on the rough surface [13]. The Wenzel equation assumes homogenous wetting, *i.e.* full wetting on the entire surface area and all asperities of the rough surface.

In case of heterogenous wetting (*i.e.*, fluid B being trapped in some solid asperities, which are not wet by the main wetting fluid A) the equation of Cassie-Baxter has to be used instead [14]. The same equation also has to be used for wetting on chemically inhomogeneous surfaces. For the case of the surface showing two different chemical properties with a partial areas A_1 and A_2 , respectively, the Cassie-Baxter equation is:

$$\cos \theta_{CB} = \frac{A_1}{A_{actual}} \cos \theta_1 + \frac{A_2}{A_{actual}} \cos \theta_2 \quad \text{Equation 11}$$

where θ_{CB} is the apparent angle θ_1 and θ_2 are the Young contact angles of the wetting liquid on homogeneous surfaces of chemical type 1 and 2, respectively [15].

While θ_Y , θ_W and θ_{CB} denote thermodynamic equilibrium angles at rest, different contact angles will appear during the process of wetting or de-wetting of a solid [16], which also strongly depend on the local surface geometry [17]. The angle during wetting, termed the advancing contact angle θ_{adv} , is higher than the equilibrium angle θ_{eq} , while the angle during de-wetting, termed the receding contact angle θ_{rec} , is lower than the equilibrium angle.

The most stable apparent contact angle may be calculated as the mean angle between advancing and receding angles, $(\theta_{adv} + \theta_{rec})/2$ [12], but this approach is not valid in all cases [18].

While the most stable apparent contact angle is the equilibrium angle θ_{eq} , there also exist some other energetically metastable contact angle where the Gibbs energy exhibits a local, but not a global minimum. These local minima, however, will lead to the appearance of a variety of such metastable contact angles $\neq \theta_{eq}$ in the range of the hysteresis for real system even when the system is at rest [12].

The angles θ_Y , θ_W and θ_{CB} are not directly affected by the contact angle hysteresis, but without information in the hysteresis, they alone will not be sufficient to explain the whole appearance of a

wetted structure [12]. The range of the hysteresis can be large. Hysteresis in the range of $\theta_{eq} \pm 20^\circ$ are easily found in literature.

1.2. Technological applications of spreading

Spreading has been the subject of many scientific research, driven by the plethora of industrial applications. Two strategies can be followed to control the spreading: the former is the functionalization of the wetted surface in order to tune the interfacial tension between the solid and the two fluid phases. This approach is preferred when the properties of the spreading liquid cannot be changed. The latter approach relies on the modification of the properties of the spreading liquid, by using specific wetting agents able to modify the interfacial tension between the liquid and the solid as well as that between the spreading liquid and the second fluid (a gas or a second immiscible liquid). It has to be noted that the second approach is based on the design of a liquid formulation with controlled wettability.

The wetting or dewetting phenomena are exploited in different fields. The large majority of applications concern water-based formulation [19].

In agriculture one of the issues is to effectively spread the fertilizer or the pesticide on the leaves, which present a hydrophobic surface. In this case the use of wetting agents is necessary to minimize the amount of formulation, with a subsequent reduction of the environmental impact [20,21].

The treatment of some illnesses, in particular lungs disease, needs the spreading of solutions with formation of a thin layer to give benefits [22].

In cosmetics the spreading is necessary to improve the capability to cover the skin and to enhance the absorption of the actives by increasing the contact area of the formulation [23-26].

In food industry the concept of spreading is applied as the basis of new coating technologies employing edible formulations [27,28], with the aim of reducing plastic packaging.

Spreading is exploited also in oil recovery, since the adhesion of oil to the rock/sand surface is minimized by the presence of wetting agents and enhanced for the increased wetted area [39,30], as well as in firefighting [31], and in inkjet printing [32].

In all these different fields the need of reducing the environmental impact has prompted the research to focus on new ecosustainable solutions. In particular, the new scientific trends point to natural, or at least bio-inspired, wetting agents.

1.3. Wetting agents

Wetting agents are an important and versatile class of fine chemicals with a variety of technological applications [33]. They can be produced through synthetic chemical processes, which are usually crude-based, or can be produced naturally from some organisms. Both synthetic and natural wetting agents show in common the main molecular architecture which consists in a hydrophilic moiety, or head, and a lipophilic moiety, or tail, allowing their adsorbing at polar/apolar interfaces [34].

1.3.1. Surfactants

Surfactant is a contraction of the terms *SURFace ACTIVE AgeNTS*. Surfactants are organic molecules that, when dissolved in a solvent at low concentration, have the ability to adsorb or locate at the interfaces, thereby altering significantly their physico-chemical properties (specifically, the surface and interfacial tension). Here, the term interface is employed to define the boundary in liquid-liquid, gas-liquid and solid-liquid systems. The chemical structure of a typical surfactant is sketched in Fig. 2.

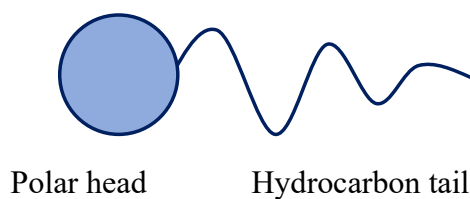


Figure 2. Typical representation of a surfactant

Numerous variations are possible within the structure of both the head and tail groups of surfactants. The simplest classification is based on the head group charge: according to it, we distinguish:

- anionic surfactants, in Fig. 3, which present a negatively charged head group (e.g., a sulfate, sulfonate, phosphate or carboxylate group):

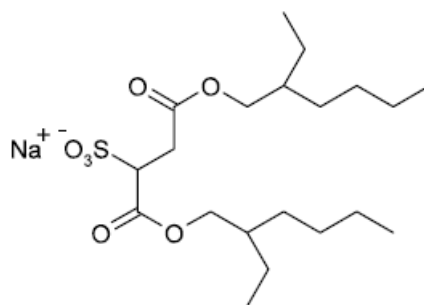


Figure 3. Example of anionic surfactant: Sodium bis(2-ethylhexyl)sulfosuccinate (Aerosol-OT or AOT).

- cationic surfactants, in Fig. 4, which present a positively charged head group (e.g., a quaternary ammonium group);

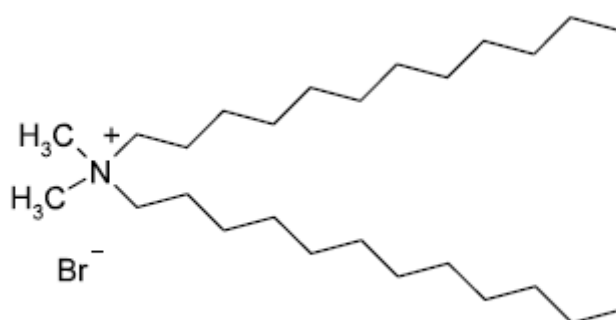


Figure 4.. Example of cationic surfactant: didodecyltrimethylammonium bromide (DDAB)

- non-ionic surfactants, in Fig. 5, which present a polar but uncharged head group (e.g., an ethoxylic chain, a saccharide):

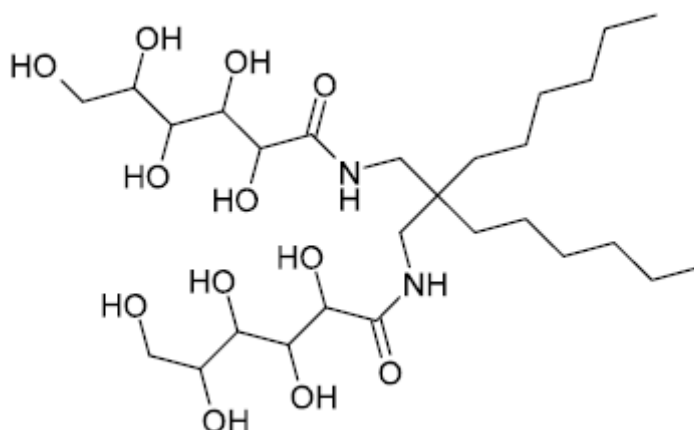


Figure 5. Example of non-ionic surfactant: di(hexyl)glucamide (di-(C6-Glu))

- zwitterionic surfactants, in Fig. 6, whose head group presents both positive and negative charges (e.g., a phosphocholine, a betaine).

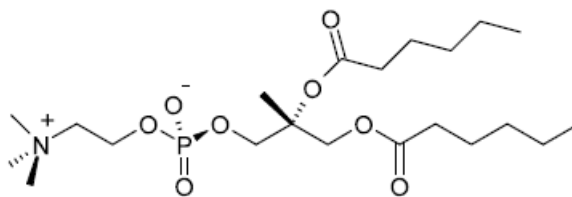


Figure 6. Example of zwitterionic surfactant: Dihexylphosphatidylcholine ((diC6)PC)

- amphoteric surfactants, in Fig. 7, whose head group charge varies with the solution pH (e.g., an amine oxide).

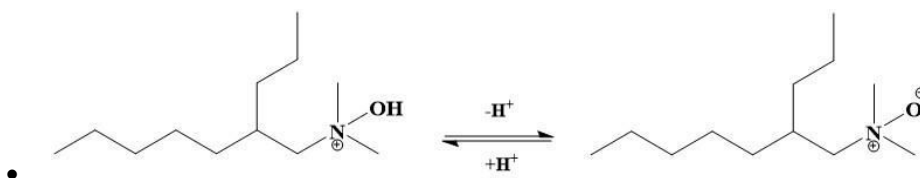


Figure 7. Example of amphoteric surfactant: *N,N*-dimethyl-2-propylheptan-1-amine oxide (C10DAO-branched)

Another possible classification is based on the molecular structure of the hydrophobic tail, which can be linear or branched, single or double. Chemical structure of typical double-chain surfactants are reported in Fig. 2-5, while Fig. 6 shows a branched surfactant.

Besides these classifications, because of the continuous research to improve surfactant properties, new interesting structures have recently emerged. These novel surfactants have attracted much interest, and include catanionics, bolaforms, gemini (or dimeric), polymeric and polymerisable surfactants. Another important driving force for this research is the need for enhanced surfactant biodegradability. For personal care products and household detergents, regulations require high biodegradability and non-toxicity of each component present in the formulation.

1.3.2. Critical packing parameter

Surfactants are distinguished by the ability to form oriented monolayers at the interfaces (e.g., air/water or oil/water) and to self-assemble in bulk phases forming well-defined nanostructures. The

particular concentration above which supramolecular aggregates, as micelles, form is called the critical micellar concentration (*cmc*) and will be analysed in a following section. The shape and dimension of the supramolecular aggregates formed by surfactants in water are extremely responsive to the variations of the mixture conditions, in terms of concentration, pH and presence of co-solvents. In dilute solutions, surfactants tend to form spherical micelle. An increase in surfactant concentration leads to a transition from spherical to rod-like or disk-like micelles. A further increment of concentration may induce the formation of mesophases such as lyotropic crystalline liquid phases (LLC), including cubic, hexagonal and lamellar phases. In Fig. 8 are shown the different aggregate morphologies. The variation of the aggregates shape can be primarily ascribed to the increase of the surfactant concentration. It causes an increase in the number and dimension of the micelle, thus decreasing the distance between the aggregates and enhancing the intermicellar interactions.

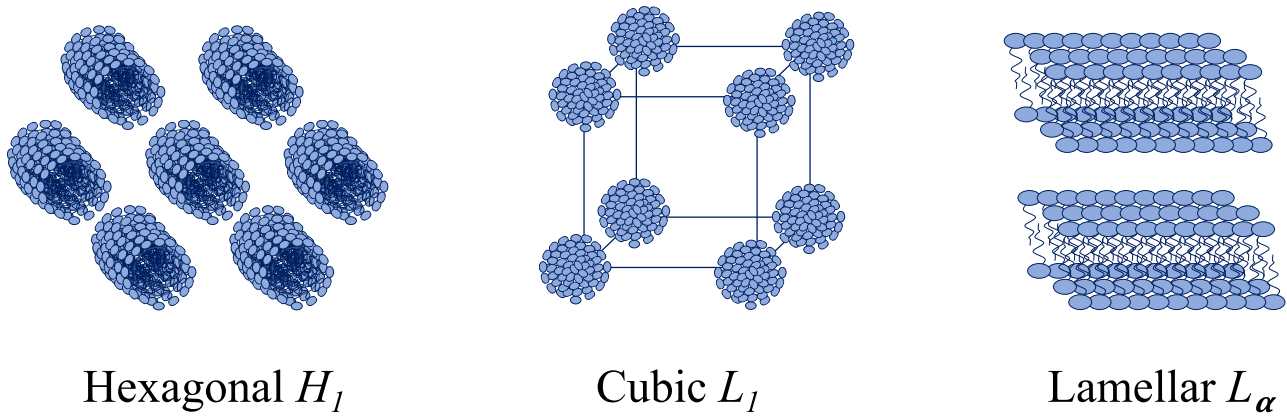


Figure 8. Shape and structure of the mesophases of surfactant aggregates

The micelle shape depends on the geometry of the surfactant molecules. To quantitatively take into account this aspect, an important parameter called *critical packing parameter* (*cpp*) is defined [35]:

$$cpp = \frac{v}{l_c a_o} \tag{Equation 12}$$

where V and l_c are the volume and the length of the hydrocarbon tail, while a_o is the effective area occupied by the polar head at the interface, see Fig. 9.

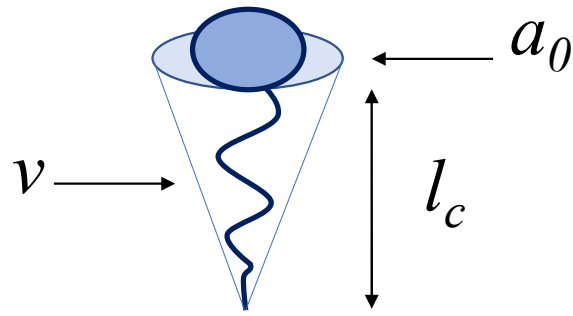


Figure 9. Molecular parameters defining the critical packing parameter.

a_0 is obtained through experimental measurements and represents the tendency of polar heads to stay close each other; this could be influenced by solution conditions, i.e., the surfactant concentration, the temperature, and the ionic strength. An estimation of this term has been derived from the following model:

$$a_0 = \sqrt{\frac{\alpha}{\sigma}}$$

Equation 13

where α represents a repulsion parameter between the surfactant heads, and σ is the interfacial energy per unit area.

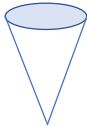
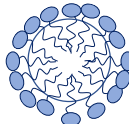
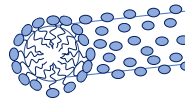
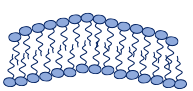
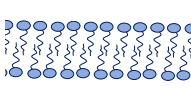
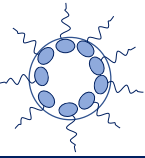
cpp $v/a_0 l_c$	$<1/3$	$1/3-1/2$	$1/2-1$	~ 1	>1
Critical Packing Shaping	Cone 	Truncated cone 	Truncated cone 	Cylinder 	Wedge 
Structures formed	Spherical micelles 	Cylindrical micelles 	Vesicles 	Planar bilayers 	Inverted micelles 

Figure 3. The aggregation structures of surfactants in aqueous solutions.

Different surfactants present distinct cpp values, depending on the dimension of the hydrophilic and hydrophobic moieties. Since the self-aggregation occurs to maximize the thermodynamic stability of the aggregate, the optimal micelle shape depends on the cpp , as shown in Fig. 10 [36].

1.3.3. Hydrophilic-Lipophilic Balance

The Hydrophilic-Lipophilic Balance (HLB) is a practical parameter which could help to understand the surfactant aggregation behavior. This parameter measures the degree of *hydrophilia* and *lipophilia* of the surfactant. The model to calculate this value was introduced by Griffin in 1949 and later revised by Davies in 1957 [37,38].

The HLB parameter is valuated from the quantitative ratio between the “effectiveness” of polar and non-polar moieties, based on their molecular weights, and its value is comprised between 0 and 20 [36], where:

- $HLB = 0$ refers to a totally lipophilic surfactant.
- $HLB = 20$ refers to a totally hydrophilic surfactant.

In particular, this parameter is fundamental for the choice of emulsifying agents. Surfactants with low HLB value ($3 < HLB < 6$) stabilize W/O emulsions, while for those with high HLB value ($8 < HLB < 18$) stabilize O/W emulsions. By a similar approach, it is possible to define the appropriate surfactant for a specific application based on its HLB value, as shown in Table 1:

Table 1 Different range of HLB for several application.

HLB value	Application
3.5-6	W/O emulsifier
7-9	Wetting agent
8-18	O/W emulsifier
13-15	Detergent
15-18	Solubilization

According to the Griffin model, the HLB value can be calculated as:

$$HLB = \frac{M_H}{M} 20$$

Equation 14

Where M_H is the molar mass of the hydrophilic moiety and M is the total molar mass of the surfactant. This equation holds for non-ionic surfactants with small hydrophilic head, while for ionic and ethoxylated surfactants a corrective factor, C^1 , must be introduced [36]:

$$HLB = \frac{M_H}{M} * 20 + C^1 \quad \text{Equation 15}$$

The Davies revision to this model decomposes the HLB value considering the chemical formulae of the surfactants in terms of group numbers, according to the equation [39]:

$$HLB = 7 + \sum(\text{hydrophilic group}) \times \text{its contribution} - \sum(\text{lypophobic group}) \times \text{its contribution} \quad \text{Equation 16}$$

The cpp parameter is probably more adherent to the molecular features of a surfactant. However, its value depends on the chemical environment (because of the α_o variation) and is hardly predictable. The HLB parameter is somehow a coarser parameter, but its value can be easily obtained and is often used for practical application.

1.4. Micellization

One of the most interesting properties of the surfactants in aqueous solution is their ability to self-assembly to form supramolecular aggregates, generating an overall lowering of the free energy of the system.

At low concentrations, the surfactant molecules preferably occupy the air-water interface, with the tails facing upwards, lowering the surface tension.

When the surfactant concentration increases, a monolayer is formed at the interface, known as a Gibbs monolayer and any additional surfactant molecule added remains in the aqueous phase.

When the concentration of the surfactant molecules in the bulk of the solution exceeds a limit value, the surfactant molecules self-aggregate. This entails a clear change in the physical-chemical properties. Fig. 11 shows a scheme of the behavior of a surfactant in solution.

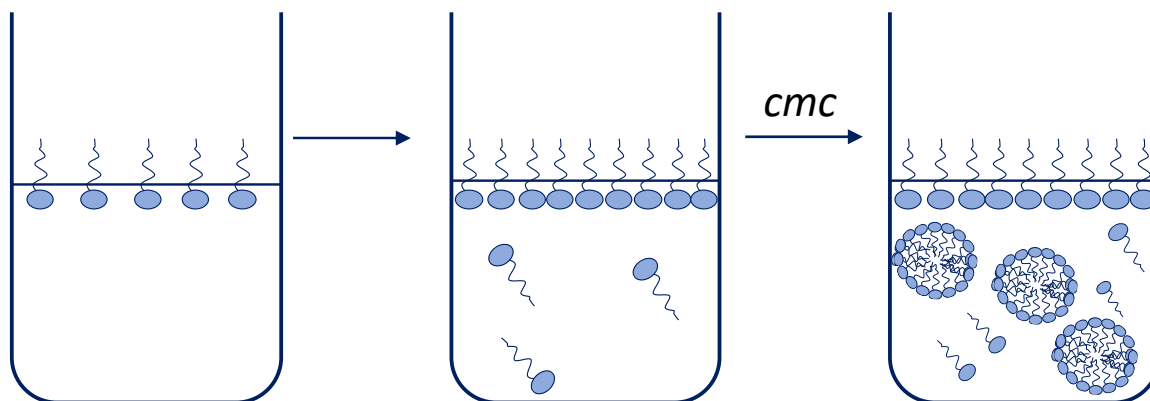


Figure 11. Scheme of the behavior of a surfactant in solution.

The particular concentration above which supramolecular aggregates are formed is called the critical micellar concentration (*cmc*).

The geometric shape of these aggregates is often similar to a sphere, or an ellipsoid of rotation, whose surface is made up of the heads of the surfactant molecules: in this way, the only hydrophilic groups interact with the water while the tails assemble inside the micelle [34]

In order to a surfactant to form micelles, it has to possess a polar group sufficiently active to promote the solubilization of the molecule until the *cmc* is reached; at the same time, it must present an apolar chain long enough to significantly reduce the solubilization in water, providing the driving force for the micellization process.

The physico-chemical description of the phenomenon of micellization is essentially based on two models [35]. The simplest one is that of the pseudo-phase separation in which the micelles are considered as a second phase microdispersed in the aqueous phase. The chemical potential of a “free” (not micellized) surfactant monomer in the aqueous phase is defined as follows:

$$\mu_F = \mu_F^0 + RT \ln a_F \quad \text{Equation 17}$$

Where, μ_F^0 is the standard chemical potential, defined as that of infinite dilution; a_F is the activity of the surfactant in water. In the micellar phase, the activity is unitary and therefore:

$$\mu_M = \mu_M^0 \quad \text{Equation 18}$$

where μ_M^0 is the standard chemical potential in the micellar phase. In conditions of equilibrium between the two phases, we have:

$$\mu_M = \mu_F \quad \text{Equation 19}$$

thus, obtaining the following expression:

$$a_F = K = \exp\left(\frac{\mu_M^0 - \mu_F^0}{RT}\right) \quad \text{Equation 20}$$

Thus, in the presence of micelles, if the *cmc* is low enough to consider ideal the aqueous phase, the concentration of the free surfactant must be a constant. This results in the formation of micelles only if the total surfactant concentration is greater the critical concentration (*cmc*), derived from the previous thermodynamic relationship. The micelles are completely absent below the *cmc*, while above the *cmc* their concentration, C_M , in the case of monodisperse aggregates with aggregation number s is given by:

$$C_M = \frac{c - cmc}{s} \quad \text{Equation 21}$$

Where c is the total concentration of surfactant present in solution and s is the aggregation number.

The phase separation model is sufficient to describe the most important aspects of the phenomenon of micellization; it predicts, at the *cmc*, a sudden change in the slope of the trend of the thermodynamic and dynamic properties of the system, in a manner similar to the phase transitions of the second order.

The short-chain hydrophobic surfactants, with a high *cmc* value, show trends in the physico-chemical properties without any angular point and often the phenomenon of micellization is barely evident. Under these conditions, a model is preferred that predicts continuous variations in the concentrations of the species in solution: the mass action model. In this model it is assumed that micellization can be represented as a simple chemical reaction.

For non-ionic surfactants:

$$sT = T_s \quad \text{Equation 22}$$

where with T we indicate a surfactant molecule and with T_s the micelle. For this reaction it is possible to estimate an equilibrium constant:

$$K = \frac{a_{T_s}}{a_T^s} \quad \text{Equation 23}$$

For ionic surfactants, partially or totally dissociated in solution, a certain number q of counter ions, C , will condense around the micellar surface to reduce the electrostatic repulsions between the heads. The reaction must then be rewritten as follows:

$$sT + qC = T_s C q^{(s-q)} \quad \text{Equation 24}$$

the equilibrium constant is changed as follows:

$$K = \frac{a_{T_s} C q}{a_T^s a_C^q} \quad \text{Equation 25}$$

The two models can appear very different; however, it should be emphasized that the results that allow to obtain coincide for aggregates with an aggregation number greater than 10 [35].

The formation of micelles is an important phenomenon not only because many interfacial phenomena, such as detergency, depend on the existence of the micelles in solution but also because their presence influences, for example, the decrease in surface tension, which does not directly involve the micelles. These aggregates have become of great interest in the catalysis of organic reactions and because of their similarity to biological membranes and globular proteins [1,5].

1.4.1. Mixed micellization

In many practical applications, blends of surfactants are used rather than pure surfactants. This is sometimes due to industrial syntheses that directly produce mixtures of surfactants of a similar nature, which would be difficult to separate. In other cases, surfactant mixtures are purposely designed and produced. They are widely used in the detergent, food and pharmaceutical industries since, their composition and concentration can be easily optimized and adapted to different tasks [36].

The physico-chemical properties of surfactant mixtures are essentially driven by the nature of the different hydrophilic heads and their interactions. There is considerable interest in the development of an adequate model to represent the formation of mixed micelles, however, the principles that govern this phenomenon are far from having been fully understood. In the literature there are only models that describe some aspects of mixed micellization. It is also difficult to identify an experimental technique that allows information on systems of this type to be obtained, in fact, very often “average” data are obtained, affected by all the different species involved, and it is difficult to separate the individual contributions.

1.4.2. Thermodynamics of mixed micellization

Several thermodynamic treatments have been developed to describe the process of formation of mixed micelles in solution. Similarly to what discussed above for the micellization of a single surfactant, the two most used models to interpret the experimental data are the pseudo-phase separation model and the mass action model [40].

The pseudo-phase separation model assumes that micelles are a separate phase whose existence begins at the critical micellar concentration (*cmc*), which represents the saturation concentration for surfactants. This model has the advantage of being simple and of adequately interpreting the composition of the micellar phase as a function of the composition of the aqueous phase.

The mass action model, on the other hand, considers that the monomeric surfactants and micellar aggregates are in association-dissociation equilibrium, so that the law of mass action can be applied. This model, which describes in a more satisfactory way the behavior of the system around the *cmc*, has the disadvantage of requiring a greater number of parameters which, due to the formation of a micelle formed by two surfactants, become difficult to determine.

In the hypothesis of pseudo-phase separation, the formation of mixed micelles can be described by means of a rather simple thermodynamic treatment. In a micellar solution, the chemical potential of the micellized surfactants is given by:

$$\mu_i^M = \mu_i^{0M} + RT \ln Y_i \gamma_i \quad \text{Equation 26}$$

where γ_i is the activity coefficient of the *i*-th surfactant in the micellar phase, μ_i^{0M} is the standard chemical potential, defined as that of the surfactant in its pure micelle, and Y_i is the mole fraction of the surfactant with respect to the total surfactant in the micellar phase.

The chemical potential of surfactants in the aqueous phase, on the other hand, is determined by the following relation:

$$\mu_i^F = \mu_i^{0F} + RT \ln c_i \quad \text{Equation 27}$$

μ_i^{0F} is the standard chemical potential, defined as that at infinite dilution of the surfactant, there is the concentration of the surfactant in the aqueous phase. It is assumed that the aqueous phase is sufficiently diluted to be considered ideal.

By equating the two chemical potentials, according to the theory of phase transitions, the following relationship is obtained:

$$Y_i \gamma_i \times cmc_i = X_i \times cmc \quad \text{Equation 28}$$

Where cmc_i is the critical micellar concentration of the i -th pure surfactant and X_i instead is its molar fraction with respect to the total surfactant present in the aqueous phase; cmc is the critical micellar concentration of the mixed system.

For mixtures of non-ionic surfactants, Clint has shown that the activity coefficient can be often considered as unitary, i.e. mixed micelles can be compared to ideal solutions [41]. In these conditions the following relationship applies:

$$cmc = \frac{1}{\sum_i \left(\frac{X_i}{cmc_i} \right)} \quad \text{Equation 29}$$

The stability of micelles in which at least one surfactant is ionic strongly depends on the condensation of counterions onto the micellar surface and consequently on the charges of the non-neutralized heads. This effect, which the mass action model cannot take into account in a simple way, in the phase pseudo-treatment model is simply included in the activity coefficients of the ionic component in the micellar phase. However, it is necessary to consider sufficiently diluted solutions in order to neglect the electrostatic interactions between the monomers in solution and between the micelles.

For mixtures in which at least one surfactant is ionic, it is necessary to evaluate the activity coefficient γ_i . Scamehorn, Rubingh and Holland used the theory of regular solutions to calculate the activity coefficients [42,43]. In this case, the following relationship applies:

$$\ln(\gamma_i) = \beta(1 - Y_i)^2 \quad \text{Equation 30}$$

The parameter β is an interaction factor and can be expressed in terms of molecular interactions between the different surfactants that form the mixed micelles:

$$\beta = \frac{N_A(W_{11} + W_{22} - 2W_{12})}{RT} \quad \text{Equation 31}$$

where W_{ij} is the interaction energy between surfactants i and j in the micelle. It has been shown that, if the β value is large and negative, the interactions between the two surfactants in mixed micelles are

favorable and such aggregates are more stable than pure aggregates. The value of β varies with the temperature and also, very mildly, with the total micelle concentration.

The model of regular solutions is used due to its simplicity and ease of application. It links very well the *cmc* trend of the mixtures to the composition of the two phases in equilibrium.

References

- [1] Sar P.; Ghosh A.; Scarso A.; Saha B., Surfactant for better tomorrow: applied aspect of surfactant aggregates from laboratory to industry, *Res Chem Intermed*, 2019, 45, 6021–6041. <https://doi.org/10.1007/s11164-019-04017-6>
- [2] Rieger M., *Surfactant in cosmetics*, New York, Taylor & Francis Group, 1997, 2nd Ed, <https://doi.org/10.1201/9780203737743>
- [3] Lin H.; Zhou H.; Xu L.; Zhu H.; Huang H., Effect of surfactant concentration on the spreading properties of pesticide droplets on Eucalyptus leaves, *Biosyst Eng*, 2016, 143, 42-49. <https://doi.org/10.1016/j.biosystemseng.2016.01.003>
- [4] Bramer T.; Dew N.; Edsman K., Pharmaceutical applications for cationic mixtures, *J. Pharm. Pharmacol.* 2007, 59 1319–1334, <http://dx.doi.org/10.1211/jpp.59.10.0001>
- [5] Abbasian A.; Ghaffarian S. R.; Mohammadi N.; Khosroshahi M. R.; Fathollahi M., Study on different planforms of paint's solvents and the effect of surfactants (on them), *Prog. Org. Coat.*, 2004, 49, 229–235. <http://dx.doi.org/10.1016/j.porgcoat.2003.09.020>
- [6] de Freitas Ferreira J.; Vieira E. A.; Nitschke M., The antibacterial activity of rhamnolipid biosurfactant is pH dependent, *Int. Food Res.*, 2019, 116, 737–744, <https://doi.org/10.1016/j.foodres.2018.09.005>.
- [7] Everett D.H. "Manual of Symbols and Terminology for Physicochemical Quantities and Units, Appendix II: Definitions, Terminology and Symbols in Colloid and Surface Chemistry" *Pure and Applied Chemistry*, 1972, 31, 4, 577-638. <https://doi.org/10.1351/pac197231040577>
- [8] Rouquerol J.; Rouquerol F., Adsorption at the Liquid-Solid Interface: Thermodynamics and Methodology. In Adsorption by Powders and Porous Solids: Principles, Methodology and Applications, 2nd ed.; Rouquerol, J., Rouquerol, F., Sing, K., Llewellyn, P., Maurin, G., Eds.; Academic Press, Inc.: London, UK, 2014; pp. 105–158, ISBN 9780080970356.
- [9] Wu S., 1982, "Modifications of polymer surfaces: Mechanisms of wettability and bondability improvements," in Polymer Interfaces and Adhesion, Marcel Dekker, New York, pp. 279–329.

- [10] Brzoska J. B.; Shahidzadeh N. and Rondelez F., 1992, "Evidence of a transition-temperature for the optimum deposition of grafted monolayer coatings," *Nature London* 360, 719. <https://doi.org/10.1038/360719a0>
- [11] Bonn D.; Eggers J.; Indekeu J.; Meunier J.; Rolley E., Wetting and spreading, *Rev. Mod. Phys.*, 2009, 81, 739. <https://doi.org/10.1103/RevModPhys.81.739>
- [12] Marmur A., Soft contact: Measurement and interpretation of contact angles, 2006, *Soft Matter*, 2, 12-17. <https://doi.org/10.1039/B514811C>
- [13] R.N. Wenzel, Resistance of a solid surfaces to wetting by water, 1936, *Industrial & Engineering Chemistry*, 28, 988-994. <http://dx.doi.org/10.1021/ie50320a024>
- [14] Marmur A., Wetting on hydrophobic rough surfaces: to be heterogeneous or not to be?, *Langmuir*, 2003, 19, 8343-3348. <https://doi.org/10.1021/la0344682>
- [15] Cassie A.B.D.; Baxter S., Wettability of porous surfaces. *Trans. Faraday Soc.*, 1944, 40, 546-551. <https://doi.org/10.1039/TF9444000546>
- [16] Detrich A.; Nyári M.; Volentiru E.; Hörvölgyi Z., Estimation of contact angle for hydrophobic silica nanoparticles in their hexagonally ordered layer, 2013, *Mater. Chem. Phys.*, 140, 602-609. <https://doi.org/10.1016/j.matchemphys.2013.04.013>
- [17] Herminghaus S.; Brinkmann M.; Seemann R., Wetting and de-wetting of complex surface geometries, *Annu. Rev. Mater. Sci.*, 2008, 38, 101-121. <https://doi.org/10.1146/annurev.matsci.38.060407.130335>
- [18] Tadmor R., Line energy and the relation between advancing, receding, and Young contact angles, *Langmuir*, 2004, 20, 3676-3678. <https://doi.org/10.1021/la049410h>
- [19] Kovalchuk N. M.; Simmons M. J. H. Surfactant-mediated wetting and spreading: Recent advances and applications, *Curr Opin Colloid Interface Sci*, 2021, 51, 101375. <https://doi.org/10.1016/j.cocis.2020.07.004>
- [20] Hagedorn O.; Fleute-Schlachter I.; Mainx H. G.; Zeisler-Diehl V.; Koch K., Surfactant-induced enhancement of droplet adhesion in superhydrophobic soybean (*Glycine max L.*) leaves. *Beilstein J. Nanotechnol.* 2017, 8, 2345–2356. <https://doi.org/10.3762/bjnano.8.234>

- [21] Fernández V.; Eichert T., Uptake of Hydrophilic Solutes Through Plant Leaves: Current State of Knowledge and Perspectives of Foliar Fertilization, *CRC Crit Rev Plant Sci*, 2009, 28, 36-68. <https://doi.org/10.1080/07352680902743069>
- [22] Stetten A. Z.; Iasella S. V.; Corcoran T. E.; Garoff S.; Przybycien T. M.; Tilton R. D., Surfactant-induced Marangoni transport of lipids and therapeutics within the lung, *Curr Opin Colloid Interface Sci*, 2018, 36, 58-69. <https://doi.org/10.1016/j.cocis.2018.01.001>
- [23] Eudier F.; Savary G.; Grisel M.; Picard C., Skin surface physico-chemistry: Characteristics, methods of measurement, influencing factors and future developments, *Adv. Colloid Interface Sci*, 2019, 264, 11-27. <https://doi.org/10.1016/j.cis.2018.12.002>
- [24] Athanasopoulos D.; Svarnas P.; Ladas S.; Kennou S.; Koutsoukos P., On the wetting properties of human stratum corneum epidermidis surface exposed to cold atmospheric-pressure pulsed plasma, *Appl. Phys. Lett.*, 2018, 112, 213703. <https://doi.org/10.1063/1.5027901>
- [25] Ahmed G.; Arjmandi Tash O.; Cook J.; Trybala A.; Starov V., Biological applications of kinetics of wetting and spreading, *Adv. Colloid Interface Sci*, 2017, 249, 17-36. <https://doi.org/10.1016/j.cis.2017.08.004>
- [26] Lodge R.A.; Bhushan B., Wetting properties of human hair by means of dynamic contact angle measurement, *J. Appl. Polym. Sci.*, 2006, 102, 5255-5265. <https://doi.org/10.1002/app.24774>
- [27] Saberi B.; Golding J. B.; Chockchaisawasdee S.; Scarlett C. J.; Stathopoulos, C. E., Effect of Biocomposite Edible Coatings Based on Pea Starch and Guar Gum on Nutritional Quality of “Valencia” Orange During Storage, *Starch - Stärke*, 2018, 70: 1700299. <https://doi.org/10.1002/star.201700299>
- [28] Galus S.; Kadzińska J., Gas barrier and wetting properties of whey protein isolate-based emulsion films, *Polym Eng Sci*, 2018, 59, E375-E383. <https://doi.org/10.1002/pen.24992>
- [29] Bertrand E.; Bonn D.; Meunier J.; Segal D., Wetting of Alkanes on Water, *Phys. Rev. Lett.*, 2001, 86, 3208. <https://doi.org/10.1103/PhysRevLett.86.3208>
- [30] Druetta P.; Raffa P.; Picchioni F., Chemical enhanced oil recovery and the role of chemical product design, *Applied Energy.*, 2019, 252, 113480. <https://doi.org/10.1016/j.apenergy.2019.113480>

- [31] Moody C. A.; Field J. A.; Perfluorinated Surfactants and the Environmental Implications of Their Use in Fire-Fighting Foams, *Environ. Sci. Technol.*, 2000, 34, 3864–3870. <https://doi.org/10.1021/es991359u>
- [32] Wijshoff H., Drop dynamics in the inkjet printing process, *Curr Opin Colloid Interface Sci*, 2018, 36, 20-27. <https://doi.org/10.1016/j.cocis.2017.11.004>
- [33] Martins P. C.; Martins V. G., Biosurfactant production from industrial wastes with potential remove of insoluble paint, *Int. Biodeterior. Biodegradation*, 2018, 127, 10–16. <https://doi.org/10.1016/j.ibiod.2017.11.005>
- [34] Rosen M. J.; Kunjappu J. T., Characteristic features of surfactants in: In Surfactants and interfacial phenomena, 2012, 4th Ed., New York: John Wiley & Sons, 1-38. <https://doi.org/10.1002/9781118228920>
- [35] Khalil R. A.; Zarari A. A., Theoretical estimation of the critical packing parameter amphiphilic self-assembled aggregates, *Appl. Surf. Sci.*, 2014, 318, 85-89. <https://doi.org/10.1016/j.apsusc.2014.01.046>
- [36] Davies J.T.; A quantitative kinetic theory of emulsion type. I. Physical chemistry of the emulsifying agent (1957), Proceedings of the International Congress of Surface Activity 1, 426-38.
- [37] M. Rashmi, Micellar aggregate structures and shapes in: Kinetic studies of some esters and amides in presence of micelles (2010), India, Pt. Ravishankar Shukla University. <http://shodhganga.inflibnet.ac.in/handle/10603/3938>
- [38] Griffin W. C.; Classification of surface-active agents by HLB, The Journal of the Society of Cosmetic Chemists, 1949, 1, 311-326.
- [39] Pasquali R. C.; Taurozzi M. P.; Bregni C., Some considerations about the hydrophilic-lipophilic balance system, *Int. J. Pharm.*, 2008, 356, 44-51. <https://doi.org/10.1016/j.ijpharm.2007.12.034>
- [40] Ogino K.; Abe M., In Mixed Surfactant Systems; Holland P.M.; Rubingh D. N., Eds.; ACS Symposium Series, American Chemical Society: Washington, DC, 1992; Chapter 8.
- [41] Clint J. H., Micellization of mixed nonionic surface-active agents, *Chem.Soc, Faraday Trans.1*, 1975, 71,1327-1334. <https://doi.org/10.1039/F19757101327>
-

[42] Scamehorn J. F.; Schechter R. S.; Wade W. H., Adsorption of surfactants on mineral oxide surfaces from aqueous-solutions : 1: Isomerically pure anionic surfactants, *J Colloid Interface Sci*, 1982, 85, 463-478. [https://doi.org/10.1016/0021-9797\(82\)90013-3](https://doi.org/10.1016/0021-9797(82)90013-3)

[43] Holland P. M.; Rubingh D. N., Nonideal multicomponent mixed micelle model, *J. Phys. Chem.*, 1983, 87, 1984–1990. <https://doi.org/10.1021/j100234a030>

Chapter II

2. Green chemistry principles in chemical formulations

In the era of industrial globalization, the increasing demand for performing surfactant-based formulations and the concerns about environmental issues, the exploitation of bio-based, biodegradable, and non-toxic raw materials continue to grow with the aim to develop environmentally friendly products.

The increasing and evolving consciousness of the eco-sustainability relevance has led to the set up of operative strategies that has significantly changed over time. At the beginning, the eco-friendly management of materials and chemicals was based on the reduction of the environmental dispersion to materials representing a hazard to health and the environment, confining them in monitored sites. Later on, the approach to reduce or eliminate the hazard at the root was accepted and implemented in the everyday practice, steering a more responsible use of chemicals. At the end of XX century the term ‘Green Chemistry’ was coined to meet the needs of the present and future generation in terms of environmental sustainability [1] and later this concept was enlarged to economic and social dimensions in order to establish a global system able to be sustained by the planet [2]. This is a dynamic and multidisciplinary approach where politics, industry, and academia converge and its aim is to eliminate the intrinsic risk, rather than focusing on reducing it by minimizing the exposure. The new approach, initially thought for chemical productions involving synthetic processes, has indeed expanded over the entire industrial chemistry, including chemical formulations.

Indeed, the twelve principles of green chemistry [3], originally focused on waste and hazard minimization in synthetic strategies, can easily be applied in formulation design and production, with minimal re-definitions, as specified below:

1. Waste prevention instead of remediation: it is better to reduce, or hopefully eliminate, the waste instead of finding a way to dispose of waste. In formulation chemistry, this means that all formulation could be safely dispersed in the environment, with no need of waste management.
2. Atom efficiency: during a process of synthetic chemistry the final product should incorporate as much as the materials used for its production. In this way there is the minimization of waste and a maximization of production. In formulation chemistry, this would translate in the strict use of components required to fulfill the real task, without any additional chemical for “esthetic benefits”.

Moreover, this also means that concentrated formulations, with a low amount of solvent, should be preferred.

3. Less hazardous/toxic chemicals: the chemicals and the methodologies used in synthetic chemistry should present the minimal or absence toxicity to the environment and the human health. This directly applies also to formulations.

4. Safer products by design: the final product should be designed in order to have the proper effectiveness and at same time a low toxicity. This applies also to formulations.

5. Innocuous solvents and auxiliaries: it is preferable the restrict use of solvent or dispersing agents where it is no necessary and if they are used, it is better to choose the innocuous ones. This is a relevant point in formulation chemistry, driving the preference for water and to bio-compatible dispersing agents.

6. Energy efficient by design: the production process should be conducted at ambient temperature and pressure in order to be economically and environmentally sustainable. This also applies to formulation production.

7. Preferably renewable raw materials: raw materials used in the processes should be renewable itself, in other words crude is not renewable. This directly applies to formulations, pointing to the relevance of bio-derived or even natural components.

8. Shorter syntheses: derivatization processes should be avoided when it is possible. Formulations with a lower number of components and production steps should be preferred.

9. Catalytic rather than stoichiometric reagents: it is better to prefer a catalytic reagent as selective as possible. To a certain extent, this applies also to formulations: components active at lower concentration (which would reduce the amount of formulation needed to fulfill a given task) should be preferred.

10. Design products for degradation: the product at the end of its life should not persist in the environment and do not produce in toxic products. This applies also to formulations.

11. Analytical methodologies for pollution prevention: a continuous and in real-time monitoring of hazardous contaminants reduce the risk of accumulation and exposition. This also applies to formulations.

12. Inherently safer processes: it is favorable to choose chemicals with the lowest risk for workers of fire, explosion and toxicity. This also applies to formulations, and is not limited to workers, but also to consumers who use the formulated products.

2.1. Eco-friendly Surfactants

The increasing ecological awareness has led the preference for surfactants which, besides the functional efficiency, present additional properties such as biodegradability and biocompatibility [4]. For conventional synthetic surfactants, it is reported that biodegradability is generally associated with linear tail, while the toxicity decreases with reducing the tail length [1]. However, the principles of “Green Chemistry”, steer the scientists’ and technologists’ interest for even more-eco-compatible alternatives, which are inspired by natural substances or directly extracted from natural sources.

2.1.1. Bioinspired and bioderived synthetic surfactants

A possible approach to apply the “Green Chemistry” guidelines is the so-called bio-inspiration: new surfactants are designed in order to mimic natural amphiphilic molecules such as phospholipids and biopolymers as peptides, proteins and nucleic acids [4]. These bio-based surfactants are generally synthesized from natural raw materials and are considered potential alternatives to currently used surfactants synthesized typically from fossil raw materials [5].

It is possible to divide bio-inspired surfactants into:

- I. amino acid-based surfactants, arising from the combination of hydrophilic amino acids or peptides (acting as polar headgroups) with long chain compounds (non-polar tails).
- II. glycerolipid-like structures, in which a single polar head and one or two non-polar tails are linked through a glycerol backbone.
- III. carbohydrate-based surfactants in which a sugar moiety is linked to a hydrophobic tails.

In these bio-inspired surfactants, the headgroup could be charged differently depending on the specific functional groups. The presence of one or more charged groups causes an increase in the electrostatic repulsions, enlarging the space they occupy at the micelle interface [4].

The food industry is interested to amino-acid based surfactants, and in particular to the arginine-based ones, because of their high antimicrobial activity against typical pathogens as *Escherichia coli* and *Salmonella*. Considering all these promising features, these surfactants can be proposed as substitutes for commercially available glycerides [6,7].

An example of the second class of bioinspired compounds is represented by diacyl glycerol arginine-based surfactants, which can be considered analogues to diglycerides. They consist in a glycerol skeleton connecting one positively charged arginine residue as polar head, and two fatty acid chains as hydrophobic tails. With respect to the conventional cationic surfactants, as the quaternary ammonium derivatives, diacyl glycerol arginine-based surfactants present a much lower cytotoxicity [8,9]. Another industrially relevant derivative of glycerol is Cremophor EL, which presents a very low *cmc* and can reduce the water surface tension to about 26 mN m⁻¹.

Carbohydrate-based amphiphiles, such as sugar esters and alkyl glycosides (AG), have long been used for their surfactant properties [10,11] and a new interest is rising for these molecules given the great available saccharidic biomass [12]. The APGs, alkyl polyglycosides, are nonionic surfactants synthesized on large scale from renewable raw materials such as glucose and xylose hydrolyzed from agricultural and food waste [13,14]. The high polar density of the carbohydrates is well suited as the polar head. The apolar moiety presents variation in chain length and degree of substitution [11]. Compared with traditional surfactants, APGs, or more in general AGs, have excellent industrial applications and medicine since they have high performing surface activity, good biodegradability, antifungal activity, low cytotoxicity/irritancy and biocompatibility [15,16].

Glycolipids present interesting physicochemical properties. Indeed, they often exhibit liquid crystalline phases. Significant differences are observed in the thermo- tropic properties depending on chain length (number of carbons between 8 and 14) [17] the presence of unsaturations, and to the position of the fatty residue on the sugar backbone [11]. Thus, several applications are founded on the use of glycosurfactant for their peculiar characteristics. They are applied in microemulsion, detergent and cleaner, personal care products, cosmetics and flooding processes. [17,10].

Other carbohydrates are used to synthesize surfactants and among them the sorbitan and sorbide esters are finding large applications. Examples of sorbitan fatty acid esters (SFEs) are Span® and Tween®. They are nonionic surfactants in which a sorbitan unit, eventually bearing polyoxyethylene chains, represents the hydrophilic moiety, while the hydrophobic moiety usually consists of fatty acids, alkyl-alcohols and alkyl-phenols. In general, the sugar-based nonionic surfactants tend to self-associate at

a lower concentration than the other surfactants. The main polysorbate used in the formulation industry is Tween 80. It is produced using polyethoxylated sorbitan and oleic acid and contains 20 ethylene oxide units. Since the ester bonds of fatty acids are subjected to hydrolysis at acid and basic condition, it is possible to carry out a hydrogenolysis of sorbitan acetals, in order to develop sorbitan ethers. The polysorbates present many important properties as high surface activity and low *cmc*, and consequently they can be employed as wetting, solubilizing and emulsifying agents. Specifically, they have been tested in ocular formulations [13,14]. Tween 80 can also be applied for soil recovery. Indeed, the presence of hydrophobic organic compounds (HOCs) makes the land toxic. Non-ionic surfactants have shown a higher efficiency than the cationic or anionic ones. In particular, Tween 80 represents a low-cost and low-toxicity compound for the degradation of the HOCs. At pre-micellar concentration, in the soil-water system, the surfactant is arranged at the solid-liquid interphase. The interactions between the pollutants and the surfactant hydrophilic heads favor the exclusion of the HOCs from the soil particle. Above the *cmc*, the Tween 80 micelles compete for the contaminant molecules with the soil particle [18].

Going beyond the limits of synthetic surfactants, although bio-inspired, a new kind of amphiphiles is gaining a large interest. They are molecules naturally produced by living organisms such as bacteria, plants yeasts and fungi; thus, they are called biosurfactants [19].

2.2. Biosurfactants

Biosurfactants are amphiphilic compounds naturally produced by bacteria, yeasts or fungi, whose structure is composed of hydrophilic and hydrophobic parts [20]. In general, the first moiety can be ionic, non-ionic or amphoteric, while the second one consists of one or more hydrocarbon chains.

Due to their molecular architecture, they tend to position themselves at the interfaces (e.g., oil/water interface) reducing the interfacial tension. Above a certain value of the critical micelle concentration (*cmc*), biosurfactant molecules form spherical or spheroidal aggregates (micelles) and surface tension reaches a plateau value [21].

The first important classification among the numerous types of biosurfactants is based on the molecular weight: low molecular weight biosurfactants, which are more efficient in lowering surface

and interface tension, and high molecular weight biosurfactants, which are better stabilizers of oil-in-water emulsions [22].

A second and more accurate classification can be achieved considering their chemical structure, according to which biosurfactants can be divided in several categories [23]. The main ones are glycolipids, whose structure is characterized by a tail made of long-chain aliphatic or hydroxyaliphatic acids and a polysaccharide as headgroup; lipopeptides, composed of a lipid moiety and a polypeptide chain [24]; fatty acids and phospholipids [24]; polymeric biosurfactants (proteins or polysaccharides) [20].

The processes of biosynthesis of biosurfactants are complex and very different from each other. Only a few have been studied in depth [24]. To allow the formation of biosurfactants, it is necessary for the microorganisms to grow on an organic substrate, which represents a source of carbon and energy [25]. In this respect, one of the advantages of biosurfactants, over chemical/conventional surfactants, lies in the used raw materials: the source of carbon can be chosen among by-products and industrial wastes. An example is given by vegetable oils, which are by-products of food industries, such as corn, sunflower and olive oil; being made of saturated and unsaturated fatty acids, they present 16-18 carbon atoms chains, so they are ideal for the purpose [26].

In addition to carbon, another essential presence is the nitrogen: low quantities of nitrogen promote cell metabolism and consequently biosurfactant production. On the contrary, high quantities of nitrogen give low C/N ratios, which reduce biosurfactant production [21].

Regarding variables like temperature and pH, it has been found that conducting the synthesis at neutral pH and temperatures between 35-40 °C leads to the maximum production of biosurfactants [27].

The functional properties of each biosurfactant are related to the physical and chemical characteristics of the molecule; nevertheless, it is possible to identify a common behavior which determines biosurfactant performances and applications.

The fundamental property of a biosurfactant in aqueous solution is to reduce surface tension. As already hinted, because of the hydrophilic-hydrophobic duality of their structure, biosurfactant molecules replace those of the solvent at the solution surface, decreasing the intermolecular forces among them [20]. In the solution bulk, above the *cmc*, biosurfactants micellize. In this respect, they are more efficient than their industrial counterparts, since their *cmc* is 10-40 times lower [28]. The *cmc* and the morphology of the micelles depends on the structure and length of the hydrocarbon

chains and it can change with temperature, pressure, pH variations, presence of co-solvent, such as ethanol and glycerol [20].

The capability to micellize makes biosurfactants solubilizing agents for hydrophobic compounds. They increase solubility not degrading molecules but favoring mass transfer of the hydrophobic compounds to the solution [29]: they incorporate hydrophobic molecules inside the micelles, in contact with the hydrocarbon chains [20].

Moving to the qualities which make biosurfactants environmentally friendly, biodegradability is another significant property, which means that a biodegradable compound can be decomposed by microorganisms, through enzymatic processes. It has been studied that, also thanks to their origin, biosurfactants are biodegradable [30] and they result more efficient compared to synthetic surfactants [18].

Biodegradability and bio-derivation are not synonymous of non-toxicity, but even if only few studies have been conducted about biosurfactant toxicity, they are considered low or non-toxic, so they can be employed in various fields [31]. Although non-toxic, it should be recalled that some of them are produced by pathogens (i.e., *Pseudomonas aeruginosa*), hence they are considered scarcely suitable for applications which involve food consumption [32].

Thanks to their characteristics and properties, biosurfactants are a valid option and are increasingly proposed as substitutes for synthetic ones. Their applications are countless, but one of the most studied is bioremediation, which relies on the combination of good surface activity and solubilization power: lowering interfacial tension of water, biosurfactants allow the transfer of hydrophobic pollutants in the mobile phase and with micelles, they increase the solubility of undesirable molecules [31]. To remedy to the big quantity of chemical used in these processes, biosurfactants are the ideal compounds, because they combine sustainability and good functionality. Indeed, their bioremediation efficiency is far greater than that of industrial surfactants [33].

Being good emulsifiers, biosurfactants can be used in cosmetic formulation. In this field, they are preferred to industrial surfactants because they are healthier and reduce the incidence of skin irritations and allergies [34].

Biosurfactants have been proposed considered even for biomedical applications. Surfactin has antibiotic, anti-inflammatory and anti-tumor functions [32]; specifically, it has been found to have

immunosuppressive activity, so it can be used in therapies for transplantations and autoimmune diseases [35].

Despite all these possible applications and their evident benefits, massive use of biosurfactants is slowed down so far by high costs of raw materials and production process. Low yields from already expensive process make biosurfactants uncompetitive compared to synthetic surfactants costs [27]. Current scientific research is focusing on development of more efficient bioprocesses, overproducing strains, and use of cheap raw material, paying attention to the preliminary purification costs, so as not to further charge the expenses [36].

2.3. Rhamnolipids

Rhamnolipids are the most important class of biosurfactants. They are arising an increasing technological and applicative interest, because of the promising detergent, emulsifying, wetting and solubilizing properties.

They are produced by the opportunistic pathogen *Pseudomonas Aeruginosa* and have a glycolipid-type structure composed of two parts:

- I. the glycon part, constituted by one or more rhamnose units,
- II. the aglycon part, constituted by one or more fatty acids [13].

2.3.1. Natural origin, biological functions, and molecular structure

Pseudomonas aeruginosa is a voracious organism, which feeds almost on anything. As an example, if placed in an oil-affluent environment, without other sources of carbon, it produces rhamnolipids to emulsify the oil, then ingest and consume them.

Therefore, the production of rhamnolipids is possible from several carbon sources that support bacterial growth. Highest productivity is achieved by using original oils such as soybean, canola and olive. Instead, among the water-soluble substrates, mannitol is the most effective. [37]

Furthermore, the biosynthesis of rhamnolipids can be also regulated at the transcriptional level by the quorum-sensing (QS) which is a cell-to-cell communications mechanism based on the exchange of lipidic intercellular signals between different bacteria or same bacterial strains. [37]

Among the biological functions of rhamnolipids is the reduction of surface and interfacial tension, in fact they are able to solubilize the adsorption of hydrophobic substrates.

In addition, given their low toxicity, high biodegradability and compatibility, they exhibit antibacterial, antiviral and antifungal activities. [37,38]

The discovery of rhamnolipids dates back to 1946 when Bergström *et al.* reported a glycolipid oil, called pyolipic acid, composed of L-rhamnose and β -hydroxydecanoic acid, produced by *Pseudomonas pyocyaneus* (today *Pseudomonas aeruginosa*), when cultivated on glucose [39]. In 1949 Jarvis and Johnson isolated the compound and defined the rhamnolipids structure as normal *l*- β -hydroxydecanoic acid connected through a 1,3-glycosidic bond to two molecules of L-rhamnose [40]. In 1965 Edwards and Hayashi discovered that the bond between the two L-rhamnose molecules is the α -1,2-glycosidic bond, as deduced through oxidation and methylation of the periodate; thus, they conclusively demonstrated the structure of rhamnolipids to be 2-O- α -L-rhamnopyranosyl- β -hydroxy-decanoyl- β -hydroxydecanoate [40].

From 1972 to 2000, through the use of various analytical instrumental techniques, various rhamnolipids, produced by *Pseudomonas Aeruginosa* strains growing on different carbon sources, were isolated and characterized; the identified structures included a large number of homologues, about 60. The main molecular features that can vary are the number of rhamnose units and the number of hydroxyalkanoic acids. Fig. 1 shows the most representative rhamnolipid structures.

The molecular features influence the rhamnolipid solubility in water and their capability to solubilize hydrophobic compounds. Specifically, the additional molecule of rhamnose gives greater hydrophilicity to the di-rhamnolipids, while additional or longer fatty acid chains increase their hydrophobicity [41,42]. Minor variable features include the fatty acid length, chain unsaturation, and the possible presence of further functional groups. In all cases, rhamnolipids present a single free carboxylic group and this gives the rhamnolipids an amphoteric behavior in water (protonated/neutral in acidic and deprotonated/anionic in alkaline conditions) [43].

The great part of surfactants usually shows a net distinction between polar head and hydrophobic tails. Rhamnolipids expose the carboxylic group at the end of the aliphatic chains which contributes to the hydrophilic region but the electric contribution is the surfactant head. and should be considered as part of the head [44].

As consequence, the presence of the carboxylic group makes rhamnolipids pH sensitive surfactants. The pKa of the carboxylic group is around 5.5 [45-47] so they behave as anionic surfactant at neutral

and basic pHs and as non-ionic surfactants at acid pH below 5.5. and thus the physico-chemical and aggregation properties are related on both the pH and the presence of ions.

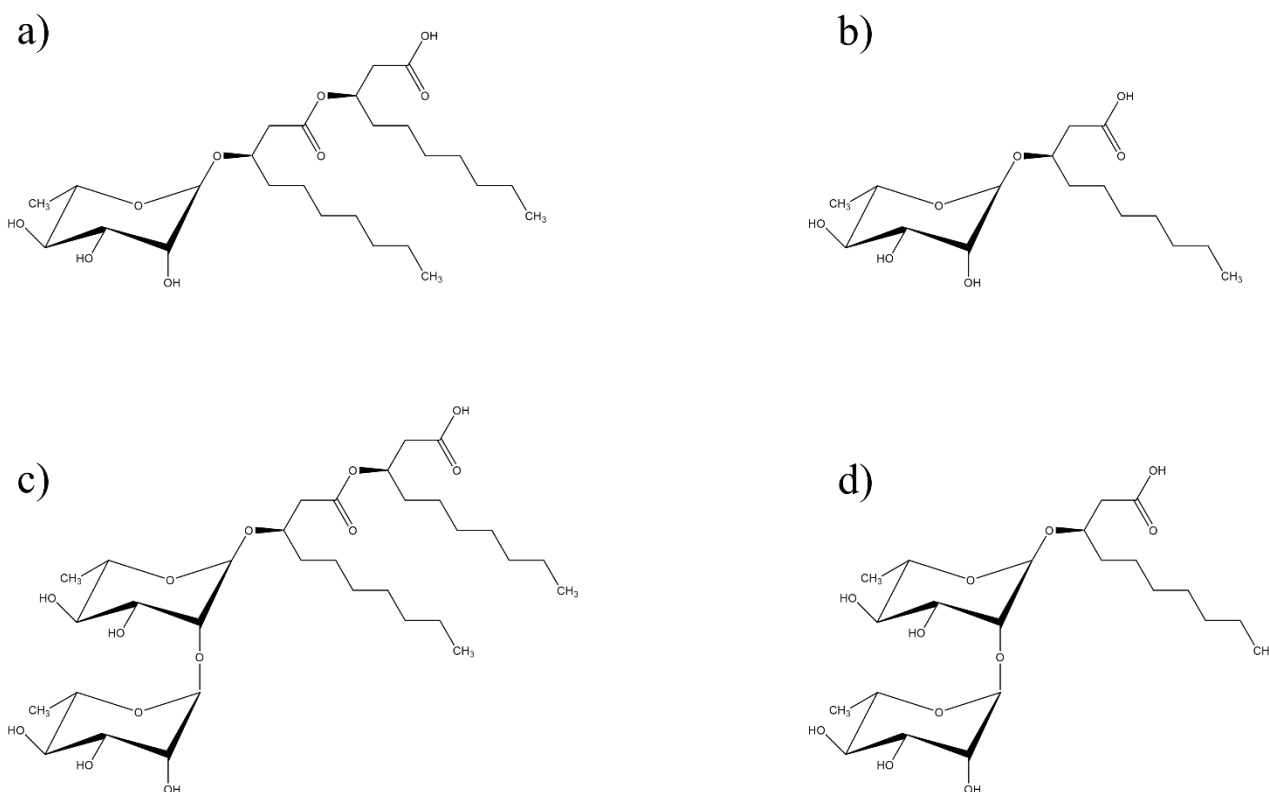


Figure 1. Common structures of rhamnolipids homologues: in panel a) and b) the structure of mono-rhamnolipid; in panel c) and d) the structure of di-rhamnolipid.

Pseudomonas Aeruginosa bacteria produce rhamnolipid mixtures, whose composition depends on the strain, its origin, the type of carbonaceous substrate, the culture conditions [40]. The enzymatic synthesis *Pseudomonas Aeruginosa* uses to produce di-rhamno-di-lipids, chosen as an example, can be summarized in three main reactions:

1. $2\beta\text{-hydroxydecanoyl-CoA} \xrightarrow{+\text{H}_2\text{O}} \beta\text{-hydroxydecanoyl-}\beta\text{-hydroxydecanoate} + 2 \text{ CoA}$
2. $\text{TDP-L-rhamnose} + \beta\text{-hydroxydecanoyl-}\beta\text{-hydroxydecanoate} \rightarrow \text{TDP} + \text{L-rhamnosyl-}\beta\text{-hydroxydecanoyl-}\beta\text{-hydroxydecanoate}$
3. $\text{TDP-L-rhamnose} + \text{L-rhamnosyl-}\beta\text{-hydroxydecanoyl-}\beta\text{-hydroxydecanoate} \rightarrow \text{TDP} + \text{L-rhamnosyl-L-rhamnosyl-}\beta\text{-hydroxydecanoyl-}\beta\text{-hydroxydecanoate}$

The double chain β -hydroxydecanoyl- β -hydroxydecanoate is obtained first, and then we have a sequence of two rhamnosyl-transfer reaction (2 and 3), catalyzed by two rhamnosyl-transferases, where the source of rhamnose is Thymidine Di- p-Phosphate-L-rhamnose. Thus, the mono-rhamnolipids are initially obtained, and eventually converted to di-rhamnolipids [41].

2.3.2. Physico-chemical properties

Probably the main property of biosurfactants is their ability to lower surface/interface tension. This ability allowed the presence of such molecules to be identified in bacterial media [48-53] and is at the basis of biosurfactant use in many different fields, being the surface tension a parameter of crucial importance in different phenomena, such as adsorption, wetting, catalysis and so on [21,54]. Moreover, self-aggregation of biosurfactants, with formation of aggregate/solvent interfaces, results in the micellization phenomenon, on which other fundamental applications, such as detergency or contaminant removal, depend [55-57].

When surfactants are added to water, given the amphiphilic nature, they adsorb at the water–air interface with the hydrophilic headgroups towards water and the hydrophobic tails towards air. The result of this preferential adsorption is the reduction of solution surface tension γ [54,57]. In thermodynamics terms, the presence of surfactants at the air/water interface reduces the surface free energy per unit area required to create new surface. Surface tension of surfactant solutions can be determined as a function of surfactant concentration by means of tensiometric titration experiments [58].

These experiments allow to determine γ_{min} , the maximum lowering of surface tension, and also the *cmc*. Moreover, from the slope of the plot of γ versus the logarithm of surfactant molar concentration c it is possible to calculate the surface concentrations Γ by means of the Gibbs equation [59-61]:

$$\Gamma = -\frac{1}{nRT} \frac{d\gamma}{d \ln c} \quad \text{Equation 1}$$

where R is the gas constant, T is the absolute temperature and n is a coefficient that takes into account the dissociation of ionic surfactants, and, in turn, the area occupied by a molecule at the surface A_{min} :

$$A_{min} = \frac{1}{\Gamma N_A} \quad \text{Equation 2}$$

where N_A is the Avogadro number. The area occupied at the surface by single surfactant gives a good idea on the packing of molecules and on their structure and interactions.

Surface properties, including γ_{min} and A_{min} , as well as self-aggregation features, such as the cmc , have been determined for a great variety of rhamnolipids, mixtures of congeners as well as purified forms, natural rhamnolipids as well as synthetic ones, and in conditions differing for pH, ionic strength and presence of additives.

Mixtures of rhamnolipids show the value of γ_{min} is 26-39 mN/m and value of cmc in the range 10-600 mg/L. These wide range are due to the different producing bacterium, and the different growth conditions. Indeed, cmc depends on the growth medium employed for rhamnolipid production: when sources of long carbon chains are used, lower cmc values are obtained, with respect to cases where glucose or other carbon sources are employed.

For pure rhamnolipids, the cmc values of monorhamnolipids range from 0.01 to 0.40 mM, while for dirhamnolipids they range from 0.01 to 0.46 mM, indicating that the presence of one or two sugar units has a limited effect on the aggregation of rhamnolipids in micelles. In acid conditions, $pH \sim 4-5 < 5.6 = pK_a$, monorhamnolipids and dirhamnolipids show a smaller value which corresponds to conditions where rhamnolipids are expected to be fully protonated, with no net charge and with minimal electrostatic repulsions. Thus at acid pH, cmc values for monorhamnolipids and dirhamnolipids are perfectly coincident when highly pure (>96%) and the pH is kept constant by the use of buffers [62]. At intermediate conditions, with $pH=6.8$, the value of cmc are very similar each other.

In alkaline conditions, $pH = 9$, the carboxylic groups is expected to be deprotonated, the monorhamnolipid show a net negative charge and electrostatic repulsion with other molecules which correspond to a cmc value that is twice that of dirhamnolipid [63], suggesting that for rhamnolipids in anionic form a slight effect of the number of rhamnose moieties in the head could exist.

The effect of ionic strength was investigated for both monorhamnolipids and dirhamnolipids at acid [45,64] and neutral [45,64-66] pHs when they are supposed to be respectively non-ionic and anionic. It was observed that addition of increasing quantities of NaCl has near no effect when both rhamnolipids are protonated, while it causes a decrease of cmc values at pH around 7, with cmc decreasing of a factor of 2-4 for monorhamnolipids and of 4-5 for dirhamnolipids with increasing NaCl concentration [45,64-66].

The average γ_{min} values are 25-36 mN/m for monorhamnolipids and 28-37 mN/m for dirhamnolipids, respectively, indicate that the more hydrophobic monorhamnolipid appears more surface active compared to the more hydrophilic dirhamnolipid. The highest values are found for both rhamnolipids

at highly basic pHs when significant dissociation might occur [49,67]. As for the smallest values, they are generally found for acid pHs when rhamnolipids fully behave as non-ionic surfactants [62]. For what concerns A_{min} values, they crucially depend on the choice of the prefactor n employed in the Gibbs equation (Equation 1) [59,61,66,67].

At $\text{pH} < \text{pKa}$ as well as at $\text{pH} > \text{pKa}$ and high ionic strength a Gibbs prefactor $n = 1$ is used. In these conditions, A_{min} values for monorhamnolipid range between 52 [63] and 84 [68] \AA^2 , a significant variation that cannot be related to the different experimental conditions, since the lowest value is found for pure monorhamnolipid in water at neutral pH and in the presence of 0.5 M NaCl [63] and the highest value in very similar conditions, *i.e.* in pure water, where the pH should be around 7, and in the presence of 1 M NaCl [68]. The main difference is the purity of the rhamnolipid employed, in the former case around 96%, in the latter significantly lower, even if not specified. When only highly pure monorhamnolipid samples are taken into account, the smallest A_{min} value, about 60 \AA^2 , is found at acid pH, when electrostatic repulsion among the headgroups should be null [65].

In the case of dirhamnolipid, A_{min} values range between 65 [65] and 84 [71] \AA^2 when a Gibbs prefactor of 1 is used. Surprisingly the highest value, found in pure water and in the absence of salts, is the same found for monorhamnolipid, and, overall, A_{min} values for dirhamnolipid are not so different nor always larger than those found for monorhamnolipid, despite the presence of two rhamnose units in the headgroup rather than one.

At $\text{pH} > \text{pKa}$ and at low ionic strength, a Gibbs prefactor of 2 should be used to take into account surfactant dissociation [59,61,66,67]. In these conditions A_{min} for dirhamnolipid is about 130 \AA^2 [62,65,68,69], while for monorhamnolipid ranges between 86 [74] and 135 [73] \AA^2 , a great variability that cannot be easily justified on the bases of the pH or the ionic strength, as, for example, A_{min} varies from 86 to 109 \AA^2 by decreasing the pH from 8 to 7 and increasing the phosphate buffer concentration from 10 mM to about 100 mM [70]. Molecular dynamic simulations of anionic Rha-C₁₀-C₁₀ at the air/water interface indicated an energetically preferred A_{min} value of $\sim 80 \text{\AA}^2$ [71]. However, values ranging from 60 to 140 \AA^2 were all found to be energetically accessible at room temperature. The highest surface concentrations, corresponding to the smallest surface areas, were found in the simulations when the monolayer began to exhibit significant undulations, which depended, in turn, on the balance of possible headgroup–headgroup and tail–tail interactions, which are difficult to predict [71]. This may justify variations of A_{min} values that cannot be easily linked to molecular structure or solution conditions.

When pure monorhamnolipid and dirhamnolipid are analysed in the same conditions, for example in pure water at pH = 6.8 [62,68,69], monorhamnolipid is characterized by a slightly larger area per molecule at interface, 135 vs 131 Å². This counterintuitive finding was explained invoking the screening effect of the double rhamnosyl group of dirhamnolipid molecules on the carboxylate group, allowing dirhamnolipid molecules to pack more densely than monorhamnolipid ones at the interface [62]. However, such a difference is indeed small and mostly suggests a very similar packing for monorhamnolipid and dirhamnolipid, irrespective of the supposed bulkiness of the polar head.

Belonging to glycolipids class which self-assemble into spherical, disk-like (oblate) and rod-like (prolate) spheroid micelles in dilute conditions [72,73], while at higher concentrations, they show a complex phase behaviour of a range of liquid crystalline states [72,74]. Rhamnolipids are able to form various structures, such as micelles, vesicles, bilayers and various mesophases. In principle, the presence of the carboxylic acid group further complicates this scenario conferring a pH dependence to rhamnolipid aggregation properties, in addition to the dependence on concentration, temperature, presence of additives, salts or impurities, as well as sample heterogeneity due to the presence of different congeners. Rhamnolipids are indeed able to form aggregates with very different dimensions, depending on the concentration, the pH and the temperature. However, a clear identification of the kind of aggregates formed is often not possible as many studies employed Dynamic Light Scattering (DLS), as the only technique to analyse aggregate features, providing only the hydrodynamic radius (R_h) or diameter. In this respect, rhamnolipids are shown to form mainly smaller aggregates with hydrodynamic radii of the order of tenth of nanometres (10-60 nm) and larger aggregates with hydrodynamic radii of the order of hundreds of nanometres. A first source of confusion arises because the former kind of aggregates are considered as micelles by some research groups and as vesicles by others. Actually, species with $R_h \sim 10/30$ nm are likely to be micelles, but because of their large dimensions they cannot be identified as simple spherical micelles and are likely to be elongated micelles, ellipsoidal or even cylindrical ones. Aggregates with $R_h \sim 50/60$ nm could be identified as vesicles, but a clear distinction between very large micelles and vesicles requires the use of additional experimental techniques in conjugation with DLS, such as Small Angle Neutron Scattering (SANS) or Polarized Optical Microscopy (POM). Nonetheless, it is worth to note that neither of these two techniques gives a clear-cut definition of the aggregate nature on its own. When SANS or POM are employed, the presence of a lamellar arrangement of rhamnolipids is assessed by a q^{-2} trend of the SANS profiles at small q or by the presence of maltese crosses in POM images, but whether we are in the presence of flat lamellae or spherical vesicles (and if the latter are uni- or multi-lamellar) cannot

be established without the combination of complementary techniques. Therefore, the actual nature of lamellar aggregates is also elusive. Finally, some ambiguous or wrong classifications could be the result of misinterpretation of the experimental data.

The aggregation behaviour of monorhamnolipids and dirhamnolipids have been also rationalized in some cases through the calculation of the critical packing parameter (*cpp*) [74,75], but very different values are reported in different papers, with *cpp* values ranging from 0.24 [68] and 1 [76] for monorhamnolipids and from 0.27 [68] and 0.73 for dirhamnolipids.

cpp is in the previous Chapter I in paragraph 1.3.2. (Eq. 12).

Within the simplicity of the above formula, calculating the *cpp* of surfactants, in particular complex surfactants like biosurfactants in general and rhamnolipids in particular, is not trivial [54]. Focusing only on the main issues, one has to consider not only the possibility of tail deformation when defining v_0 and l_0 , but also, in the case of rhamnolipids, the presence of two tails and their actual lengths, since delimitation of hydrophobic and hydrophilic regions is much more blurred than in canonical surfactants. The most difficult geometrical parameter to calculate among those present in the *cpp* definition is a_e . Often it is regarded as an index of the steric hindrance of the headgroups, and, also considering this oversimplification, the conformational flexibility of the rhamnolipid headgroup, particularly for di-rhamnolipids, significantly complicates a_e evaluation. In addition, a_e strictly represents an equilibrium area per molecule, obtained from the minimization of the free energy of micellization. Therefore, it includes effects deriving from electrostatic interaction, hydration of the headgroup, binding and hydration of counterions and hydrophobicity of the headgroup [54,77], all of them are effects difficult to evaluate and more significant for rhamnolipids than for canonical surfactants. Finally, the influence of the hydrophobic region usually is not accounted in a_e calculation [75,78], but is likely to play a crucial role in determining headgroup conformation in the case of rhamnolipids. For all these reasons the observed variability of *cpp* values is not surprising; moreover, great caution is required when assessing a specific morphology to rhamnolipid aggregates based on *cpp* values.

2.3.3. Technological application

Rhamnolipids are of great interest for industrial applications, such as enhanced oil recovery, agriculture (control of zoosporic plant pathogen by affecting motility), food (multipurpose ingredients), cosmetic (health care formulations), biomedicine (cellular immunosuppression) and a bioremediation (metal flushing agents, biodegradation of organics) [40-48]. Interestingly, an

extensive characterization of rhamnolipid mixture obtained from different strains of *P. aeruginosa* (NCIM 5514 [79], BS20 [80], SG [81]) and from *Pseudomonas stutzeri* Rhl [82] subjected to different, extreme, conditions of temperature (from 4 to 120°C), pH (from 2 to 13) and ionic strength (from 0 to 20 % w/v NaCl) well highlighted the incredible resistance of biosurfactants and the possibility to employ them also in industrial applications where canonical surfactants undergo degradation and inactivation [79,80,82]. Thus, these findings prove the rhamnolipids advantages.

Furthermore, rhamnolipids are excellent candidates for bioremediation, because of their excellent tension surface and emulsifying activity as well as high stability at elevated temperatures, high salinities, and over a wide pH range [83].

The main issues for industrial applications of rhamnolipids are safety, performance and costs. Concerning safety, it has to be reminded that *Pseudomonas Aeruginosa* is a well-known pathogen. This has driven:

- the heterologous production of rhamnolipid in non-pathogenic bacteria.
- the identification of non-pathogenic bacteria naturally producing rhamnolipid [84].

In the second direction, some researchers have shown that *Pseudomonas chlororaphis* is able to produce rhamnolipids using glucose as a carbon source, and a strain of *Thermus thermophilus* HB8 produces both polyhydroxyalkanates and rhamnolipids using glucose or sodium gluconate as a carbon source. However, in both cases the produced amounts are much lower lower than those of *Pseudomonas Aeruginosa* [85].

Regarding performances, the main problem is that they change with the rhamnolipid mixture composition. Different carbon source, such as soybean oil or glycerol, cause *Pseudomonas Aeruginosa* to produce rhamnolipids mixtures with different applicative potentials [86].

About the costs, the biotechnological production of rhamnolipids is much more expensive if compared to synthetic surfactants [87]. To reduce this drawback, the use of waste as a carbon source, the identification of low-cost purification strategies, and the direct application of unrefined products appears as suitable strategies [85].

References

- [1] Nogueira A. R.; da Graça M.; Popi C. B.; Sanchez Moore C. C.; Kulay L., Environmental and energetic effects of cleaner production scenarios on the Sodium Lauryl Ether Sulfate production chain, *J. Clean. Prod.*, 2019, 240, 118203. <https://doi.org/10.1016/j.jclepro.2019.118203>
- [2] Elkington, J., 2004, Enter the Triple Bottom Line. In: Henriques. A. and Richardson, J., Eds., *The Triple Bottom Line, Does It All Add up? Assessing the Sustainability of Business and CSR*, Earthscan Publications Ltd., London, 1-16. <https://doi.org/10.1108/13598540910941948>
- [3] Sheldon R. A., Fundamentals of green chemistry: efficiency in reaction design, *Chem. Soc. Rev.*, 2012, 41, 1437–145. <https://doi.org/10.1039/C1CS15219J>
- [4] *Green Chemistry: Theory and Practice*, ed. P. Anastas and J. C. Warner, Oxford University Press, Oxford, 1998; for an alternative twelve principles see: N. Winterton, *Green Chem.*, 2001, 3, G73.
- [5] Li J.; Zhang J.; Chen L.; Zhang G.; Liao J., Surface Properties and Liquid Crystal Properties of Alkyltetra(oxyethyl) β -d-Glucopyranoside. *J. Agric. Food Chem.*, 2021, 69, 10617–10629. <https://doi.org/10.1021/acs.jafc.1c03630>
- [6] Rashedi H.; Mazaheri Assadi M.; Bonakdarpour B.; Jamshidi E., Environmental importance of rhamnolipid production from molasses as a carbon source, *Int. J. Environ. Sci. Tech.*, 2005, 2, 59–62. <https://doi.org/10.1007/BF03325858>
- [7] Tripathy D. B.; Mishra A.; Clark J.; Farmer T., Synthesis, chemistry, physicochemical properties and industrial applications of amino acid surfactants: A review, *C R Chim.*, 2018, 21, 112-130. <https://doi.org/10.1016/j.crci.2017.11.005>.
- [8] Kopsahelis A.; Kourmentza C.; Zafiric C.; Kornaros M., Gate-to-gate life cycle assessment of biosurfactants and bioplasticizers production via biotechnological exploitation of fats and waste oils, *J. Chem. Technol. Biotechnol.* 2018, 93, 2833–2841. <http://dx.doi.org/10.1002/jctb.5633>
- [9] Tavano L.; Pinazoc A.; Abo-Riya M.; Infantec M. R.; Manresa M. A.; Muzzalupo R.; Pérezc L.; Cationic vesicles based on biocompatible diacyl glycerol-arginine surfactants: Physicochemical properties, antimicrobial activity, encapsulation efficiency and drug release, *Colloids Surf. B: Biointerfaces*, 2014, 120, 160–167. <http://dx.doi.org/10.1016/j.colsurfb.2014.04.009>

- [10] von Rybinski W.; Hill K., Alkyl Polyglycosides - Properties and Applications of a new Class of Surfactants. *Angewandte Chemie International Edition*, 1998, 37, 1328–1345. [https://doi.org/10.1002/\(SICI\)1521-3773\(19980605\)37:10<1328::AID-ANIE1328>3.0.CO;2-9](https://doi.org/10.1002/(SICI)1521-3773(19980605)37:10<1328::AID-ANIE1328>3.0.CO;2-9)
- [11] Trombotto S.; Danel M.; Fitremann J.; Bouchu A.; Queneau Y., Straightforward Route for Anchoring a Glucosyl Moiety onto Nucleophilic Species: Reaction of Amines and Alcohols with Carboxymethyl 3,4,6-Tri-O-acetyl- α -d-glucopyranoside 2-O-Lactone, *J. Org. Chem.*, 2003, 68, 6672–6678. <https://doi.org/10.1016/j.carres.2008.02.008>
- [12] Dal Bó A. G.; Soldi V.; Giacomelli F. C.; Travelet C.; Borsali R.; Fort S., Synthesis, micellization and lectin binding of new glycosurfactants. *Carbohydr. Res.*, 2014, 397, 31–36. <https://doi.org/10.1016/j.carres.2014.07.021>
- [13] Eslami P.; Hajfarajollah H.; Bazsefidpar S., Recent advancements in the production of rhamnolipid biosurfactants by *Pseudomonas aeruginosa*, *RSC Adv.*, 2020, 10, 34014–34032. <https://doi.org/10.1039/D0RA04953K>
- [14] Mohan P. K.; Nakhla G.; Yanful E. K., Biokinetics of biodegradation of surfactants under aerobic, anoxic and anaerobic conditions, *Water Res.*, 2006, 40, 533–540. <https://doi.org/10.1016/j.watres.2005.11.030>
- [15] Smulek W.; Burlaga N.; Hricovíni M.; Medved'ová A.; Kaczorek E.; Hricovíniová Z., Evaluation of surface active and antimicrobial properties of alkyl D-lyxosides and alkyl L-rhamnosides as green surfactants. *Chemosphere.*, 2021, 271, 129818. <https://doi.org/10.1016/j.chemosphere.2021.129818>
- [16] Lu B.; Miao Y.; Vigneron P.; Chagnault V.; Grand E.; Wadouachi A.; Postel D.; Pezron I.; Eglesa C.; Vayssade M., Measurement of cytotoxicity and irritancy potential of sugar-based surfactants on skin-related 3D models. *Toxicol. In Vitro*, 2017, 40, 305–312. <https://doi.org/10.1016/j.tiv.2017.02.002>
- [17] Chen S.; Han M.; Al Sofi A. M.; Fahmi M.M., Experimental evaluation of non-ionic mixed surfactant formulations at high-temperature and high-salinity conditions. *J. Pet. Sci.*, 2022, 219, 111084. <https://doi.org/10.1016/j.petrol.2022.111084>
- [18] Cheng M.; Zeng G.; Huang D.; Yang C.; Lai C.; Zhang C.; Liu Y., Tween 80 surfactant-enhanced bioremediation: toward a solution to the soil contamination by hydrophobic organic compounds, *Crit. Rev. Biotechnol.*, 2018, 38, 17–30. <https://doi.org/10.1080/07388551.2017.1311296>.
- [19] Lourith N.; Kanlayavattanakul M., Natural surfactants used in cosmetics: glycolipids. *Int J Cosmet Sci.*, 2009, 31, 255–261. <https://doi.org/10.1111/j.1468-2494.2009.00493.x>

- [20] Jahan R.; Bodratti A. M.; Tsianou M.; Alexandridis P., Biosurfactants, natural alternatives to synthetic surfactants: physicochemical properties and applications, *Adv. Colloid Interface Sci.*, 2020, 275, 102061. <https://doi.org/10.1016/j.cis.2019.102061>.
- [21] Santos D. K. F.; Rufino R. D.; Luna J. M.; Santos V. A.; Sarubbo L. A., Biosurfactants: Multifunctional Biomolecules of the 21st Century., *Int J Mol Sci*, 2016, 17, 401. <https://doi.org/10.3390/ijms17030401>.
- [22] Rosenberg E.; Ron E.Z., High- and low-molecular-mass microbial surfactants, *Appl. Microbiol. Biotechnol.*, 1999, 52, 154-162. <https://doi.org/10.1007/s002530051502>.
- [23] Le Guenic S.; Chaveriat L.; Lequart V.; Joly N.; Martin P., Renewable surfactants for biochemical applications and nanotechnology, *J Surfactants Deterg*, 2019, 22, 5-21. <https://doi.org/10.1002/jsde.12216>.
- [24] Vijayakumar S.; Saravanan V., Biosurfactants-types, sources and applications, *Res. J. Microbiol*, 2015, 10, 181-192. <https://doi.org/10.3923/jm.2015.181.192>
- [25] Lin S. C., Biosurfactants: recent advances, *J. Chem. Technol.*, 1996, 66, 109-120. [https://doi.org/10.1002/\(SICI\)1097-4660\(199606\)66:2<109::AID-JCTB477>3.0.CO;2-2](https://doi.org/10.1002/(SICI)1097-4660(199606)66:2<109::AID-JCTB477>3.0.CO;2-2).
- [26] Makkar R. S.; Cameotra S. S.; Banat I. M., Advances in utilization of renewable substrates for biosurfactant production, *AMB Express* 1, 2011, 5. <https://doi.org/10.1186/2191-0855-1-5>
- [27] Bertrand B.; Martínez-Morales F.; Rosas-Galván N. S.; Morales-Guzmán D.; Trejo-Hernández M.R., Statistical design, a powerful tool for optimizing biosurfactant production: a review, *Colloids Interfaces*, 2018, 2, 36. <https://doi.org/10.3390/colloids2030036>.
- [28] Muthusamy K.; Gopalakrishnan S.; Kochupappy Ravi T.; Sivachidambaram P., Biosurfactants: properties, commercial production and application, *Curr. Sci*, 2008, 94, 736-747. <https://www.jstor.org/stable/24100627>
- [29] Miller R. M.; Zhang Y. (1997). Measurement of Biosurfactant-Enhanced Solubilization and Biodegradation of Hydrocarbons. In: Bioremediation Protocols. Methods in Biotechnology™, vol 2. Humana Press. <https://doi.org/10.1385/0-89603-437-2:59>
- [30] Frank N.; Lißner A.; Winkelmann M.; Hüttl R.; Mertens F. O.; Kaschabek S. R., Schlömann M., Degradation of selected (bio-)surfactants by bacterial cultures monitored by calorimetric methods, 2010, *Biodegradation*, 21, 179–191. <https://doi.org/10.1007/s10532-009-9292-9>
- [31] Mulligan C.N.; Eftekhari F., Remediation with surfactant foam of PCP-contaminated soil, *Eng Geol*, 2003, 70, 269-279. [https://doi.org/10.1016/S0013-7952\(03\)00095-4](https://doi.org/10.1016/S0013-7952(03)00095-4)

- [32] Banat I. M.; Franzetti A.; Gandolfi I.; Bestetti G.; Martinotti M. G.; Fracchia L.; Smyth T. J.; Marchant R., Microbial biosurfactants production, applications and future potential, *Appl. Microbiol. Biotechnol.*, 2010, 87, 427-444. <https://doi.org/10.1007/s00253-010-2589-0>
- [33] Mulligan C. N., Recent advances in the environmental applications of biosurfactants, *Curr Opin Colloid Interface Sci*, 2009, 14, 372-378. <https://doi.org/10.1016/j.cocis.2009.06.005>
- [34] Vecino X.; Cruz J. M.; Moldes A. B.; Rodrigues L. R., Biosurfactants in cosmetic formulations: trends and challenges, *Crit. Rev. Biotechnol.*, 2017, 37, 911-923. <https://doi.org/10.1080/07388551.2016.1269053>
- [35] Park S. Y.; Kim Y., Surfactin inhibits immunostimulatory function of macrophages through blocking NK- κ B, MAPK and Akt pathway, *Int. Immunopharmacol.*, 2009, 9, 886-893. <https://doi.org/10.1016/j.intimp.2009.03.013>
- [36] Edwards J. R.; Hayashi J. A., Structure of a rhamnolipid from *Pseudomonas aeruginosa*, *Arch. Biochem. Biophys.*, 1965, 111, 415-421. [https://doi.org/10.1016/0003-9861\(65\)90204-3](https://doi.org/10.1016/0003-9861(65)90204-3)
- [37] Soberon-Chavez G.; Lepine F.; Deziel E., Production of rhamnolipids by *Pseudomonas aeruginosa*, *Appl Microbiol Biotechnol*, 2005, 68, 718-725. <https://doi.org/10.1007/s00253-005-0150-3>
- [38] Lotfabad T.; Shahcheraghi F.; Shooraj F., Assessment of Antibacterial capability of Rhamnolipids Produced by Two Indigenous *Pseudomonas aeruginosa* Strains, *Jundishapur Journal of Microbiology*, 2013, 6, 29-35. <https://doi.org/10.5812/jjm.2662>
- [39] Rikalović M. G.; Vrvic M. M.; Karadžić I. M., Rhamnolipid biosurfactant from *Pseudomonas Aeruginosa*-from discovery to application in contemporary technology, *J. Serb. Chem. Soc*, 2015, 80, 279-304. <https://doi.org/10.2298/JSC140627096R>
- [40] Jarvis F. G.; Johnson M. J., A glyco-lipide produced by *Pseudomonas Aeruginosa*, *J. Am. Chem. Soc.*, 1949, 71, 4124-4126. <https://doi.org/10.1021/ja01180a073>
- [41] Burger M. M.; Glaser L.; Burton R. M., The enzymatic synthesis of a rhamnose-containing glycolipid by extracts of *Pseudomonas aeruginosa*, *J. Biol. Chem.*, 1963, 238, 2595-2602. [https://doi.org/10.1016/S0021-9258\(18\)67872-X](https://doi.org/10.1016/S0021-9258(18)67872-X)
- [42] Abdel-Mawgoud A. M.; Lépine F.; Déziel E., Rhamnolipids: diversity of structures, microbial origins and roles, *Appl. Microbiol. Biotechnol.*, 2010, 86, 1323-1336. <https://doi.org/10.1007/s00253-010-2498-2>
- [43] Nitschke M.; Costa S.G.V.A.O.; Contiero J., Rhamnolipid surfactants: an update on the general aspects of these remarkable biomolecules, *Biotechnol. Progr.*, 2005, 21, 1593-1600. <https://doi.org/10.1021/bp050239p>
-

- [44] Palos Pacheco R.; Kegel L. L.; Pemberton J. E., Interfacial and Solution Aggregation Behavior of a Series of Bioinspired Rhamnolipid Congeners Rha-C14-C_x (x = 6, 8, 10, 12, 14). *J. Phys. Chem. B*, 2021, 125, 13585–13596. <https://doi.org/10.1021/acs.jpcc.1c09435>.
- [45] Abbasi H.; Noghabi K. A.; Hamed M. M.; Zahiri H. S.; Moosavi-Movahedi A. A.; Amanlou M.; Teruel J. A.; Ortiz A., Physicochemical Characterization of a Monorhamnolipid Secreted by *Pseudomonas Aeruginosa* MA01 in Aqueous Media. An Experimental and Molecular Dynamics Study, *Colloids Surf. B*, 2013, 101, 256–265. <https://doi.org/10.1016/j.colsurfb.2012.06.035>.
- [46] Lebrón-Paler A.; Pemberton J. E.; Becker B. A.; Otto W. H.; Larive C. K.; Maier R. M., Determination of the Acid Dissociation Constant of the Biosurfactant Monorhamnolipid in Aqueous Solution by Potentiometric and Spectroscopic Methods, *Anal. Chem.*, 2006, 78, 7649–7658. <https://doi.org/10.1021/ac0608826>.
- [47] Ishigami Y.; Gama Y.; Nagahora H.; Yamaguchi M.; Nakahara H.; Kamata T., The PH-Sensitive Conversion of Molecular Aggregates of Rhamnolipid Biosurfactant., *Chem. Lett.*, 1987, 16, 763–766. <https://doi.org/10.1246/cl.1987.763>.
- [48] Benincasa M.; Abalos A.; Oliveira I.; Manresa A., Chemical Structure, Surface Properties and Biological Activities of the Biosurfactant Produced by *Pseudomonas Aeruginosa* LBI from Soapstock. *Antonie Van Leeuwenhoek*, 2004, 85, 1–8. <https://doi.org/10.1023/B:ANTO.0000020148.45523.41>.
- [49] Mohammed I. U.; Deeni Y.; Hapca S. M.; McLaughlin K.; Spiers A. J, Predicting the Minimum Liquid Surface Tension Activity of *Pseudomonads* Expressing Biosurfactants. *Lett Appl Microbiol*, 2015, 60, 37–43. <https://doi.org/10.1111/lam.12331>.
- [50] Georgiou G.; Lin S.-C.; Sharma M. M., Surface-Active Compounds from Microorganisms., *Nat Biotechnol*, 1992, 10, 60–65. <https://doi.org/10.1038/nbt0192-60>.
- [51] Das P.; Yang X.-P.; Ma L. Z., Analysis of Biosurfactants from Industrially Viable *Pseudomonas* Strain Isolated from Crude Oil Suggests How Rhamnolipids Congeners Affect Emulsification Property and Antimicrobial Activity., *Front. Microbiol.*, 2014, 5. <https://doi.org/10.3389/fmicb.2014.00696>
- [52] Bognolo G., Biosurfactants as Emulsifying Agents for Hydrocarbons, *Colloids Surf. A Physicochem. Eng. Asp.*, 1999, 152, 41–52. [https://doi.org/10.1016/S0927-7757\(98\)00684-0](https://doi.org/10.1016/S0927-7757(98)00684-0)
- [53] Del Regno A.; Warren P. B.; Bray D. J.; Anderson R. L., Critical Micelle Concentrations in Surfactant Mixtures and Blends by Simulation., *J. Phys. Chem. B*, 2021, 125, 5983–5990. <https://doi.org/10.1021/acs.jpcc.1c00893>.
-

- [54] Baccile N.; Seyrig C.; Poirier A.; Castro S. A.; Roelants S. L. K. W.; Abel S., Self-Assembly, Interfacial Properties, Interactions with Macromolecules and Molecular Modelling and Simulation of Microbial Bio-Based Amphiphiles (Biosurfactants). A Tutorial Review. *Green Chemistry*, 2021, 23, 3842–3944. <https://doi.org/10.1039/D1GC00097G>.
- [55] Vinarov Z.; Katev V.; Radeva D.; Tcholakova S.; Denkov N. D., Micellar Solubilization of Poorly Water-Soluble Drugs: Effect of Surfactant and Solubilize Molecular Structure., *Drug Dev Ind Pharm*, 2018, 44, 677–686. <https://doi.org/10.1080/03639045.2017.1408642>.
- [56] Perinelli D. R.; Cespi M.; Lorusso N.; Palmieri G. F.; Bonacucina G.; Blasi P., Surfactant Self-Assembling and Critical Micelle Concentration: One Approach Fits All?, *Langmuir*, 2020, 36, 5745–5753. <https://doi.org/10.1021/acs.langmuir.0c00420>.
- [57] Ghosh S.; Ray A.; Pramanik N., Self-Assembly of Surfactants: An Overview on General Aspects of Amphiphiles. *Biophys. Chem.*, 2020, 265, 106429. <https://doi.org/10.1016/j.bpc.2020.106429>.
- [58] Prosser A. J.; Franses E. I., Adsorption and Surface Tension of Ionic Surfactants at the Air–Water Interface: Review and Evaluation of Equilibrium Models. *Coll. Surf A: Physicochem. Eng. Asp.*, 2001, 178, 1–40. [https://doi.org/10.1016/S0927-7757\(00\)00706-8](https://doi.org/10.1016/S0927-7757(00)00706-8).
- [59] Mchedlov-Petrosyan N. O., Adsorption of Ionic Surfactants on Water/Air Interface: One More Transformation of the Gibbs Equation., *Surf. Engin. Appl. Electrochem.*, 2014, 50, 173–182. <https://doi.org/10.3103/S1068375514020100>.
- [60] Martínez-Balbuena L.; Arteaga-Jiménez A.; Hernández-Zapata E.; Márquez-Beltrán C., Applicability of the Gibbs Adsorption Isotherm to the Analysis of Experimental Surface-Tension Data for Ionic and Nonionic Surfactants., *Adv. Colloid Interface Sci.*, 2017, 247, 178–184. <https://doi.org/10.1016/j.cis.2017.07.018>.
- [61] Bae S.; Haage K.; Wantke K.; Motschmann H., On the Factor in Gibbs Equation for Ionic Surfactants. *J. Phys. Chem. B*, 1999, 103, 1045–1050. <https://doi.org/10.1021/jp9822992>.
- [62] Özdemir G.; Peker S.; Helvacı S. S., Effect of PH on the Surface and Interfacial Behavior of Rhamnolipids R1 and R2. *Coll. Surf. A Physicochem. Eng. Asp.*, 2004, 234, 135–143. <https://doi.org/10.1016/j.colsurfa.2003.10.024>.
- [63] Chen M. L.; Penfold J.; Thomas R. K.; Smyth T. J. P.; Perfumo, A.; Marchant R.; Banat I. M.; Stevenson P.; Parry A.; Tucker I.; Grillo I., Mixing Behavior of the Biosurfactant, Rhamnolipid, with a Conventional Anionic Surfactant, Sodium Dodecyl Benzene Sulfonate, *Langmuir*, 2010, 26, 17958–17968. <https://doi.org/10.1021/la1031834>.

- [64] Sánchez M.; Aranda F. J.; Espuny M. J.; Marqués A.; Teruel J. A.; Manresa Á.; Ortiz A., Aggregation Behaviour of a Dirhamnolipid Biosurfactant Secreted by *Pseudomonas Aeruginosa* in Aqueous Media, *J. of Colloid Interface Sci*, 2007, 307, 246–253. <https://doi.org/10.1016/j.jcis.2006.11.041>.
- [65] Wu L.; Lai L.; Lu Q.; Mei P.; Wang Y.; Cheng L.; Liu Y., Comparative Studies on the Surface/Interface Properties and Aggregation Behavior of Mono-Rhamnolipid and Di-Rhamnolipid. *Coll. Surf. B*, 2019, 181, 593–601. <https://doi.org/10.1016/j.colsurfb.2019.06.012>.
- [66] Santos F. K. G.; Neto E. L. B.; Moura M. C. P. A.; Dantas T. N. C.; Neto A. A. D., Molecular Behavior of Ionic and Nonionic Surfactants in Saline Medium, *Coll. Surf. A Physicochem. Eng. Asp.*, 2009, 333, 156–162. <https://doi.org/10.1016/j.colsurfa.2008.09.040>.
- [67] Eastoe J.; Nave S.; Downer A.; Paul A.; Rankin A.; Tribe K.; Penfold J., Adsorption of Ionic Surfactants at the Air–Solution Interface, *Langmuir*, 2000, 16, 4511–4518. <https://doi.org/10.1021/la991564n>.
- [68] Helvacı Ş. Ş.; Peker S.; Özdemir G., Effect of Electrolytes on the Surface Behavior of Rhamnolipids R1 and R2., *Coll. Surf. B*, 2004, 35, 225–233. <https://doi.org/10.1016/j.colsurfb.2004.01.001>.
- [69] Peker S.; Helvacı Ş.; Özdemir G., Interface–Subphase Interactions of Rhamnolipids in Aqueous Rhamnose Solutions, *Langmuir*, 2003, 19, 5838–5845. <https://doi.org/10.1021/la0269964>.
- [70] Eismin R. J.; Munusamy E.; Kegel L. L.; Hogan D. E.; Maier R. M.; Schwartz S. D.; Pemberton J. E., Evolution of Aggregate Structure in Solutions of Anionic Monorhamnolipids: Experimental and Computational Results, *Langmuir*, 2017, 33, 7412–7424. <https://doi.org/10.1021/acs.langmuir.7b00078>.
- [71] Munusamy E.; Luft C. M.; Pemberton J. E.; Schwartz S. D., Unraveling the Differential Aggregation of Anionic and Nonionic Monorhamnolipids at Air–Water and Oil–Water Interfaces: A Classical Molecular Dynamics Simulation Study, *J. Phys. Chem. B*, 2018, 122, 6403–6416. <https://doi.org/10.1021/acs.jpcc.8b03037>.
- [72] Kitamoto D.; Morita T.; Fukuoka T.; Konishi M.; Imura T., Self-Assembling Properties of Glycolipid Biosurfactants and Their Potential Applications, *Curr Opin Colloid Interface Sci*, 2009, 14, 315–328. <https://doi.org/10.1016/j.cocis.2009.05.009>.
- [73] Söderman O.; Johansson I., Polyhydroxyl-Based Surfactants and Their Physico-Chemical Properties and Applications, *Curr Opin Colloid Interface Sci*, 1999, 4, 391–401. [https://doi.org/10.1016/S1359-0294\(00\)00019-4](https://doi.org/10.1016/S1359-0294(00)00019-4).
- [74] Imura T.; Hikosaka Y.; Worakitkanchanakul W.; Sakai H.; Abe M.; Konishi M.; Minamikawa H.; Kitamoto D., Aqueous-Phase Behavior of Natural Glycolipid Biosurfactant Mannosylerythritol Lipid A: Sponge, Cubic, and Lamellar Phases, *Langmuir*, 2007, 23, 1659–1663. <https://doi.org/10.1021/la0620814>.

- [75] Nagarajan R., Molecular Packing Parameter and Surfactant Self-Assembly: The Neglected Role of the Surfactant Tail, *Langmuir*, 2002, 18, 31–38. <https://doi.org/10.1021/la010831y>.
- [76] Zhang Y.; Placek T. L.; Jahan R.; Alexandridis P.; Tsianou M., Rhamnolipid Micellization and Adsorption Properties, *Int. J Mol. Sci.*, 2022, 23, 11090. <https://doi.org/10.3390/ijms231911090>.
- [77] Srinivasan V.; Blankshtein D., Effect of Counterion Binding on Micellar Solution Behavior: 2. Prediction of Micellar Solution Properties of Ionic Surfactant–Electrolyte Systems, *Langmuir*, 2003, 19, 9946–9961. <https://doi.org/10.1021/la030070u>.
- [78] Nagarajan R., Constructing a Molecular Theory of Self-Assembly: Interplay of Ideas from Surfactants and Block Copolymers, *Adv. Coll. Interface Sci.*, 2017, 244, 113–123. <https://doi.org/10.1016/j.cis.2016.12.001>.
- [79] Varjani S. J.; Upasani V. N., Core Flood Study for Enhanced Oil Recovery through Ex-Situ Bioaugmentation with Thermo- and Halo-Tolerant Rhamnolipid Produced by *Pseudomonas Aeruginosa* NCIM 5514, *Bioresource Technology*, 2016, 220, 175–182. <https://doi.org/10.1016/j.biortech.2016.08.060>.
- [80] Abdel-Mawgoud A. M.; Aboulwafa M. M.; Hassouna N. A. H., Characterization of Rhamnolipid Produced by *Pseudomonas Aeruginosa* Isolate Bs20, *Appl Biochem Biotechnol*, 2009, 157, 329–345. <https://doi.org/10.1007/s12010-008-8285-1>.
- [81] Zhao F.; Shi R.; Ma F.; Han S.; Zhang Y., Oxygen Effects on Rhamnolipids Production by *Pseudomonas Aeruginosa*, *Microbial Cell Factories*, 2018, 17, 39. <https://doi.org/10.1186/s12934-018-0888-9>.
- [82] Zhao F.; Shi R.; Zhao J.; Li G.; Bai X.; Han S.; Zhang Y., Heterologous Production of *Pseudomonas Aeruginosa* Rhamnolipid under Anaerobic Conditions for Microbial Enhanced Oil Recovery. *Journal of Applied Microbiology*, 2015, 118, 379–389. <https://doi.org/10.1111/jam.12698>.
- [83] Clint J.H., Micellization of mixed nonionic surface-active agents, *Chem.Soc, Faraday Trans.1*, 1975, 71,1327-1334. <https://doi.org/10.1039/F19757101327>
- [84] Chong H.; Li Q., Microbial production of rhamnolipids: opportunities, challenges and strategies, *Microbial Cell Factories*, 2017, 16. <https://doi.org/10.1186/s12934-017-0753-2>
- [85] Li Q., Rhamnolipid synthesis and production with diverse resources, *Front Chem Sci Eng*, 2016, 11, 27-36. <https://doi.org/10.1007/s11705-016-1607-x>
- [86] Zhao F.; Han S.; Zhang Y., Comparative studies on the structural composition, surface/interface activity and application potential of rhamnolipids produced by *Pseudomonas Aeruginosa* using hydrophobic or

hydrophilic substrates, *Bioresour. Technol.*, 2020, 295, 122269.
<https://doi.org/10.1016/j.biortech.2019.122269>.

[87] Shatila F.; Diallo M. M.; Şahar U.; Ozdemir G.; Tansel Yalçın H., The effect of carbon, nitrogen and iron ions on mono-rhamnolipid production and rhamnolipid synthesis gene expression by *Pseudomonas aeruginosa* ATCC 15442, *Arch. Microbiology*, 2020, 202, 1407-1417. <https://doi.org/10.1007/s00203-020-01857-4>.

Chapter III

3. Molecular structure of glycosurfactants interfacial layers

Emulsions are kinetically stable dispersions of droplets in another nonmiscible continuous liquid phase. They can be distinguished among water-in-oil, W/O, oil-in-water, O/W, and a more complex emulsion of water-oil-water, W/O/W. The interfacial tension between the two liquids is usually lowered by adding an emulsifying agent. Surfactants represent the most used emulsifiers in industrial formulations [1,2,3] given their peculiar characteristics. They form a monolayer at the droplet surface, pointing their polar head groups to water, while the apolar tails point towards the oil phase [1].

When the diameter of the droplets is low around 50–200 nm, the system is called nanoemulsion [4,5]. It is a kinetically stable system, since Brownian motion overcomes the gravity forces that drive the system separation, avoiding creaming and sedimentation. The application of nanoemulsion in different field stands due to the ability to solubilize a wide range of substances. Therefore, these systems have found numerous applications over a wide range of areas such as pharmaceuticals [6], foods [7], cosmetics [8], agrochemicals [9] and fuels [10], and new applications are continuously being reported [5,11]. In the recent year the trend of a formulation with high performance and low environmental impact is arising. Thus, the physico-chemical characterization remains a fundamental challenge for many research groups. Indeed, the stability of emulsions and nanoemulsions depends on the combination of a large number of factors, including temperature, oil type, oil and water relative amounts, surfactant(s) type and concentration [12]. New classes of surfactants, such as the glycolipids, have been studied to accomplish the requirement of green chemistry principles, which should present a low environmental impact and to ensure no risk for human health. Sorbitan esters (commercially known as Span surfactants) are among the most employed emulsifiers [13,14]. The properties of these surfactants can be finely tuned by changing the length and saturation of the acyl chain [15]. Moreover, their hydrophilicity can be increased by decorating the sugar ring with poly (ethylene glycol) chains (resulting in the Tween surfactant series). These sugar-based nonionic surfactants are recognized as safe and biocompatible products; they are affected neither by pH changes of the mixture nor by the presence of other components [16,17]. In order to increase the emulsion stabilization, a mixture of surfactants is preferred with respect to single surfactants [7,18] since their composition can be finely tuned depending on conditions and requirements. In this part of the present PhD thesis, a mixture of Span80 and Tween80, two sugar-based surfactants belonging to

glycolipid class, have been used to formulate Oil-in-Water (O/W) and Water-in-Oil (W/O) emulsions by using alternatively a linear or a branched oil [15,19]. In particular, mixtures of these surfactants have been recently demonstrated to effectively stabilize nanoemulsions [20-24].

Firstly, the pseudo-phase diagrams is determined, delimiting composition regions in which samples showed a uniform milky appearance with no evidence of demixing, as a function of time. Then a fine analysis on the surfactant microscopic organization and dynamics has been investigated through electron paramagnetic resonance (EPR). Specifically, the Span80/Tween80 layer interposing between water and oil domains is characterized by using two amphiphilic spin-labeled probes, 5- and 16-doxyl stearic acids (abbreviated as 5- and 16-DSA, respectively) which provide information on the microenvironment polarity, the surfactant orientation, mobility and segmental ordering of the acyl chains.

3.1 Materials and samples preparation

In Fig. 1 are presented the molecular formulae of both used surfactants. Span80 and Tween80 were purchased from Sigma-Aldrich (St. Louis, MO, USA). Span and Tween are registered trademarks of Croda Inc. (New Castle, DE, USA).

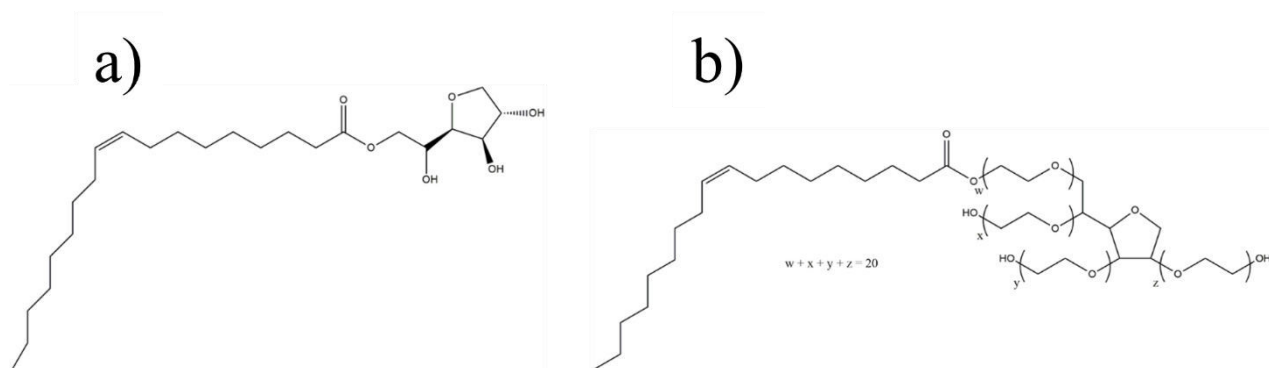


Figure 1 Molecular formulae of (a) Span80, (b) Tween80

Span80 (sorbitan monooleate) is a biodegradable surfactant synthesized from the natural fatty acid oleic acid and the sugar alcohol sorbitol; the appearance is a viscous, brown, liquid, lipophilic surfactant with low hydrophilic–lipophilic balance ($HLB_{Span80} = 4.3$). Tween80 (polyethylene glycol

sorbitan monooleate) is a hydrophilic derivative of Span80, obtained from polyethoxylated sorbitan and oleic acid, with an amber, sticky liquid aspect and $HLB_{Tween80} = 15$. The emulsion were obtained by using Millipore water Millipore Milli-Q system with an electrical conductivity less than 1×10^{-6} S cm⁻¹ at 25 °C and two types of oil with linear alkanes for the first and a large fraction of branched alkanes for the second. Both oils present a negligible content of aromatics and unsaturated chains and are polydisperse samples with an average number of carbon atoms per molecule equal to ~12. The former one, commercially called Alboles 2701 (from Lubra S.p.A., Cornaredo, MI, Italy), is a mixture of linear aliphatic hydrocarbons with a distillation range between 180 and 240 °C. Its kinematic viscosity at 40 °C is 1.8 mm² s⁻¹ and the density at 15 °C is 0.78 kg dm⁻³. The latter one, commercially called Isopar G (from Exxon Mobil Chemicals, Parkway Spring, TX, USA), is mainly composed of isoalkanes with a distillation range comprised between 165 and 177 °C. The kinematic viscosity at 40 °C is 1.19 mm² s⁻¹ and the density at 15 °C is 0.75 kg dm⁻³.

The spin-labeled fatty acids 5-doxyl stearic acid (5-(1-oxyl-2,2-dimethyl-oxazolidin) stearic acid, 5-DSA) and 16-doxyl stearic acid (16-(1-oxyl-2,2-dimethyloxazolidin) stearic acid, 16-DSA), used for EPR measurements, were also purchased from Sigma-Aldrich and stored at -20 °C and showed in Fig. 2.

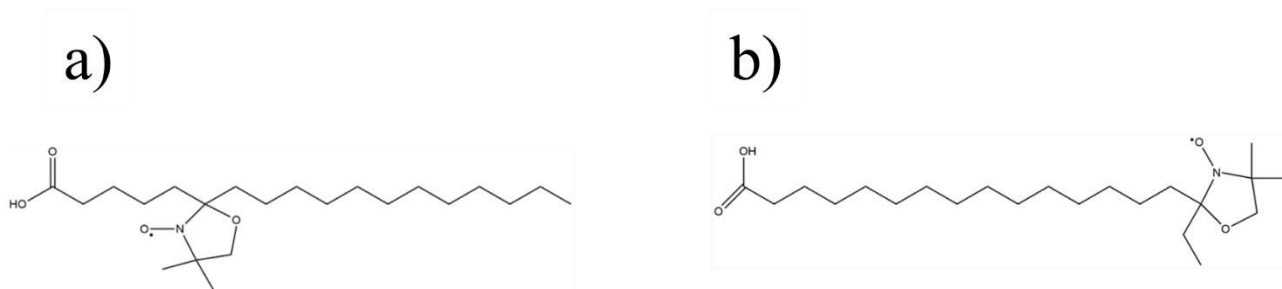


Figure 2 Molecular formulae of (a) 5-doxyl stearic acid (5-DSA) and (b) 16-doxyl stearic acid (16-DSA).

The samples were prepared as described:

- i) Proper amounts of linear oil, L.O., or branched oil, B.O., with and Span80 were weighted in a vial and thoroughly mixed by using a bench-type vortex (ArgoLab Mix, Carpi, Italy).
- ii) Proper amounts of water and Tween80 were weighted in another vial and thoroughly mixed by vortexing. The pH of this solution was checked to be from neutral to weakly acid (pH = 6–7).

- iii) The contents of the two vials were combined, briefly vortexed and then sonicated using a Sonics Vibracell VCX 130 PB ultrasonic processor (Sonics&Materials, Newtown, CT, USA) equipped with a 3 mm titanium probe running at an amplitude of 40% for 20 min in an ice bath.

Systems of water/L.O./(Tween80+Span80) and water/B.O./(Tween80 + Span80) have been analyzed. The relative amount of water and oil in each sample was quantified as the oil weight percent with respect to the total solvent, denoted by *L.O.%* and *B.O.%*, respectively. In all the samples the total amount of the surfactant mixture (Tween80+Span80) was fixed to 4% in weight with respect to the total sample amount. On the contrary, the fraction of the two surfactants was varied as the Span80 content increases with respect to the total surfactant weight and it is indicated with α_{Span80} . The entire α_{Span80} range was analyzed. The thermodynamic equilibrium is waited and thus the emulsions were monitored by the ocular inspection after 3, 24 and 96 h from preparation stored at 25 ± 1 °C as showed in Fig. 3.

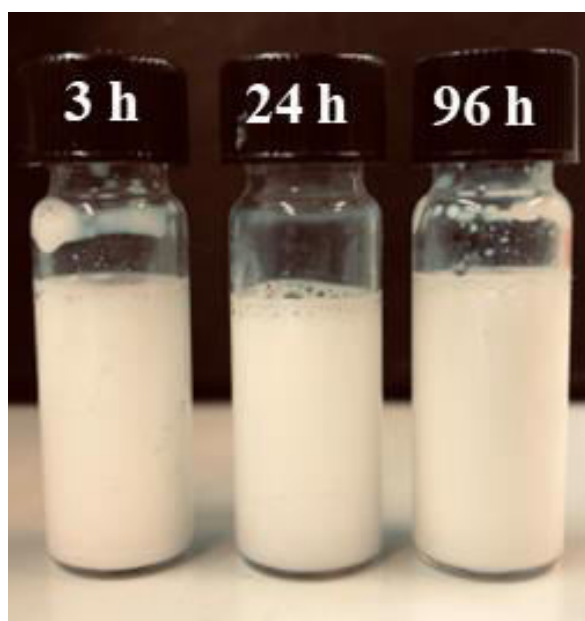


*Figure 3 Water/L.O./(Tween80 + Span80) emulsion samples. The total surfactant amount was fixed to 4% in weight with respect to the total sample amount, surfactant composition and the oil content were $\alpha_{Span80} = 0.4$ and *L.O.%* = 40 in all the samples. Time from preparation is indicated in the labels*

3.2. Measurements

3.2.1. Pseudo-Phase diagram determination

Systems of water/L.O./(Tween80+Span80) and water/B.O./(Tween80 + Span80) have been analyzed. The relative amount of water and oil in each sample was quantified as the oil weight percent with respect to the total solvent, denoted by *L.O.%* and *B.O.%*, respectively. In all the samples the total amount of the surfactant mixture (Tween80+Span80) was fixed to 4% in weight with respect to the total sample amount. At contrary, the fraction of the two surfactants was varied as the Span80 content increases with respect to the total surfactant weight and it is indicated with α_{Span80} . The entire α_{Span80} range was analyzed. The thermodynamic equilibrium is waited and thus the emulsions were monitored by the ocular inspection after 3, 24 and 96 h from preparation stored at 25 ± 1 °C.

3.2.2 Conductometric measurements

Specific conductivity measurements were performed on water/L.O./(Tween80 + Span80) samples using a CDM 210 conductometer (Radiometer Analytical, Villeurbanne, France) with a conductivity cell having a constant of 0.1 cm^{-1} . The cell was calibrated by determining the cell constant *K* before the measure. The cell constant was determined by measuring the conductivity of a KCl standard solution with a specific conductivity known with great accuracy at several concentrations and temperatures. The specific conductivity, χ ($\mu\text{S cm}^{-1}$), was then obtained as the product of the cell constant and the conductivity of the solution. The conductometric measurements were performed in a thermostated room (25 ± 1 °C) using samples which present the same temperature. Specific conductivity were repeated thrice on independently prepared samples with the same nominal composition. The results are reported as mean value \pm standard deviation.

3.2.3. Electron Paramagnetic Resonance characterization

Local polarity, tail order and mobility of the surfactant layer were performed through EPR measurements by using two spin-labelled saturated fatty acids as probes: 5-DSA and 16-DSA. The first presents a nitroxide group reporter in position 5 of the backbone which is relatively close to

surfactant polar head and so the second probe shows the nitroxide group reporter on the acyl chain terminus. The spin-labelled stearic acid are pH dependent ($pK_a = 7.45$) [25,26]. The measurements were carried out at pH value below the pK_a so the the carboxylic group was in the un-dissociated form. A probe thin film had been obtained by drying under nitrogen the proper amount of a 1 mg mL^{-1} probe solution in ethanol placed in a round-bottom glass vial in order to have a concentration of 2% by mass with respect to the surfactants in the samples. The probes were incorporated after the sonication step, shaken for 15 min and finally left at rest for another 15 min. The same procedure was repeated for the two spin probes. The probe-containing nanoemulsions were purged with nitrogen (10 min) before being transferred to a $25 \text{ }\mu\text{L}$ glass capillary and flame sealed to avoid Oxygen-induced line broadening in EPR spectra that occur when oily samples are analyzed [27].

EPR spectrometer is an X-band (9 GHz) Bruker Elexsys E-500 (Rheinstetten, Germany). The capillaries with the samples were placed in a standard 4 mm quartz sample tube to record measurements at room temperature ($25 \pm 1 \text{ }^\circ\text{C}$). The settings for spectra record were:: frequency 9.87 GHz; non-saturating incident power, 6.40 mW; sweep width, 140 G; center magnetic field 3510 G; resolution, 1024 points; time constant, 10.24 ms; conversion time, 20.48 ms; modulation frequency, 100 kHz; modulation amplitude, 1.0 G. Several scans, typically 128, were accumulated to improve the signal-to-noise ratio. The error in the determination of the distance between the peaks in EPR spectra depended on their width; the highest possible error was $\pm 0.3\%$. Thus, EPR measurements were repeated thrice on independently prepared samples with the same nominal composition. The results are reported as mean value \pm standard deviation.

3.3 Results and discussions

3.3.1 Pseudo-Phase diagram and specific conductometry

Fig. 4 panel a and b, show the pseudo-phase diagrams of the systems water/L.O./(Tween80 + Span80) and water/B.O./(Tween80 + Span80), respectively. As mentioned above, the total amount of the surfactant mixture (Tween80 + Span80) is constant and equal to 4% in weight with respect to the total sample amount. The horizontal axes report the α_{Span80} value, which its increasing leads to the increase of the the HLB of the surfactant mixture from 15 ($\alpha_{Span80} = 0.0$) to 4.3 (α_{Span80} is 1.0). The vertical

axes report the oil weight percent on the total solvent (water + oil) weight ($L.O.\%$ and $B.O.\%$, respectively). The macroscopic observed demixing of the emulsion is reported in the pseudo-phase diagram as a different colored area depending on the time (3, 24 or 96 h from sample preparation).

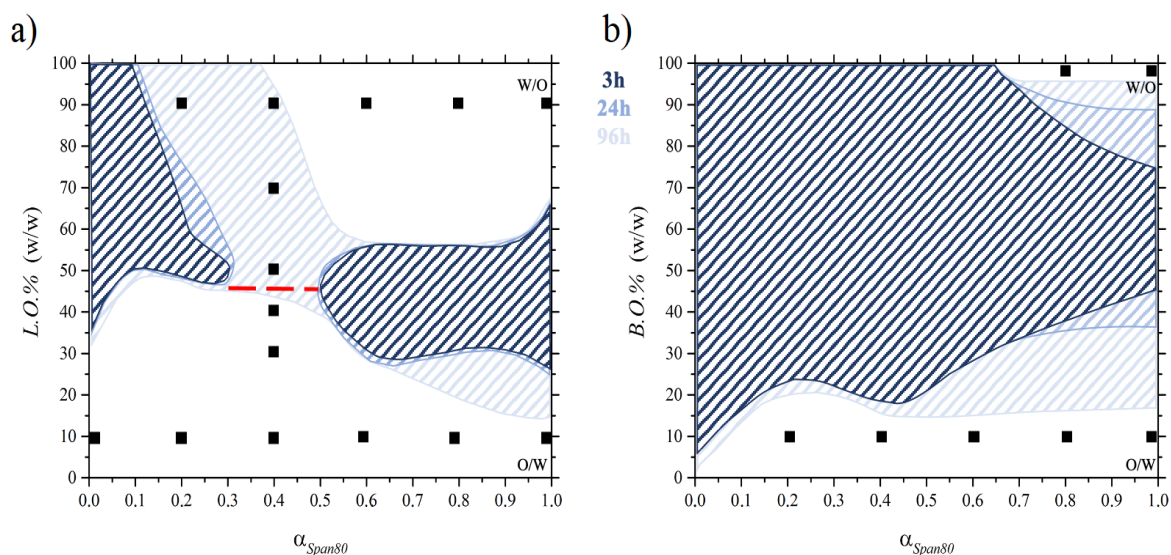


Figure 4 Pseudo-phase diagrams of the systems: (a) water/L.O. (linear oil)/(Tween80 + Span80) and (b) water/B.O. (branched oil)/(Tween80 + Span80) at 25 °C. Shaded areas represent composition domains in which samples show macroscopic demixing when inspected after 3, 24 and 96 h from preparation, according to the reported legend. Black markers indicate the compositions of the samples analyzed by electron paramagnetic resonance (EPR). The red dashed line indicates the composition at which the inversion from O/W to W/O emulsions occurs, as detected by specific conductivity measurements.

The shaded in deep blue in Fig. 4(a) stands for the water/L.O./ (Tween80 + Span80) system where two different regions of instability were detected after 3 h. The first region is on the left-hand-side of the diagram ($\alpha_{Span80} < 0.3$) that extends from $L.O.\%$ equal to 35 up to 100. This evidence indicates that the Tween80-rich system is not able to stabilize oil-rich emulsions. The second region of instability, on the right-hand-side of the diagram ($\alpha_{Span80} > 0.5$), cover an area from $L.O.\% = 25$ up to 65. This behavior is due to the ability of Span80-rich systems to stabilize emulsions rich in one of the two solvents.

After 3h, the pseudo-phase diagram shows a large double-T shaped stability area, where at bottom water-rich stable emulsions are present for the entire α_{Span80} range, with a presumable O/W structure. At the top of the diagram, oil-rich stable emulsions are present from $\alpha_{Span80} > 0.1$ with a presumable W/O structure. The central vertical part of the diagram is interesting because for $0.3 < \alpha_{Span80} < 0.5$ ($11.8 < HLB < 9.7$), the emulsions are stable at all the composition solvent range. This area was subsequently investigated through conductometric investigations on samples at $\alpha_{Span80} = 0.4$ to

observe the change in structure of the emulsion. In Fig. 5 the specific conductivity trend shows detectable values at low $L.O.\%$. When the content of oil increases, in particular above $L.O.\% = 40$, null values are detected.

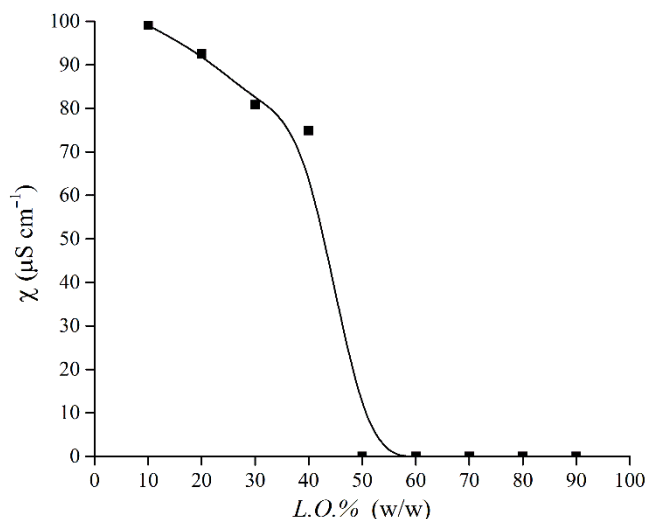


Figure 5 Specific conductivity of water/L.O./(Tween80 + Span80) emulsions as a function of the oil content $L.O.\%$ at $\alpha_{Span80} = 0.4$ at 25 °C.

These results clearly highlight a sudden inversion of the emulsion from a O/W to a W/O structure, with no evidence of an intermediate bicontinuous organization. In the pseudo-phase diagram, the oil content at which the inversion occurs is indicated by a red dashed line.

After 24 h from the sample preparations, (middle blue areas in Fig. 4(a)), there are not particular changes in the instability area, only a slight enlargement of the instability regions is observed

Finally after 96 h, the instability regions merge into a single zone as reported in Fig. 4(a), shaded in light blue. At the bottom of the figure, nothing has changed: the emulsion stability is observed for all α_{Span80} range, as the first inspection. At the top part, the W/O stability is diminished for low α_{Span80} and it is guaranteed for α_{Span80} up to around 0.5.

The panel b of Fig. 4 shows the emulsion stability of the system water/B.O./(Tween80 + Span80). Here it is notable a large instability region after 3 h from sample preparation.

The stability is reached in two separated areas of the diagram occupying the top and the bottom of the graph. The first area is where the O/W emulsions are stable in the entire α_{Span80} investigated range and the amount of $B.O.\%$ increases from 5% up to 45% when Span80 fraction is increased. In the

second area, the W/O emulsions are stable only for $\alpha_{Span80} \geq 0.5$. The amount of water increases, reaching 25% in samples where only Span80 is present as surfactant.

After 24 h, the instability zone tends to expand on the right-hand-side side; see the middle blue zone in Fig. 4(b).

A four-day aging leads to a notable widening of the instability region, shaded in light blue. Only a very narrow range of W/O emulsion stability remains for $B.O.\% > 95$. In the bottom of the O/W, structures are stable for $B.O.\% < 15$ at $\alpha_{Span80} > 10\%$.

3.3.2 Electron Paramagnetic Resonance results

The local polarity, the order parameter and microviscosity of the interfacial surfactant layer in water/L.O./(Tween80+Span80) and water/B.O./(Tween80+ Span80) emulsions were performed by EPR spectroscopy. The black squares in Fig. 4(a) and Fig. 4(b) are the considered samples in this measurement.

Two spin labelled stearic acids were employed as probes: 5-DSA and 16-DSA [5]. These probes are able to intercalate into the surfactant layer given their amphiphilic behavior and their spectroscopic features furnish detailed information on the microenvironment where the paramagnetic label resides. Since the position of the reporter group, 5-DSA monitors the surfactant structuring and dynamics at the oil-water interface next to the head moieties. 16-DSA allows the exposure in the core of the droplet next to the surfactant tails.

Fig. 6(a) and Fig. 6(b) show the EPR spectra of 5-DSA and 16-DSA in water/L.O./(Tween80 +Span80) emulsions at constant surfactant mixture composition ($\alpha_{Span80} = 0.4$) at increasing relative amount of the oil phase ($10 \leq L.O.\% \leq 90$).

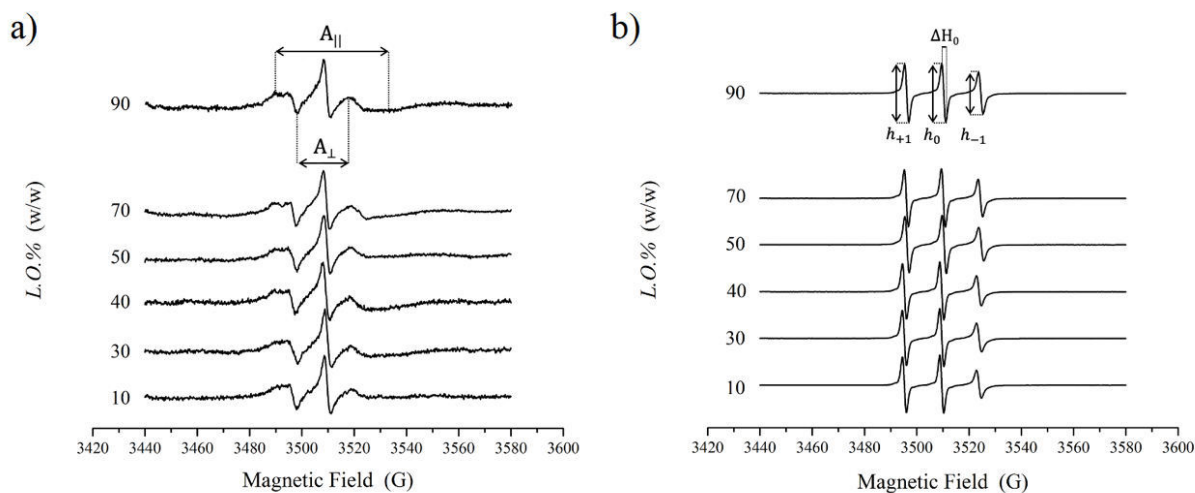


Figure 6. Electron paramagnetic resonance (EPR) spectra of 5-DSA (a) and 16-DSA (b) in water/L.O./ (Tween80+Span80) emulsions at 25 °C, recorded within 3 h from sample preparation. The total surfactant amount was fixed to 4% in weight with respect to the total sample amount and surfactant compositions was $\alpha_{Span80} = 0.4$ in all samples. The oil content was progressively increased as indicated by the labels in the figures.

The spectra are constituted by the three hyperfine lines due to the coupling between the unpaired electron spin, with spin equal to 1/2, and the nitrogen ^{14}N with nuclear spin equal to 1.

5-DSA the low- and high-field lines are further broadened and partially split in two components: these results demonstrate that the spin probes are inserted in the surfactant layer at the oil-water interface and preferentially rotate around the long molecular axis [28]. In the case of 16-DSA spectra are characterized by the presence of three lines of unequal heights and widths. The different rotation rate implies a different lineshape: for 16-DSA, the anisotropic motion of the nitroxide moiety is sufficiently rapid to average the hyperfine interaction, while for 5-DSA the motion is much slower [25]. Indeed, the label mobility is significantly more hindered close to the surfactant heads for 5-DSA. Furthermore, Inspection of the figures shows, for both spin probes, no dramatic changes are observed for both probes with the increasing oil content in the systems, suggesting that structural reorganization occurs upon emulsion phase inversion and thus, the interfacial surfactant layer is only slightly perturbed.

The EPR spectra can furnish several information con the microenvironment of the samples by a Quantitative analysis. The 5-DSA spectra allow the evaluation of the hyperfine coupling constant, A_N , and the order parameter, S . A_N is an index of the micropolarity experienced by the nitroxide label. S , which measures the label wobbling mobility, depends on the spatial ordering of the labeled segment of the probe tail with respect to the normal to the surfactant monolayer surface. These parameters can

be evaluated from the distance (in G) between maxima and minima of the spectra, (see Fig.6 (a)) according to [29]:

$$A_N = \frac{1}{3}(A_{\parallel} + 2A_{\perp}) \quad \text{Equation 1}$$

$$S = \frac{A_{\parallel} - A_{\perp}}{A_{zz} - \frac{1}{2}(A_{xx} + A_{yy})} \frac{A_N^0}{A_N} \quad \text{Equation 2}$$

A_{xx} , A_{yy} and A_{zz} are the principal elements of the real hyperfine splitting tensor in the spin Hamiltonian of the spin-label and A_N^0 is the isotropic hyperfine coupling constant in crystal state. The values of these parameters are reported in the literature [30].

As mentioned before, no dramatic changes are observed when the oil content increases as reported by the A_N and S values (Fig. 7(a)). The S value is typical of 5-DSA probe inserted in quite ordered surfactant layers [5,27,31] and weakly increases with $L.O.\%$, indicating an increase of the order of the surfactant tails close to the headgroups. These data confirm again the absence of a bicontinuous mesophase form in the investigated system: if a phase inversion had occurred, the S parameter passes through a maximum [25], which is not observed here.

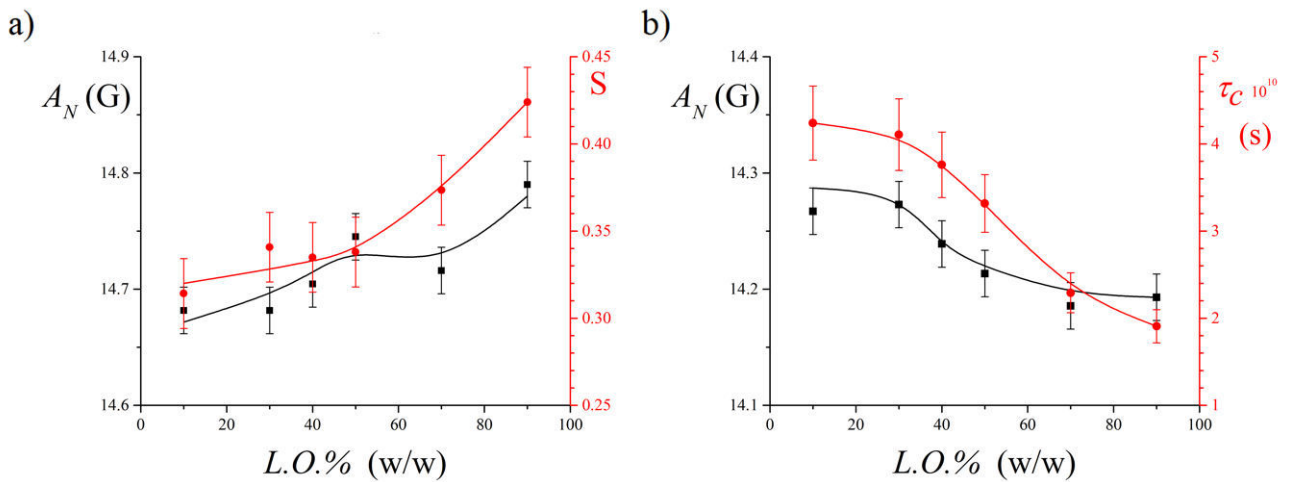


Figure 7. Dependence on oil content, $L.O.\%$, of the EPR spectroscopic parameters of 5-DSA (a) and 16-DSA (b) in water/ $L.O./$ (Tween80+Span80) emulsions at 25 °C. For both spin-probes the hyperfine coupling constant A_N is reported (on the left-hand side ordinate). The right-hand side ordinate reports the order parameter, S , and the correlation time, τ_c , for 5-DSA and 16-DSA, respectively. The total surfactant amount was fixed to 4% in weight with respect to the total sample amount and surfactant compositions was $\alpha_{Span80} = 0.4$ in all samples.

The A_N value do not show an abrupt change, but a slight increase, indicating that the nitroxide label is progressively more exposed to the aqueous medium.

The 16-DSA spectra are characterized by three well-defined lines and so the A_N values can be directly derived as the distance among them. In addition, the tumbling correlation time of the spin-probe, τ_c , can be derived, which reflects the label rotational mobility, as determined by the microenvironment viscosity. τ_c is obtainable by the relation [32]:

$$\tau_c = 6 \times 10^{-10} \Delta H_0 \left[\left(\frac{h_0}{h_{+1}} \right)^{1/2} + \left(\frac{h_0}{h_{-1}} \right)^{1/2} - 2 \right] \quad \text{Equation 3}$$

h_{+1} , h_0 and h_{-1} are the intensities of the low-field, central and high-field lines of the EPR spectrum, respectively, and ΔH_0 is the width of the central line (see Fig. 6(b)). This equation is applicable for rotational correlation times in the range $10^{-11} < \tau_c < 3 \times 10^{-9}$ s.

The τ_c values decrease (Fig. 7(b)) indicating that the rotational mobility of the terminal part of the tails increases, this result suggests that the tail termini, linked to the nitroxide probe, are in a less viscous environment.

The interpretation of the order, polarity and rotational parameters derived from EPR spectra suggests that during the emulsion transition from an O/W to a W/O structure the surfactant layer undergoes a slow structural re-arrangement where the polar heads position themselves at the interface in both the emulsions.

In the O/W emulsion, the lipophilic are in the oil droplet interior experiencing steric repulsion and entangling with each other and experiencing steric repulsion. This results in a relatively disordered and blocked surfactant molecule meso-structuring (see the 5-DSA S value the 16-DSA τ_c value, respectively). Thus, surfactants arrange to form a compact layer distancing the water phase, as confirmed by the 5-DSA A_N value which indicate a quite apolar environments experienced by the first segments of the acyl tails. This evidence is confirmed by literature which highlights a more generally disordered conformations of surfactants in O/W aggregates [33]. At contrary, in W/O systems the chains point towards the external medium, experiencing less steric constraints resulting a more ordered and dynamic surfactant organization, due to also by an enhanced water penetration among the surfactant headgroups and closer tail segments.

The “hedgehog” model can figuratively clarify this behavior [32]: by curving its back, the hedgehog can modify the relative position of its spines, increasing or decreasing the space between the edges of the spines.

The EPR spectral parameters significantly change from a O/W to a W/O structure (see Fig. 6) when the *L.O.%* increases and they do not show an appreciable spectral change variation when α_{Span80} increases.

This result highlights that the microstructure of the hydrophobic domain formed by the surfactant tails is poorly affected by changes of the headgroup layer composition, provided that the surface curvature, mainly determined by the solvent ratio, remains unvaried in emulsions stabilized by Tween80+Span80 mixtures. Average values of A_N , S and τ_c determined in water/L.O./(Tween80+Span80) emulsions with *L.O.%* equal to 10 (O/W) and 90 (W/O), and α_{Span80} varying in the range in which samples present a uniform appearance, are collected in Table 1.

In Table 1 are collected the average values of A_N , S and τ_c for water/L.O./(Tween80+Span80) systems in which *L.O.%* amount is fixed at 10 (O/W) and 90 (W/O) and α_{Span80} varies in the range in which samples present a uniform appearance. The assumptions given above on $\alpha_{Span80} = 0.4$ on the two different emulsions structures (O/W and W/O) can be extended to the other investigated α_{Span80} values. Indeed, in 5-DSA O/W emulsions the difference of the A_N values are much lower than in 16-DSA W/O ones due to a less extended conformation of the acyl chains in the former systems than in the latter ones.

The A_N , S and τ_c values for water/B.O./(Tween80+Span80) systems are also reported in Table 1. The EPR spectral parameters are significantly affected by the oil content. Indeed, at same oil content, L.O. and B.O., the A_N values are almost the same. At contrary, the S value is lower in systems with the branched oil indicating a more disordered environment compared to linear oil and it is in O/W emulsions than in W/O ones. This evidence could be ascribed to the bulkiness of the branched oil which is not able to insert among surfactant tails forcing them to assume twisted conformations leading to a less ordered surfactant layer.

Even the τ_c values obtained for 16-DSA are lower for the systems in which the branched oil was used. Due to a lower viscosity of the branched oil with respect to the linear one, the lower compactness of the surfactant tails and the increased droplet mobility destabilize the

water/B.O./(Tween80+Span80) emulsions (particularly the W/O ones), whose stability domains are much narrower with respect to those of the water/L.O./(Tween80+Span80) ones (see Fig. 4).

Table 1. EPR spectral parameters of 5-DSA and 16-DSA in water/L.O./(Tween80+Span80) and water/B.O./(Tween80+Span80) emulsions at 25 °C.

System	Spin-probe	A_N (G)	S	$\tau_c 10^{10}$ (s)
water/L.O./(Tween80+Span80)				
$L.O.\% = 10$ $\alpha_{Span80} = 0.0-1.0$ (O/W)	5-DSA	14.7 ± 0.2	0.35 ± 0.02	
	16-DSA	14.29 ± 0.05		4.5 ± 0.4
$L.O.\% = 90$ $\alpha_{Span80} = 0.2-1.0$ (W/O)	5-DSA	14.8 ± 0.2	0.45 ± 0.03	
	16-DSA	14.13 ± 0.03		2.3 ± 0.6
water/B.O./(Tween80+Span80)				
$B.O.\% = 10$ $\alpha_{Span80} = 0.2-1.0$ (O/W)	5-DSA	14.6 ± 0.2	0.16 ± 0.04	
	16-DSA	14.3 ± 0.1		2.7 ± 0.6
$B.O.\% = 97$ $\alpha_{Span80} = 0.8-1.0$ (W/O)	5-DSA	15.0 ± 0.1	0.07 ± 0.02	
	16-DSA	14.20 ± 0.02		0.7 ± 0.1

3.4 Conclusions

Emulsions are unstable complex systems which need the presence of emulsifying agents, adsorbed at interface between the dispersed droplets and the continuous medium, to guarantee their stability. In the first part of this PhD thesis the pseudo-phase diagrams of emulsions formed by water and, alternatively, a linear or a branched mineral oil, stabilized by mixtures of Span80 and Tween80 glycosurfactants, is studied. In particular, the investigation is carried out on these systems by optical measurements for the rationalization of the pseudo-phase diagrams and by EPR spectroscopy the surfactant microscopic organization at the droplet interface is investigated.

The results from pseudo-phase diagrams show that Span80+Tween80 mixtures are able to stabilize O/W emulsions in whole range of α_{Span80} (surfactant mixture composition). This evidence is confirmed by the EPR measurements in which the microstructure of the surfactant layer at the interface oil-water is almost unaffected by the ratio between the two glycosylated surfactants. Indeed, Span80 and Tween80 show the same hydrophobic tail with a sugar-based head which is bulkier for the latter. The surface of O/W droplets, which presents a positive curvature, are able to accommodate both type of headgroups with negligible effects of the surfactant tail arrangement. At contrary, W/O emulsions appear less stable than O/W ones. In this case, the negative curvature of the droplets reduces the space available to the headgroups and, consequently, surfactants with smaller head, Span80, are favored; the hydrophobic layer formed by the surfactant tail is scarcely affected by the surfactant mixture composition. Emulsions containing similar amounts of oil and water generally show a good stability when the linear oil is used. Indeed, samples are stable in the intermediate α_{Span80} range, going from $\alpha_{Span80} = 0.3$ to 0.5.

Overall, these results confirm that glycosurfactants are good emulsifier, flexibly able to adapt to different types of mesostructures. Particularly, if rationally used, they are able to stabilize also W/O emulsions, whose industrial and commercial interest is continuously growing. Thus, they are effective green alternatives to conventional surfactants currently in use in formulative practice.

The microstructure of the surfactant layer is mainly determined by α_{Span80} value and the presence of linear or branched oil, alternatively. In the emulsions formulated with the linear oil, the change of microstructure occurs as the *L.O.%* value increases when α_{Span80} is constant at 0.4 value. When a stable O/W emulsion is reached, the tails of the surfactants adsorb at the droplet interface forming a disordered layer in which the mobility of the entangled chains is hindered. In W/O emulsions the tails point to the external apolar environment forming an ordered array of extended chains. The linear oil molecules are able to intercalate among the tails increasing the hydrophobicity of environment which is poorly permeable to water molecules. The surfactant layer microstructure shows a gradual variation which can be pictorially figured according to the “hedgehog” model during the phase inversion form O/W to W/O structures even though this change in structure is definitely abrupt above *L.O.%* =40 as demonstrated by specific conductivity measurements.

When the emulsions are prepared with the branched oil, their instability increases in whole explored composition range, except for a small domain of the phase diagram at very low or very high *B.O.%*. Given its low viscosity, the Ostwald ripening rate is likely to play a role in this instability which

favors droplet impact . Furthermore, the emulsion instability can derive from the inability of the bulky branched oil to intercalate among the surfactant tail termini, hindering their extension towards the oil phase increasing the disorder and dynamics of the microscopic surfactant self-organization.

These results show a clear relation between the emulsion macroscopic stability and the surfactant layer microstructure. In particular, glycosurfactants are good emulsifier, flexibly able to adapt to different types of mesostructures. The surfactant tail ordering and dynamics are key parameters, which have to be finally tuned on a rational basis in order to achieve emulsions designed to accomplish the requirements in the various application fields. Thus, if rationally used, glycosurfactant are able to stabilize also W/O emulsions, whose industrial and commercial interest is continuously growing. Thus, they are effective green alternatives to conventional surfactants currently in use in formulative practice.

Reference

- [1] Tadros T.F. *Emulsion Formation and Stability*. Wiley-VCH Verlag GmbH & Co. KGaA. Weinheim, Germany, 2013. <https://doi.org/10.1002/9783527647941>
- [2] Jafari S.; McClements D.J., *Nanoemulsions: Formulation, Applications, and Characterization*. Academic Press: Cambridge, MA, USA, 2018. <https://doi.org/10.1016/C2016-0-01985-X>
- [3] Nor Bainun I.; Nur Hashimah, A.; Syed-Hassan S.S.A., Nanoemulsions: formation, characterization, properties and applications – a review. *Adv. Mat. Res.*, 2015, 1113, 147–152. <https://doi.org/10.4028/www.scientific.net/AMR.1113.147>
- [4] Nikolic I.; Mitsou E.; Pantelic I.; Randjelovic D.; Markovic B.; Papadimitriou V.; Xenakis A.; Lunter D.J.; Zugic A.; Savic S., Microstructure and biopharmaceutical performances of curcumin-loaded low-energy nanoemulsions containing eucalyptol and pinene: Terpenes' role overcome penetration enhancement effect? *Eur. J. Pharm. Sci.*, 2020, 142, 105135. <https://doi.org/10.1016/j.ejps.2019.105135>
- [5] Demisli S.; Theochari I.; Christodoulo P.; Zervoua M.; Xenaki A.; Papadimitriou V., Structure, activity and dynamics of extra virgin olive oil-in-water nanoemulsions loaded with vitamin D3 and calcium citrate. *J. Mol. Liq.*, 2020, 306, 112908. <https://doi.org/10.1016/j.molliq.2020.112908>
- [6] Chellapa P.; Ariffin F.D.; Eid A.M.; Almahgoubi A.A.; Mohamed A.T.; Issa Y.S.; Elmarzugi N.A., Nanoemulsion for cosmetic application. *Eur. J. Biomed. Pharm. Sci.*, 2016, 3, 8–11. ISSN:2349-8870
- [7] Mustafa I.F.; Hussein M.Z., Synthesis and technology of nanoemulsion-based pesticide formulation. *Nanomaterials*, 2020, 10, 1608. <https://doi.org/10.3390/nano10081608>
- [8] Azmi N.A.N.; Elgharbawy A.A.M.; Motlagh S.R.; Samsudin N.; Salleh H.M., Nanoemulsions: factory for food, pharmaceutical and cosmetics. *Processes*, 2019, 7, 617. <https://doi.org/10.3390/pr7090617>
- [9] Takamura A.; Minowa T.; Noro S.; Kubo T., Effects of Tween and Span group emulsifiers on the stability of O/W emulsions. *Chem. Pharm. Bull.* 1979, 27, 2921–2926. <https://doi.org/10.1248/cpb.27.2921>
-

- [10] Lv G.; Wang F.; Cai W.; Li H.; Zhang X., Influences of addition of hydrophilic surfactants on the W/O emulsions stabilized by lipophilic surfactants. *Colloids Surf. A: Physicochem. Eng. Aspects*, 2014, 457, 441–448. <http://dx.doi.org/10.1016/j.colsurfa.2014.06.031>
- [11] Hou W.; Papadopoulos K.D., W1/O/W2 and O1/W/O2 globules stabilized with Span80 and Tween80. *Colloids Surf. A: Physicochem. Eng. Aspects*, 1997, 125, 181–187. [https://doi.org/10.1016/S0927-7757\(96\)03861-7](https://doi.org/10.1016/S0927-7757(96)03861-7)
- [12] Sagiri S.S.; Behera B.; Sudheep T.; Pal K., Effect of composition on the properties of Tween80–Span80-based organogels. *Des. Monomers Polym.*, 2012, 15, 253–273. <http://dx.doi.org/10.1163/156855511X615669>
- [13] Peng L.C.; Liu C.H.; Kwan C.C.; Huang K.F., Optimization of water-in-oil nanoemulsions by mixed surfactants. *Colloids Surf. A Physicochem. Eng. Asp.*, 2010, 370, 136–142. <https://doi.org/10.1016/j.colsurfa.2010.08.060>
- [14] Lv G.; Wang F.; Cai W.; Zhang X., Characterization of the addition of lipophilic Span 80 to the hydrophilic Tween 80-stabilized emulsions. *Colloids Surf. A: Physicochem. Eng. Aspects*, 2014, 447, 8–13. <http://dx.doi.org/10.1016/j.colsurfa.2014.01.066>
- [15] Preetika R.; Mehta P.S.; Kaisare N.S.; Basavaraj M.G., Kinetic stability of surfactant stabilized water-in-diesel emulsion fuels. *Fuel*, 2019, 236, 1415–1422. <https://doi.org/10.1016/j.fuel.2018.09.074>
- [16] Chong W.-T.; Tan C.-P.; Cheah Y.-K.; Lajis A.F.B.; Dian N.L.H.M.; Kanagaratnam S.; Lai O.-M., Optimization of process parameters in preparation of tocotrienol-rich red palm oil-based nanoemulsion stabilized by Tween80-Span 80 using response surface methodology. *PLoS ONE*, 2018, 13, e0202771. <https://doi.org/10.1371/journal.pone.0202771>
- [17] Manchun S.; Dass C.R.; Sriamornsak P., Designing nanoemulsion templates for fabrication of dextrin nanoparticles via emulsion cross-linking technique. *Carbohydr. Polym.*, 2014, 101, 650–655. <http://dx.doi.org/10.1016/j.carbpol.2013.09.049>
- [18] Fu Z.; Liu M.; Xu J.; Wang Q.; Fan Z., Stabilization of water-in-octane nano-emulsion. Part I: Stabilized by mixed surfactant systems. *Fuel*, 2010, 89, 2838–2843. <http://dx.doi.org/10.1016/j.fuel.2010.05.031>

- [19] Zhang W.; Qin Y.; Gao Z.; Ou W.; Zhu H.; Zhang Q., Phase behavior and stability of nano-emulsions prepared by D phase emulsification method. *J. Mol. Liq.*, 2019, 285, 424–429. <https://doi.org/10.1016/j.molliq.2019.04.112>
- [20] Zhang W.; Qin Y.; Chang S.; Zhu H.; Zhang Q., Influence of oil types on the formation and stability of nano-emulsions by D phase emulsification. *J. Dispers. Sci. Technol.*, 2021, 42, 1225–1232. <https://doi.org/10.1080/01932691.2020.1737538>
- [21] Tedeschi A.M.; D’Errico G.; Busi E.; Basosi R.; Barone V., Micellar aggregation of sulfonate surfactants studied by electron paramagnetic resonance of a cationic nitroxide: An experimental and computational approach. *Phys. Chem. Chem. Phys.*, 2002, 4, 2180–2188. <https://doi.org/10.1039/b106833d>
- [22] Tedeschi A.M.; Busi E.; Paduano L.; Basosi R.; D’Errico G., Influence of the headgroup molecular structure on the anionic surfactant-PVP interaction studied by electron paramagnetic resonance of a cationic nitroxide. *Phys. Chem. Chem. Phys.*, 2003, 5, 5077–5083. <https://doi.org/10.1039/b305739a>
- [23] Vitiello G.; Falanga A.; Petruk A.A.; Merlino A.; Fragneto G.; Paduano L.; Galdiero S.; D’Errico G., Fusion of raft-like lipid bilayers operated by a membranotropic domain of the HSV-type I glycoprotein gH occurs through a cholesterol-dependent mechanism. *Soft Matter*, 2015, 11, 3003–3016, <https://doi.org/10.1039/c4sm02769h>.
- [24] Chatzidaki M.D.; Mitsou E.; Yaghmur A.; Xenakis A.; Papadimitriou V., Formulation and characterization of food-grade microemulsions as carriers of natural phenolic antioxidants. *Colloids Surf. A: Physicochem. Eng. Aspects*, 2015, 483, 130–136. <http://dx.doi.org/10.1016/j.colsurfa.2015.03.060>
- [25] Zuev Y.F.; Vylegzhanina N.N.; Zakhartchenko N.L., Effects of protein solubilization on the structure of the surfactant shell of reverse micelles. *Appl. Magn. Reson.*, 2003, 25, 29–42. <https://doi.org/10.1007/BF03166964>
- [26] Izquierdo P.; Esquena J.; Tadros T.F.; Dederen J.C.; Feng J.; Garcia-Celma M.J.; Azemar N.; Solans C., Phase behavior and nano-emulsion formation by the phase inversion temperature method. *Langmuir*, 2004, 20, 6594–6598, <https://doi.org/10.1021/la049566h>.
-

- [27] Rozner S.; Kogan A.; Mehta S.; Somasundaran S.; Aserin A.; Garti N.; Ottaviani M.F., Characterization of nonionic microemulsions by EPR. Part II. The effect of competitive solubilization of cholesterol and phytosterols on the nanostructure. *J. Phys. Chem. B*, 2009, 113, 700–707. <https://doi.org/10.1021/jp807163t>
- [28] Rokach S.; Ottaviani M.F.; Shames A.I.; Nir I.; Aserin A.; Garti N., W/O Microemulsions as dendrimer nanocarriers: An EPR study. *J. Phys. Chem. B*, 2012, 116, 12633–12640. <https://doi.org/10.1021/jp307616b>
- [29] Kommareddi N.S.; John V.T.; Waguespack Y.Y.; McPherson G.L., Temperature and gas pressure induced microstructural changes in AOT water-in-oil microemulsions: characterization through electron paramagnetic resonance spectroscopy. *J. Phys. Chem.*, 1993, 97, 5752–5761. <https://doi.org/10.1021/j100123a048>
- [30] Gaffney B.J.; McConnell H.M., The paramagnetic resonance spectra of spin labels in phospholipid membranes. *J. Magn. Reson.*, 1974, 16, 1–28. [https://doi.org/10.1016/0022-2364\(74\)90193-0](https://doi.org/10.1016/0022-2364(74)90193-0)
- [31] Kogan A.; Rozner S.; Mehta S.; Somasundaran P.; Aserin A.; Garti N.; Ottaviani M.F., Characterization of the nonionic microemulsions by EPR. I. Effect of solubilized drug on nanostructure. *J. Phys. Chem. B*, 2009, 113, 691–699. <https://doi.org/10.1021/jp807161g>
- [32] Avramiotis S.; Cazianis C.T.; Xenakis A., Interfacial properties of lecithin microemulsions in the presence of lipase. A membrane spin-probe study. *Langmuir*, 1999, 15, 2375–2379. <https://doi.org/10.1021/la9814236>
- [33] Baglioni P.; Gambi C.M.C.; Goldfarb D., Electron spin echo modulation study of Winsor microemulsions. *J. Phys. Chem.*, 1991, 95, 2577–2583. <https://doi.org/10.1021/j100159a086>

Chapter IV

4. Rhamnolipids and their mixtures with conventional surfactants

Biosurfactants, amphiphilic molecules naturally produced by bacteria, yeast and plants, represent a valid alternative to synthetic ones, allowing a reduction of environmental and potential health problems [1]. A large variety of biosurfactants are found in nature, presenting very different biochemical structures still keeping the hydrophilic/lipophilic duality [2]. They are coarsely classified in high- (lipoproteins, lipopolysaccharides, proteins, polysaccharides and biopolymer complexes) and low-molecular weight molecules (glycolipids, lipopeptides, phospholipids) [3]. Biosurfactants present interfacial activity comparable to, or even better than, conventional synthetic surfactants, and show several advantages, such as tolerance to temperature, pH and ionic strength changes, low toxicity and biodegradability.

Nowadays, industrial application of several biosurfactants is becoming possible thanks to the optimization of their massive biotechnological production using renewable raw materials [4]. Rhamnolipids are among the most promising ones under this viewpoint. These glycolipids are electively produced by *Pseudomonas aeruginosa* as secondary metabolites [5,6], and are generally found as a mixture of homologues, sharing the general amphiphilic molecular architecture given by a polar head composed by one or two L-rhamnose residues and an apolar tail composed by one or two fatty acid residues, generally 3-hydroxyalkanoic acid [7]; all the homologues also present a carboxylic moiety, which is deprotonated at neutral pH, imparting an anionic or non-ionic character to the molecules [8]. Rhamnolipids are available on a large scale thanks to fermentation bioreactors [9]. Besides the great interfacial and ecological features, they are endowed with a good antibacterial activity [10] and have been considered as multipurpose ingredients in food processing [10], emulsion, bioremediation, cosmetic and nanotechnologies [11].

Recent studies address the mixed micellization of Rha with anionic [12-14], nonionic surfactants [15-17], and both [18]; however, mixtures with conventional synthetic surfactants have remained poorly investigated so far [19]. At neutral pH, the deprotonation of the carboxylic group is reported to impart a negative charge to the Rha headgroup [20]; consequently, Rha mixtures with charged surfactants are expected to behave as anionic-anionic and catanionic systems, respectively. Catanionic surfactant mixture self-aggregate in a variety of supramolecular aggregates [21-23]. Because of this versatility, their application has been proposed in many different fields, including oil recovery [24], purification

processes [25], biomedicine and pharmaceuticals [26–28]. Biocompatibility and ecosustainability concerns have driven the design of cationic aggregates based on natural and bio-derived components [29], e.g., bile salts [30], fatty acids [31], and modified aminoacids [32]. A few studies have addressed the inclusion of sugar-based surfactants in cationic mixtures [33–35].

4.1. Rhamnolipid and sodium lauryl ether sulfate

In the framework of the eco-sustainable product design, rhamnolipids can be proposed as suitable candidates to totally or, at least, partially replace conventional surfactants in several industrial formulations. For this reason, the investigation of their mixtures with largely employed synthetic surfactants is strategic. In the present thesis, we compare the physico-chemical and functional properties of a commercial rhamnolipid sample (Rha) in aqueous solution with those of sodium lauryl ether sulfate (SLES), an anionic surfactant massively used in laundry and household cleaning detergents as well as in personal care and consumer products [36], see Fig.1 for the molecular structures.

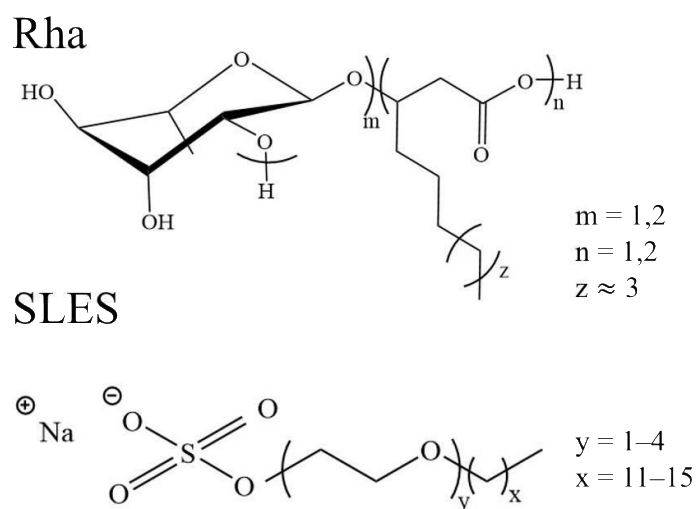


Figure 1. Molecular structures of the surfactants used in this study: rhamnolipids (Rha) and sodium lauryl ether sulfate (SLES).

The study is conducted at neutral pH, so that both surfactants are negatively charged. The mixtures of these two anionic surfactants are also investigated, analyzing whether, and to what extent, synergistic/antagonistic interactions alter the system behavior with respect to that of the single components. In the first part of our study, we analyze the self-aggregation behavior of Rha–SLES mixtures in aqueous solutions. Specifically, the critical micelle concentrations (*cmc*) are determined by surface tension measurements. The dimension of the micellar aggregates is measured by Dynamic

Light Scattering (DLS). The surfactant organization and dynamics within the micelles is investigated by Electron Paramagnetic Resonance (EPR). The experimental results are discussed in terms of molecular interactions and quantitatively analyzed in order to estimate the partitioning of each surfactant between the aqueous medium and the micellar aggregate. In the second part of this work, we investigate the wetting, emulsifying, and foaming ability of Rha-SLES aqueous mixtures. The comprehension of the relationships between the physico-chemical properties of this system and its functional behavior is strategic to drive the rational exploitation of rhamnolipids in chemical formulations. Last, to support these biosurfactants as “green” alternatives to conventional anionic surfactants, we present the results of ecotoxicological tests.

4.1.1. Materials and samples preparation

The rhamnolipid sample employed in the present work (hereafter named Rha) was purchased from AGAE Technologies (Corvallis, OR, USA). It appears as a light-brown powder containing 90% w/w rhamnolipids and is a biotechnological product obtained by *P. aeruginosa* culture using vegetable oils as carbon source. Rhamnolipid samples obtained under these production conditions contain more mono- than di-saccharides (60 wt%) and more di- than single-tailed species (80 wt%). Fatty acids are generally saturated, even though the presence of mono-unsaturated chains is non-negligible (30 wt%). The tail length is polydisperse, ranging from C6 to C16, with a dominant presence of C10. The average molar mass is $M_w \approx 530 \text{ g mol}^{-1}$ and the dispersity is 1.05 [37]. The Hydrophilic-Lipophilic Balance (HLB) is about 10 [38] and the average packing parameter (pp) is 0.66 [39].

Sodium lauryl ether sulfate (SLES) was provided by Procter and Gamble (Bruxelles, Belgium) as a 70 wt% aqueous mixture. It is a polydisperse substance, with a C12 to C16 tail conjugated to a short chain of 1–4 ethylene oxide units terminated by the sulfate group. The HLB is above 20 [40] and the pp is $< 1/3$ [18].

All water-Rha-SLES mixtures were prepared using ultrapure deionized water from a Millipore Milli-Q system with an electrical conductivity less than $1 \times 10^{-6} \text{ S cm}^{-1}$ at 25 °C. The pH was buffered at 7.1 ± 0.2 using sodium dihydrogen phosphate hydrate ($\text{NaH}_2\text{PO}_4 \cdot \text{H}_2\text{O}$, purity >99%) and disodium hydrogen phosphate anhydrous (Na_2HPO_4 , purity >99%), both purchased from Sigma-Aldrich (Milan, Italy). Buffer concentration was maintained as low as possible to minimize the effect the increased ionic strength on the measured physico-chemical parameter. For this reason, added ion

concentration was fixed at ten times the total surfactant concentration (the maximum total concentration in the case of tensiometric titrations).

For EPR measurements two spin-probes were alternatively added to the water-Rha-SLES mixtures. The spin-labeled fatty acids 5-doxyl stearic acid (5-(1-oxyl-2,2-dimethyl-oxazolidin)stearic acid, 5-DSA) and 16-doxyl stearic acid (16-(1-oxyl-2,2-dimethyl-oxazolidin) stearic acid, 16-DSA) were purchased from Sigma-Aldrich. The probe concentration was fixed at 2 wt% with respect to the surfactants, and was obtained by pouring a proper amount of each surfactant mixture onto a thin probe film deposited at the round-bottom of a glass vial, which was then shaken for 10 min and finally left at rest for other 10 min. The probe thin film had been previously obtained by drying under nitrogen the proper amount of a 1 mg mL⁻¹ probe solution in ethanol.

Single-side polished silicon wafer substrates (3-inch diameter, 375µm thickness), used for contact angle measurements, were purchased from Sigma-Aldrich. They were washed with chloroform (HPLC-grade), acetone (≥99.5% purity) and ethanol (GC-grade ≥99.8% purity), all from Sigma-Aldrich, and Milli-Q water. Hydrogen peroxide (30 wt%) and ammonium hydroxide (≥25 v%) aqueous solutions were used for hydrophilic functionalization of the silicon wafer, while toluene (GC-grade ≥99.7% purity) and octadecyltrichlorosilane (OTS, ≥90% purity) were used for its hydrophobic functionalization; all chemicals used for these surface treatments were purchased from Sigma-Aldrich.

4.1.2. Measurements

4.1.2.1. Tensiometry

The surface tension, γ , of water-Rha-SLES mixtures was determined with a Sigma 70 tensiometer (KSV, Stockholm, Sweden) by the Du Noüy ring method as reported in a previous work [41]. Successive aliquots of a concentrated surfactant solution at a given surfactant composition, defined as:

$$x_{\text{Rha}} = \frac{m_{\text{Rha}}}{m_{\text{Rha}} + m_{\text{SLES}}} \quad \text{Equation 1}$$

were added to the instrument vessel with a known volume of the same buffer used to prepare the surfactant solution. In Eq. 1 m_{Rha} and m_{SLES} are the molalities of Rha and SLES, respectively. By

using this procedure, the surfactant concentration ($m_{\text{surf}} = m_{\text{Rha}}$ and m_{SLES}) was progressively increased while the surfactant composition x_{Rha} and the buffer ion concentration were kept constant. After each aliquot addition, the sample was mixed using a magnetic stirrer and allowed to equilibrate 3 min prior to measuring the surface tension.

4.1.2.2. Dynamic Light Scattering

Micelle dimensions were determined by DLS. After some preliminary test performed to assess the effect of surfactant concentration, a set of samples spanning the whole x_{Rha} range at constant $m_{\text{surf}} = 0.045 \text{ mol kg}^{-1}$ was analysed. The total surfactant concentration was optimized in order to obtain reliable measurements for all the considered mixture composition. Measurements were carried out with a home-assembled apparatus constituted by a SMD 6000 50 mW light source (Laser Quantum, Fremont, CA, USA) operating at 5325 Å, a compact goniometer (Photocor Ltd., Moscow, Russia), a photomultiplier (PMT-120-OP/B) and a correlator Flex02-01D (Correlator.com, Shenzhen, China). The experiments were run at $(25.0 \pm 0.1) \text{ }^\circ\text{C}$, at a scattering angle $q = 90^\circ$. A regularization algorithm was used to analyze the scattered intensity correlation function [42]. The diffusion coefficient of each population of diffusing particles was calculated as the z-average of the coefficients of the corresponding distributions [43]. Considering that the mixtures are diluted, the Stokes–Einstein equation was used to evaluate the hydrodynamic radius of the aggregates, R_{H} , from their translational diffusion coefficient, D :

$$R_{\text{H}} = \frac{k_{\text{B}}T}{6\pi\eta D} \quad \text{Equation 2}$$

where k_{B} is the Boltzmann constant, T is the absolute temperature, and h is the medium viscosity whose value was assumed to be that of the buffer solution [44].

4.1.2.3. Electron Paramagnetic Resonance

The local polarity and microviscosity experienced by the surfactant molecules in the micellar aggregates was investigated by EPR measurements, using the spin-labelled fatty acids 5-DSA and 16-DSA as molecular probes. ESR spectra were recorded with a 9 GHz Bruker Elexys E-500 spectrometer (Bruker, Rheinstetten, Germany). Samples were loaded in capillaries and flame sealed. The capillaries were placed in a standard 4 mm quartz sample tube containing light silicone oil for

thermal stability. All the measurements were performed at (25 ± 1) °C. The instrumental settings were as follows: sweep width, 120 G; resolution, 1024 points; time constant, 20.48 ms; modulation frequency, 100 kHz; modulation amplitude, 1.0 G; incident power, 6.37 mW. Several scans, typically 16, were accumulated to improve the signal-to-noise ratio.

Spectra simulations were performed using the program of Budil and Freed [45]. The main parameters of computation, which changed in function of Rha content, were the correlation time for the diffusional rotational motion of the radical, τ_C , and the A_{zz} component of the hyperfine coupling tensor between the electron spin and the nuclear spin (taking constant $A_{xx} = A_{yy} = 6$ G).

4.1.2.4 Emulsification Index and foaming test

The ability of Rha-SLES mixtures to emulsify two immiscible liquids was quantified by determining the emulsification index, E . Each measurement was carried out by pouring 2 mL of the aqueous surfactant solution and 3 mL of sunflower in a round-bottom, cylindric glass test tube (1 cm i.d.). The sample was then vortexed for 1 min and left to stand for a pre-fixed resting time. The emulsification index E_X was then calculated as the percentage of the height of milky emulsified layer with respect to the total height of test tube content [46]. X (= 2 or 24) is the resting time expressed in hours. All tests were run in triplicate.

The foaming ability of the Rha-SLES mixtures was also determined. The experiments were conducted by transferring 5 mL of each surfactant solution in a screwcap tube (1 cm i.d.), adding 2 mL of phosphate buffer (0.004 M) and vigorously handshaking for 2 minutes. The samples were left at rest for 10 minutes and then the foaming ability was calculated as the percentual height of the foam with respect to the liquid layer [47]. All tests were run in triplicate.

4.1.2.5. Contact angle

In order to verify the wetting ability of the surfactant mixtures, contact angle measurements were carried out using the OCA 15EC system (DataPhysics, Filderstadt, Germany), and the drop shape was analysed with the SCA20 software (DataPhysics). For each measurement, a sample droplet of 3 μ L was placed on a solid support. Silicon wafers {1.1.1} in three different states of surface activation (native, hydrophilic and hydrophobic) were employed as supports. The wafers were cut

approximately into $1 \times 1 \text{ cm}^2$ and then washed in chloroform, acetone, ethanol, deionized water (15 min for each solvent) in ultrasonic bath at room temperature to remove all the organic residues and the impurity from the surface. The obtained supports were dried with nitrogen (native surface). Some of these supports were treated in a beaker with a mixture of hydrogen peroxide, ammonium hydroxide solutions and deionized water H_2O (1:1:2 v/v/v) for 15 min at $60 \text{ }^\circ\text{C}$ and then washed with deionized water (hydrophilic surface) [48]. In turn, some of the hydrophilic wafers were carefully dried with nitrogen and dipped in toluene. After the addition of OTS, the beaker was sonicated for 1 h; the wafers were then rinsed with chloroform, ethanol, deionized water for 10 min for each solvent in ultrasonic bath at room temperature (hydrophobic surface) [49].

4.1.2.6. Ecotoxicity tests

The eco-toxicity of Rha and SLES was assessed towards three organisms, *Aliivibrio fischeri*, *Raphidocelis subcapitata* and *Daphnia magna*. The acute luminescence assay was detected with the *A. fischeri* (NRRLB-11177, supplied by MicroBioTest, Gent, Belgium) according to ISO 11348-3:2007 [50] and was carried out with a luminometer Microtox (Model 500 analyzer, New Castle, DE, USA). To provide the required osmotic pressure for the test organism, the assay was conducted using a saline water solution (2% sodium chloride, NaCl). After activation of *A. fischeri* by rehydration with a reconstitution solution, the luminescence intensity of bacteria was measured after 30 min at 490 nm of exposition to the test solutions at $15 \text{ }^\circ\text{C}$. The test was performed in triplicate with a control, and pharmaceutical and toxic effects were quantified as the ratio of the decrease in bacterial light production to the remaining light. The algal growth inhibition assay was carried out according to ISO 8692:2012 using *R. subcapitata* [51]. Algal inoculum (104 cell/mL) was added to the test solutions for 72 h. Algal toxicity was assessed in three replicates. The samples were maintained under continuous illumination (white fluorescent light) at $22 \pm 4 \text{ }^\circ\text{C}$ for incubation and were mixed twice a day by hand. The algal growth was measured at 670 nm (HachLange DR 5000, Loveland, CO, USA). The difference between the growth rate in the control group and the solutions provided inhibition rate in each sample. The immobilization test with *D. magna* was performed according to ISO 6341:2012 [52]. Daphnids (less than 24 h old) obtained from a laboratory culture were used (20 organisms for each test solution and control). Four replicates were carried out, and the number of immobilized organisms was determined under stereomicroscopy (Leica EZ4-HD, Wetzlar, Germany) after 48 h of exposure.

4.1.3. Results and discussions

4.1.3.1. Rha-SLES mixed micellization: surface tension and DLS data

The ternary system water-Rha-SLES (pH = 7.1) was investigated by tensiometric titrations conducted increasing the total surfactant molality, m_{surf} , at constant composition of the surfactant mixture, x_{Rha} . The whole composition range was considered ($0.0 \leq x_{\text{Rha}} \leq 1.0$). Surface tension data collected at selected x_{Rha} values are reported in Fig. 2(a) as a function of m_{surf} .

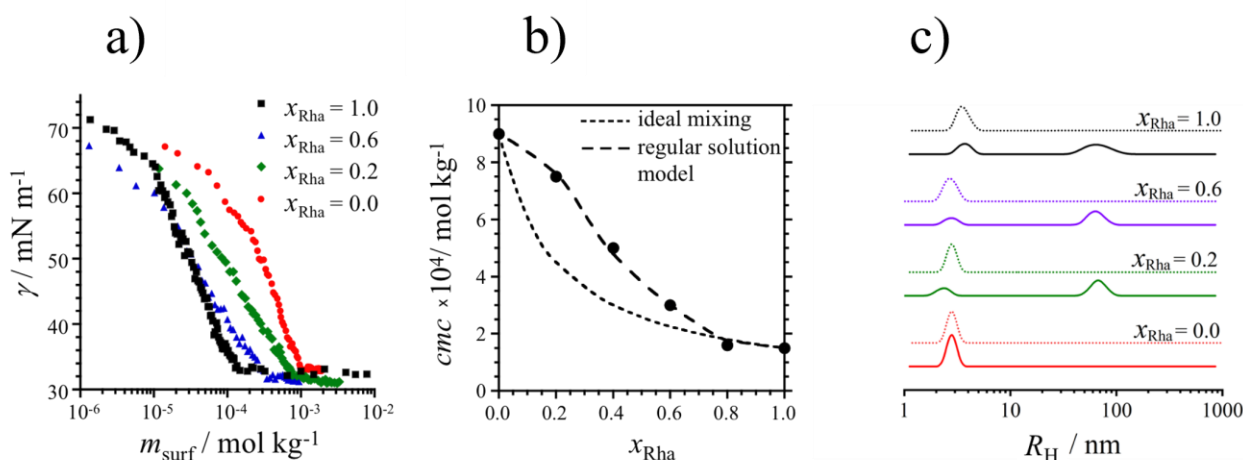


Figure 2. Physico-chemical characterization of the ternary system water-Rha-SLES at pH = 7.1 and 25 °C. (a) Surface tension vs. total surfactant concentration at the surfactant mixture compositions indicated in the legend. (b) Critical micelle concentration vs. surfactant mixture composition; the experimental data (black circles) are compared with the predictions of mixed micellization models as indicated in the legend. For the regular solution model, the trend obtained with $\beta = 5$ is shown. (c) Intensity-weighted (continuous line) and number-weighted (dotted line) hydrodynamic radius distributions of Rha-SLES micelles at total surfactant concentration equal to 0.045 mol kg⁻¹ and surfactant mixture composition indicated in the legend.

Qualitatively, all the curves present the same trend: with increasing m_{surf} , the surface tension decreases; as micellization starts, the curves change the slope and approach to constant values, γ_{cmc} . In each titration a single, abrupt slope change was observed, indicating that the two surfactants co-micellize. The cmc value for each curve can be evaluated as the concentration corresponding to the intersection between two straight lines fitting the data in the pre-micellar and micellar concentration range, respectively, as shown in the figure. The cmc and γ_{cmc} values determined at the various x_{Rha} are collected in Table 1. The average area at the air–solution interface per surfactant molecule at the cmc , A , was estimated through the Gibbs isotherm:

$$A = -\frac{1}{N_A} \left[\frac{1}{nRT} \left(\frac{\partial \gamma}{\partial \ln m_{\text{surf}}} \right)_{T,p} \right]^{-1} \quad \text{Equation 3}$$

where N_A is the Avogadro constant, R is the gas constant and p is the pressure. $\frac{\partial \gamma}{\partial \ln m_{\text{surf}}}$ is the slope of the γ trend in the premicellar concentration range, evaluated close to the *cmc*. n is a coefficient taking into account the dissociation of ionic surfactants; its value is 2 for completely dissociated species, as anionic surfactants at low ionic strength. The A values obtained from the curves at constant x_{Rha} are collected in Table 1.

Table 1. *cmc*, surface tension parameters and micelle dimension for the system water-Rha-SLES at $pH = 7.1$ and 25°C .

x_{Rha}	$cmc \times 10^4$ (mol kg ⁻¹)	γ_{cmc} (mN m ⁻¹)	A (Å ²)	R_{H1} (nm)	R_{H2} (nm)
0.0	9.0±0.9	33.2±0.5	60±4	2.9±0.4	-
0.2	7.5±0.4	30.1±0.3	90±3	2.4±0.6	67.0±1.0
0.4	4.9±0.5	31.3±0.6	98±4	2.6±0.3	60.0±0.5
0.6	3.1±0.2	31.7±0.4	117±7	2.7±0.3	63.3±0.3
0.8	1.6±0.2	31.2±0.4	97±7	3.0±0.4	65.5±0.7
1.0	1.5±0.3	32.8±0.6	67±3	3.8±0.4	67.2±0.8

The *cmc* values determined for the binary systems water-SLES ($x_{\text{Rha}} = 0.0$, $cmc_{\text{SLES}} = 9.0 \times 10^{-4}$ mol kg⁻¹) and water-Rha ($x_{\text{Rha}} = 1.0$, $cmc_{\text{Rha}} = 1.5 \times 10^{-4}$ mol kg⁻¹) are in good agreement with the values reported in the literature [53, 37]. Rha self-aggregates at a concentration lower by almost one order of magnitude compared to SLES. This is connected to the lower HLB value (10 vs. 20 for Rha and SLES, respectively) and can be ascribed to the bulkier hydrophobic moiety (an average of 16 carbon atoms prevalently distributed in two tails for Rha vs. an average of 14 carbon atoms in a single tail for SLES). The *cmc* value of the ternary mixtures water-Rha-SLES monotonically decreases when reported as a function of x_{Rha} , Fig. 2(b), indicating a gradual increase of the self-aggregation driving force the Rha content in the mixture is increased.

The γ_{cmc} values of the two binary systems are similar both being in good agreement with literature data [54,39], see Table 1. Concerning the ternary systems, this parameter is scarcely affected by the surfactant mixture composition, the average value (31.0±0.7 mN m⁻¹) being slightly lower than that observed for the binary systems. The A values of the two surfactants, taken individually, are also quite

similar [54,39]. However, as they are mixed, the average area per molecule significantly increases, passing through a maximum at $x_{\text{Rha}} \approx 0.6$, see Fig. 2(b). This suggests antagonistic interactions among the surfactant molecules at the interface, an opposite trend being expected for mixtures presenting a synergistic behavior [55].

The dimensions of the micellar aggregates formed in Rha-SLES aqueous mixtures was investigated by DLS measurements. Samples with x_{Rha} spanning the entire composition range were analysed. After having checked that m_{surf} value scarcely affected the results, a constant $m_{\text{surf}} = 0.045 \text{ mol kg}^{-1}$ was chosen for all the considered systems. The intensity-weighted plots show a single population of small micellar aggregates for the water-SLES binary system, see Fig. 2(c). Concerning the water-Rha binary system, two populations are present, indicating the co-presence of small and large aggregates. This finding confirms previous literature data reporting the co-existence of micelles and vesicles [56,57], due to the prevalent di-chained structure of Rha which favours aggregates with lower surface curvature such as vesicles, as expected from the surfactant *pp*. Two populations are also present in all the ternary systems water-Rha-SLES. The average hydrodynamic radii of the populations observed at the various x_{Rha} values are collected in Table 1. R_{H1} and R_{H2} refer to the small and large aggregates, respectively. It must be recalled that the intensity weighted plots enhance the presence of larger aggregates; the same results, reported in the number-weighted form clearly demonstrate the prevalence of small micelles.

For the water-SLES binary system, the R_{H1} value, close to the length of the surfactant molecule in the extended conformation ($\sim 28 \text{ \AA}$ [58]), is compatible with the formation of small spherical aggregates [59], as expected from the surfactant *pp*. On the other hand, the larger value observed for the water-Rha binary system is not compatible with spherical micelles and should only be taken as an indication that bulky aggregates with different shape are formed. This result is in agreement with literature data reporting the formation of cylindrical micelles at concentrations well above the *cmc* [60]. Concerning the Rha-SLES mixtures, the relatively low R_{H1} values, similar to that observed for the pure SLES micelles, indicate the formation of spherical aggregates.

4.1.3.2 Microstructure and local dynamics in Rha-SLES mixed micelles: EPR data

Information about the structure and dynamics of the surfactants within the aggregate was gained by analysing the EPR spectra of two spin-labelled fatty acids inserted in the micelles as molecular

probes. 5-DSA presents the cyclic nitroxide label close to the carboxylic group and provides information on the more external layer of the micelles, while in 16-DSA the reporter group is positioned at the chain terminus. Examples of EPR spectra of 5-DSA and 16-DSA in water-Rha-SLES mixtures are shown in Fig. 3(a) and Fig. 3(b), respectively. They show the typical nitroxide signal in micellar systems: a triplet due to the hyperfine coupling between the unpaired electron and the nitrogen nucleus, with the high- and low-field lines broadened by the slow tumbling of the label [61]. Interestingly, perusal of the 5-DSA spectrum relative to the water-Rha binary system ($x_{\text{Rha}} = 1.0$) reveals two clear features belonging to a different signal with respect to the usual 5-DSA spectrum; they are highlighted by the arrows in the figure. This signal was extracted by spectra subtraction and is shown in the insert of Fig. 3(a). It is constituted by a triplet of triplets with $A_1 = 15.5$ G ($I = 1$) and $A_2 = 4.5$ G ($I = 1$ or two similar $I = \frac{1}{2}$ nuclei).

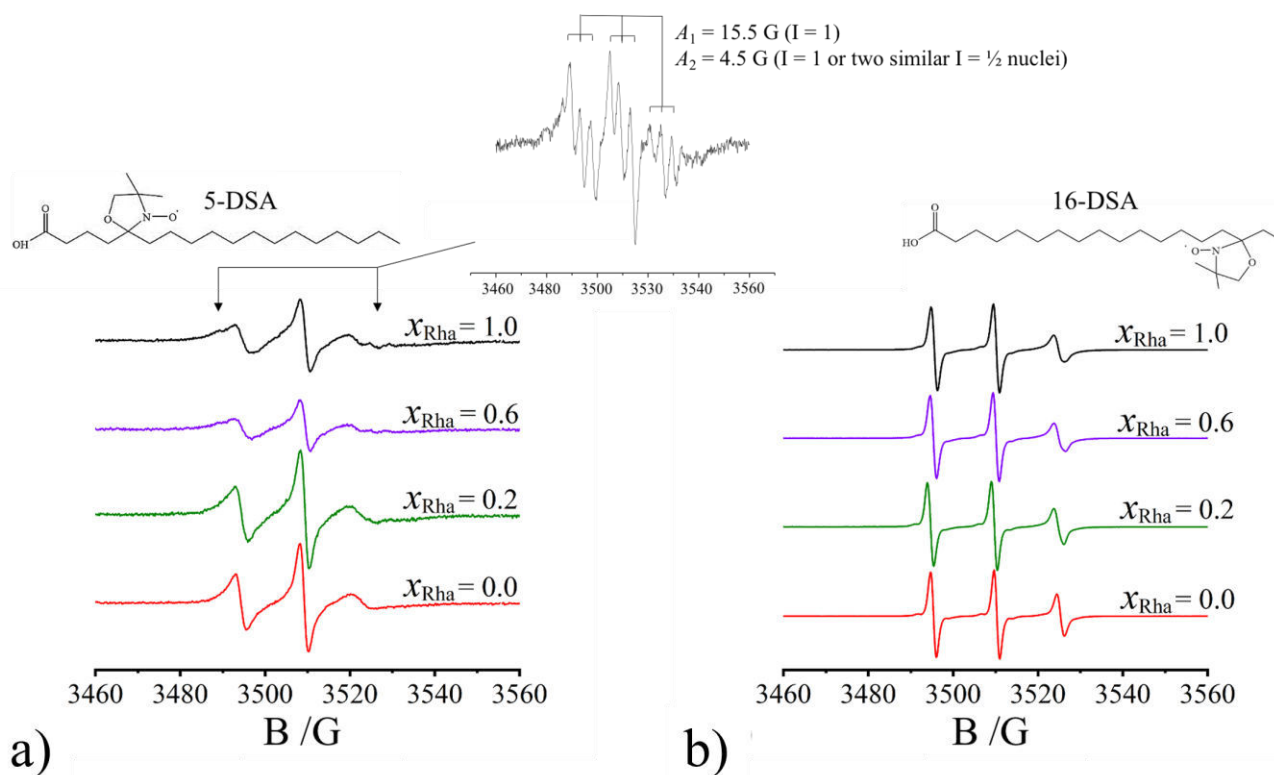


Figure 3. EPR characterization of the ternary system water-Rha-SLES using spin-labelled fatty acids at pH = 7.1 and 25 °C. (a) 5-DSA spectra in surfactant mixtures at the compositions indicated in the legend. (b) 16-DSA spectra in surfactant mixtures at the compositions indicated in the legend. The insert of panel (a) shows the spectrum of the radical detected in the 5-DSA spectrum at $x_{\text{Rha}} = 1.0$ and obtained by subtraction.

The ability of Rha to participate to electron exchange processes is supported by its antioxidant activity which has been recently demonstrated [62]. The A_2 value of the second triplet may come from two almost equivalent protons. The same superimposed spectrum is detected for all the water-Rha-SLES mixtures, while it is absent in the water-SLES system ($x_{\text{Rha}} = 1.0$). In agreement with the hypothesis of Rha as responsible of the radical formation with the involvement of the nitroxide moiety, two collateral effects were found by increasing the Rha content: (a) a decrease in the intensity of the nitroxide spectrum (by almost 30% between $x_{\text{Rha}} = 0.0$ and $x_{\text{Rha}} = 1.0$); (b) an increase in the relative percentage of the radical signal (up to 15% at $x_{\text{Rha}} = 1.0$, see Fig. 3). Last, inspection of Fig. 3(b) reveals that no superimposed signal is observed in the 16-DSA spectra. This indicates that the rhamnose moieties positioned at the aggregate interface are the main responsible for the radical generation, while the micellar core is not involved. This is consistent with the electron trapping ability reported for rhamnose [63]. This interesting point, which could potentially open new perspectives in the practical applications of rhamnolipids in chemical formulations, has to be deepened in future investigations.

The 5-DSA and 16-DSA EPR spectra allow important information on the molecular organization of surfactant aggregates to be gained [64-68]. Comparison between the spectra reported in Fig. 3(a) and in Fig. 3(b) shows that, for all the investigated systems, the signals of the nitroxide triplet appear broader for 5-DSA than for 16-DSA, as particularly evident for the low- and high-field lines, suggesting the motion of the nitroxide label to be more hindered by the local environment, i.e., by the interactions with the neighbouring molecules.

The values of the optimized parameters are reported in Fig. 4(a) and Fig. 4(b) for 5-DSA and 16-DSA, respectively. The correlation time for the diffusional rotational motion of the radical, τ_C , measures the microviscosity experienced by the label in its rotation, while the A_{zz} component of the hyperfine coupling tensor measures the micropolarity at the nitroxide site. For all the water-Rha-SLES mixtures, τ_C and A_{zz} values are higher for 5-DSA than for 16-DSA. This evidence confirms that the reporter group of 5-DSA is embedded just below the surfactant headgroups, where it experiences a more viscous and polar microenvironment compared to the reporter group of 16-DSA, which is positioned in the micelle interior where the surfactant tails form a disordered fluid core.

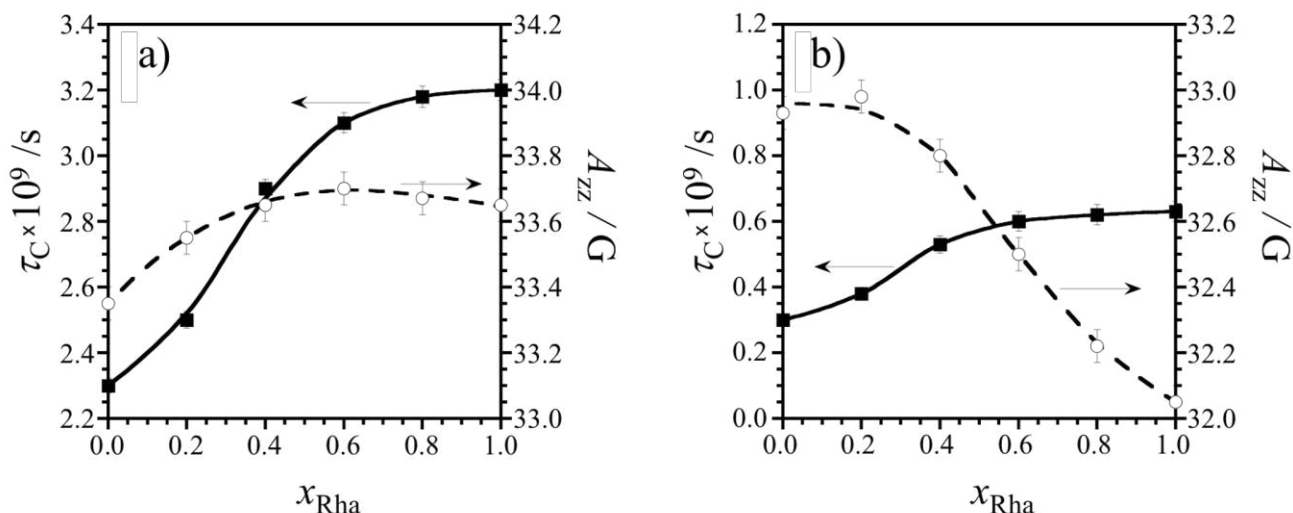


Figure 4. Dependence on Rha content of the EPR spectroscopic parameters of 5-DSA (a) and 16-DSA (b) in water-Rha-SLES mixtures at pH = 7.1 and 25 °C. For both spin-probes, the correlation time, t_C , is reported on the left-hand side ordinate, and the hyperfine coupling tensor component A_{zz} is reported on the right-hand side ordinate.

For both 5-DSA and 16-DSA, τ_C increases with increasing increasing the Rha content, showing a steeper variation up to $x_{\text{Rha}} = 0.6$. This evidence indicates that the di-chained biosurfactant induces a higher microviscosity within the aggregates, most likely connected with a more compact surfactant tail packing. This hypothesis is supported by the A_{zz} trend observed for 16-DSA, showing a marked decrease with x_{Rha} , indicating that the Rha chains form a more hydrophobic microenvironment around the doxyl group. Interestingly, for 5-DSA the A_{zz} variation is smaller than for 16-DSA, and the effect of increasing amount of Rha is the opposite, causing an increase up to $x_{\text{Rha}} = 0.6$. Thus, the presence of the Rha headgroups increases the polarity of micelle more external layer, suggesting that Rha disturbs the packing of the SLES headgroups. At higher Rha content the trend reverses, possibly because of the micellar aggregate increased size, as indicated by DLS results.

4.1.3.3 Rha-SLES mixed micellization: models and molecular interactions

Analysis of the experimental findings in terms of theoretical models of mixed micellization provides important information on the molecular determinants of the observed behavior. In the pseudo-phase separation model [69], the *cmc* of Rha-SLES mixtures is considered as a saturation value of surfactants solubility, above which both Rha and SLES partition between the co-existing aqueous monomer solution and the mixed micelles.

The compositions of the two pseudo-phases can be described in terms of the surfactant mole fractions, defined as:

$$X_{\text{Rha}} = \frac{m_{\text{Rha}}^{\text{mon}}}{m_{\text{Rha}}^{\text{mon}} + m_{\text{SLES}}^{\text{mon}}} \quad \text{Equation 4}$$

and

$$Y_{\text{Rha}} = \frac{m_{\text{Rha}}^{\text{mic}}}{m_{\text{Rha}}^{\text{mic}} + m_{\text{SLES}}^{\text{mic}}} \quad \text{Equation 5}$$

where $m_{\text{Rha}}^{\text{mon}}$ and $m_{\text{SLES}}^{\text{mon}}$ are the molalities of Rha and SLES in monomeric form while $m_{\text{Rha}}^{\text{mic}}$ and $m_{\text{SLES}}^{\text{mic}}$ are those in micellized form ($m_{\text{Rha}}^{\text{mon}} + m_{\text{Rha}}^{\text{mic}} = m_{\text{Rha}}$ and $m_{\text{SLES}}^{\text{mon}} + m_{\text{SLES}}^{\text{mic}} = m_{\text{SLES}}$). At the *cmc*, most of the surfactants are in aqueous pseudo-phase, and consequently $X_{\text{Rha}} \approx x_{\text{Rha}}$.

By imposing the chemical potentials of each surfactant to be equal in the two pseudo phases at equilibrium, the following relation between the *cmc* of Rha-SLES mixtures and those of the pure components is obtained:

$$\frac{1}{\text{cmc}} = \frac{X_{\text{Rha}}}{\gamma_{\text{Rha}} \text{cmc}_{\text{Rha}}} + \frac{(1-X_{\text{Rha}})}{\gamma_{\text{SLES}} \text{cmc}_{\text{SLES}}} \quad \text{Equation 6}$$

where γ_{Rha} and γ_{SLES} are the activity coefficient of Rha and SLES in the mixed micelles, respectively, whereas the monomer solution is assumed to behave ideally. As a first attempt, one could assume an ideal behavior also for the micellar pseudo-phase ($\gamma_{\text{Rha}} = \gamma_{\text{SLES}} = 1$, [70]). Fig. 2(b) shows that the experimental *cmc* values for the Rha-SLES mixtures are systematically higher than those predicted by the ideal mixed micellization, suggesting that Rha-SLES interactions disfavour self-aggregation.

Holland and Rubingh introduced the regular solution model to interpret the micellar pseudo-phase behavior, assuming ideal entropy variation for the surfactants mixing within the aggregates [71]. In this model, the activity coefficients can be expressed as a function of the micelle composition by introducing a single interaction parameter, β :

$$\gamma_{\text{Rha}} = \exp[\beta(1 - Y_{\text{Rha}})^2] \quad \text{Equation 7}$$

and

$$\gamma_{\text{SLES}} = \exp[\beta Y_{\text{Rha}}^2] \quad \text{Equation 8}$$

β corresponds to the energy interaction difference between equal and nonequal surfactant molecules, and can be estimated by using the equation:

$$\beta = \frac{\ln[X_{\text{Rha}} \text{cmc} / (Y_{\text{Rha}} \text{cmc}_{\text{Rha}})]}{(1-Y_{\text{Rha}})^2} \quad \text{Equation 9}$$

A negative value of β indicates that there is some synergism between the two surfactants, i.e., micellization is promoted by their mixing. On the other hand, a positive value denotes antagonism between the surfactants.

Y_{Rha} can be evaluated from the equation:

$$\frac{Y_{\text{Rha}}^2 \ln[X_{\text{Rha}} \text{cmc} / (Y_{\text{Rha}} \text{cmc}_{\text{Rha}})]}{(1-Y_{\text{Rha}})^2 \ln\{(1-X_{\text{Rha}}) \text{cmc} / [(1-Y_{\text{Rha}}) \text{cmc}_{\text{Rha}}]\}} = 1 \quad \text{Equation 10}$$

Solution of Eqs. 6-10 by an iterative minimization routine using the experimental cmc and X_{Rha} as input values allows the simultaneous estimation of Y_{Rha} and β [72,73]. The cmc trend predicted by this approach with the value $\beta = 5 \pm 1$, shown in Fig. 2b, satisfactorily interpolates the experimental values. The positive β value clearly points to unfavorable interactions between Rha and SLES. The corresponding Y_{Rha} values are reported as a function of X_{Rha} in Fig. 5(a), where the values predicted by the ideal solution model, computed by the equation:

$$Y_{\text{Rha}} = \frac{X_{\text{Rha}} \text{cmc}_{\text{SLES}}}{X_{\text{Rha}} \text{cmc}_{\text{SLES}} + (1-X_{\text{Rha}}) \text{cmc}_{\text{Rha}}} \quad \text{Equation 11}$$

are also reported. The figure clearly shows that micelle composition obtained by fitting the experimental data deviates from ideality. For $X_{\text{Rha}} < 0.3$ (i.e., in SLES-rich mixtures), Y_{Rha} values are higher than those predicted by ideal mixing, indicating that Rha molecules tend to crowd in the micellar aggregates. This means that, once a Rha molecule enters the micelle, it attracts other Rha molecules to reduce interactions with SLES. In contrast, for $X_{\text{Rha}} > 0.3$ (i.e., in Rha-rich mixtures), Y_{Rha} values are lower than those predicted by ideal mixing, indicating that SLES molecules tend to crowd in the aggregates.

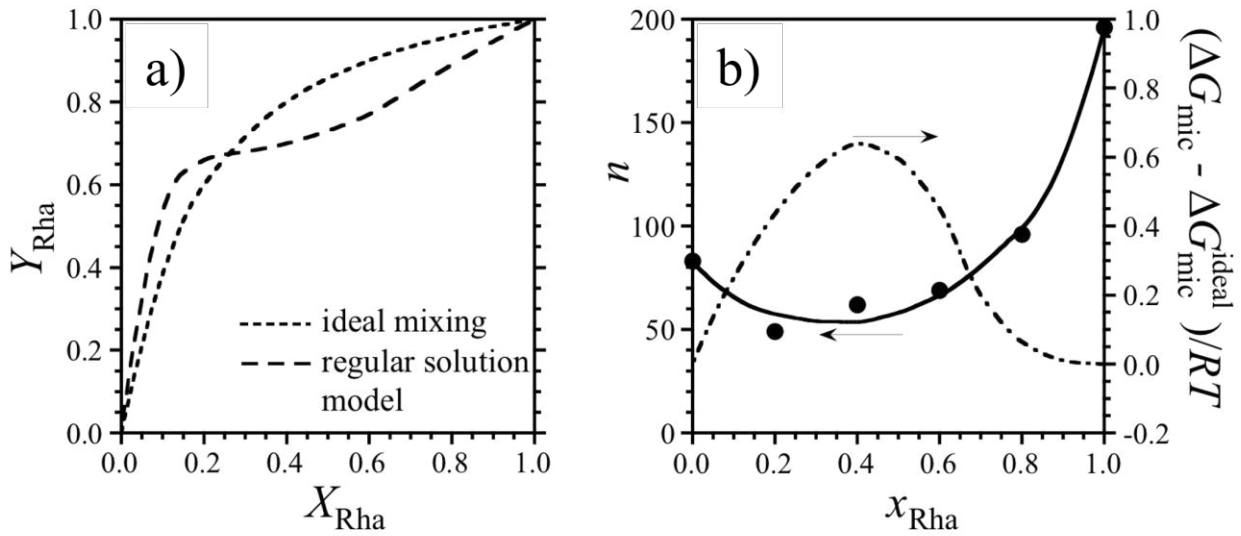


Figure 5. Parameters describing the mixed micellization for the ternary system water-Rha-SLES at pH = 7.1 and 25 °C. (a) Micellar pseudo-phase composition vs. aqueous pseudo-phase composition obtained by the models reported in the legend. For the regular solution model, the trend obtained with $\beta = 5$ is shown. (b) variation of the micellization Gibbs energy (regular solution model in respect to ideal mixing, dashed-dotted line) and surfactant aggregation number (continuous line) vs. surfactant mixture composition.

Once X_{Rha} and Y_{Rha} are known, it is possible to calculate the Gibbs energy of micellization, ΔG_{mic} , as defined by Maeda [74]:

$$\Delta G_{mic} = \ln(cmc) + (1 - Y_{Rha}) \ln \frac{(1 - X_{Rha})}{(1 - Y_{Rha})} + Y_{Rha} \ln \frac{X_{Rha}}{Y_{Rha}} \quad \text{Equation 12}$$

The ΔG_{mic} computed from the Y_{Rha} values obtained from the regular solution model is less negative than that computed from the ideal solution model, ΔG_{mic}^{ideal} . The difference between these two quantities, reported in Fig. 5(b), is positive in the entire composition range becoming negligible only at high x_{Rha} . This confirms that, because of antagonistic Rha-SLES interactions, the formation of mixed micelles is less favoured than expected from ideal surfactant mixing.

The knowledge of the micelle composition allows the aggregation number, n , to be estimated from the ratio between the volume of the micellar aggregate, V , and the average value of the surfactant volumes.

$$n = \frac{V}{Y_{Rha} V_{Rha} + (1 - Y_{Rha}) V_{SLES}} \quad \text{Equation 13}$$

V can be computed starting from the R_{H1} values obtained by DLS measurements, assuming a spherical shape of the aggregates. As discussed in the previous subsection, this assumption is reliable for all

considered samples, with the exception of the water-Rha binary mixture in which case Eq. 12 furnishes only a qualitative indication. The molar volumes of micellized Rha ($470 \text{ cm}^3 \text{ mol}^{-1}$ [75]), SLES ($412 \text{ cm}^3 \text{ mol}^{-1}$ [76,77]) and the hydration numbers of rhamnose (4 [78]), carboxylate group (5 [79]), ethoxylic unit (4 [80]), sulfate group (6 [81]), were taken from the literature. The trend of the n values estimated by Eq. 12 is shown in Fig. 5(b). The aggregation number of the mixed aggregates is lower than those of the micelles formed by the single surfactants.

Summarizing, the cmc values, the maximum in the A trend [55], the positive β value, the ΔG_{mic} values, and the minimum in the n trend agree in showing that, although Rha and SLES form mixed aggregates, micellization is less favored than expected for ideal mixtures, pointing to antagonistic interactions between the two surfactants. This point deserves further comments in light of previous studies assessing the ability of these surfactants to co-micellize with other amphiphiles.

Despite the large exploitation for SLES in complex industrial formulations, its mixtures with other surfactants have been poorly investigated. In a few works in which mixed micellization with nonionic ethoxylated surfactants have been considered, SLES show synergistic interactions leading to a cmc lowering and aggregate enlargement [53,82-84]. This behavior has been ascribed to the strong ion-dipole attractive interactions occurring between the sulfate moiety and the ether oxygens of adjacent nonionic headgroups, favored by the ethoxylic chains flexibility [53]. Our results indicate that such interactions are not occurring between the SLES and Rha headgroups, because these last are rigid and sterically hindered. Indeed, we note that favorable interactions between the sulfate group and the ethoxylic chain could set up in single-component SLES micelles between neighboring headgroups [85]. Favorable interactions among the SLES headgroups could also arise from the H-bonding between hydrated ethoxylic chains [86,87]. The result is a rather compact micelle hydrophilic interface, which is disturbed by the Rha insertion, as suggested by EPR results.

Mixed micellization of Rha with other surfactants has been investigated in some recent studies. Rha shows a strong synergism with anionic surfactants such as sodium dodecyl sulfate (SDS) [13] or sodium dodecyl 6-benzene sulfonate (LAS) [14]; this is mainly ascribed to the reduction of the electrostatic repulsion between the densely charged sulfate groups due to the interposition of the weakly charged Rha headgroups. Our results show that a similar effect is not occurring for SLES, further supporting the hypothesis that the electrostatic repulsion among the sulfate groups is partially masked by their interaction with ethoxylic linkers [88].

Other studies converge in showing an important role played by the molecular packing in determining the effects of surfactant mixing in the aggregates [18]. A synergistic effect has been observed between Rha and nonionic surfactants with a bulky hydrophobic moiety (i.e., a highly branched single chain [89,15] or a double chain [16]). Thus, we can hypothesize that the mismatch between the size and shape of the hydrophobic moieties of Rha (which presents two short tails) and SLES (which bears a single linear long chain) could disfavor their mixed aggregation.

Importantly, Rha shows a strong synergism in forming mixed micelles with other glycosidic biosurfactants such as sophorolipids [90,91], pointing to the setup of attractive interactions among the carbohydrate moieties at the micelle interface [92,93].

Overall, our results could be reasonably interpreted as follows: Rha and SLES form mixed micelles in aqueous solution; however, because of the unfavorable interactions between the headgroups and the mismatch of the tails each surfactant molecule prefer to be surrounded by other molecules of the same type, as highlighted by the Y_{Rha} vs. X_{Rha} trend, thus reducing the Gibbs energy gain deriving from surfactant mixing.

4.1.3.4 Rha-SLES aqueous mixtures: functional behavior

Anionic surfactants are largely exploited in modern cleaning liquid formulations, being regarded as effective emulsifiers as well as good foaming and wetting agents. Currently, SLES is preferred to previously used anionic surfactants (*e.g.*, alkyl sulfates and alkyl benzene sulfonates) since it is milder for the skin [94,95]. The present study aims at evaluating the opportunity to gradually move from SLES to anionic biosurfactants in the direction of even more sustainable formulations. The functional performances of detergent formulations critically depend on their interfacing with oils, air, and solid surfaces. For this reason, we analyzed the emulsifying, foaming and wetting ability of Rha-SLES mixtures.

Both SLES and Rha are hydrophilic surfactants able to stabilize W/O emulsions [55,96,97]. Below, we investigate the ability of Rha-SLES mixtures to emulsify sunflower oil in water (pH = 7.1). In Fig. 6(a) the emulsification index evaluated after two hours (E_2) is reported. The values show a dose-dependent behavior at all mixture composition. Particularly, E_2 is lower at 200 mg L⁻¹ while for 500 and 1000 mg L⁻¹ similar higher values are observed, suggesting a sort of saturation of the trend. The value observed for Rha is close to that relative to SLES. Moreover, the Rha-SLES mixtures present

almost the same value for all molar ratios, so that above 500 mg L⁻¹ data do not display significant variations with both composition and concentration. On the other side, the E_{24} values are dose dependent at all the surfactant mixture compositions, see Fig. 6(b), and show a lower emulsification activity as the content of rhamnolipid increases. These results confirm that both SLES and Rha are able to emulsify sunflower oil in water. However, oil droplets are longer-lasting when coated by SLES molecules than by Rha ones. This could be due to a combination of factors: the higher surface charge of SLES layers hinders more efficiently the droplets coalescence; moreover, the attractive interactions occurring between adjacent SLES headgroups enhances the compactness of the surfactant layer; last, the emulsions stability increases with the length of the apolar tail and is rather limited for the short-tailed Rha [98]. Surfactant layers formed by Rha-SLES mixtures show a durability intermediate between that of the pure surfactants.

The foaming tests were carried out at two total surfactant concentration, 500 mg L⁻¹ and 1000 mg L⁻¹, respectively, and at different surfactant mixture compositions. Fig. 6(c) shows a good foamability for all the investigated samples. However, the Foam% value is higher for SLES than for Rha, as is particularly evident at 1000 mgL⁻¹. The values obtained for the surfactant mixtures are similar to the SLES one and are scarcely affected by the total surfactant concentration.

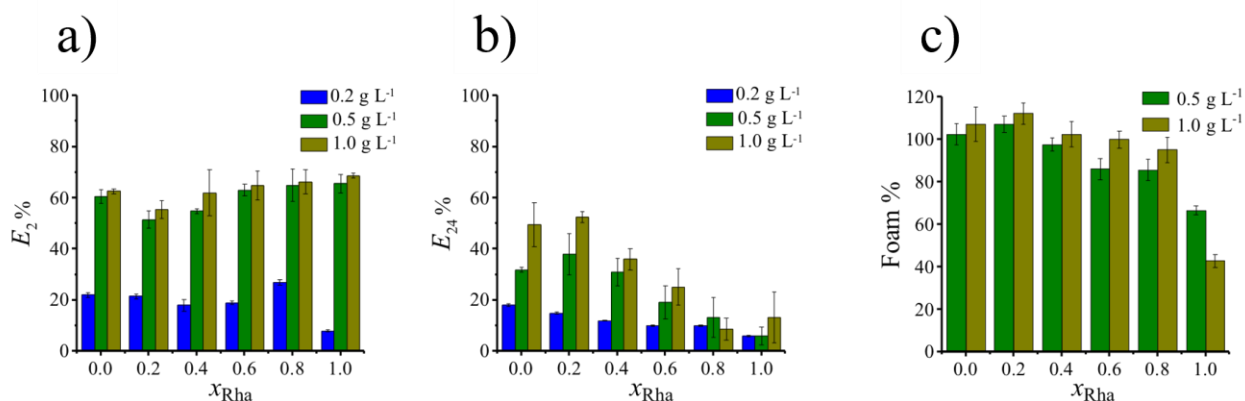


Figure 6. Parameters describing the functional features of the Rha-SLES surfactant mixtures at pH = 7.1 and 25 °C. Emulsification index after 2 h (a) and 24 h (b) from shaking vs. surfactant mixture composition at the total surfactant concentration reported in the legend. (c) Foaming ability vs. surfactant mixture composition.

The foamability is governed by a delicate equilibrium between different factors, including equilibrium surface tension and adsorption kinetics [99]. Micellar aqueous solutions of SLES and Rha have almost the same surface tension, see Section 3.1; on the other hand, the adsorption of Rha at the air/water interface is much slower for Rha than for SLES [55,100], due to the overall higher

bulkiness of the molecule and the steric or packing constraints of the larger headgroup [101,102]. For the surfactant mixtures the foamability is independent of the composition, being almost equal to that of SLES alone. This evidence suggests that the fast adsorption of SLES at the interface rules the foam formation also in these mixtures.

In Fig. 7 the values of the contact angle (θ) between Rha-SLES aqueous mixtures and selected solid surfaces are reported as a function of the surfactant mixture composition. In all cases, the measured values were found to be negligibly affected by the total surfactant concentration. Fig. 7(a) shows the data obtained using a native silicon wafer as support. This support, when exposed to atmospheric oxygen, presents a thin layer of SiO₂. The contact angle with the aqueous phosphate buffer (pH = 7.1, dashed line in the figure) is relatively low (58°), which confirms the surface to be quite hydrophilic. The presence of surfactants significantly reduces θ : an average value of about 20° is observed, independent of the surfactant mixture composition and concentration. The θ decrease points to the positioning of surfactant molecules (with the possible formation of a bilayer) at the solid-liquid interface [103]. Exposure of the silicon wafer to an oxidizing solution leads to the formation of silanol groups on its surface, which increases its hydrophilicity, see Fig. 7(b). On this surface the extremely low contact angle of the aqueous buffer (16°) is unaffected by the presence of surfactants. Hydrophobic derivatization of the wafer surface with OTS results in an extremely high contact angle with the aqueous buffer (109°). Surfactants significantly lower this value, indicating the formation of a monolayer at the solid-liquid interface. Rha is more effective than SLES (50° vs. 65°), and their mixtures present θ values decreasing with the Rha content. The dependence of the contact angle with the hydrophobic surface on the mixture composition deserves some further comment. The Young equation:

$$\gamma_{SV} - \gamma_{SL} = \gamma_{LV} \cos\theta \tag{Equation 14}$$

correlates the contact angle and the solid-vapor, solid-liquid, and liquid-vapor interface tensions (γ_{SV} , γ_{SL} and γ_{LV} , respectively). γ_{SV} remains constant for all the data shown in Fig. 7(c), as the same solid surface is considered. γ_{LV} coincides with the γ_{cmc} reported in Table 1 and is almost independent of the surfactant mixture composition. As a consequence, the significant decrease of θ as the Rha content increases is ascribable to a γ_{SL} decrease. The higher wettability of Rha compared to SLES is related to the lower hydrophilic-lipophilic balance of the di-tailed surfactant [104,105].

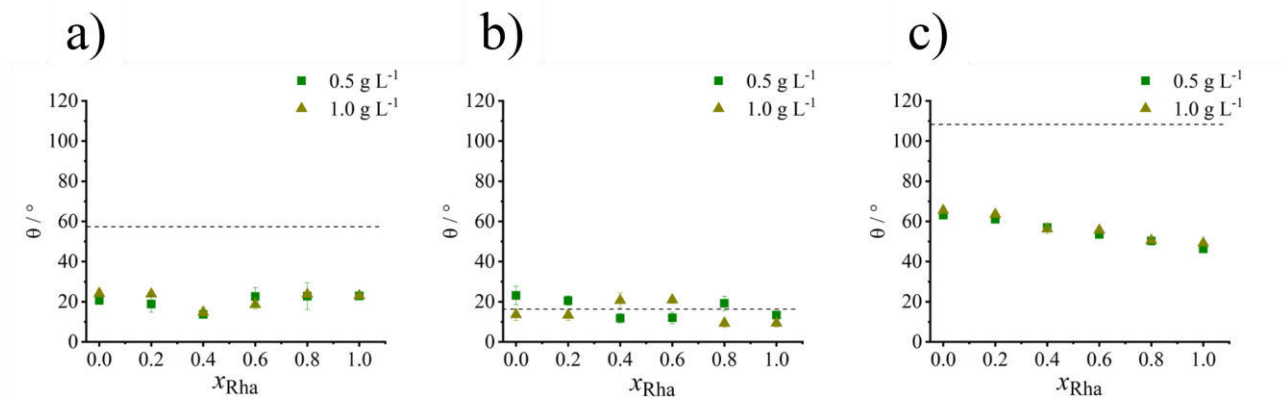


Figure 7. Parameters describing the functional features of the Rha-SLES surfactant mixtures at pH = 7.1 and 25 °C. Contact angle between the Rha-SLES surfactant mixtures and a native (a), oxidized hydrophilic (b) and hydrophobically modified (c) silicon wafer surface. The dashed line represents the value determined for the aqueous phosphate buffer (pH = 7.1).

4.1.3.5. Ecotoxicity assay

In regard to ecotoxicity, both SLES and Rha are generally considered non-harmful for the environment. However, the available scientific literature does not allow a direct comparison between them. Given the different applications, assays have been conducted in different conditions and on different indicators. SLES is a suitable foaming agent in mechanized tunneling and some studies focused on its ecotoxicity in excavated soils [106-108

]. On the other hand, Rha has been proposed for environmental remediation and its toxicity has been tested on plants, algae, soil microbes and yeast [109,110]. The ecotoxicological studies of Rha on aquatic and terrestrial organisms are scarce [111].

In this scenario, in order to align the results obtained for SLES and Rha, we decided to perform a rational comparative ecotoxicological assay, using the same organisms at the same conditions. According to the environmental guidelines, three different tests were carried out: i) luminescence inhibition test on the bacterium *Aliivibrio fischeri*, ii) growth inhibition test on the alga *Raphidocelis subcapitata*, iii) immobility test on the crustacean *Daphnia magna*. The chosen organisms belong to different trophic levels, being classified as decomposer, primary producer and primary consumer, respectively.

Table 2. Ecotoxicity of the Rha and SLES as EC50 values, expressed as luminescence inhibition (%) of the bacterium *A. fischeri*, growth inhibition of alga *R. subcapitata* and immobility (%) of the crustacean *D. magna*. CI 95%= 95% of confidence intervals.

Tested species	EC50 (g L ⁻¹) (CI 95%)	
	SLES	Rha
<i>A. fischeri</i>	0.003 (0.002-0.003)	0.007 (0.007-0.008)
<i>R. subcapitata</i>	0.009 (0.007-0.012)	0.033 (0.028-0.038)
<i>D. magna</i>	0.015 (0.010-0.020)	0.030 (0.022-0.040)

A dose–response relationship was found, where the 100% effect was caused only by high surfactant concentrations. The EC50 values estimated for SLES are in line with the values reported in the literature for other anionic surfactants [112], while those obtained for Rha are in all cases higher, the more relevant difference being observed for the alga. Particularly, SLES can be classified as toxic, while Rha is only harmful, definitely demonstrating the lower ecotoxicity of Rha [109].

4.2 monorhamnolipid and CTAC

Catanionic surfactant mixture self-aggregate in a variety of supramolecular aggregates [21-23]. Because of this versatility, their application has been proposed in many different fields, including oil recovery [24], purification processes [25], biomedicine and pharmaceuticals [26-28]. Biocompatibility and ecosustainability concerns have driven the design of catanionic aggregates based on natural and bio-derived components [29], e.g., bile salts [30], fatty acids [31], and modified aminoacids [32]. A few studies have addressed the inclusion of sugar-based surfactants in catanionic mixtures [33-35].

In this part of the research, we study the mixed micellization of mono-rhamnolipids (mRha) and cetyltrimethylammonium chloride (CTAC, IUPAC name hexadecyltrimethylammonium chloride) in aqueous solution at neutral and acidic pH, see Fig. 8 for the molecular structures.

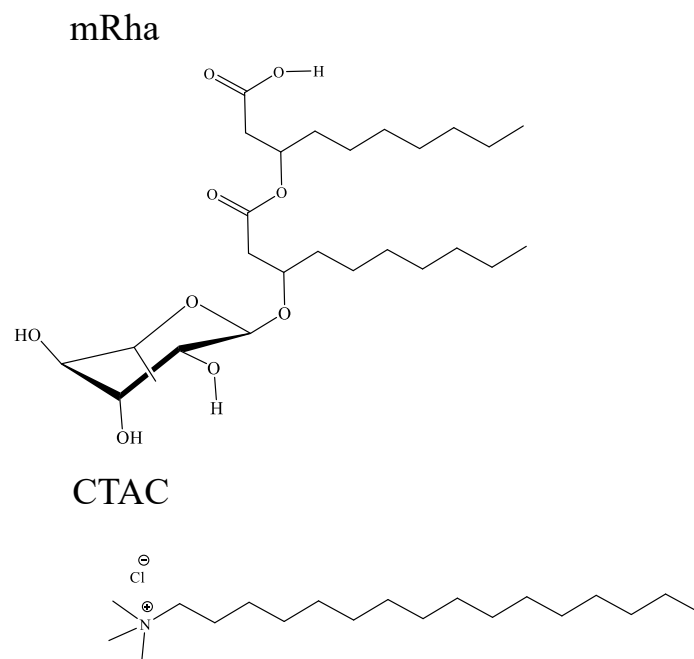


Figure 8. Molecular structures of the surfactants used in this study.

mRha is one of the rhamnolipid congeners produced by *Pseudomonas aeruginosa* as secondary metabolites. Its molecular architecture presents one L-rhamnose unit linked as polar headgroup to and two 3-hydroxyalkanoic acids as apolar tails. For the present investigation, mRha was preferred to the rhamnolipid mixture with the aim to avoid possible ambiguity in data interpretation arising from the sample polydispersity [113].

CTAC is a cationic surfactant largely used in personal care products as hair conditioners [114], whose mixtures with other (co)surfactants are actively investigated to improve the formulation functionality and safety [115,116].

Hereafter, the self-aggregation behavior of the ternary system water-mRha-CTAC is investigated by combining different experimental techniques: the critical micelle concentration (*cmc*) is estimated by surface tension measurements at two pH (pH = 7.1 and pH = 3.4); the dimension and the morphology of the micellar aggregates is analysed by Dynamic Light Scattering (DLS) in acidic and neutral pH, and Small Angle Neutron Scattering (SANS) at neutral pH; the condensation of counterions at the aggregate interface is investigated by conductimetry. Finally, the results are analysed and rationalized in the framework of the regular solution model of mixed micellization.

4.2.1 Materials and samples preparation

The mono-rhamnolipid C10-C10 sample (a colourless gel-like solid with a purity grade of $\geq 95\%$, hereafter named mRha) was purchased by AGAE Technologies (Corvallis, OR, USA). 1-Hexadecyl trimethylammonium chloride (CTAC, purity 96%,) was provided by ALFA AESAR (Kandel Germany). The molar masses of mRha and CTAC are 504 g mol^{-1} and 320 g mol^{-1} , respectively. Ultrapure deionized water from a Millipore Milli-Q system was used as solvent for all sample preparation, except for those prepared for SANS measurements for which deuterium oxide (99.8 atom % D, obtained from Sigma Aldrich, Milan, Italy) was used. All water-mRha-CTAC mixtures was buffered at $\text{pH } 7.1 \pm 0.2$ using phosphate buffer at concentration 0.04 M (ionic strength around 0.1 mol kg^{-1}). The phosphate buffer was prepared by using Na_2HPO_4 and NaH_2PO_4 , both obtained from Sigma-Aldrich with a purity $> 99\%$. The citrate buffer at 3.4 ± 0.2 was prepared using Sodium Citrate dihydrate ($\text{Na}_3\text{C}_6\text{H}_5\text{O}_7 \cdot 2\text{H}_2\text{O}$, purity $> 99\%$) and citric acid ($\text{C}_6\text{H}_8\text{O}_7$ purity $> 99\%$), both purchased from Sigma-Aldrich (Milan, Italy).

The ternary system water-mRha-CTAC ($\text{pH} = 7.1$ and $\text{pH} = 3.4$) was investigated by varying both the surfactant mixture composition, calculated as

$$x_{\text{mRha}} = \frac{m_{\text{mRha}}}{m_{\text{mRha}} + m_{\text{CTAC}}} \quad \text{Equation 15}$$

and the total surfactant concentration, which is

$$m_{\text{surf}} = m_{\text{mRha}} + m_{\text{CTAC}} \quad \text{Equation 16}$$

where m_{mRha} and m_{CTAC} are the molalities of mRha and CTAC, respectively. Specifically, surface tension and conductivity measurements were performed by adding successive aliquots of a concentrated surfactant solution at a given surfactant composition to a known volume of the same buffer used to prepare the surfactant solution; in such a way, m_{surf} was progressively increased (from 0 to maximum $2 \times 10^{-3} \text{ mol kg}^{-1}$), while x_{mRha} was kept constant at a chosen value ($x_{\text{mRha}} = 0.0, 0.1, 0.2, 0.4, 0.5, 0.6, 0.7, 1.0$ for surface tension and $x_{\text{mRha}} = 0.0, 0.2, 0.4, 1.0$ for conductivity). DLS measurements were performed at the same x_{mRha} investigated by surface tension and at constant $m_{\text{surf}} = 1 \times 10^{-3} \text{ mol kg}^{-1}$. This m_{surf} was previously checked to allow reliable measurements at all the considered x_{mRha} . All experiments were performed at $25 \text{ }^\circ\text{C}$.

4.2.2. Measurements

Surface tension and Dynamic light scattering measurements were carried out as described previously in 4.1.2.1 and 4.1.2.2 paragraphs of this chapter.

Specific conductivity, c , was measured using a CDM 210 conductometer (Radiometer Analytical, Villeurbanne, France) which was calibrated as previously reported in chapter 3 (3.3.2). Contact angle measurements are carried out as described in 4.1.2.5 paragraph.

4.2.2.1 Small Angle Neutron Scattering (SANS)

SANS measurements were carried out on the Sans2d beamline at the ISIS Pulsed Neutron Source (STFC Rutherford Appleton Laboratory, Didcot, UK). A simultaneous Q-range of 0.004-1 Å⁻¹ was achieved utilizing an incident wavelength range of 1.75-16.5 Å in time of light mode and employing an instrument set up of L1 = L2 = 4m and two detectors to measure small and wide angles, with the front detector at 2.4 m from the sample. Each raw data set was corrected for detector efficiencies, sample transmission, and background scattering and converted to scattering intensity $I(q)$ versus the scattering vector $q=4\pi/\lambda\sin(\theta/2)$, where λ and θ represented the wavelength of the neutron beam and scattering angle, respectively [117]. The structural information can be extrapolated by choosing the appropriate model to fit the experimental data. In this case, the core-shell ellipsoidal model was used to fit the data of $x_{mRha} = 0.0$. Using this model, the scattering intensity is calculated in the following way:

$$P(q) = \frac{scale}{V} F^2(q) + bkg \quad \text{Equation 17}$$

Where

$$F(q) = \frac{3\Delta\rho V (\sin[q(R_e^2 + R_p^2)^{1/2}] - \cos[q(R_e^2 + R_p^2)^{1/2}])}{(q[R_e^2 + R_p^2]^{1/2})^3} + f(q, R_e + t_{shell}, R_e x_{core} + t_{shell}, x_{shell})$$

Equation 18

where $V = \frac{4}{3}\pi R_p R_e^2$ is the volume of the ellipsoid, R_p is the polar radius, R_e is the equatorial radius, and t_{shell} is the thickness of the shell. In addition, for the $x_{mRha} = 0.0$ sample the Hayter-Penfold

Rescaled Mean Spherical Approximation factor for the charged sample was considered. On the other hand, the $x_{\text{mRha}} = 0.6$ sample was fitted using the vesicle model, for which the scattering intensity is:

$$P(q) = \frac{\phi}{V_s} \left[\frac{3V_c(\rho_{\text{solv}} - \rho_s)j_1(qr_c)}{qr_c} + \frac{3V_{\text{tot}}(\rho_s - \rho_{\text{solv}})j_1(qr_c)}{qr_c} \right]^2 + bkg \quad \text{Equation 19}$$

where ϕ is the volume fraction of shell, V_s is the volume of the shell, V_{tot} is the total volume. Finally, the $x_{\text{mRha}} = 1$ was fitted using the core-shell-sphere model:

$$P(q) = \frac{\text{scale}}{V} F^2(q) + bkg \quad \text{Equation 20}$$

Where

$$F(q) = \frac{3}{V_s} \left[V_c(\rho_c - \rho_s) \frac{\sin(qr_c) - qr_c \cos(qr_c)}{(qr_c)^3} + V_s(\rho_c - \rho_{\text{solv}}) \frac{\sin(qr_s) - qr_s \cos(qr_s)}{(qr_s)^3} \right] \quad \text{Equation 21}$$

where V_s is the volume of the whole particle, V_c is the volume of the core, r_s is the radius of the particle, r_c is the radius of the core, ρ_c is the scattering length density of the core, ρ_s is the scattering length density of the shell, and ρ_{solv} is the scattering length density of the solvent.

All fittings were performed with SasView software (version 5.0).

4.2.3 Results and discussions

4.2.3.1. mRha-CTAC mixed micellization: surface tension

In Fig. 9 are reported the parameters obtained by surface tension titration. In Fig. 9 (a) the *cmc* values at both pH are reported for the mixed system water-mRha-CTAC. In general, both systems at different pH show quite the same trend.

In particular, the CTAC *cmc* is not affected by the pH ($x_{\text{mRha}} = 0.0$, $cmc_{\text{CTAC}} = 7.2 \times 10^{-4}$ mol kg⁻¹) which is higher than that of the binary system water-mRha ($x_{\text{mRha}} = 1.0$ $cmc_{\text{mRha}} = 1.4 \times 10^{-4}$ mol kg⁻¹ at neutral pH and $x_{\text{mRha}} = 1.0$ $cmc_{\text{mRha}} = 0.5 \times 10^{-4}$ mol kg⁻¹ at acidic pH), indicating that the glycolipid has a stronger tendency to micellize than the cationic surfactant.

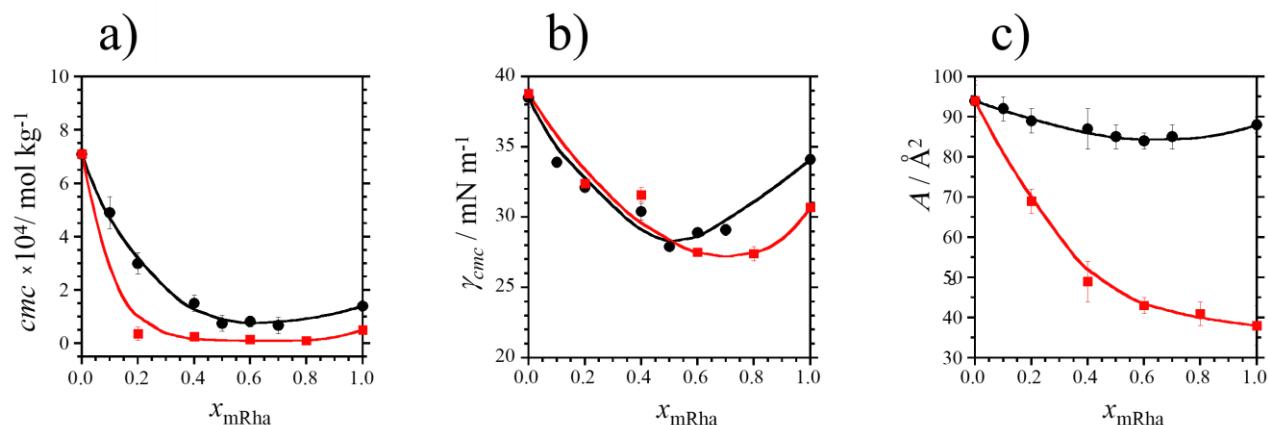


Figure 9. Physico-chemical characterization of the ternary system water-mRha-CTAC at pH = 7.1 (black line) and at pH = 3.4 (red line) and 25 °C. (a) Critical micelle concentration vs. surfactant mixture composition; (b) surface tension at micellization vs. surfactant mixture composition; (c) value of A vs. surfactant mixture composition. The pH = 7.1 is black-colored and pH = 3.4 is red colored.

At low x_{mRha} value, the cmc of the ternary mixtures water-mRha-CTAC steeply decreases with increasing the mRha content in the mixture, reaching a shallow minimum at $x_{mRha} = 0.5-0.7$ suggesting a kind of synergistic behavior in the mixed micellization process. With further increasing the mRha content, the cmc increases, finally reaching cmc_{mRha} .

The constant surface tension value, γ_{cmc} , found in each data set collected at constant x_{mRha} for $m_{surf} \geq cmc$ Fig. 9(b). The general, the trends seem to not be affected by pH where mRha alone is more effective than CTAC in lowering the surface tension of micellar solutions ($\gamma_{cmc} = 34.1 \text{ mN m}^{-1}$ vs. 38.5 mN m^{-1} at neutral pH and $\gamma_{cmc} = 30.7 \text{ mN m}^{-1}$ at acidic pH). As the two surfactants are mixed, even lower γ_{cmc} values are reached, and a shallow minimum is observed for $x_{mRha} \sim 0.5 - 0.7$. The third parameter, Fig. 9(c), is the average area at the air-solution interface per surfactant molecule at the cmc , A , calculated by the Gibbs isotherm. At neutral pH the experimental data do not seem to be affected by the composition of the system being quite constant. At acidic pH, since the mRha is uncharged and thus, the electrostatic repulsion do not occur, present an abrupt decrease of its value from 89 \AA^2 to 45 \AA^2 .

4.2.3.2 mRha-CTAC mixed micellization: thermodynamic models

In Fig. 10 the experimental cmc trend at both pH are compared with that predicted by ideal mixing and regular solution model as described previously in 4.1.3.3 paragraph [70,71]

The cmc trends obtained by applying the model of regular solution are shown in Fig. 9(a).

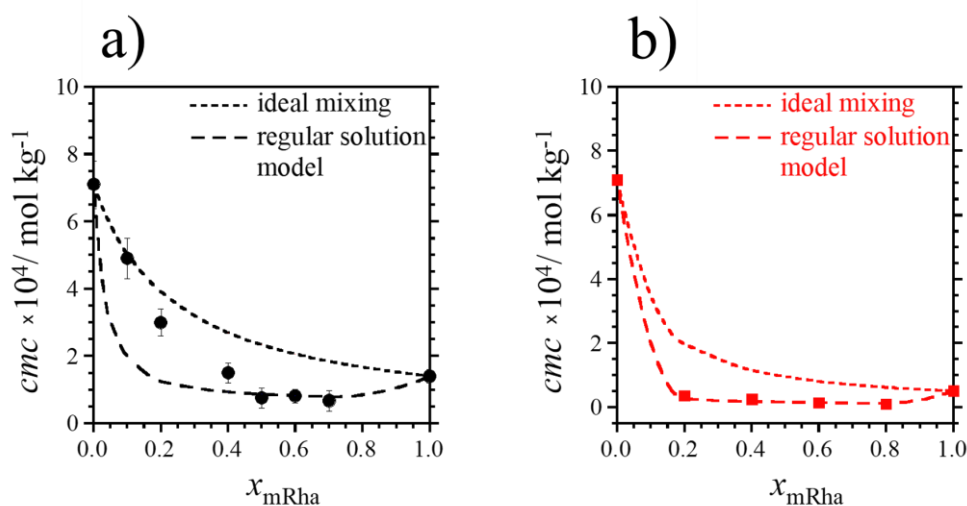


Figure 10. Critical micelle concentration vs. surfactant mixture composition; the experimental data (circles) are compared with the predictions of mixed micellization models as indicated in the legend. For the regular solution model, the trend obtained with $\beta = -7.1$ (a) and $\beta = -8.8$ (b), respectively. The pH = 7.1 is black-coloured and pH=3.4 is red coloured.

The β value was optimized considering simultaneously all the experimental *cmc* data; the result ($\beta = -7.1 \pm 0.5$ at neutral pH and $\beta = -8.8 \pm 0.7$ at acidic pH) confirms very favorable interactions between mRha and CTAC in the micellar aggregates. Inspection of Fig. 10(a) reveals that the predicted *cmc* trend satisfactorily fits the experimental values for $x_{\text{mRha}} \geq 0.5$. On this basis, in this composition range the mRha-CTAC mixtures can be proposed to follow the Y_{mRha} trend predicted by the Holland and Rubingh model (solid line). It is interesting to observe that the values are lower than those predicted by the Clint model. Thus, in mRha-rich mixtures, micelles are enriched by CTAC with respect to the ideal mixing, further confirming that mRha is able to bring along CTAC in the mixed micelles. At acidic pH there is a good agreement between the experimental data and the computed model of regular solutions. Thus, the processes are synergistic and energetically favored at both pH, as confirmed by the negative values of β and interestingly they are quite similar suggesting a weak affection of the electrostatic interaction at different pH during the mixed micellization process.

4.2.3.3 mRha-CTAC mixed micellization: specific conductometry

mRha-CTAC mixed micellization in aqueous solutions buffered at pH = 7.1 was further investigated by electrical conductivity measurements. The experimental results are shown in Fig. 11. mRha-CTAC mixed micellization in aqueous solutions buffered at pH = 7.1 was further investigated by electrical conductivity measurements. The experimental results are shown in Fig. 11. The solution specific

conductivity increases with the surfactant concentration at all considered x_{mRha} values. For the single CTAC ($x_{mRha} = 0.0$) a clear slope change is observed at the *cmc*, due to the condensation of a fraction of added counterions at the micellar interface to reduce the electrostatic repulsion among the positively charged headgroups.

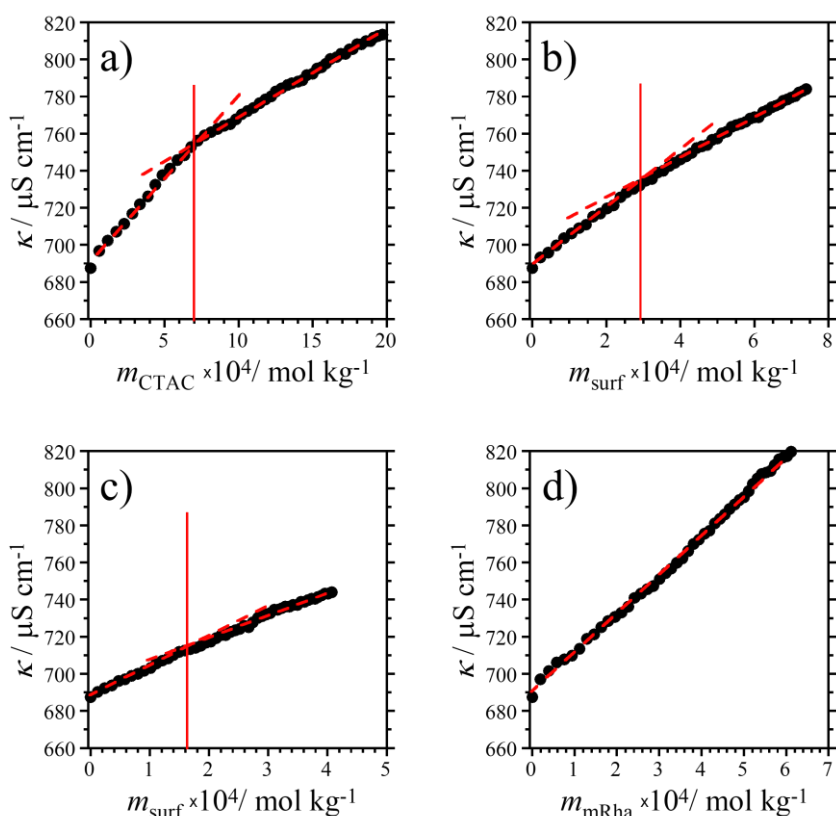


Figure 11. Specific conductivity of water-CTAC (a), water-mRha (d), and water-CTAC-mRha mixtures at $x_{mRha} = 0.2$ (b) and $x_{mRha} = 0.4$ (c) at $pH=7.1$ and $25\text{ }^{\circ}\text{C}$.

The *cmc* value determined by conductometry is in close agreement with that determined by tensiometry. The degree of micellar ionization was calculated as the ratio of the slopes of the conductivity in the micellar and premicellar concentration range, obtaining $\alpha = 0.50 \pm 0.02$. This value is slightly higher than that reported in the literature for CTAC in neat water [118], due to the presence of the buffering ions. With increasing x_{mRha} the slope change becomes less marked, and the micelle ionization increases ($\alpha = 0.75 \pm 0.03$ at $x_{mRha} = 0.2$ and $\alpha = 0.87 \pm 0.05$ at $x_{mRha} = 0.4$), indicating that the interposition of the mRha headgroups among the CTAC ones reduces the need of counterion condensation. At higher mRha content in the surfactant mixture no slope change was

observed in the conductivity trends. Particularly, no break point was observed for the pure mRha ($x_{\text{mRha}} = 1.0$). The absence of counterion condensation onto the mRha aggregates, in line with literature results [113], suggests a low charge density of their surface.

4.2.3.4 mRha-CTAC mixed micellization: Dynamic Light Scattering

The dimensions of the aggregates formed in water-mRha-CTAC systems were investigated by DLS measurements. The intensity-weighted plots (Fig. 12) show three populations of different size at pH = 7.1 and two populations at pH = 3.4.

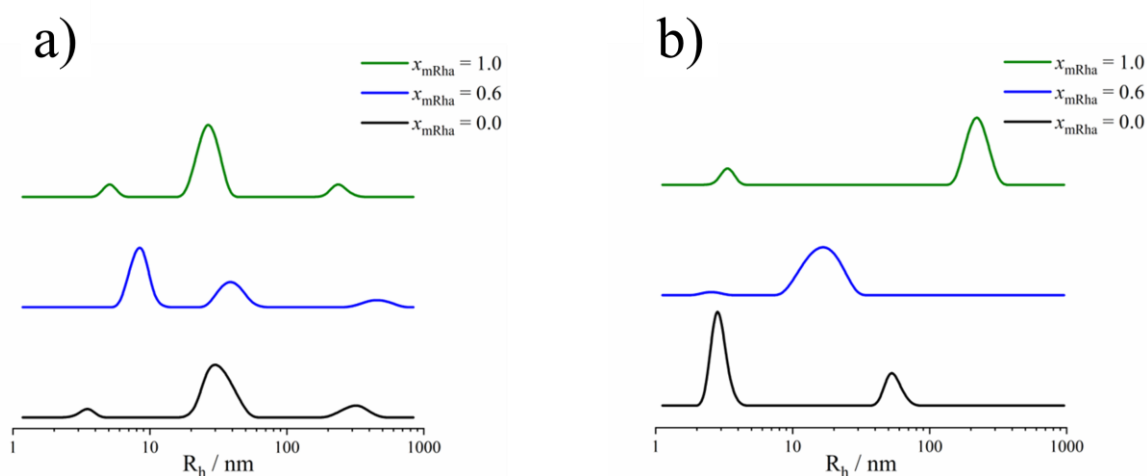


Figure 12. Intensity-weighted hydrodynamic radius distributions of mRha-CTAC aggregates at (a) pH = 7.1 and (b) pH = 3.4. The total surfactant concentration is equal to $0.045 \text{ mol kg}^{-1}$ and surfactant mixture composition are $x_{\text{mRha}} = 0.0, 0.6, 1.0$.

The average hydrodynamic radii of the populations observed at the various compositions are collected in Table 3. R_{H1} , R_{H2} and R_{H3} refer to the small and large aggregates, respectively.

Table 3. Aggregate dimension for the system water-mRha-CTAC at pH = 7.1 and 25 °C, and at pH = 3.4 and 25 °C as obtained by DLS measurements.

x_{mRha}	pH = 7.1			pH = 3.4	
	R_{H1}	R_{H2}	R_{H3}	R_{H1}	R_{H2}
	(nm)	(nm)	(nm)	(nm)	(nm)
0.0	5.6 ± 0.3	50 ± 2	440 ± 120	2.6 ± 0.3	54 ± 15
0.6	13.2 ± 1.5	50 ± 20	600 ± 200	2.5 ± 0.3	16 ± 1
1.0	9 ± 1	44 ± 1	410 ± 140	3.30 ± 0.13	200 ± 70

Particles with R_{HI} radius can confidently assumed to be micelles, which are smaller at pH = 3.4 than at pH 7.1, indicating uncharged mRha molecules to pack in the aggregates more tightly. In all the cases, these micelles co-exist with one or two populations of larger aggregates, possibly vesicles [56,57,101].

4.2.3.3 mRha-CTAC mixed micellization: SANS

SANS data, shown in Fig. 13, shows that the morphology of the aggregates in the systems are quite different.

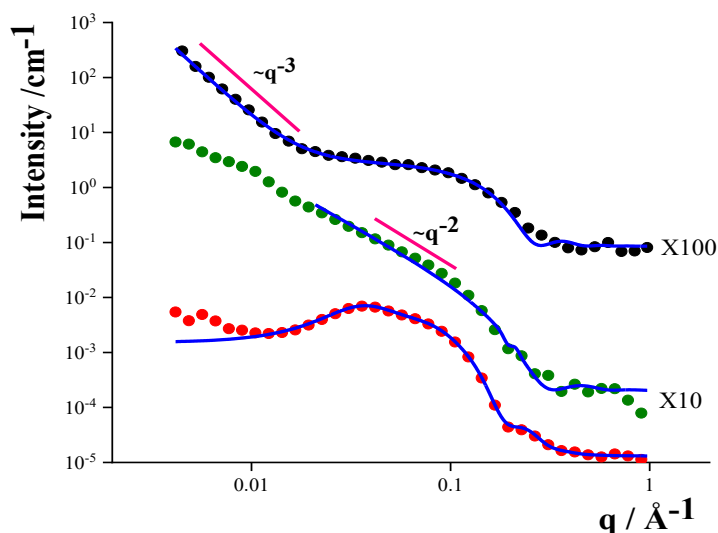


Figure 13. SANS data (cirles) and best fit curve (solid blue line) of $x_{mRha}=0.0$ (pink), $x_{mRha}=0.6$ (green), and $x_{mRha}=1.0$ (black) in D_2O .

The intensity scattering profile for the samples $x_{mRha}=0.0$ and 1.0 suggest the presence of micelles. In the absence of monorhamnolipid ($x_{mRha}=0.0$) the micelle is characterized by a charge density on surface. This is expected as the micelle is formed by a charged CTAC surfactant [136]. On the other hand, for sample ($x_{mRha}=1.0$) no presence of shoulder or peak in the intermediate q value suggest the presence of charge on the surface of micelle. Furthermore, at low values of q , the decreasing profile of $I(q)$ as a power law with $q \sim -3$) suggests the presence of large aggregates. Sample $x_{mRha}=0.6$ shows a slope at intermediate q of about 2, that is typical of bilayer scattering object [101]. According

to those considerations Samples $x_{mRha} = 0.0$ has been fitted with a core-shell-ellipsoid model, adding a structure factor, while the sample $x_{mRha} = 0.6$ with a lamellar model, finally $x_{mRha} = 1.0$ has been fitted with a core-shell-sphere model. The fitted curves and the obtained data are shown in Fig. 13 and Table 4.

Table 4. Experimental data obtained from SANS data fitting.

	$x_{mRha}=0.0$	$x_{mRha}=0.6$	$x_{mRha}=1.0$
Semiminor axis / Å	29 ± 2		
Semimajor axis / Å	36 ± 1		
Charge / e	27		
Thickness / Å		27 ± 3	
Core / Å			10 ± 1
Shell / Å			11 ± 1
slope			-3.38 ± 0.05

From the values obtained from the fitting of the SANS data it can be assert that the micelle of the only CTAC is prolate with an aggregation number of 150 [119]. While the only mRha is spherical, typical shape of mRha micelle in dilute solution [101], with an aggregation number of 45. The thickness value obtained from the fitted SANS data of CTAC-mRha system is slightly lower than the sum of the length of the alkyl chains of the two surfactants calculated with the Tanford equation [120], $l_{CTAC} = 21.8 \text{ Å}$ and $l_{mRha} = 10.4 \text{ Å}$. This last value agrees with the experimental core value [120].

4.2.3.4 mRha-CTAC mixed micellization: contact angle

The wettability of these surfactant mixtures was investigated. Fig. 14 shows the values of the contact angle (θ) between water-CTAC-mRha mixtures and selected solid surfaces as a function of the surfactant mixture composition at both the investigated pH. Samples at concentration 10, 50 and 100 times the *cmc* of mRha were tested; inspection of the figure shows that the concentration does not affect the ability of the mixture to decrease the contact angle. The data obtained using a native silicon wafer as support are shown in Fig. 14(a) (pH = 7.1) and Fig. 14(d) (pH = 3.4). This support exposes

a thin layer of SiO₂; the contact angle with the aqueous buffers (pH = 7.1 and pH = 3.4, dashed line in the figure) is relatively low (55°), which confirms the surface to be quite hydrophilic.

The presence of surfactants reduces θ , the effect becoming stronger with increasing the mRha content, independently of the pH. The θ decrease points to the positioning of surfactant molecules (with the possible formation of a bilayer) at the solid-liquid interface [103].

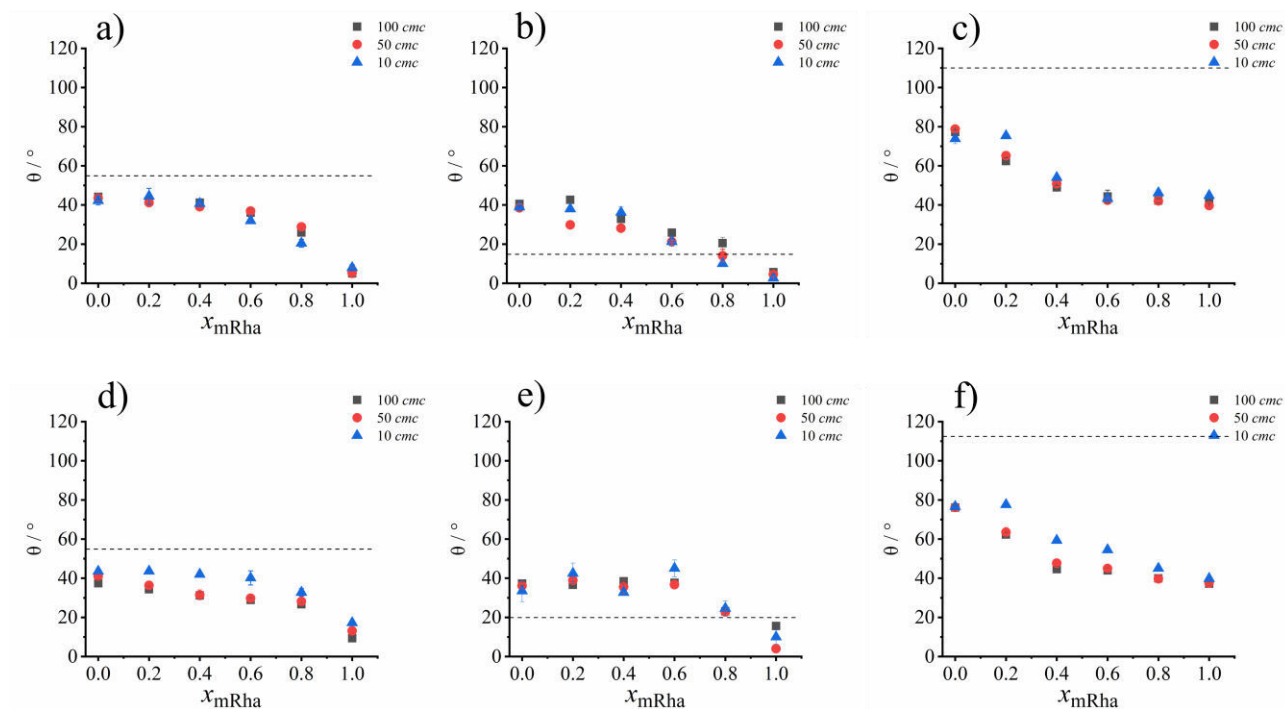


Figure 1. The CTAC-mRha surfactant mixtures contact angle on a native (a,d), oxidized hydrophilic (b,e) and hydrophobically modified (c,f) silicon wafer surface, at pH = 7.1 (a,b,c) and pH = 3.4 (d,e,f), at 25 °C. Data are reported as a function of the surfactant mixture composition; the total surfactant concentration is indicated in the legend. The dashed line represent the values determined for the aqueous phosphate (pH = 7.1) and citrate buffer (pH = 3.4).

Exposure of the silicon wafer to an oxidizing solution leads to the formation of silanol groups on its surface, which increases its hydrophilicity, as confirmed by the extremely low contact angle with the aqueous buffers (15° at pH = 7.1 and 20° at pH = 3.4, see Fig.14(b) and Fig. 14(c), respectively). For both neutral and acidic surfactant mixtures, θ value is higher than that determined with the buffer when $0.0 < x_{mRha} < 0.6$, probably due to the long CTAC hydrophobic tails. As the content of mRha increases, the contact angles decrease, becoming lower than those observed for the buffers. Hydrophobic derivatization of the wafer surface with OTS results in an extremely high contact angle with the aqueous buffers (about 110° for both investigated pH). Surfactants significantly lower these

values, indicating the formation of a monolayer at the solid-liquid interface. mRha is twice effective than CTAC (40° vs. 80° , independently of the pH), and their mixtures present θ values decreasing with increasing x_{mRha} . The dependence of the contact angle on the mixture composition deserves some further comment. The Young equation:

$$\gamma_{\text{SV}} - \gamma_{\text{SL}} = \gamma_{\text{LV}} \cos\theta \quad \text{Equation 22}$$

correlates the contact angle and the solid-vapor, solid-liquid, and liquid-vapor interface tensions (γ_{SV} , γ_{SL} and γ_{LV} , respectively). γ_{SV} remains constant for a given solid support. γ_{LV} coincides with the γ_{cmc} and is only weakly dependent on the surfactant mixture composition, see Fig. 10(b). Therefore, the significant decrease of θ as the mRha content increases is ascribable to a γ_{SL} decrease. The higher wettability of mRha compared to CTAC could be related to the attitude of the di-tailed surfactant to form interfacial monolayer [105].

4.3 Conclusions

Rhamnolipids are biosurfactants whose good functional properties could be fruitfully exploited in detergency. They are still more expensive than synthetic surfactants, but the genetic engineering efforts to obtain bacterial strain with higher productivity and the identification of energy-efficient unit operations make us confident that the costs will significantly decrease in the near future. This will open new perspective in the design of eco-sustainable industrial formulations.

For most practical applications surfactant mixtures are preferred to the single components, because their composition can be optimized for each specific task. The evaluation of the physico-chemical properties of rhamnolipid as mixtures or single pure homologues with conventional surfactants is thus fundamental for the rational design of formulations conjugating functionality and eco-friendliness. SLES is an anionic surfactant massively used in laundry, household cleaning and personal care detergents and CTAC is a cationic surfactant largely used in personal care products as hair conditioners.

In this chapter, we have deeply investigated the physico-chemical properties of rhamnolipid with SLES and CTAC, alternatively, aqueous mixtures at neutral and acidic pH in the bulk solution and at the interface with air, oil and solids with various polarity. Our results can be interpreted on the basis of the different molecular features of the different surfactants.

SLES presents a rather long single tail connected to the sulfate group by a flexible polar ethoxylic linker. Rha is a mixture of rhamnolipids, being the double-tailed mono-rhamnolipid the prevalent species. Thus, it prevalently presents two rather short tails linked to a bulky and sterically hindered headgroup including the saccharide moiety and one carboxylic group. Compared to SLES, the HLB indicates that Rha is much more hydrophobic than SLES and the *pp* predicts that Rha will form supramolecular aggregates with lower curvature. In agreement with these molecular features, our data on the two binary systems confirm that Rha self-aggregates at a concentration lower by almost one order of magnitude compared to SLES and that SLES forms small spherical aggregates while in the case of Rha large cylindrical micelles co-exist with vesicles. Rha micelles are characterized by a viscous inner core, as expected for double-tailed surfactants. In contrast, the packing of the bulky headgroups at the micelle interface is sterically hindered. On the other hand, SLES micelles present a compact external layer, likely due to the ion-dipole interaction between the sulfates and the neighboring ethoxylic chains.

For what concerns the ternary system, our results show that Rha and SLES form mixed micelles in the whole composition range. Significant deviations from the ideal mixing are found, pointing to antagonistic Rha-SLES interactions within the aggregates. Being both negatively charged, this evidence cannot be ascribed to electrostatic interactions. Rather, they could be determined by the mismatch between the molecular architecture of the two surfactants, concerning both headgroups and tails. Particularly, Rha headgroups disturb the SLES organization at the micelle interface.

The balance between the different molecular features of SLES and Rha determines the functional behavior of their mixtures in terms of wetting, foamability and emulsion stability. The wettability of planar hydrophobic surfaces increases with the Rha content, due to its low HLB and high *pp*. On the other hand, emulsion stability increases with the SLES content, due to the close packing among the neighboring SLES headgroups and the long hydrophobic tail. Even the foamability improves with increasing the SLES content, due to its fast adsorption at the air/water interface, while decreases with the Rha content, due to the steric and packing constraints of the large headgroup. Thus, the properties of SLES-Rha mixtures can be optimized for each specific task by tuning the mixture composition. Furthermore, these results also indicate that, as an added value of the biosurfactant application in industrial formulations, these molecules exhibit specific properties which derive from their evolutionary fine tuning. Particularly, Rha shows an unexpected ability to participate to radical processes involving electron exchange, thus suggesting its possible anti- or pro-oxidant activity,

which could be of interest in many fields. To complete the study, we analyzed to what extent Rha can be considered eco-sustainable with respect to conventional surfactants, such as SLES. The ecotoxicological profile of Rha is significantly better than that of SLES, even though differences are not dramatic. This result, along with the greener production and the faster biodegradability, fully confirms the biosurfactant eco-sustainability.

Concerning the system composed by monorhamnolipid and CTAC, an in-depth investigation of the physico-chemical properties of mRha-CTAC aqueous mixtures at neutral and acid pH in the bulk solution and at the interface with air and solids with various polarity was performed. Overall, the results were interpreted in a unifying framework based on of the molecular features of the two surfactants. mRha and CTAC mixed micellization is energetically favored at all mixture composition and at both investigated pHs. It is worth noting that CTAC, which bears a positively charged headgroup, could be expected to interact much more favorably with mRha at neutral pH, at which the latter is in anionic form, than at acidic pH, at which mRha is uncharged. However, our results show a comparable synergism in the two conditions, suggesting that electrostatic interactions play a minor role. mRha presents a bulky headgroup which screens and somehow hides the negative charge. Therefore, mixed micellization is rather favored by the better molecular packing in the aggregates upon surfactant mixing, this effect being more evident at acidic pH, at which mRha molecules are tightly packed. This interpretation is supported by DLS data showing larger aggregates in neutral than in acid solution.

The peculiar mRha molecular structure, presenting two alkyl chains and a relatively bulky headgroup, is also responsible for its good wettability. The contact angle between mRha-CTAC solutions and planar surfaces with different hydrophobicity can be reduced by more than 35° by increasing the x_{mRha} , independently of the pH.

Reference

- [1] Johnson P.; Trybala A.; Starov V.; Pinfield V.J., Effect of synthetic surfactants on the environment and the potential for substitution by biosurfactants, *Adv. Colloid Interface Sci.*, 2021, 288, 102340, <https://doi.org/10.1016/j.cis.2020.102340>
- [2] Manga E.B.; Celik P.A.; Cabuk A.; Banat I.M., Biosurfactants: Opportunities for the development of a sustainable future, *Curr. Opin. Colloid Interface Sci.*, 2021, 56, 101514, <https://doi.org/10.1016/j.cocis.2021.101514>
- [3] Sobrinho H.B.S.; Luna J.M.; Rufino R.D.; Porto A.; Sarubbo L.A., Biosurfactants: classification, properties and environmental application, in: J.N. Govil (Ed.), *Recent Developments in Biotechnology*, Studium Press LLC, USA, 2013, pp. 303–330
- [4] Martins P. C.; Martins V. G., Biosurfactant production from industrial wastes with potential remove of insoluble paint, *Int. Biodeterior. Biodegradation*, 2018, 127, 10–16, <https://doi.org/10.1016/j.ibiod.2017.11.005>
- [5] Ghorbani M.; Hosseini M.; Najafpour G.; Hajimohammadi R., Synthesis and characterization of rhamnolipid biosurfactant produced by *Pseudomonas aeruginosa* PTCC 1340 for emulsification of oil sludge in oil storage tank, *Arab. J. Sci. Eng.* 2021, 47, 219-226. <https://doi.org/10.1007/s13369-021-05872-5>.
- [6] Varjani S.J.; Upasani V.N., Evaluation of rhamnolipid production by a halotolerant novel strain of *Pseudomonas aeruginosa*, *Bioresour. Technol.*, 2019, 288, 121577, <https://doi.org/10.1016/j.biortech.2019.121577>
- [7] Varjani S.J.; Upasani V.N., Critical review on biosurfactant analysis, purification and characterization using rhamnolipid as a model biosurfactant, *Bioresour. Technol.*, 2017, 232, 389–397, <http://dx.doi.org/10.1016/j.biortech.2017.02.047>
- [8] Abbasi H.; Noghabi K.A.; Hamed M.M.; Zahiri H.S.; Moosavi-Movahedi A.A.; Amanlou M.; Teruel J.A.; Ortiz A., Physicochemical characterization of a monorhamnolipid secreted by *Pseudomonas aeruginosa* MA01 in aqueous media. An experimental and molecular dynamics study, *Colloids Surf. B*, 2013, 101, 256-265. <http://dx.doi.org/10.1016/j.colsurfb.2012.06.035>
- [9] Radzuan M.N.; Winterburn J.; Banat I., Bioreactor Rhamnolipid Production Using Palm Oil Agricultural Refinery By-Products, *Processes*, 2021, 9, 2037, <https://doi.org/10.3390/pr9112037>
-

- [10] de Freitas Ferreira J.; Vieira E. A.; Nitschke M., The antibacterial activity of rhamnolipid biosurfactant is pH dependent, *Int. Food Res.*, 2019, 116, 737–744, <https://doi.org/10.1016/j.foodres.2018.09.005>
- [11] Rikalović M.G.; Vrvic M.M.; Karadžić I.M., Rhamnolipid biosurfactant from *Pseudomonas aeruginosa* – from discovery to application in contemporary technology, *J. Serb. Chem. Soc.*, 2015, 80, 279–304, <https://doi.org/10.2298/JSC140627096R>
- [12] Esposito R.; Ingenito L.; Cavasso D.; Siciliano A.; Alfieri M.L.; Chiappisi L.; Fragneto G.; Ottaviani M.F.; Guida M.; Paduano L.; D’Errico G., Rhamnolipid–SLES aqueous mixtures: from the molecular self-aggregation to the functional and ecotoxicological properties, *J. Mol. Liq.*, 2022, 367, 120547, <https://doi.org/10.1016/j.molliq.2022.120547>
- [13] Manko D.; Zdziennicka A.; Janczuk B., Adsorption and aggregation activity of sodium dodecyl sulfate and rhamnolipid mixture, *J. Surfact. Deterg.*, 2017, 20, 411–423, <https://doi.org/10.1007/s11743-016-1916-6>
- [14] Chen M.L.; Penfold J.; Thomas R.K.; Smyth T.J.P.; Perfumo A.; Marchant R.; Banat I.M.; Stevenson P.; Parry A.; Tucker I.; Grillo I., Mixing Behavior of the Biosurfactant, Rhamnolipid, with a Conventional Anionic Surfactant, Sodium Dodecyl Benzene Sulfonate, *Langmuir*, 2010, 26, 17958–17968, <https://doi.org/10.1021/la1031834>
- [15] Liu J.; Wang Y.; Li H., Synergistic Solubilization of phenanthrene by mixed micelles composed of biosurfactants and a conventional non-ionic surfactant, *Molecules*, 2020, 25, 4327, <http://dx.doi.org/10.3390/molecules25184327>
- [16] Nahir Haidar C.; Martini G.; Pellegrini Malpiedi L.; Beatriz Nerli B., Rhamnolipids biosurfactants as potential modulators of phase and partitioning behavior in micellar systems of aliphatic alcohol ethoxylate surfactants, *J. Mol. Liq.*, 2020, 309, 113125, <https://doi.org/10.1016/j.molliq.2020.113125>
- [17] Rekiel E.; Zdziennicka A.; Szymczyk K.; Jańczuk B., Thermodynamic analysis of the adsorption and micellization activity of the mixtures of rhamnolipid and surfactin with Triton X-165, *Molecules*, 2022, 27, 3600, <https://doi.org/10.3390/molecules27113600>
- [18] Liley J.R.; Penfold J.; Thomas R.K.; Tucker I.M.; Petkov J.T.; Stevenson P.S.; Banat I.M.; Marchant R.; Rudden M.; Terry A.; Grillo I., Self-assembly in dilute mixtures of non-ionic and

anionic surfactants and rhamnolipid biosurfactants, *J. Colloid Interface Sci.*, 2017, 487, 493–503, <http://dx.doi.org/10.1016/j.jcis.2016.10.071>

[19] Mei Q.-X.; Lai L.; Li S.-J.; Mei P.; Wang Y.-Q.; Ma Q.-L.; Liu Y., Surface properties and phase behavior of Gemini/conventional surfactant mixtures based on multiple quaternary ammonium salts, *J. Mol. Liq.*, 2019, 281, 506–516, <https://doi.org/10.1016/j.molliq.2019.02.126>

[20] Jahan R.; Bodratti A.M.; Tsianou M.; Alexandridis P., Biosurfactants, natural alternatives to synthetic surfactants: Physicochemical properties and applications, *Adv. Colloid Interface Sci.*, 2020, 275, 102061, <https://doi.org/10.1016/j.cis.2019.102061>

[21] Hao J.C.; Hoffmann H., Self-assembled structures in excess and salt-free cationic surfactant solutions, *Curr. Opin. Colloid Interface Sci.*, 2004, 9, 279–293, <http://dx.doi.org/10.1016/j.cocis.2004.06.004>

[22] Marques E.F.; Regev O.; Khan A.; Lindman B., Self-organization of double-chained and pseudodouble-chained surfactants: counterion and geometry effects, *Adv. Colloid Interface Sci.*, 2003, 100, 83–104, [https://doi.org/10.1016/S0001-8686\(02\)00068-4](https://doi.org/10.1016/S0001-8686(02)00068-4)

[23] Kume G.; Gallotti M.; Nunes G., Review on anionic/cationic surfactant mixtures, *J. Surfact. Deterg.*, 2008, 11, 1–11, <https://doi.org/10.1007/s11743-007-1047-1>

[24] Li Z.; Wu H.; Hu Y.; Chen X.; Yuan Y.; Luo Y.; Hou J.; Bai B.; Kang W., Ultra-low interfacial tension biobased and cationic surfactants for low permeability reservoirs, *J. Mol. Liq.*, 2020, 309, 113099, <https://doi.org/10.1016/j.molliq.2020.113099>

[25] Lioi S.B.; Wang X.; Islam M.R.; Danoff E.J.; English D.S., Cationic surfactant vesicles for electrostatic molecular sequestration and separation, *Phys. Chem. Chem. Phys.*, 2009, 11, 9315–9325, <https://doi.org/10.1039/b908523h>

[26] Dhawan V.V.; Nagarsenker M.S., Cationic systems in nanotherapeutics – Biophysical aspects and novel trends in drug delivery applications, *J. Control. Release*, 2017, 266, 331–345, <http://dx.doi.org/10.1016/j.jconrel.2017.09.040>

[27] Ghosh S.; Ray A.; Pramanik N.; Ambade B., Can a cationic surfactant mixture act as a drug delivery vehicle? *C. R. Chim.*, 2016, 19, 951–954, <http://dx.doi.org/10.1016/j.crci.2016.03.020>

- [28] Bramer T.; Dew N.; Edsman K., Pharmaceutical applications for catanionic mixtures, *J. Pharm. Pharmacol.*, 2007, 59, 1319–1334, <http://dx.doi.org/10.1211/jpp.59.10.0001>
- [29] Marqués A.M.; Pérez L.; Farfán M.; Pinazo A., Green surfactants: Production, properties, and application in advanced medical technologies, in: H. Sarma, M.N.V. Prasad (Eds.), *Biosurfactants for a Sustainable Future: Production and Applications in the Environment and Biomedicine*, Wiley, Hoboken, NJ, 2021, pp. 207–243. <https://doi.org/10.1002/9781119671022.ch10>.
- [30] di Gregorio M.C.; Severoni E.; Travaglini L.; Gubitosi M.; Sennato S.; Mura F.; Redondo-Gómez C.; Jover A.; Pavel N.V.; Galantini L., Bile acid derivative-based catanionic mixtures: versatile tools for superficial charge modulation of supramolecular lamellae and nanotubes, *Phys. Chem. Chem. Phys.*, 2018, 20, 18957–18969, <https://doi.org/10.1039/c8cp02745e>
- [31] Fameau A.-L.; Zemb T., Self-assembly of fatty acids in the presence of amines and cationic components, *Adv. Colloid Interface Sci.*, 2014, 207, 43–64, <http://dx.doi.org/10.1016/j.cis.2013.11.017>
- [32] Oliveira I.S.; Pereira C.; Borges E.; do Vale M.L.; Gomes A.C.; Marques E.F., Formation of catanionic vesicles by threonine-derived surfactants and gemini surfactants based on conventional or serine-derived headgroups: designing versatile and cytocompatible nanocarriers, *Soft Matter*, 2021, 17, 7099–7110. <https://doi.org/10.1039/d1sm00766a>
- [33] Mahle A.; Dashaputre N.; DeShong P.; Stein D.C., Catanionic surfactant vesicles as a new platform for probing glycan–protein interactions, *Adv. Funct. Mater.*, 2018, 28, 1706215, <https://doi.org/10.1002/adfm.201706215>
- [34] Thomas G.B.; Rader L.H.; Park J.; Abezgauz L.; Danino D.; DeShong P.; English D.S., Carbohydrate modified catanionic vesicles: Probing multivalent binding at the bilayer interface, *J. Am. Chem. Soc.*, 2009, 131, 5471–5477, <https://doi.org/10.1021/ja8076439>
- [35] Soussan E.; Mille C.; Blanzat M.; Bordat P.; Rico-Lattes I., Sugar-derived tricatener catanionic surfactant: Synthesis, self-Assembly properties, and hydrophilic probe encapsulation by vesicles, *Langmuir*, 2008, 24, 2326–2330, <https://doi.org/10.1021/la702171s>
- [36] Zoller U., *Handbook of Detergents, Part E: Applications*, sixth ed., CRC Press, Taylor & Francis Group, Boca Raton, FL, 2008, <https://doi.org/10.1201/9781420018165>
-

- [37] Zhao F.; Han S.; Zhang Y., Comparative studies on the structural composition, surface/interface activity and application potential of rhamnolipids produced by *Pseudomonas Aeruginosa* using hydrophobic or hydrophilic substrates, *Bioresour. Technol.*, 2020, 295, 122269. <https://doi.org/10.1016/j.biortech.2019.122269>
- [38] Abalos A.; Viñas M.; Sabaté J.; Manresa M.A.; Solanas A.M., Enhanced biodegradation of Casablanca crude oil by a microbial consortium in presence of a rhamnolipid produced by *Pseudomonas aeruginosa* AT10, *Biodegradation.*, 2004, 15, 249–160. <https://doi.org/10.1023/B:BIOD.0000042915.28757.fb>
- [39] İközler B.; Arslan G.; Kıpçak E.; Dirik C.; Çelenk D.; Aktuğlu T.; Helvacı Ş.; Peker S., Surface adsorption and spontaneous aggregation of rhamnolipid mixtures in aqueous solutions, *Colloids Surf. A*, 2017, 519 125–136, <http://dx.doi.org/10.1016/j.colsurfa.2016.06.056>
- [40] Kim S.; Park H.; Kim T., The study on stable emulsion system and selective addition of active ingredient in w/o/w one step multiple emulsion, *J Soc. Cosmet. Scientists Korea*, 1998, 24, 96–102
- [41] Ortona O.; D’Errico G.; Paduano L.; Vitagliano V., Interaction between cationic, anionic, and non-ionic surfactants with ABA block copolymer Pluronic PE6200 and with BAB reverse block copolymer Pluronic 25R4, *J. Colloid Interface Sci.*, 2006, 301, 63–77 <https://doi.org/10.1016/j.jcis.2006.04.041>
- [42] Lomakin A.; Teplow D.B.; Benedek G.B., Quasielastic Light Scattering for Protein Assembly Studies, in: E.M. Sigurdsson (Ed.), *Amyloid Proteins: Methods and Protocols*, vol. 299, Humana Press, Totowa, New Jersey, 2005, <https://doi.org/10.1385/1-59259-874-9:153>
- [43] Zhang H.X.; Annunziata O., Effect of macromolecular polydispersity on diffusion coefficients measured by Rayleigh interferometry, *J. Phys. Chem. B*, 2008, 112, 3633–3643, <https://doi.org/10.1021/jp7104456>
- [44] Lide D.R., *Handbook of Chemistry and Physics*, 84th ed. CRC Press, Boca Raton FL, 2003, <https://doi.org/10.1021/ja0336372>
- [45] Budil D.E.; Lee S.; Saxena S.; Freed J.H., Nonlinear-least-squares analysis of slow-motion EPR spectra in one and two dimensions using a modified Levenberg-Marquardt algorithm, *J. Magn. Reson. A*, 1996, 120, 155–189, <https://doi.org/10.1006/jmra.1996.0113>
-

- [46] Cooper D.G.; Goldenberg B.G., Surface-active agents from two bacillus species, *Appl. Environ. Microbiol.*, 1987, 53, 224–229. <https://doi.org/10.1128/aem.53.2.224-229.1987>
- [47] Fraga A.K.; Rezende D.A.; Santos R.F.; Mansur C.R.E., Method to evaluate foaming in petroleum, *Braz. J. Pet. Gas*, 2011, 5, 25–33. <http://dx.doi.org/10.5419/bjpg2011-0004>
- [48] Kern W., The evolution of silicon wafer cleaning technology, *J. Electrochem. Soc.*, 1990, 137, 1887–1891, <https://doi.org/10.1149/1.2086825>
- [49] Flinn D.H.; Guzonas D.A.; Yoon R.H., Characterization of silica surfaces hydrophobized by octadecyltrichlorosilane, *Colloids Surf. A*, 1994, 87, 163-176. [https://doi.org/10.1016/0927-7757\(94\)80065-0](https://doi.org/10.1016/0927-7757(94)80065-0)
- [50] I.S.O., 11348-3:2007 Water quality — Determination of the inhibitory effect of water samples on the light emission of *Vibrio fischeri* (Luminescent bacteria test) — Part 3: Method using freeze-dried bacteria.
- [51] I.S.O., 8692:2012 Water quality — Fresh water algal growth inhibition test with unicellular green algae.
- [52] I.S.O., 6341:2012 Water quality — Determination of the inhibition of the mobility of *Daphnia magna Straus* (Cladocera, Crustacea) — Acute toxicity test.
- [53] Aoudia M.; Al-Maamari T.; Al-Salmi F., Intramolecular and intermolecular ion–dipole interactions in sodium lauryl ether sulfates (SLES) self-aggregation and mixed micellization with Triton X-100, *Colloids Surf. A*, 2009, 335, 55–61 <https://doi.org/10.1016/j.colsurfa.2008.10.026>.
- [54] Petrović L.; Milinković J.; Fraj J.; Bučko S.; Katona J.; Spasojević L., Study of interaction between chitosan and sodium lauryl ether sulfate, *Colloid Polym. Sci.*, 2017, 295, 2279–2285 <https://doi.org/10.1007/s00396-017-4205-7>
- [55] [56] Desai S.V.; Bhagwat S.S., Synergism and interfacial property study of sodium lauryl ether sulfate and polysorbate 80 at the air–water interface, *J. Surfact. Deterg.*, 2019, 22, 237–247, <http://dx.doi.org/10.1002/jsde.12229>
- [56] [57] Palos Pacheco R.; Kegel L.L.; Pemberton J.E., Interfacial and solution aggregation behavior of a series of bioinspired rhamnolipid congeners Rha-C14-Cx (x = 6, 8, 10, 12, 14), *J. Phys. Chem. B*, 2021, 125, 13585–13596, <https://doi.org/10.1021/acs.jpcc.1c09435>
-

- [57] ~~[58]~~ Dahrazma B.; Mulligan C.N.; Nieh M.-P., Effects of additives on the structure of rhamnolipid (biosurfactant): A small-angle neutron scattering (SANS) study, *J. Colloid Interface Sci.*, 2008, 319, 590–593, <http://dx.doi.org/10.1016/j.jcis.2007.11.045>
- [58] ~~[59]~~ Savignano L.; Fabozzi A.; Vitiello R.; Fornasier M.; Murgia S.; Guido S.; Guida V.; Paduano L.; D’Errico G., Effect of tail branching on the phase behavior and the rheological properties of amine oxide/ethoxysulfate surfactant mixtures, *Colloids Surf. A*, 2021, 613, 126091, <https://doi.org/10.1016/j.colsurfa.2020.126091>
- [59] ~~[60]~~ Song Y.; Lee J.H.; Jung I.; Seo B.; Hwang H., Molecular dynamics simulations of micelle properties and behaviors of sodium lauryl ether sulfate penetrating ceramide and phospholipid bilayers, *J. Phys. Chem. B*, 2020, 124, 5919–5929, <https://doi.org/10.1016/j.colsurfa.2020.126091>
- [60] ~~[61]~~ Luft C.M.; Munusamy E.; Pemberton J.E.; Schwartz S.D., A classical molecular dynamics simulation study of interfacial and bulk solution aggregation properties of dirhamnolipids, *J. Phys. Chem. B*, 2020, 124 814–827, <https://dx.doi.org/10.1021/acs.jpcc.9b08800>
- [61] ~~[62]~~ Tedeschi A.M.; D’Errico G.; Busi E.; Basosi R.; Barone V., Micellar aggregation of sulfonate surfactants studied by electron paramagnetic resonance of a cationic nitroxide: an experimental and computational approach, *Phys. Chem. Chem. Phys.*, 2002, 4, 2180–218, <https://dx.doi.org/10.1039/b106833d>
- [62] ~~[63]~~ Sanjivkumar M.; Deivakumari M.; Immanuel G., Investigation on spectral and biomedical characterization of rhamnolipid from a marine associated bacterium *Pseudomonas aeruginosa* (DKB1), *Arch. Microbiol.*, 2021, 203, 2297–2314, <https://doi.org/10.1007/s00203-021-02220-x>
- [63] ~~[64]~~ Sagstuen E.; Lindgren M.; Lund A., Electron trapping and reactions in rhamnose by ESR and ENDOR, *Radiat. Res.*, 1991, 128, 235–242, <https://doi.org/10.2307/3578045>
- [64] ~~[65]~~ Kogan A.; Rozner S.; Mehta S.; Somasundaran P.; Aserin A.; Garti N.; Ottaviani M.F., Characterization of the non-ionic microemulsions by EPR. I. Effect of solubilized drug on nanostructure. *J. Phys. Chem. B*, 2009, 113, 691–699. <https://doi.org/10.1021/jp807161g>
- [65] ~~[66]~~ Esposito R.; Cavasso D.; Niccoli M.; D’Errico G., Phase inversion and interfacial layer microstructure in emulsions stabilized by glycosurfactant mixtures, *Nanomaterials*, 2021, 11, 331, <https://doi.org/10.3390/nano11020331>
-

- [66] Kieber M.; Ono T.; Oliver R.C.; Nyenhuis S.B.; Tieleman D.P.; Columbus L., The fluidity of phosphocholine and maltoside micelles and the effect of CHAPS, *Biophys. J.*, 2019, 116, 1682–1691, <https://doi.org/10.1016/j.bpj.2019.03.019>
- [67] Lewinska A.; Wilk K.A.; Jezierski A., Characterization of the microenvironments of alkylamidoamine-N-oxide surfactant aggregates by the EPR spin labeling method, *J. Solution Chem.*, 2012, 41, 1210–1223. <https://doi.org/10.1007/s10953-012-9859-7>
- [68] Santiago P.S.; de Sousa Neto D.; Barbosa L.R.S.; Itri R.; Tabak M., CTAC micelles investigated by small angle X-ray scattering (SAXS) and electron paramagnetic resonance (EPR), *J. Colloid Interface Sci.*, 2007, 316, 730–740, <https://doi.org/10.1016/j.jcis.2007.08.010>
- [69] Shinoda K.; Hutchinson E., Pseudo-phase separation model for thermodynamic calculations on micellar solutions, *J. Phys. Chem.*, 1962, 66, 577–582, <https://doi.org/10.1021/j100810a001>
- [70] Clint J.H., Micellization of mixed nonionic surface active agents, *J. Chem. Soc., Faraday Trans. 1*, 1975, 71, 1327–1334, <http://dx.doi.org/10.1039/F19757101327>
- [71] Holland P. M.; Rubingh D. N., Nonideal multicomponent mixed micelle model, *J. Phys. Chem.*, 1983, 87, 1984–1990. <https://doi.org/10.1021/j100234a030>
- [72] Ren Z.H.; Huang J.; Zheng Y.C.; Lai L.; Hu L.L., Effect of isopropanol on the micellization of binary mixture containing amino sulfonate amphoteric surfactant in aqueous solution: Mixing with octylphenol polyoxyethylene ether (7), *J. Mol. Liq.*, 2017, 236, 101–106, <http://dx.doi.org/10.1016/j.molliq.2017.03.083>
- [73] Ren Z.; Luo Y.; Shi D., Mechanism on the interaction between amino sulfonate amphoteric surfactant and sodium dodecyl benzene sulfonate in aqueous solution, *Colloids Surf. A*, 2013, 428, 18–24, <http://dx.doi.org/10.1016/j.colsurfa.2013.03.036>
- [74] Maeda H.; Muroi S.; Ishii M.; Kaimoto H.; Kakehashi R.; Nakahara T.; Motomoura K., Effects of ionization on the critical micelle concentration and the surface excess of dodecyl dimethylamine oxide in salt solutions, *J. Colloid Interface Sci.*, 1995, 175, 497–505, <https://doi.org/10.1006/jcis.1995.1481>
- [75] Zdziennicka A.; Krawczyk J.; Jańczuk B., Volumetric properties of rhamnolipid and surfactin at different temperatures, *J. Mol. Liq.*, 2018, 255, 562–571, <https://doi.org/10.1016/j.molliq.2018.02.015>
-

- [76] Buwalda R.; Engberts J.B.F.N.; Høiland H.; Blandamer M.J., Volumetric properties and compressibilities of alkyltrimethylammonium bromides and sodium alkylsulphates in aqueous solution, *J. Phys. Org. Chem.*, 1998, 11, 59–62, [https://doi.org/10.1002/\(SICI\)1099-1395\(199801\)11:1<59::AID-POC971>3.0.CO;2-1](https://doi.org/10.1002/(SICI)1099-1395(199801)11:1<59::AID-POC971>3.0.CO;2-1)
- [77] Ambrosone L.; Costantino L.; D’Errico G.; Vitagliano V., Density and viscosity studies of poly(ethylene-oxide) alkyl alcohols, *J. Solution Chem.*, 1996, 25, 757–772, <http://dx.doi.org/10.1007/BF00973783>
- [78] Juskiewicz A.; Antosiewicz J., Ultrasonic velocity studies on carbohydrates in aqueous ethanolic solutions, *Z. Phys. Chem.*, 1986, 148, 185–195, <https://doi.org/10.1524/zpch.1986.148.2.185>
- [79] Liang T.; Walsh T.R., Molecular dynamics simulations of peptide carboxylate hydration, *Phys. Chem. Chem. Phys.*, 2006, 8, 4410–4419, <https://doi.org/10.1039/B608672A>
- [80] Ambrosone L.; Costantino L.; D’Errico G.; Vitagliano V., Thermodynamic and dynamic properties of micellar aggregates of nonionic surfactants with short hydrophobic tails, *J. Colloid Interface Sci.*, 1997, 190, 286–293, <https://doi.org/10.1006/jcis.1997.4860>
- [81] Mangiapia G.; Ricciardi R.; Auriemma F.; De Rosa C.; Lo Celso F.; Triolo R.; Heenan R.K.; Radulescu A.; Tedeschi A.M.; D’Errico G.; Paduano L., Mesoscopic and microscopic investigation on poly(vinyl alcohol) hydrogels in the presence of sodium decylsulfate, *J. Phys. Chem. B*, 2007, 111, 2166–2173, <https://doi.org/10.1021/jp0663107>
- [82] Pandya N.; Rajput G.; Janni D.S.; Subramanyam G.; Ray D.; Aswal V.; Varade D., SLES/CMEA mixed surfactant system: Effect of electrolyte on interfacial behavior and microstructures in aqueous media, *J. Mol. Liq.*, 2021, 325, 115096, <https://doi.org/10.1016/j.molliq.2020.115096>
- [83] Blagojević S.M.; Erić N.; Nešović M.; Blagojević S.N., Micellization and foamability of sodium laureth sulfate and polysorbate surfactant mixtures, *Russ. J. Phys. Chem. A*, 2019, 93, 2804–2811, <https://doi.org/10.1134/S0036024419130053>
- [84] Blagojević S.M.; Pejić N.D.; Blagojević S.N., Synergism and physicochemical properties of anionic/amphoteric surfactant mixtures with nonionic surfactant of amine oxide type, *Russ. J. Phys. Chem. A*, 2017, 91, 2690–2695, <https://doi.org/10.1134/S0036024417130064>

- [85] Ciccarelli D.; Costantino L.; D'Errico G.; Paduano L.; Vitagliano V., Mixed micellar aggregates of anionic and non-ionic surfactants with short hydrophobic tails. A PGSE-NMR study, *Langmuir*, 1998, 14, 7130–7139, <https://doi.org/10.1021/la9804583>
- [86] Vergara A.; Paduano L.; D'Errico G.; Sartorio R., Network formation in polyethyleneglycol solutions. An intradiffusion study, *Phys. Chem. Chem. Phys.*, 1999, 1, 4875–4879, <https://doi.org/10.1039/A905035C>
- [87] D'Errico G., On the segregative tendency of ethoxylated surfactants in non-ionic mixed micelles, *Langmuir*, 2011, 27, 3317–3323, <https://doi.org/10.1021/la1039283>
- [88] El-Dossoki F.I.; Gomaa E.A.; Hamza O.K., Solvation thermodynamic parameters for sodium dodecyl sulfate (SDS) and sodium lauryl ether sulfate (SLES) surfactants in aqueous and alcoholic-aqueous solvents, *SN Appl. Sci.*, 2019, 1, 933, <https://doi.org/10.1007/s42452-019-0974-6>
- [89] Manko D.; Zdziennicka A.; Janczuk B., Composition of surface layer at the water–air interface and micelles of Triton X-100 + Rhamnolipid mixtures, *J. Solution Chem.*, 2017, 46, 1251–1271, <http://dx.doi.org/10.1007/s10953-017-0642-7>
- [90] Song D.; Li Y.; Liang S.; Wang J., Micelle behaviors of sophorolipid/rhamnolipid binary mixed biosurfactant systems, *Colloids Surf. A*, 2013, 436, 201–206, <http://dx.doi.org/10.1016/j.colsurfa.2013.06.011>
- [91] Song D.; Liang S.; Yan L.; Shang Y.; Wang X., Solubilization of polycyclic aromatic hydrocarbons by single and binary mixed rhamnolipid–sophorolipid biosurfactants, *J. Environ. Qual.*, 2016, 45, 1405–1412, <http://dx.doi.org/10.2134/jeq2015.08.0443>
- [92] Peker S.; Helvacı S.; Özdemir G., Interface-subphase interactions of rhamnolipids in aqueous rhamnose solutions, *Langmuir*, 2003, 19, 5838–5845, <http://dx.doi.org/10.1021/la0269964>
- [93] Hinz H.-J.; Kuttnerreich H.; Meyer R.; Renner M.; Fründ R.; Koynova R.; Boyanov A.I.; Tenchov B.G., Stereochemistry and size of sugar head groups determine structure and phase behavior of glycolipid membranes: Densitometric, calorimetric, and X-ray studies, *Biochemistry*, 1991, 30, 5125–5138, <https://doi.org/10.1021/bi00235a003>
- [94] Ananthapadmanabhan K.; Moore D.J.; Subramanyan K.; Misra M.; Meyer F., Cleansing without compromise: the impact of cleansers on the skin barrier and the technology of mild cleansing, *Dermatol. Ther.*, 2004, 17, 16–25, <https://doi.org/10.1111/j.1396-0296.2004.04s1002.x>
-

- [95] Takagi Y.; Shimizu M.; Morokuma Y.; Miyaki M.; Kiba A.; Matsuo K.; Isoda K.; Mizutani H., A new formula for a mild body cleanser: sodium laureth sulphate supplemented with sodium laureth carboxylate and lauryl glucoside, *Int. J. Cosmet.*, 2014, 36, 305–311, <https://doi.org/10.1111/ics.12127>
- [96] Lovaglio R.B.; dos Santos F.J.; Jafelicci Junior M.; Contiero J., Rhamnolipid emulsifying activity and emulsion stability: pH rules, *Colloids Surf. B: Biointerfaces*, 2011, 85, 301–305. <https://doi.org/10.1016/j.colsurfb.2011.03.001>
- [97] Pornsunthorntawe O.; Wongpanit P.; Chavadej S.; Abe M.; Rujiravanit R., Structural and physicochemical characterization of crude biosurfactant produced by *Pseudomonas aeruginosa* SP4 isolated from petroleum-contaminated soil., *Bioresour Technol.*, 2008, 99, 1589–1595. <https://doi.org/10.1016/j.biortech.2007.04.020>
- [98] Alizadeh S.; Suleymani M., A mechanistic study of emulsion flooding for mobility control in the presence of fatty acids: Effect of chain length, *Fuel*, 2020, 276, 118011. <https://doi.org/10.1016/j.fuel.2020.118011>
- [99] Beneventi D.; Carre B.; Gandini A., Role of surfactant structure on surface and foaming properties, *Colloids Surf. A: Physicochem. Eng. Aspects*, 2001, 189, 65–73. [https://doi.org/10.1016/S0927-7757\(01\)00602-1](https://doi.org/10.1016/S0927-7757(01)00602-1)
- [100] Wu L-M; Lai L.; Lu Q.; Mei P.; Wang Y.-Q.; Cheng L.; Liu Y., Comparative studies on the surface/interface properties and aggregation behavior of mono-rhamnolipid and di-rhamnolipid, *Colloids Surf. B: Biointerfaces*, 2019, 181, 593–601, <https://doi.org/10.1016/j.colsurfb.2019.06.012>
- [101] Chen M.L.; Penfold J.; Thomas R.K.; Smyth T.J.P.; Perfumo A.; Marchant R.; Banat I.M.; Stevenson P.; Parry A.; Tucker I.; Grillo I., Solution self-assembly and adsorption at the air-water interface of the monorhamnolipid and dirhamnolipid and their mixtures, *Langmuir*, 2010, 26, 18281–18292, <https://doi.org/10.1021/la1031812>
- [102] Liley J.R.; Thomas R.K.; Penfold J.; Tucker I.M.; Petkov J.T.; Stevenson P.S.; Banat I.M.; Marchant R.; Rudden M.; Webster J.R.P., Adsorption at the air–water interface in biosurfactant–surfactant mixtures: quantitative analysis of adsorption in a five-component mixture. *Langmuir*, 2017, 33, 13027–13039, <https://doi.org/10.1021/acs.langmuir.7b03187>

- [103] Zdziennicka A.; Jańczuk B., Wetting and adhesion properties of rhamnolipid and surfactin, *Int. J. Adhes. Adhes.*, 2018, 84, 275–282. <https://doi.org/10.1016/j.ijadhadh.2018.04.005>
- [104] Özdemir G.; Malayoglu U., Wetting characteristics of aqueous rhamnolipids solutions, *Colloids Surf. B*, 2004, 39, 1–7, <https://doi.org/10.1016/j.colsurfb.2004.08.006>
- [105] Costa S.G.V.A.O.; de Souza S.R.; Nitschke M.; Franchetti S.M.M.; Jafelicci Jr M.; Lovaglio R.B.; Contiero J., Wettability of aqueous rhamnolipids solutions produced by *Pseudomonas aeruginosa* LBI, *J. Surfact. Deterg.*, 2009, 12, 125–130. <https://doi.org/10.1007/s11743-008-1102-6>
- [106] Patrolecco L.; Pescatore T.; Mariani L.; Rolando L.; Grenni P.; Finizio A.; Spataro F.; Rauseo J.; Ademollo N.; Muzzini V.G.; Donati E.; Lacchetti I.; Padulosi S.; Barra Caracciolo A., Environmental fate and effects of foaming agents containing sodium lauryl ether sulphate in soil debris from mechanized tunneling. *Water*, 2020, 12, 2074. <https://doi.org/10.3390/w12082074>
- [107] Finizio A.; Patrolecco L.; Grenni P.; Galli E.; Muzzini V.G.; Rauseo J.; Rizzi C.; Barra Caracciolo A., Environmental risk assessment of the anionic surfactant sodium lauryl ether sulphate in site-specific conditions arising from mechanized tunnelling, *J. Hazard. Mater.*, 2020, 383, 121116. <https://doi.org/10.1016/j.jhazmat.2019.121116>
- [108] Baderna D.; Lomazzi E.; Passoni A.; Pogliaghi A.; Ifigeneia Petoumenou M.; Bagnati R.; Lodi M.; Viarengo A.; Sforzini S.; Benfenati E.; Fanelli R., Chemical characterization and ecotoxicity of three soil foaming agents used in mechanized tunneling, *J. Hazard. Mater.*, 2015, 296, 210-220. <https://doi.org/10.1016/j.jhazmat.2015.04.040>
- [109] Lopes C.S.C.; Teixeira D.B.; Braz B.F.; Santelli R.E.; de Castilho L.V.A.; Gomez J.G.C.; Castro R.P.V.; Seldin L.; Freire D.M.G., Application of rhamnolipid surfactant for remediation of toxic metals of long- and short-term contamination sites, *Int. J. Environ. Sci. Technol.*, 2021, 18, 575–588. <https://doi.org/10.1007/s13762-020-02889-5>
- [110] Wei Z.; Wang J.J.; Meng Y.; Li J.; Gaston L.A.; Fultz L.M.; DeLaune R.D., Potential use of biochar and rhamnolipid biosurfactant for remediation of crude oil-contaminated coastal wetland soil: Ecotoxicity assessment, *Chemosphere*, 2020, 253, 126617. <https://doi.org/10.1016/j.chemosphere.2020.126617>

- [111] Johann S.; Seiler T.B.; Tiso T.; Bluhm K.; Blank L.M.; Hollert H., Mechanism-specific and whole-organism ecotoxicity of mono-rhamnolipids, *Sci. Total Environ.*, 2016, 548–549, 155–163. <http://dx.doi.org/10.1016/j.scitotenv.2016.01.066>
- [112] Hammer J.; Tukker A.M.; Postma J.F.; Haftka J.J.-H.; Hermens J.L.M.; de Voogt P.; Kraak M.H.S., Solubility constraints on aquatic ecotoxicity Testing of anionic surfactants, *Bull. Environ. Contam. Toxicol.*, 2018, 101, 99-104. <https://doi.org/10.1007/s00128-018-2361-1>
- [113] Manko D.; Zdziennicka A.; Janczuk B., Thermodynamic properties of rhamnolipid micellization and adsorption, *Colloids Surf. B*, 2014, 119, 22–29, <https://doi.org/10.1016/j.colsurfb.2014.04.020>
- [114] Zhou Z.; Xu J.; Zhu S.; Yu W.; Li J.; Li J.; Wang B.; Chen K., A design with natural polysaccharide particles and cationic conditioning agent as efficient emulsifier for hair care, *Carbohydr. Polym.*, 2022, 286, 119311, <https://doi.org/10.1016/j.carbpol.2022.119311>
- [115] Colafemmina G.; Palazzo G.; Mateos H.; Amin S.; Fameauc A.-L.; Olsson U.; Gentile L., The cooling process effect on the bilayer phase state of the CTAC/cetearyl alcohol/water surfactant gel, *Colloids Surf. A*, 2020, 597, 124821, <https://doi.org/10.1016/j.colsurfa.2020.124821>
- [116] Russo Krauss I.; Imperatore R.; De Santis A.; Luchini A.; Paduano L.; D’Errico G., Structure and dynamics of cetyltrimethylammonium chloride-sodium dodecylsulfate (CTAC-SDS) catanionic vesicles: High-value nano-vehicles from low-cost surfactants, *J. Colloid Interface Sci.*, 2017, 501, 112–122, <http://dx.doi.org/10.1016/j.jcis.2017.04.032>
- [117] Pota G.; Vitiello G.; Venezia V.; Della Sala F.; Borzacchiello A.; Costantini A.; Paduano L.; Cavalcanti L.P.; Tescione F.; Silvestri B.; Luciani G., Shall We Tune? From Core-Shell to Cloud Type Nanostructures in Heparin/Silica Hybrids. *Polymers*. 2022, 14, 3568. <https://doi.org/10.3390/polym14173568>
- [118] El-Dossoki F.I.; Gomaa E.A.; Hamza O.K., Solvation thermodynamic parameters for alkyl benzyl dimethyl ammonium chloride and cetyl trimethyl ammonium chloride surfactants in water and alcoholic-water solvents, *J. Chem. Eng. Data*, 2019, 64, 4482–4492, <https://doi.org/10.1021/acs.jced.9b00527>

[119] Aswal V. K.; Goyal P. S., Counterions in the growth of ionic micelles in aqueous electrolyte solutions: A small-angle neutron scattering study, *Phys. Rev. E* 61 (2000) 2947, <https://doi.org/10.1103/PhysRevE.61.2947>

[120] C. Tanford, Micelle shape size, *J. Phys. Chem.*, 1972, 26, 30200.

Chapter V

5. Micellization of rhamnolipids in water/bioglycerol co-solvent mixtures

Co-solvents are compounds of various kinds, which, added to the solvent, generally water, modify its properties [1]. The reasons why co-solvents are used are several, but the main one is linked to the solubility of hydrophobic solutes in aqueous solution, just as an example. It has been seen in different studies that a co-solvent (usually termed hydrotrope) can enhance this solubility, in order to adapt the system to the conditions required for a specific chemical process [2] or application [3,4].

Moreover, a co-solvent can also be used to regulate the aggregation of solutes: always acting on solubility, they can promote aggregation of compounds, which could influence the mixture functionality [1,5].

5.1. Bio-Glycerol

Given the urgent need for new technologies and green alternatives in the cosmetic field to reduce or eliminate the use of substances obtained starting from fossil sources as raw materials, the interest of scientists and technologists is increasingly directed towards chemicals obtained from renewable sources, able to conjugate environmental and human health benefits [6].

In the present work of thesis, the behavior of rhamnolipids, natural products of bacterial metabolism, is evaluated in the presence of different contents of bio-glycerol, a by-product of different industrial processes conducted by NICL (Naples Industrial Chemistry Laboratory) group of the University of Naples Federico II on pilot plants.

Bio-glycerol is obtained during the production of biodiesel fuel, based on a transesterification reaction in which there is an interchange between the glycerides and an alcohol. The traditional process comprises a transesterification reaction between methanol and vegetable oil catalyzed by KOH. The reaction product is a mixture of biodiesel and a glycerol-methanol solution. Through centrifugation, glycerol traces are eliminated from the oil. The mixture of glycerol, methanol, water, catalyst residues, free fatty acids, unreacted mono-, di- and triglycerides, methyl esters and other MONG (Matter Organic Non-Glycerol) obtained as side product can be distilled to lead glycerol which meets

the standards for cosmetic applications [7]. The prefix bio- means that glycerol has been obtained by natural sources as glycerides.

The use of bio-glycerol reduces the costs of production and it represents an economic gain. Therefore, this can be considered as an example of circular economy where a by-product of a process can be the raw material for a new process. Circular economy represents a new industrial strategy, which is based on sharing and recycle of materials. The development of this economic model is necessary because of the increased demand of raw materials and, on the other hand, to the shortage of them. So, eco-design and materials re-use are the principles on which the fine industry will have to be based in the future [8].

In this scenario, the combined use of rhamnolipids and bio-glycerol in formulations could lead to environmental, economic and human benefits.

5.1.1. Glycerol in formulations and its effect on surfactant micellization

Glycerol is an organic molecule, the polyol 1,2,3-propanetriol, which is stabilized in aqueous phase by the intramolecular hydrogen bonds and intermolecular solvation of the hydroxyl groups. It was discovered in 1779 by the Swedish chemist Carl W. Scheele and it is one of the most commonly used compounds in fine chemistry. The main advantage of the use of glycerol in formulations is its non-toxicity, non-irritability, stability, miscibility, and high compatibility. The latter property is very important in the formulations field and, in particular, for pharmaceutical and cosmetic applications. Indeed, glycerol can be used as solvent or co-solvent, humectant, emollient and it can also control water activity [7].

Its surface tension is 63.4 dyn cm^{-1} at $20 \text{ }^\circ\text{C}$, lower than that of water, which is 72.5 dyn cm^{-1} . When glycerol is added in aqueous solution at increasing concentrations, it causes a reduction of water chemical potential. By using the Gibbs's isotherm adsorption equation, it appears that glycerol surface excess is independent of alcohol content [9].

The wide use of glycerol in fine industry is due to its environmental friendliness. Indeed, because of its low vapor pressure and the lack of odor, it is considered not dangerous for wastewater. It is employed as a solvent in food industry to prepare flavor extracts, i.e., vanillin and spices; it is, also, applied as preservative for fruits and vegetables. In pharmaceutical industry it is used in ointments,

parental solutions and also in capsules and suppositories. Another application of glycerol is as solvent for tobacco, hydraulic fluid formulations and it also applied in paper industry [10].

In cosmetic industry glycerol is present in the personal care products as shaving creams, soaps, skin and hair care formulations. The 28% of the glycerol market is represented by cosmetic, pharmaceutical and toothpaste products [7].

Since surfactants and glycerol are both used in large scale in aqueous formulations, the behavior of the surfactants in the presence of glycerol as co-solvent is of great interest. In different studies the effect of glycerol on the micellization of various surfactants is investigated.

The work conducted by Ruiz et al. in 2007 underlines that the micellization of cationic surfactants such as alkyl trimethyl ammonium bromides is not affected by the presence of glycerol up to 20 wt%: apparently the systems seem to contain only water as solvent. A further increase in glycerol content leads to a slight increase of the *critical micelle concentration (cmc)* and a decrease of the aggregation number. According to the authors, this effect is controlled by the increasing of the surface area per surfactant headgroup due to the participation of the co-solvent in the solvation of the micellized surfactant. To understand this effect, the thermodynamics parameters should be considered. In particular, the micellization is influenced by the enthalpic and entropic contributions through the following equation:

$$\Delta G_{mic}^0 = \Delta H_{mic}^0 - T\Delta S_{mic}^0 \quad \text{Equation 1}$$

ΔH_{mic}^0 is ascribed to the variation of hydrogen bond number and electrostatic interaction strength. According to these authors, the negative value of enthalpy variation is given by the prevalence of the London-force dispersion in the micellar process. The analysis of $T\Delta S_{mic}^0$ value provides more information given that its value is positive and larger than ΔH_{mic}^0 both in water and in the presence of 20 wt% glycerol. The results suggest that the hydrophobic effect is predominant in glycerol-poor formulations. Indeed, the solubility of the hydrophobic tail is unfavored because of the ordered disposition of water molecules around the surfactant tails, which leads to consequentially $\Delta S_{mic}^0 > 0$. So, $\Delta G_{mic}^0 < 0$ and the micellar process is favored. When glycerol content increases, the micellization is controlled by enthalpic term because the hydrophobic effect decreases, the solubility of hydrophobic moiety is favored due to reduction of polarity of the solvent. In this way, $\Delta G_{mic}^0 < 0$ even if it is less negative than in aqueous solution, as shown by the *cmc* increase [11].

D'Errico and coworkers highlighted the glycerol effects on the water structure. They assume that there are structure-breakers compounds which allow a reduction of the number of hydrogen bonds, and structure-makers compounds which promote the hydrogen bonds in aqueous phase. In this scenario, glycerol presents a structure-makers behavior. Thus, the addition of the alcohol in aqueous phase causes the increase of the *cmc* because the micellization driving force decreases. The glycerol effect on the micellization of ionic surfactants can be interpreted as due to a modulation of the electrostatic repulsion due to the reduction of the dielectric constant, while for nonionic ethoxylated surfactants the water structuring effect of glycerol prevails [12].

A similar effect is also confirmed by Ruiz et.al 2008. In their work these authors affirm that the *cmc* increase is due to a reduction of cohesive energy density which increases the solubility of the surfactant. Glycerol increases the electrostatic repulsion of the headgroups, and improves the solvation of the hydrophobic tails, opposing to micellization. Moreover, the presence of alcohol causes the formation of smaller micelles [13].

Carnes et al. analyzed the effect of glycerol in the presence of the nonionic biosurfactant *Plantcare 2000*. They showed that the addition of the alcohol from 0 to 70 wt% in aqueous formulation causes a slight increase of the *cmc* value, from 3×10^{-3} M to 8×10^{-3} M, while the surface tension of micellar solutions presents a fixed value around 29 mN/m independently of the glycerol concentration. The almost constant value of surface tension is justified due to the salting-out effect, which causes the competition between glycerol and surfactant for water molecules. This effect is the responsible of the dehydration of the ethoxylic surfactant head groups [14].

Considering that the biosurfactants used in this project, rhamnolipids, present a negative charge at neutral pH, it is interesting to consider the work of Khan et al. in which they analyze glycerol effect on SDS micellization. This work reports a minimum of the *cmc* value when glycerol content is around 20 wt%, while above 40 wt% the *cmc* value increases exponentially. The initial decrease depends on a reduction of water hydrogen bonds favored by the interactions with glycerol molecules. Above 30 wt% alcohol the cohesive energy, the dielectric constant and the polarity of the solvent decrease. In this condition the solubility of the hydrophobic moieties and the electrostatic repulsion between the headgroups increase [15].

5.2. Materials and samples preparation

The rhamnolipid sample employed in the present work was purchased from AGAE Technologies (Corvallis, OR, USA) and it is the same used in Chapter 4, described in 4.1.1 subsection. The bioglycerol was kindly provided by the NICL (Naples Industrial Chemistry Laboratory) group of the University of Naples Federico II. All sample mixtures were prepared using ultrapure deionized water from a Millipore Milli-Q system with an electrical conductivity less than $1 \times 10^{-6} \text{ S cm}^{-1}$ at 25 °C. The pH was buffered at 7.1 ± 0.2 using sodium dihydrogen phosphate hydrate ($\text{NaH}_2\text{PO}_4 \cdot \text{H}_2\text{O}$, purity >99%) and disodium hydrogen phosphate anhydrous (Na_2HPO_4 , purity >99%), both purchased from Sigma-Aldrich (Milan, Italy). Buffer concentration was maintained as low as possible to minimize the effect the increased ionic strength on the measured physico-chemical parameter. For this reason, added ion concentration was fixed at ten times the total surfactant concentration (the maximum total concentration in the case of tensiometric titrations).

5.3. Measurements

5.3.1. Tensiometry

The surface tension, γ , of water-Rha and water-Rha-Gly mixtures was determined with a Sigma 70 tensiometer (KSV, Stockholm, Sweden) by the Du Noüy ring method as reported in a previous work [16]. Successive aliquots of ten times the rhamnolipid *cmc* solution were added to the instrument vessel with a known volume of the same buffer used to prepare the surfactant solution. Alternatively, the measurements were carried out at increasing amount of bio-glycerol in the titrating and titrated solutions as fixed percentage in weight (5, 10, 15, 20, 30, 40, 50, 60, 70, 80 wt%) of total liquid. After each aliquot addition, the sample was mixed using a magnetic stirrer and allowed to equilibrate 3 min prior to measuring the surface tension.

5.3.2. Dynamic Light Scattering

Size and distribution of the aggregates were determined by DLS. The procedure was carried out at different percentage content of bio-glycerol (0 wt%, 20 wt%, 40 wt%, 70 wt%) and constant concentration of rhamnolipids. It is to be highlighted that at the first two considered bio-glycerol

contents (20 and 40 wt%) the rhamnolipid *cmc* remains more or less unaltered by the presence of co-solvent, while the third considered bio-glycerol content (70 wt%) refers to a situation in which the *cmc* is significantly increased. In detail, for the binary system at 0 wt% of bio-glycerol, solutions 50, 75, 100, 150, 200 and 300 times the *cmc* (1.1×10^{-4} M) were prepared. When the amount of bio-glycerol was set at 20 wt%, solutions 50, 100, 200 and 300 times the *cmc* of rhamnolipid (0.7×10^{-4} M) were prepared. At 40 wt% of bio-glycerol, solutions 50, 100, 200 and 300 times the *cmc* (1.01×10^{-4} M) were used. Finally, at high content of bio-glycerol, 70 wt%, solutions 100, 200 and 300 times the *cmc* (1.83×10^{-4} M) are analyzed. Measurements were carried out with a home-assembled apparatus as described above in Chapter 4.

5.4. Results and discussion

5.4.1. water-Rha-Gly micellization: surface tension

The surface tension of the systems of biosurfactants in aqueous buffer/co-solvent mixtures was investigated as a function of both rhamnolipid and bio-glycerol concentration. Different sets of measurements were performed. In each set the bio-glycerol concentration was kept constant at a value ranging from 0 to 80 wt%, while the rhamnolipid concentration was progressively increased. Fig. 1 reports the surface tension of the ternary system water-Rha-Gly (pH =7.1) versus the rhamnolipids concentration.

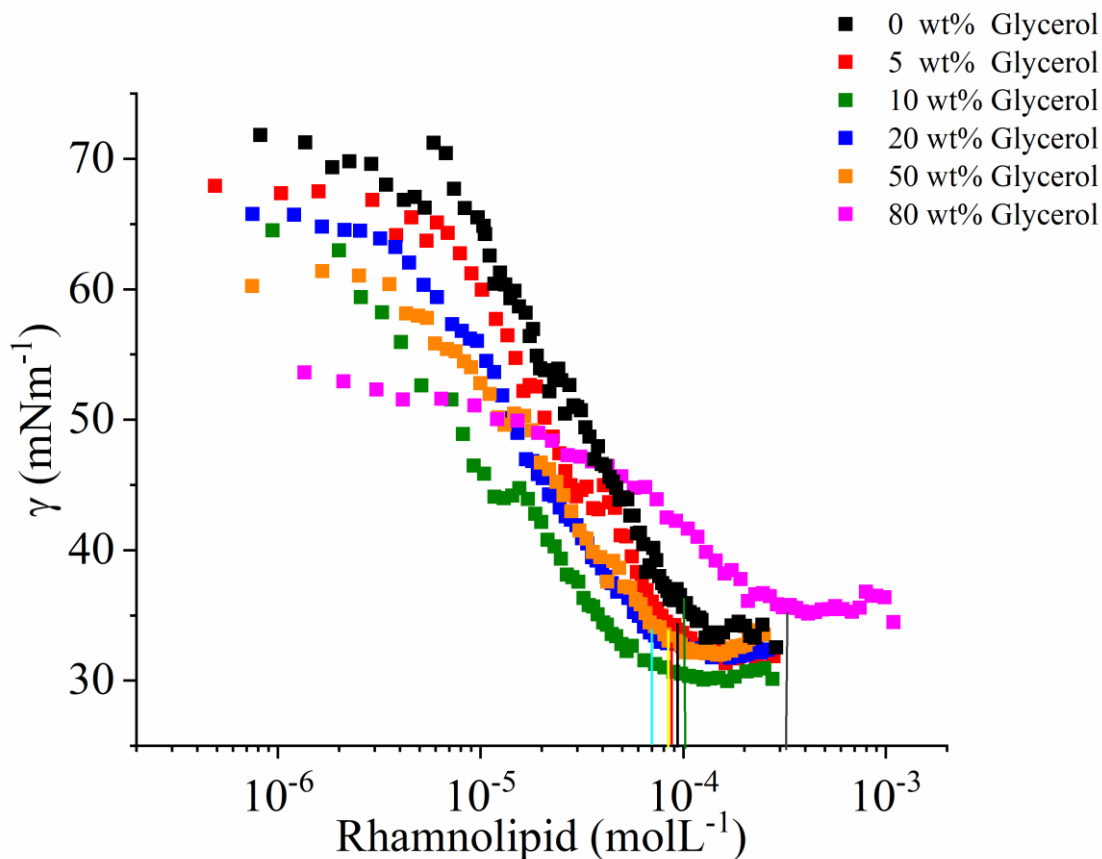


Figure 1. Surface tension versus rhamnolipids concentration for the water-Rha-Gly ($pH=7.1$) system at different percentage of bio-glycerol as reported in legend.

The surface tension value observed in the absence of surfactants ($\sim 72 \text{ mN m}^{-1}$) is coincident with literature values reported for water, thus confirming the reliability of the experimental setup. With increasing of bio-glycerol in the solution, the initial surface tension decreases. In Fig. 1 we can distinguish an initial region, in which only a slight decrease of the surface tension is observed; an intermediate region, in which surface tension sharply decreases; a final plateau, in which the surface tension value can be consider substantially constant. Thus, the first two concentrations regions comprise the premicellar composition range while the last one corresponds to the micellar composition range. From the surface tension we can obtain important experimental parameters which are collected in Table 1.

Table 1. summary of the surface tension results.

System	Glycerol percentual (%wt)	$\gamma_{w/gly}$ (mN m ⁻¹)	cmc^* (μM)	γ_{mic} (mN m ⁻¹)	A (\AA^2)
Rha-buffer	0	70.5	115	33.7 \pm 0.6	66 \pm 1
Rha-buffer-gly	5	71.8	97	32.3 \pm 0.7	70 \pm 2
Rha-buffer-gly	10	59.4	98	30.6 \pm 0.3	83 \pm 2
Rha-buffer-gly	15	73.0	88	33.7 \pm 0.8	75 \pm 2
Rha-buffer-gly	20	66.6	71	32.1 \pm 0.3	75 \pm 2
Rha-buffer-gly	30	70.2	69	33.3 \pm 0.4	67 \pm 2
Rha-buffer-gly	40	70.0	101	34.6 \pm 0.6	76 \pm 2
Rha-buffer-gly	50	62.3	95	32.5 \pm 0.5	90 \pm 2
Rha-buffer-gly	60	57.8	216	31.6 \pm 0.5	151 \pm 6
Rha-buffer-gly	70	53.9	183	35.8 \pm 0.6	132 \pm 7
Rha-buffer-gly	80	53.9	322	35.9 \pm 0.8	159 \pm 5

(*) Where the error on the determination of the cmc has been estimated to be around 10%.

For a better understanding, the experimental parameters are reported in Fig. 2.

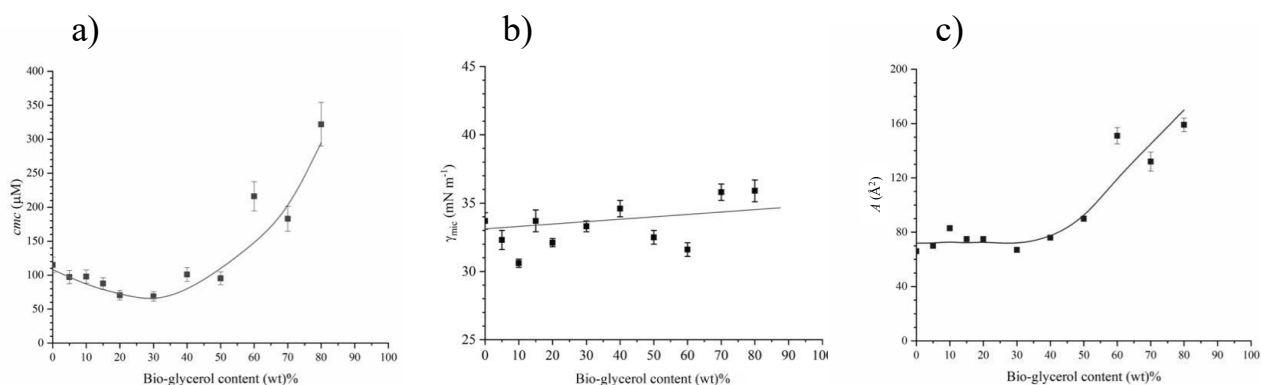


Figure 2. Surface tension parameter obtained from experimental curves: (a) cmc value in function of bio-glycerol wt%; (b) γ_{mic} value in function of bio-glycerol wt%; (c) A value in function of bio-glycerol wt.

In particular, Fig 2(a) figure shows rather limited cmc changes from 0 to 50 wt% of bio-glycerol, while an evident increase is observed at higher co-solvent content. Indeed, a perusal of the data reveals that the cmc reaches a shallow minimum around 25-30 wt% of bio-glycerol. The γ_{mic} data, in Fig.

2(b), are substantially constant, indicating a limited effect of the bio-glycerol on the surface activity exerted by the rhamnolipids. The area occupied by a single molecule of solute at the interface, A , is reported as a function of the bio-glycerol content in Fig. 2(c). Up to 40 wt% A exhibits rather constant values. An evident and pronounced increment of the parameter is observed with increasing the bio-glycerol percent.

The increment in the cmc due to bio-glycerol can be explained in terms of an indirect effect on micellization deriving from modifications of the aqueous medium due to the co-solvent. As detailed in the previous paragraph, the cmc is related to the variation of the Gibbs energy of the system upon surfactant micellization. In the glycerol-poor content systems, the solvent mixtures present properties similar to neat water. Because of the high medium polarity, the solubility of the hydrophobic tails is unfavored because there is a loss of entropy due to the ordered organization of water molecules around them. Consequently, the formation of micellar aggregates, in which the surfactant tails are shielded from the contact with the solvent, is favored ($\Delta G_{mic}^0 < 0$). As the bio-glycerol content increases, the medium polarity decreases favoring solubility of hydrophobic moiety and the hydrophobic effect is depressed. Thus, $\Delta G_{mic}^0 < 0$ but its absolute value is lower than in aqueous solution.

5.4.2. water-Rha-Gly micellization: DLS

Fig. 3, Fig. 4, Fig. 5, and Fig. 6 show the hydrodynamic radius distribution for the samples prepared in absence and presence of bio-glycerol. In panel (a) of all following figures, the data are reported in an intensity-weighted mode. This representation enhances large aggregates, which efficiently scatter the light. The DLS is in principle more sensitive to large objects than to smaller ones, with the intensity proportional to the sixth power of radius, so in panel (b) we converted the intensity-weighted profiles into number-weighted profiles giving us an indication of the concentration of the different aggregates in the sample [17].

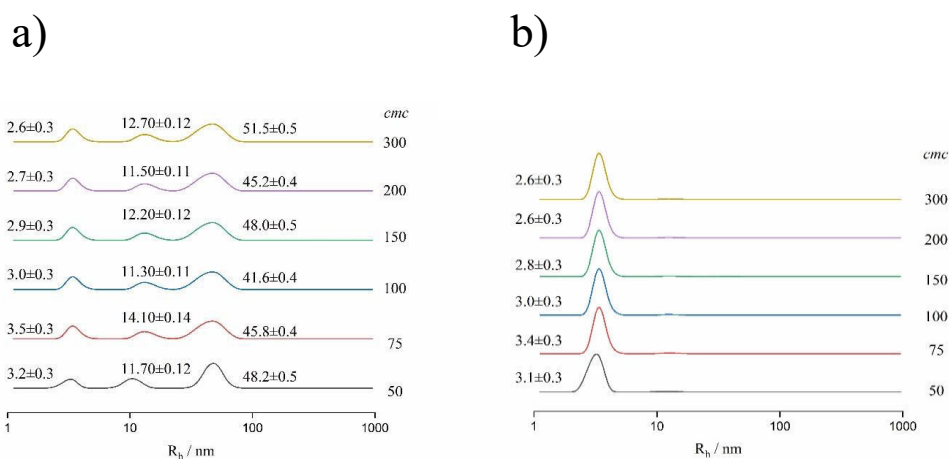


Figure 3. Hydrodynamics radius distributions of rhamnolipid aggregates in the binary system water (pH=7.1, phosphate buffer)/rhamnolipids at 25 °C. Panel (a): intensity-weighted distributions; panel (b): number-weighted distributions.

Inspection of Fig. 3(a) shows the presence of various aggregates in all the considered samples: small aggregates, with an average radius equal to about 3 nm, coexist with two distributions of larger aggregates, whose size is about 10 and 50 nm, respectively. Small aggregates can be confidently classified as almost spherical micelles, while larger aggregates can presumably to be assumed as vesicles or elongated micelles. Fig. 3(b) clearly shows that spherical micelles constitute by far the large majority of the aggregates in the sample.

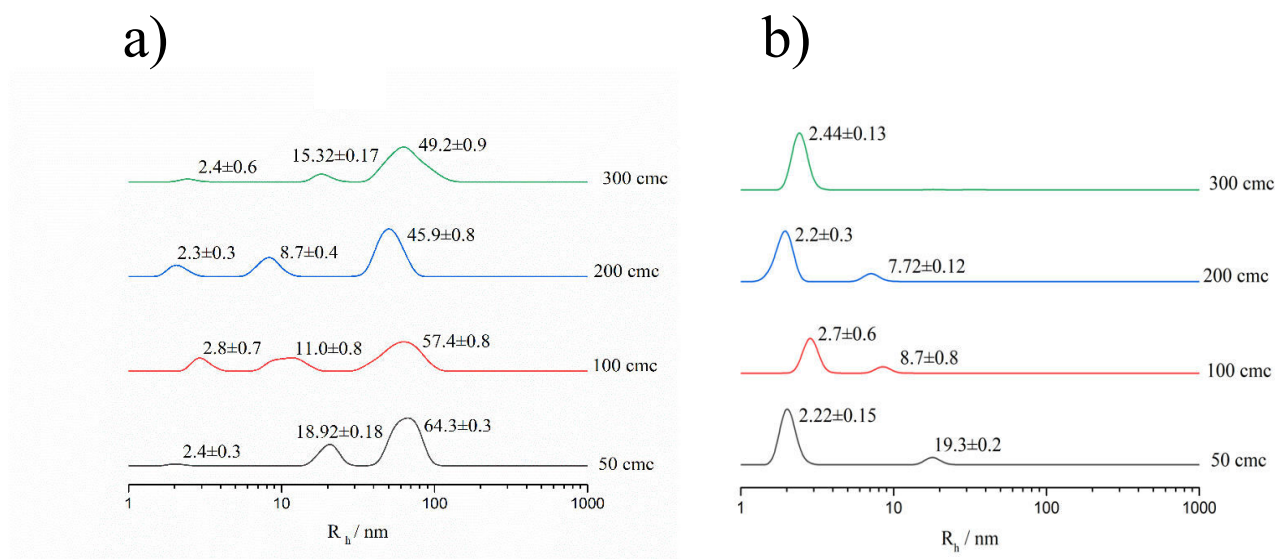


Figure 4. Hydrodynamics radius distributions of rhamnolipid aggregates in the ternary system water (pH=7.1, phosphate buffer)/bio-glycerol (20 wt%)/rhamnolipid at 25 °C. Panel (a): intensity-weighted distributions; panel (b): number-weighted distributions.

Similarly to what observed in the absence of bio-glycerol, Fig. 4(a) shows the presence of various aggregates in all the considered samples at 20wt% bio-glycerol: small micellar aggregates, with an average radius equal to about 2.5 nm, coexist with two distributions of larger aggregates, with a size of around 10 and 50 nm. Fig. 4(b) clearly shows that micelles constitute by far the large majority of the aggregates in the sample even though some larger aggregates are detectable. Indeed, comparison between Fig. 4 and Fig. 3 shows that bio-glycerol enhances the populations with large dimension.

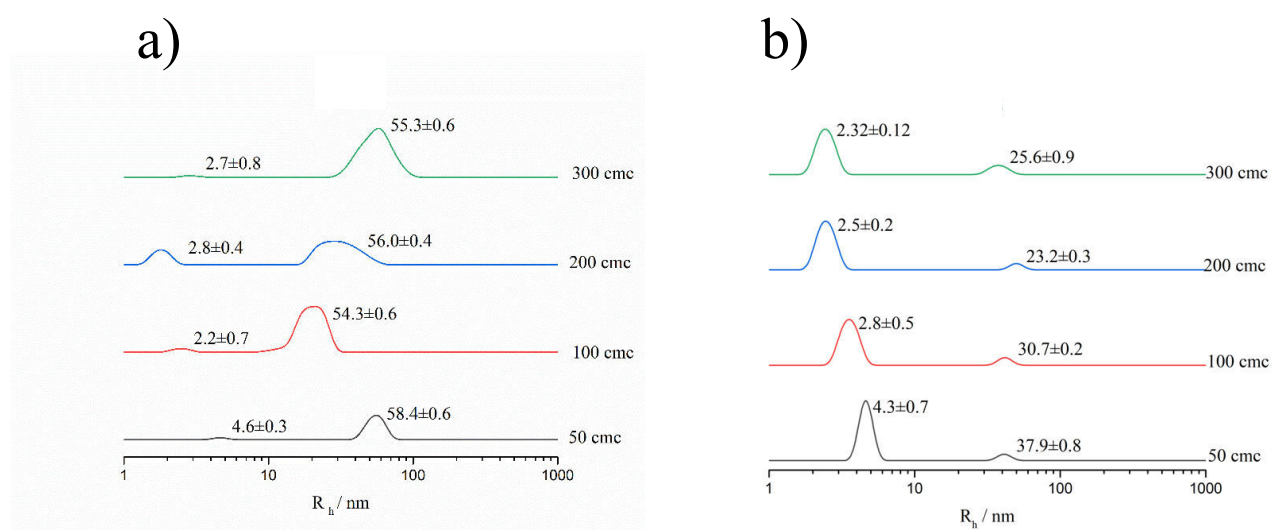


Figure 5. Hydrodynamics radius distributions of rhamnolipid aggregates in the ternary system water (pH=7.1, phosphate buffer)/bio-glycerol(40 wt%)/rhamnolipid at 25 °C. Panel (a): intensity-weighted distributions; panel (b): number-weighted distributions.

Fig. 5(a) highlights the presence of various aggregates in all the considered samples at 40wt% bio-glycerol: small micellar aggregates, with an average radius equal to about 3 nm, coexist with one distribution of larger aggregates, with a size of around 56 nm, respectively, which is likely of vesicular nature. Under this viewpoint it is to be noted that at this bio-glycerol content only one type of large aggregates is found, corresponding to the larger aggregates found at lower bio-glycerol content. Panel B clearly shows that micelles constitute by far the large majority of the aggregates in the sample even though vesicles are detectable. The comparison between Fig. 5 and Fig. 2 confirms that bio-glycerol enhances the populations with large dimension, while the size of the micellar aggregates remains more or less constant.

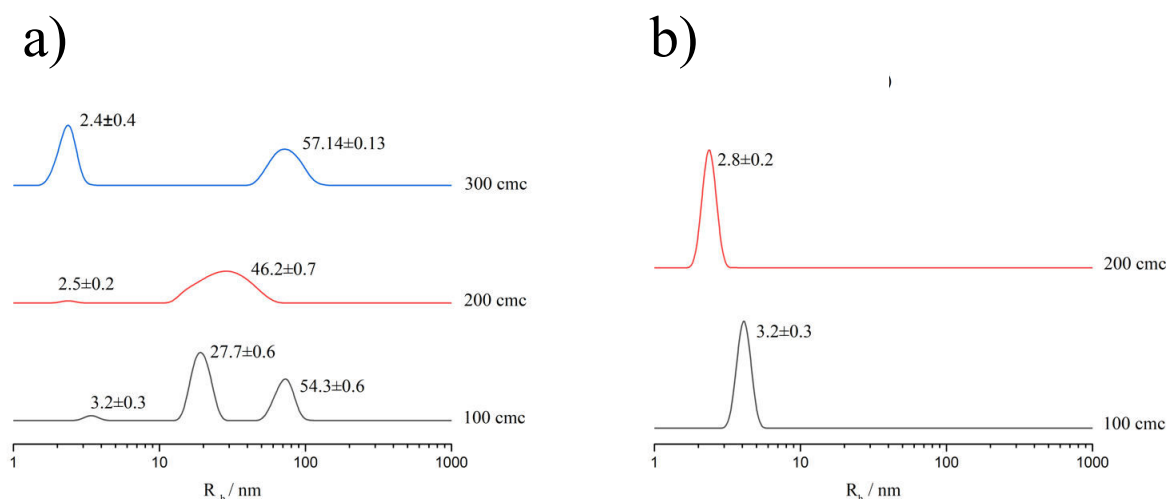


Figure 6. Hydrodynamics radius distributions of rhamnolipid aggregates in the ternary system water ($pH=7.1$, phosphate buffer)/bio-glycerol(70 wt%)/rhamnolipid at 25 °C. Panel (a): intensity-weighted distributions; panel (b): number-weighted distributions.

Fig. 6(a) shows the presence of various aggregates in all the considered samples at 70wt% bio-glycerol: small micellar aggregates, with an average radius equal to about 3 nm, coexist with one or two distributions of larger aggregate, which are likely of vesicular nature. Fig. 6(b) clearly shows that micelles constitute by far the large majority of the aggregates. Indeed, comparison between Fig. 4, Fig 5 and Fig. 6 shows that at high concentration of bio-glycerol populations with large dimensions are unfavoured, while the size of the micellar aggregates remains more or less constant.

5.5. Conclusions

In the present chapter, the bio-glycerol effect on the rhamnolipid micellization process has been evaluated. The study has been carried out by performing surface tension measurement for aqueous solutions at co-solvent percentages ranging from 0 to 80 wt%. Furthermore, the effect of bio-glycerol at 0 wt%, 20 wt%, 40 wt%, 70 wt% content was investigated by Dynamic Light Scattering measurements, focusing on the size and distribution of the aggregates formed during the micellization process.

The experimental data shows that the addition of bio-glycerol to the rhamnolipid aqueous solution does not perturb the aggregation process up to 50 wt%, while an evident effect is observed at higher

co-solvent content. A perusal of the data reveals that the *cmc* reaches a shallow minimum around 25-30 wt% of bio-glycerol content and increases at higher co-solvent concentration. Instead, the γ_{mic} value can be considered substantially constant, indicating a limited effect of the bio-glycerol on the surface activity exerted by the rhamnolipids. The area occupied by a single surfactant molecule, *A*, exhibits rather constant values up to 40 wt%, while an evident and pronounced increment of the parameter is observed with increasing the bio-glycerol percent.

The *cmc* increment due to bio-glycerol content can be explained in terms of an indirect effect on micellization deriving from modifications of the aqueous medium related the co-solvent presence. This parameter is related to the variation of the Gibbs energy of the system upon surfactant micellization. In the glycerol-poor content systems, the solvent mixtures present properties similar to neat water. Because of the high medium polarity, the solubility of the hydrophobic tails is unfavored because there is a loss of entropy due to the ordered organization of water molecules around them. Consequently, the formation of micellar aggregates, in which the surfactant tails are shielded from the contact with the solvent, is favored. As the bio-glycerol content increases, the medium polarity decreases favoring solubility of hydrophobic moiety and the hydrophobic effect is depressed. However, all these effects are seen only at very high glycerol content.

DLS data showed a weak dependence of the rhamnolipid micellization process on glycerol concentration. At low bio-glycerol content, the prevalence of vesicle-type aggregates with surface curvature point to a de-hydration of the surfactant headgroups. This could be related to a *salting out* effect of the co-solvent. In other words, bio-glycerol competes with surfactant molecules for water molecule, so that the surfactant has fewer water molecules available. The driving force behind the formation of low-curvature aggregates could be identified with the reduced ability of bio-glycerol molecules to enter the hydration sphere of the rhamnolipid headgroups. The hydrophilic moieties of the surfactants are less hydrated, so they approach each other promoting the formation of vesicle-like aggregates.

At high concentrations of glycerol, DLS data show that micelles become the predominant population. Evidently in these samples it is possible, as is already reported in the literature [12], that the presence of bio-glycerol decreases the dielectric constant. If the dielectric constant is lower, the electrostatic repulsions are greater and since we are in a range where the rhamnolipids are anionic it is possible that there is repulsion between the heads. The low dielectric constant enhances this repulsion and therefore aggregates with greater surface curvature are favored, that is micelles.

In conclusion, the limited effect of bio-glycerol at low-to-intermediate concentration demonstrates that this particular co-solvent can be employed to reduce the water content in the formulation, inspired by the water-free or water-poor formulation trend. In addition, it is interesting to note that throughout the analysed range of bio-glycerol the size of the micellar aggregates remains more or less constant. This implies that bio-glycerol is an excellent co-solvent and can be used in formulations. The present research contributes to build a reliable scientific platform for the exploitation of rhamnolipids in chemical formulations such as detergent, cosmetic, dermatological and pharmaceutical products.

References

- [1] Moelbert S.; Normand B.; De Los Rios P., Kosmotropes and chaotropes: modelling preferential exclusion, binding and aggregate stability, *Biophys. Chem.*, 2004, 112, 45-57. <https://doi.org/10.1016/j.bpc.2004.06.012>
- [2] Sawangkeaw R.; Bunyakiat K.; Ngamprasertsith S., Effect of co-solvents on production of biodiesel via transesterification insupercritical methanol, *Green chemistry*, 2007, 9, 679-685. <https://doi.org/10.1039/B614064E>
- [3] Dobbs J.M.; Wong J.M.; Johnston K.P., Nonpolar co-solvents for solubility enhancement in supercritical fluid carbon dioxide, *J. Chem. Eng. Data*, 1989, 31, 303-308. [https://doi.org/10.1016/0378-3812\(90\)85145-Z](https://doi.org/10.1016/0378-3812(90)85145-Z)
- [4] Montañés F.; Corzo N.; Olano A.; Reglero G.; Ibáñez E.; Fornari T., Selective fractionation of carbohydrate complex mixtures by supercritical extraction with CO₂ and different co-solvents, *J. Supercrit. Fluids*, 2008, 45, 189–194. <https://doi.org/10.1016/j.supflu.2007.08.012>
- [5] van Franeker J.J.; Turbiez M.; Li W.; Wienk M.M.; Janssen R.A.J., A real-time study of the benefits of co-solvents in polymer solar cell processing, *Nature communications*, 2015, 6, 6229. <https://doi.org/10.1038/ncomms7229>
- [6] Anastas P.; Eghbali N., *Green Chemistry: Principles and Practice*, 2009, Chemical Society Review.
- [7] Pagliaro M.; Rossi M., *Glycerol: properties and production in: The Future of Glycerol: New Uses of a Raw Material*, 2018, RSC Green Chemistry Book Series, 1-17.
- [8] *Economia circolare: definizione, importanza e vantaggi*, Attualità Parlamento Europeo, 2015, <https://www.europarl.europa.eu/news/it/headlines/economy/20151201STO05603/economia-circolare-definizione-importanza-e-vantaggi>
- [9] Takamura K.; Fischer H.; Morrow N.R., Physical properties of aqueous glycerol solutions, *J. Pet. Sci.*, 2012, 98–99, 50–60. <https://doi.org/10.1016/j.petrol.2012.09.003>
- [10] Christoph R.; Schmidt B.; Steinberner U.; Dilla W.; Karinen R., *Glycerol*, 2006, Ullmann's Encyclopedia of Industrial Chemistry, 17, 68-82.

- [11] Carnero Ruiz C.; Díaz-López L.; Aguiar J., Self-assembly of tetradecyltrimethylammonium bromide in glycerol aqueous mixtures: A thermodynamic and structural study, *J. Colloid Interface Sci.*, 2007, 305, 293–300. <https://doi.org/10.1016/j.jcis.2006.09.074>
- [12] D’Errico G.; Ciccarelli D.; Ortona O., Effect of glycerol on micelle formation by ionic and nonionic surfactants at 25°C, *J. Colloid Interface Sci.*, 2005, 286, 747–754.
- [13] Carnero Ruiz C.; Díaz-López L.; Aguiar J., Micellization of Sodium Dodecyl Sulfate in Glycerol Aqueous Mixtures, *J. Dispers Sci Technol.*, 2008, 29, 266–273. <https://doi.org/10.1080/01932690701707571>
- [14] Roques-Carmes T.; Mathieu V.; Gigante A., Experimental contribution to the understanding of the dynamics of spreading of Newtonian fluids: Effect of volume, viscosity and surfactant, *J. Colloid Interface Sci.*, 2010, 344, 180-197. <https://doi.org/10.1016/j.jcis.2009.12.039>
- [15] Khan H.; Seddon J.M.; Law R.V.; Brooks N.J.; Robies E.; Cabral J.T.; Ces O., Effect of glycerol with sodium chloride on the Krafft point of sodium dodecyl sulfate using surface tension, *J. Colloid Interface Sci.*, 2019, 538, 75-82. <https://doi.org/10.1016/j.jcis.2018.11.021>
- [16] Accardo A.; Tesauro D.; Roscigno P.; Gianolio E.; Paduano L.; D’Errico G.; Pedone C.; Morelli G., Physicochemical properties of mixed micellar aggregates containing CCK peptides and Gd complexes designed as tumor specific contrast agents in MRI, *J. Am. Chem. Soc.*, 2004, 126, 10, 3097–3107. <https://doi.org/10.1021/ja039195b>
- [17] Santis A.; Vitiello G.; Appavou M.; Scoppola E.; Fragneto G.; Barnsley L. C.; Clifton L. A.; Ottaviani M.F.; L Paduano.; Russo Krauss I.; D’Errico G., Not just a fluidifying effect: omega-3 phospholipids induce formation of non-lamellar structures in biomembranes, *Soft Matter*, 2020, 16, 10425-10438.

Conclusions

The aim of this PhD thesis was the identification and characterization of new ecofriendly surfactants as wetting agents in order to foster their application in industrial chemical formulations. In the last decades new concerns are arising on environmental and health issues caused by the massive use of chemical products, including liquid formulations. The total or partial replacement of synthetic surfactants with “green” alternatives is a fundamental step towards a new generation of water-based industrial formulations with an eco-sustainable profile.

In the various chapters of this thesis, it was shown that bio-inspired glycosurfactants and natural glycolipids have physico-chemical features comparable to (or even better than) those of conventional surfactants, presenting at the same time a significantly improved ecological footprint.

A first example, driven by the industrial interests and the collaboration for this thesis with Soltar srl, is given by mixtures of bio-inspired surfactants such as sorbitan esters. These mixtures were demonstrated to be able to stabilize both W/O and O/W emulsions, a result of relevant applicative interest. The emulsion stability was correlated to the glycosurfactant supramolecular organization at the oil–water interface, which was finely tuned by optimizing the surfactant mixture composition.

An even more meaningful example of eco-sustainable alternatives to conventional wetting agents is given by biosurfactants, natural molecules produced by bacteria, yeasts, and plants. Here, the attention focused on rhamnolipids, amphiphiles produced by *Pseudomonas aeruginosa* and nowadays available at a large scale thanks to optimized biotechnological production processes. The lower ecotoxicity of rhamnolipids, compared to synthetic surfactants, was confirmed by preliminary biological assays. These kinds of analysis need to be expanded on different models in order to define the final composition and potential applications of rhamnolipid-containing formulations. Then, a deep and wide physico-chemical characterization of rhamnolipid behavior in aqueous solution highlighted on the one side features similar to those of conventional surfactants, such as the surface tension lowering and the supramolecular aggregation above a well-defined *cmc*, while on the other side specific properties were found, such as the co-existence of small micelles with larger aggregates even close to the *cmc*. More importantly, rhamnolipid were found to be a promising wetting agent, lowering the contact angle between aqueous solutions and a variety of solid supports much more effectively than synthetic surfactants. This evidence was interpreted in terms of the peculiar rhamnolipid molecular structure, which presents a bulky and composite headgroup constituted by one or two sugar units and

one carboxylic group whose dissociation depends on the pH, joined to a hydrophobic counterpart composed by one or two rather short tails.

Importantly, rhamnolipids were found to co-micellize with both anionic and cationic surfactants. This capability is of great importance for applications in industrial formulations, in which the possibility to mix different surfactants offers the opportunity to design mixtures optimized for each specific tasks. The mixture of rhamnolipids with the largely diffused anionic surfactant SLES were investigated from both structural and functional viewpoints. In this mixture both surfactants present a negative charge at neutral pH. The results showed that they are able to co-aggregate in the whole composition range with a slight antagonism behavior in the mixed micellization process, as confirmed by the comparison with thermodynamic models. Furthermore, this mixed system forms small spherical micelles, which is a useful property for some industrial formulations, i.e., detergent formulation, with a transition to elongated micelles as the composition becomes rhamnolipid-rich.

The physico-chemical study on monorhamnolipid-CTAC mixed system highlighted further important properties. In this system the surfactants present opposite charges at neutral pH, while in acidic solutions a non-ionic-cationic mixture is formed. The mixture shows a synergism in the mixed micellization process, as confirmed by comparison with thermodynamic models. Interestingly, the synergism seems to be insensitive to the pH, i.e., to scarcely depend on the monorhamnolipid charge. This is again due to the peculiar structure of monorhamnolipids where the bulky rhamnose unit is able to screen the negative charge of the carboxylic group. This results in a system which is able to co-micellize, to form aggregates of different dimensions, and to spread onto solid surface independently on pH. This is an important feature which expands the field where rhamnolipids can be considered as alternative to conventional surfactants.

The last part of this PhD thesis is devoted to exploring a more applicative feature of rhamnolipid mixture in aqueous solution in presence of a “green” co-solvent, bioglycerol. Glycerol is a largely used cosolvent in cosmetic and detergent formulations, in which is used a humectant and hygroscopic (anti-dessiccant) agent. Bio-glycerol is the common name of glycerol obtained as side-product of processes involving natural triglycerides, such as biodiesel production. Results showed that glycerol scarcely affects rhamnolipid micellization. Only at very high glycerol content the decrease of the medium polarity results in increased *cmc* values.

Overall, the results presented in this thesis contribute to build a robust platform for the rationalization of the use of surfactants projected towards the design of a new-generation of “green” chemical

formulations. Bio-inspiration could represent a strategy to face the environmental issue, even though the production of the bio-inspired surfactants is still nonrenewable resource based. Biosurfactants at contrary offer several advantages, such as bio-sustainable production processes, reduced emissions, reduced environmental impact, high biodegradability, low toxicity and, particularly, excellent physico-chemical properties as wetting agents which definitely point to their implementation in chemical formulation industry.

Experimental techniques

The physico-chemical characterization of different systems composed by biosurfactant and conventional surfactant is carried out in order to investigate their properties at interface (contact angle and surface tension), the self-aggregation in bulk, the dimension and morphology of the aggregates (Dynamic Light Scattering) and the molecular features of the amphiphiles within the aggregates (Electron Paramagnetic Resonance). Furthermore, a thermodynamic interpretation is given to highlight the driving force and the main energies involved when these two surfactants are in the same system. Below, we report a summary of the theoretical principles on which all these techniques are based.

1. Surface tension

The analysis of surface tension values allows detailed information on the surfactant aqueous mixture to be obtained. Surface tension, dimensionally, is defined as the force per unit length of the surface boundary or as the energy per unit area of the surface. Its origin stands in the different energy among molecules at liquid-vapor interphase and molecules in the aqueous bulk. In the solution interior, as illustrated in Fig. 1, the molecules move with the same probability in all directions; at the liquid-vapor interphase, the molecular interactions are not balanced, so a force is generated which tends to draw them at the surface [1].

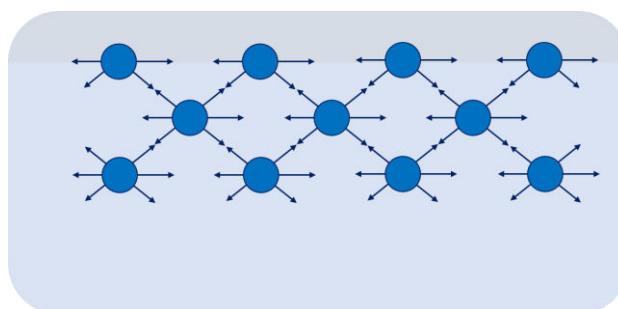


Figure 1. Interactions in solution of liquid molecules.

A liquid film at the interphase behaves like a stretched membrane. We can consider a U-shaped metallic loop closed at the bottom by a sliding wire with a length L , see Fig. 2. When the system is leaned on a liquid surface, a liquid film is created inside the loop with a behaviour similar to that of an elastic membrane. A force F is required to extend the liquid film moving the sliding wire by a

distance dx , until the equilibrium is reached between the applied force and the surface tension of the liquid film.

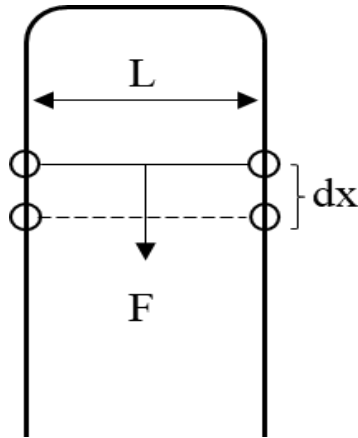


Figure 2. A wire loop with a slide wire upon which a liquid film might be formed and stretched by an applied force F .

The surface tension, γ , is defined as a force per unit of length:

$$\gamma = \frac{f}{l} \quad \text{Equation 1}$$

The work associated with the interfacial area expansion is given by the force times the displacement:

$$dw = f dx \quad \text{Equation 2}$$

Substitution of Eq. 1 into Eq. 2 leads to:

$$dw = \gamma l dx = \gamma dA \quad \text{Equation 3}$$

where A is the area of the interphase delimited by the loop.

Assuming that the expansion process is adiabatic and that T and P are constant, the work for the liquid film expansion is the only contribute to its Gibbs energy variation:

$$dG = \gamma dA \quad \text{Equation 4}$$

From Eqs. 2 and 4, it is evident that the surface tension can be defined as a force per unit length (expressed in Nm^{-1}) and, equivalently, as an energy per unit area (expressed in Jm^{-2}).

The liquid-vapor interphase is not the only one to generate a surface tension. A similar phenomenon also occurs at the solid-vapor and at the solid-liquid interphases. It is possible to connect the surface tension values to the energy associated with liquid droplet spreading onto a solid surface. Let's

consider a system constituted by a solid and a vapor interfaced each other. We put a liquid droplet on the solid horizontal surface. Two scenarios are possible:

the liquid remains as a lens drop and does not wet the surface.

the liquid spreads onto the surface as a uniform film.

The different behaviour is regulated by the value of the spreading factor, S , defined as:

$$S = \gamma_{sv} - (\gamma_{sl} + \gamma_{lv}) \quad \text{Equation 5}$$

Where γ_{sv} is the surface tension at solid-vapor interphase, γ_{sl} is the surface tension at solid-liquid interphase and γ_{lv} is the surface tension at liquid-vapor interphase. S can assume different values and it gives information about the wettability of the liquid solution:

- if $S \geq 0$, the wettability condition is satisfied and the drop spreads on the surface;
- if $S < 0$, the wettability condition is not satisfied, and a well-defined liquid lens remains.

In the latter case, we introduce θ , the contact angle between the solid-liquid and liquid-vapor interphases, see Fig. 3. The Young equation says that the equilibrium is reached when the vector sum of the different surface tensions is zero:

$$\gamma_{sv} = \gamma_{sl} + \gamma_{lv} \cos \theta \quad \text{Equation 6}$$

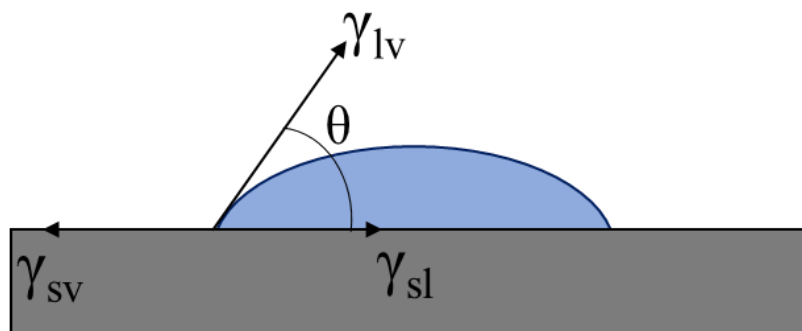


Figure 3. Components of interfacial tension needed to derive Young's equation

1.2. The Gibbs isotherm

Surfactants are composed by hydrophobic and hydrophilic moieties. In aqueous solutions, surfactants are positioned at the liquid-vapor interphase, exposing their hydrophobic tails toward the air. In this

way, they reduce the number of water molecules at interphase, where the interactions are not balanced in all directions. This involves a reduction of surface tension of the water. In particular it is possible to determine the area occupied by a surfactant monomer at the interphase by using the Gibbs equation. This equation describes the γ variation as a function of the surfactant concentration in solution on a logarithmic scale. We can obtain the Gibbs equation from thermodynamic considerations [2].

The differential form of the first law of thermodynamic for a system constituted by one component in a single phase is:

$$dU = \delta q + \delta w \quad \text{Equation 7}$$

If only pressure-volume work is considered and the process is reversible, we can write:

$$dU = TdS - pdV \quad \text{Equation 8}$$

For an open system composed by a single component present in two phases and one interphase (i.e., a pure liquid in equilibrium with its vapor), we have to consider the work required to create the interphase and the internal energy variation correlated to the matter input or output, dn , so the relation becomes:

$$dU = TdS - pdV + \gamma dA + \mu dn \quad \text{Equation 9}$$

Where μ is the chemical potential of the component.

We remind that the extensive variables are additive, and U is a homogenous first order function of the variables S, V, A, n .

$$U = TS - pV + \gamma A + \mu n \quad \text{Equation 10}$$

Differentiating, we obtain:

$$dU = TdS + SdT - PdV - VdP + \gamma dA + Ad\gamma + \mu dn + nd\mu \quad \text{Equation 11}$$

Comparison of Eqs. 11 and 9 leads to:

$$SdT - VdP + Ad\gamma + nd\mu = 0 \quad \text{Equation 12}$$

If the considered system has two components, the previous relation becomes:

$$SdT - VdP + Ad\gamma + n_1 d\mu_1 + n_2 d\mu_2 = 0 \quad \text{Equation 13}$$

In this expression, which is an extension of the Gibbs-Duhem relation, S is the total entropy of the system, including the two phases and the interphase; the same consideration stands for V , A , n_1 , n_2 .

Indicating with α the liquid phase and with β the vapor phase, and assuming each phase to be constituted from two components, named 1 and 2, we consider now an arbitrary volume V^α in the α phase far enough from the interphase and the same for V^β in the β phase; the Gibbs-Duhem equation for each phase can be written:

$$S^\alpha dT - V^\alpha dP + Ad\gamma + n_1^\alpha d\mu_1 + n_2^\alpha d\mu_2 = 0 \quad \text{Equation 14}$$

$$S^\beta dT - V^\beta dP + Ad\gamma + n_1^\beta d\mu_1 + n_2^\beta d\mu_2 = 0 \quad \text{Equation 15}$$

The three equations (13-14) give three relations on five variables (T , P , γ , μ_1 , μ_2) with two degrees of freedom of the system, f , defined as the difference between the number of independent variables and the number of relations among them.

Dividing Eqs. 14 and 15 by V^α and V^β , respectively, we obtain:

$$S^\alpha dT - dP + c_1^\alpha d\mu_1 + c_2^\alpha d\mu_2 = 0 \quad \text{Equation 16}$$

$$S^\beta dT - dP + c_1^\beta d\mu_1 + c_2^\beta d\mu_2 = 0 \quad \text{Equation 17}$$

where c_1 and c_2 are the concentrations of the two components in the two phases and S is the entropy per unit volume. If T is assumed to be constant, we have only one degree of freedom.

Subtracting Eq. 16, multiplied by x , and Eq. 17, multiplied by y , from Eq. 13 we obtain:

$$-(V - x - y)dP + Ad\gamma + (n_1 - xc_1^\alpha - yc_1^\beta)d\mu_1 + (n_2 - xc_2^\alpha - yc_2^\beta)d\mu_2 = 0 \quad \text{Equation 18}$$

This expression must be valid for all x and y values and also for those values which make the coefficients of dP and $d\mu_1$ null:

$$x + y = V \quad \text{Equation 19}$$

$$xc_1^\alpha + yc_1^\beta = n_1 \quad \text{Equation 20}$$

In these conditions it is possible to obtain:

$$x = \frac{c_1^\beta V - n_1}{c_1^\beta - c_1^\alpha} \quad \text{Equation 21}$$

$$y = \frac{n_1 - c_1^\alpha V}{c_1^\beta - c_1^\alpha} \quad \text{Equation 22}$$

The Gibbs equation is obtained by introducing Eqs. 21 and 22 in Eq. 18:

$$\left(\frac{\delta\gamma}{\delta\mu_2}\right)_{T,P} = -\Gamma_1 \quad \text{Equation 23}$$

Where

$$\Gamma_2 = A^{-1} \left[n_2 - \frac{c_1^{\beta}V - n_1}{c_1^{\beta} - c_1^{\alpha}} c_2^{\alpha} - \frac{n_1 - c_1^{\alpha}V}{c_1^{\beta} - c_1^{\alpha}} c_2^{\beta} \right] \quad \text{Equation 24}$$

Following the same procedure, it is possible to obtain:

$$\left(\frac{\delta\gamma}{\delta\mu_1}\right)_{T,P} = -\Gamma_1 \quad \text{Equation 25}$$

where:

$$\Gamma_1 = A^{-1} \left[n_1 - \frac{c_1^{\beta}V - n_1}{c_1^{\beta} - c_1^{\alpha}} c_1^{\alpha} - \frac{n_1 - c_1^{\alpha}V}{c_1^{\beta} - c_1^{\alpha}} c_1^{\beta} \right] \quad \text{Equation 26}$$

Considering the denominator of Eqs. 21 and 22, we can hypothesize that if the concentration of solvent 1 in the liquid β is much larger than that in the vapor phase α , $c_1^{\beta} \gg c_1^{\alpha}$, the equations become:

$$x \cong V - \frac{n_1}{c_1^{\beta}} \quad \text{Equation 27}$$

$$y \cong \frac{n_1}{c_1^{\beta}} \quad \text{Equation 28}$$

In order to obtain the relation Eq. 28, we also hypothesize $n_1 \gg c_1^{\alpha}V$, meaning that the average concentration ($\frac{n_1}{V}$) of component 1, which is the solvent, is much larger in phase β than in phase α .

The ratio $\frac{n_1}{c_1^{\beta}}$ is the hypothetical volume occupied by the solvent if it is all condensed in the liquid phase. The increase of the volume of the condensed phase due to the vapor phase condensation is certainly slight, therefore y is approximately equal to the volume occupied by the liquid phase and x is approximately equal to the volume occupied by the vapor phase. The following relation shows the approximate number of moles of component 2 (the solute) in vapor phase:

$$x c_2^{\alpha} = \frac{c_1^{\beta}V - n_1}{c_1^{\beta} - c_1^{\alpha}} c_2^{\alpha} \quad \text{Equation 29}$$

Similarly, the following relation shows the number of solute moles in liquid phase:

$$yc_2^\beta = \frac{n_1 - c_1^\alpha V}{c_1^\beta - c_1^\alpha} c_2^\beta \quad \text{Equation 30}$$

The difference between the sum of these values and the total number of solute moles in the system, n_2 , expresses the number of moles of solute which are neither in the liquid nor in the vapor bulk, so it can be assumed that they are positioned at the interphase. We can now calculate the number of moles of solute per unit area at the interphase:

$$\Gamma_2 = A^{-1}[n_2 - xc_2^\alpha - yc_2^\beta] \quad \text{Equation 31}$$

Eq. 20 implies that n_1 , the total moles of solvent, equals the sum of the moles in liquid and vapor phases, thus the net value at interphase is null.

For adequately diluted solutions, which behave as ideal, we can assume that:

$$d\mu_2 = \frac{RT}{c_2^\beta} dc_2^\beta \quad \text{Equation 32}$$

So, Eq. 23 becomes:

$$-\Gamma_2 = \frac{c_2^\beta d\gamma}{RT dc_2^\beta} = \frac{1}{RT} \frac{d\gamma}{d \ln c_2^\beta} \quad \text{Equation 33}$$

where Γ_2 represent the number of moles of solute per unit area adsorbed at interphase. Consequently, in a graph reporting surface tension data as a function of the logarithm of solute concentration in the liquid phase, the slope gives $-\Gamma_2 RT$. The area occupied by a single molecule of solute at the interphase is:

$$a = \frac{1}{N_A \Gamma_2} \quad \text{Equation 34}$$

where N_A is the Avogadro constant. If the solution is sufficiently diluted, we can approximate the molar concentration with the molal concentration.

The Gibbs isotherm allows the exact location of the interphase to be identified, defining a putative interface or Gibbs Dividing Surface (GDS). Indeed, while in solid systems the concentration variations at the interphases are abruptly evident on an angstrom scale, in liquid systems the concentrations vary across an interfacial region on a nanometer scale. Fig. 4(a) shows the variations of the concentration of component 1, the solvent, which show no excess at the interphase, as quantitatively reported in Eq. 20. If we choose to locate the exact value of the interface position, z_0 ,

as shown in the figure, Γ_1 is zero. Fig. 4(b) shows the concentration profile for c_2 . It is evident that c_2^α and c_2^β are both smaller than c_2 at the interface, so the Γ_2 assumes positive value.

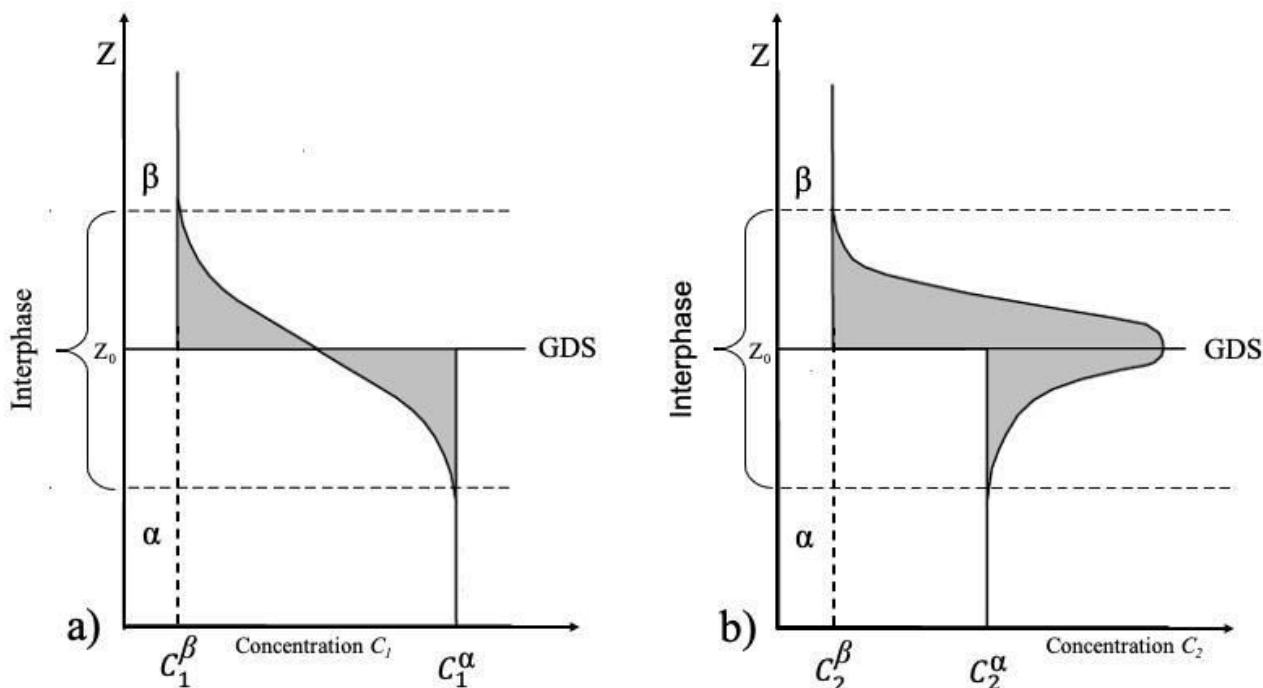


Figure 4. In the Gibbs approach to defining the surface excess concentration, the Gibbs dividing surface (GDS) is defined as the plane in which the solvent excess concentration become zero as in (a). the surface excess of c_2 will then be the difference in the concentrations of that component on either side of the plane (b).[3]

2. Electron Paramagnetic Resonance

Electron Paramagnetic Resonance (EPR), or Electron Spin Resonance (ESR) spectroscopy is useful for studying of paramagnetic species, including organic or inorganic radicals and triples states. The basic theoretical principles of EPR spectroscopy are very complex. They are very similar to the NMR spectroscopy, but here the spectroscopy focuses on the interaction of the unpaired electrons in a molecule when an external field is applied, not on the nuclei of individual atoms [4]. If it is true that the almost all pure substances contain magnetic nuclei and are thus accessible to NMR, this is not true for EPR because only few pure substances contain unpaired electrons and are thus accessible to this type of spectroscopy. This is because chemical binding is based on electron pair formation with

spin cancellation. Thus, the compounds that can be seen by EPR have to be paramagnetic and not only diamagnetic.

2.1. Basic theoretical principles

Molecules present a well-defined state of energy such as the atoms. Spectroscopy is able to detect and to measure the energy differences between the atomic or molecular states. Through the knowledge of these energy differences, we can obtain information on the identity, structure and dynamics of the sample. It is possible to measure the energy differences, ΔE , and the absorption of energy, such as an electroparamagnetic radiation. According to Planck law, electromagnetic radiation will be absorbed if:

$$\Delta E = h\nu \quad \text{Equation 35}$$

where h is Plank constant and ν is the frequency of the radiation. The absorption of energy causes a transition of the energetical state of a molecule, where the electrons are present at the lower energy state and then to the higher energy state.

In the EPR spectroscopy the unpaired electrons in a sample are studied by applying an external magnetic field produced by a magnet which produces a change of energy [4].

This is called the Zeeman effect. Since the electron has a magnetic moment, it acts like a compass or a bar magnet when placed in a magnetic field, B_0 . If the electron is aligned with the magnetic field, the moment of the electron, μ , present a state of lowest energy or a state of highest energy when μ is aligned against the magnetic field. These two states can be labeled as the projection of the electron spin, M_s , on the direction of the magnetic field. The parallel state is designated as $M_s = -1/2$ and the antiparallel state is $M_s = +1/2$. From quantum mechanics, the most basic equations of EPR are obtained:

$$E = g\mu_B B_0 M_s = \pm \frac{1}{2} g\mu_B B_0 \quad \text{Equation 36}$$

and

$$\Delta E = h\nu = g\mu_B B_0 \quad \text{Equation 37}$$

Where g is the g-factor, which is equal to 2.0023 and about constant for the most samples (its variation depends on the electronic configuration of the radical or ion); μ_B is the Bohr magneton, which is the natural unit of the electronic magnetic moment.

Eq. 36 and Eq. 37 suggest that the two spin states have the same energy in the absence of a magnetic field and that the energies of the spin states diverge linearly as the magnetic field increases. Furthermore, there is no energy difference to measure if a magnetic field is not applied, thus, the measured energy difference depends linearly on the magnetic field. Exploiting this characteristic of electron, we can carry on different strategies to obtain spectra, since the energy differences between the two spin states is related to the variation of the magnetic field strength. The first option can be to apply a constant magnetic field and scan the frequency of the electromagnetic radiation as in conventional spectroscopy, or, the second option is to keep the electromagnetic radiation frequency constant and scan the magnetic field.

If the magnetic field tunes the two spin states and their energy difference matched the energy of the radiation, a peak in the absorption will occur: this is called the field of resonance, as showed in Fig. 5.

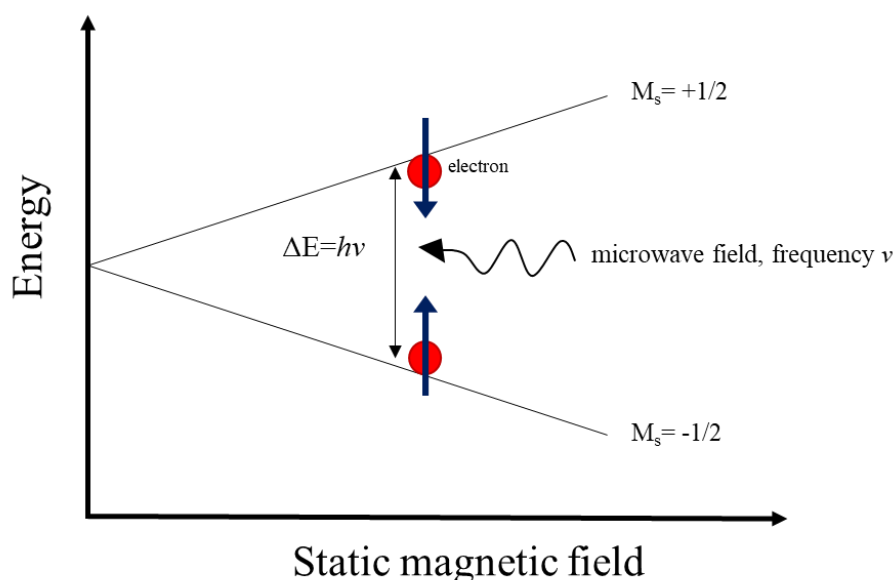


Figure 5 Variation of the spin state energies as a function of the applied magnetic field.

Unfortunately, the field of resonance do not give specific information of the investigated species because spectra can be acquired at several different frequencies, being independent of the microwave frequency, the g-factor $g = g = h\nu / (\mu_B B_0)$ is much better for that purpose. Indeed, the measurement of the g-factor can give us some useful information, but not on the molecular structure of the sample.

Fortunately, the unpaired electrons are very sensitive to their local surroundings: the nuclei of the atoms in a molecule often present a magnetic moment, which produces a local magnetic field at the electron. The interaction between the electron and the nuclei is called the hyperfine interaction. This kind of interaction allows to have several information about the sample such as the identity and the number of atoms which make up a molecule or complex as well as their distance from the unpaired electron.

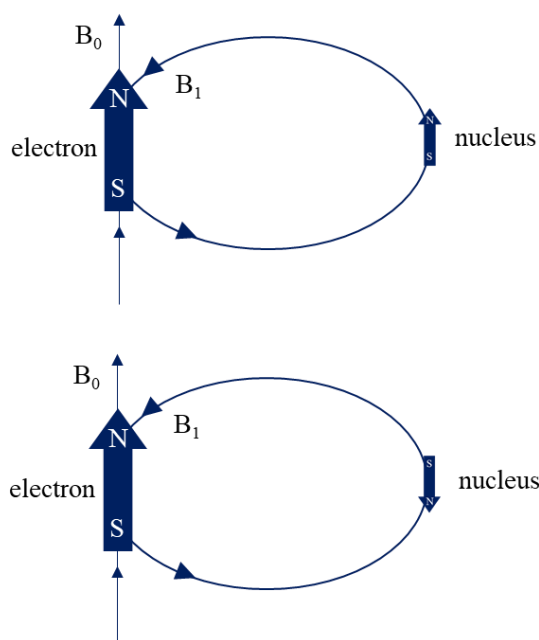


Figure 6. Local magnetic field at the electron, B_1 , due to a nearby nucleus [5]

Fig. 6 explains the origin of the hyperfine interaction. The magnetic moment of the nucleus acts like a bar magnet and produces a magnetic field at the electron, B_1 . This magnetic field opposes or adds to the magnetic field from the laboratory magnet, depending on the alignment of the moment of the nucleus. B_0

When B_1 adds to the magnetic field, we need less magnetic field from our laboratory magnet and therefore the field for resonance is lowered by B_1 . The opposite is true when B_1 opposes the laboratory field. For a spin $\frac{1}{2}$ nucleus such as a hydrogen nucleus, it is possible to observe that the single EPR absorption signal splits into two signals which are each B_1 away from the original signal, as shown in Fig. 7.

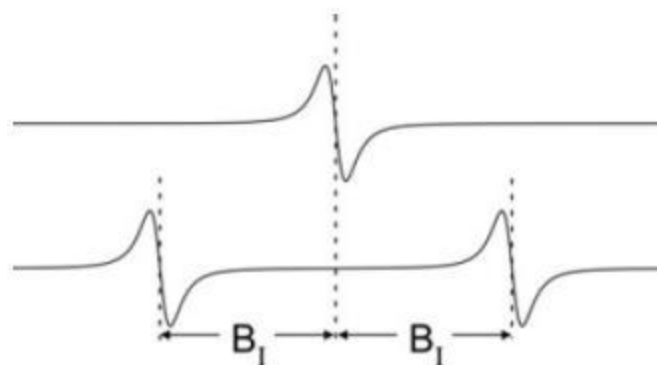


Figure 7. Splitting in an EPR signal due to the local magnetic field of a nearby nucleus [5]

If there is a second nucleus, each of the signals is further split into a pair, resulting in four signals. For N spin $\frac{1}{2}$ nuclei 2^N EPR signals will be generally observed. As the number of nuclei gets larger, the number of signals increases exponentially. Sometimes there are so many signals that they overlap and we only observe the one broad signal.

2.2. Electron Paramagnetic Resonance instrument

An EPR spectrometer is composed by four fundamental elements:

a monochromatic microwave source.

A waveguide for guiding the microwave power to the sample

A cavity designed to ensure a proper coupling between the sample and the incoming wave.

A detector for microwave power to detect the response of the sample to microwave irradiation.

A schematic drawing of an EPR spectrometer is represented in Fig. 8.

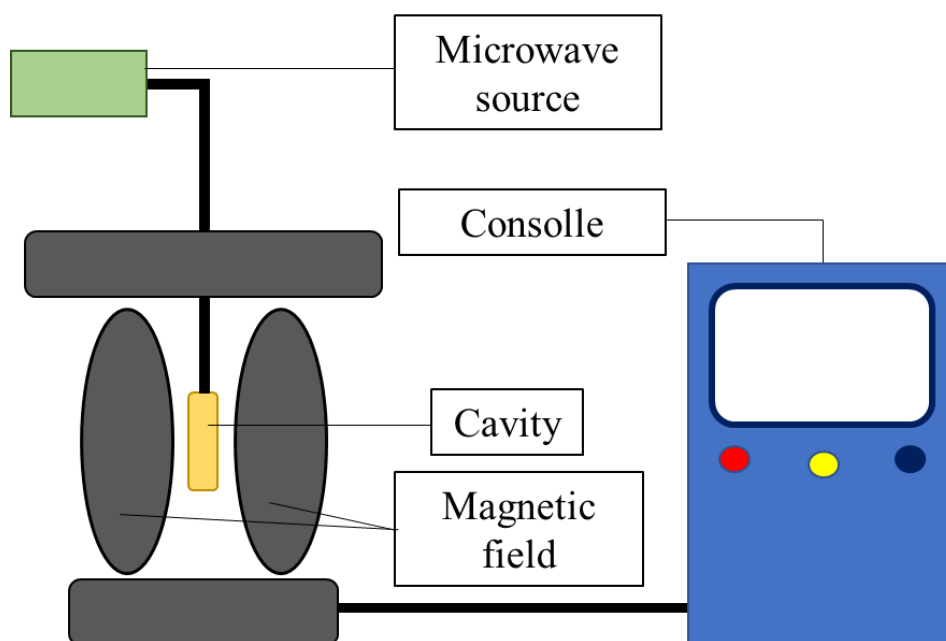


Figure 8. Schematic representation of a EPR spectrometer

The magnetic field is generated by an electromagnet, usually water-cooled, which is able to provide a stable and uniform field in the area where the sample is placed. The microwave source can be a gun diode or a klystron; in both cases, a microwave beam is generated at a fixed frequency between 9 and 19 GHz (X-Band). This generated microwave beam is sent through the waveguide to the sample. The cavity, in which the sample is placed, is at the center of the two magnetic field poles and receives the microwave through the waveguide. The cavity is designed in order to get inside a regular distribution of the magnetic field lines generated by the electromagnetic radiation coming from the source and perpendicular the static magnetic field generated by a solenoid. Finally, the “consoles” is the interface between the spectrometer and the user from which it is possible to make all the settings and set the parameters for the spectra recording.

Samples for EPR can be gases, single crystals, solution, powders, and frozen solutions. For solutions, solvents with high dielectric constant are not advisable, as they will absorb microwaves. For frozen solutions, solvents that will form a glass when frozen are preferable. Good glasses are formed from solvents with low symmetry and solvents that do not hydrogen bond. A sample is usually placed in a quartz tube, which is the material devoid of paramagnetic impurities, of 3-5 mm in diameter that is inserted into the cavity and secured in place by the media. The side walls of the resonant cavity are

coils that modulate the amplitude of the signal, usually at a frequency of 100kHz, generating the first derivative of the absorption curve, as shown in Fig. 9.

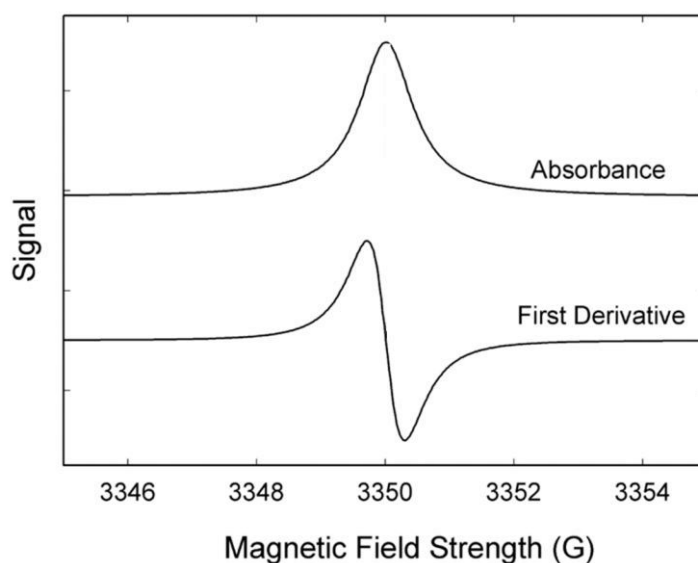


Figure 9. Example of first derivative of the absorption curve in EPR spectrum

3. Dynamic Light Scattering

Dynamic light scattering is a technique used to determine the size distribution profile of small particles in suspension or polymer in solution [6].

3.1. Basic theoretical principles

A light beam scatters in all directions when it hits a polarizable medium due to the presence of aggregates in the solution. They are the scattering centers, *scatters*, which give a stronger signal compared to the background [7]. This is due to the interaction of light with matter which induces an electronic polarization and the resulting oscillating dipoles become a secondary source of light, called scattered light. When the light source is constituted by a monochromatic incident laser, the time-dependent fluctuations of scattering intensity, I_s , are observed. Constructive and destructive interference phenomena of the scattered light can be caused by the presence of other particles nearby in the

solution; thus, these variations can give information on the reciprocal movement of the aggregates in solution. A schematic representation of the scattering process is reported in Fig. 10.

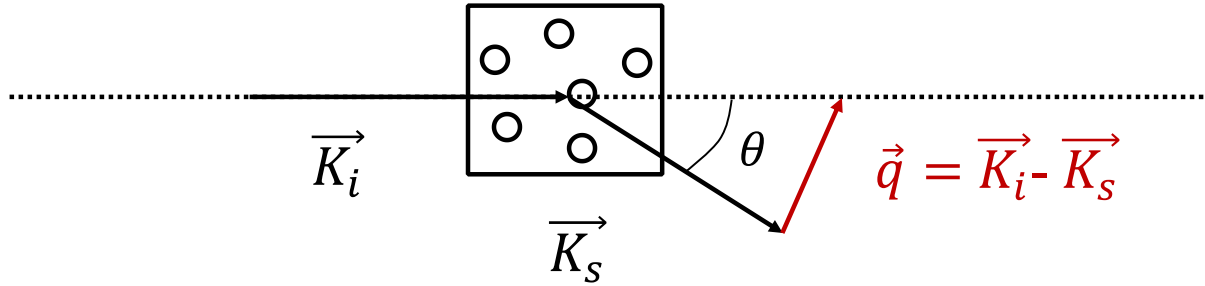


Figure 10. Schematic representation of scattering process; \vec{K}_i is the wave vector of incident light; \vec{K}_s is the wave vector of scattered light; \vec{q} is the scattering vector; θ is the scattering angle; the box is the scattering volume.

An incident monochromatic laser beam of wavelength λ_i and wave vector \vec{K}_i irradiates the scattering volume V_s containing N particles. The scattered light, with wave vector \vec{K}_s is observed at a scattering angle θ .

The scattering vector q is defined as the vector difference between the two wave vectors K_i and K_s .

In elastic scattering, which is predominant in the DLS experiments, the impact of photons occurs without changes in energy and then:

$$|\vec{K}_i| = |\vec{K}_s| = \frac{2\pi}{\lambda/n} \quad \text{Equation 38}$$

$$|\vec{q}| = |\vec{K}_i - \vec{K}_s| = \frac{4\pi}{\lambda/n} (\sin(\theta/2)) \quad \text{Equation 39}$$

Where λ is the laser wavelength in vacuum and n is the refractive index of the solution.

Scattering light intensity I_s is a complex function that depends on many factors and can be described by the following relation:

$$I_s \propto I_0 \frac{n_0^2}{\lambda^4} \left(\frac{\partial n}{\partial C} \right)^2 R^6 N P_{(q)} S_{(q;C)} \quad \text{Equation 40}$$

Where I_0 is the incident light intensity, λ its wavelength in vacuum, n_0 and n are the refractive indexes of the solvent and the solution respectively, $\partial n / \partial C$ is the refractive index increment, R is the radius of the particles, N is the number of scattering particles in the irradiated volume, $P_{(q)}$ and $S_{(q;C)}$ are the form factor and structure factor respectively.

$P_{(q)}$ gives useful information on the shape of macromolecules in solution while the $S_{(q;C)}$ take into account the effects of interference between the particles, so it depends on concentration (for dilute solution $S \approx 1$) and allows for an assessment of the structure of the solution.

In diluted sample in which aggregates can act as scatterers, the scattered light intensity depends on several parameters:

- The optical contrast factor compared to the solvent (refractive index of the particle).
- The considered angle measurements.
- Number, size and shape of particle.
- Relative position of the particles.

In particular, a good signal of the suspended particles is detected experimentally only if their refractive index is sufficiently different from that of the solvent.

For this purpose, it is often introduced a relative index of refraction:

$$m = \frac{n_p}{n_s} \tag{Equation 41}$$

Where subscripts p and s are related to particles and solvent respectively. Particle/solvent systems with relative refractive index very close to 1 will be hardly visible in a light scattering experiment, since the aggregates will produce a weak signal compared to the background of the scattered light by molecules of the solvent.

Assuming spherical particles, in the case in which factors $S_{(q;C)}$ and $P_{(q)}$ are close to 1 (diluted solution and particles that are small in comparison to the incident radiation wavelength, the scattered light varies with the sixth power of the radius of the involved particles. Within the approximation made, in condition of elastic scattering (Reyleigh regime), a particle with a radius of 50 nm diffuse light a million times more than a particle having a radius 5 nm. Therefore, the technique is more sensitive to the presence of large particles, rather than small ones. Focusing on the dependence of scattering light intensity from scattering angle, we have:

$$I_{(q)} = P_{(q)}S_{(q;C)} \tag{Equation 42}$$

Where $S_{(q;c)}$ considers interferences between particles, providing information regarding the distribution of the aggregates in space, while $P_{(q)}$ models the effect of the shape of the particles, and is important only if the particle size is comparable to the radiation wavelength λ .

Particles with sizes much smaller than λ can be considered point-like, so that $P \rightarrow 1$. And the diffused radiation is isotropic. In contrast, particles of a size comparable to the radiation wavelength λ , are characterized by an angular dependence of the shape of such particles.

In a DLS experiment the fluctuation of the scattered light intensity, originated by Brownian motions of particles, are measured as a function of time at a constant scattering light angle.

The temporal variation of the intensity is measured and represented usually through the so-called intensity autocorrelation function.

In practice, temporal fluctuations of the scattered light are recorded and analyzed by estimating the time correlation function of the electric field:

$$g^1(\tau) \propto \langle E_s(t)E_s(t + \tau) \rangle \quad \text{Equation 43}$$

Where $E_s(t)$ and $E_s(t + \tau)$ represent the electrical field intensity of the scattered light at time t and $(t + \tau)$ and described the correlation level of a dynamic quantity in a delay time τ . This function is obtained by the intensity autocorrelation function:

$$g^2(\tau) \propto \langle I_s(t)I_s(t + \tau) \rangle \quad \text{Equation 44}$$

The two functions are correlated by Siegert relation [8]

$$g_2(\tau) = 1 + \beta |g^1(\tau)|^2 \quad \text{Equation 45}$$

Where β is the coherence factor, which accounts for deviation from ideal correlation and depends on the experimental geometry.

For a monodisperse system, $g^1(\tau)$ will decay as a single exponential function with a characteristic relaxation time τ [9]:

$$g^1(q, \tau) = \exp(-q^2 D \tau) \quad \text{Equation 46}$$

Whereas for a polydisperse system $g^1(t)$ will be multiexponential:

$$g^1(q, \tau) = \sum_j w_j \exp(-q^2 D_j \tau) \quad \text{Equation 47}$$

Where q is the scattering vector, D is the mutual diffusion coefficient, the subscript j indicates particles of different size present in solution and the weights w_j are related to particles concentration and their molecular weight.

Measuring the reciprocal of the characteristic decay time $\Gamma = 1/\tau$ from the first moment of the relaxation time distribution, it is possible to estimate apparent translational diffusion coefficient D , through this relation [10]:

$$D = \lim_{q \rightarrow 0} \frac{\Gamma}{q^2} \quad \text{Equation 48}$$

D is thus obtained from the slope of Γ as a function of q^2 , where Γ is measured at different scattering angles.

Finally, using the Stokes-Einstein equation [6,8] the value of the hydrodynamic radius (R_h) of the equivalent sphere can be determined from:

$$D = \frac{k_b T}{6\pi\eta R_h} \quad \text{Equation 49}$$

Valid for infinite dilute dispersions, where η is the solvent viscosity, k_b is the Boltzmann constant and T the absolute temperature.

3.2. Dynamic Light Scattering instrument

The main components of DLS instrument, as reported in Fig. 11, used in this experimental work are:

- Laser (SMD 6000 Laser Quantum, 50 mW) that provides a light source to illuminate the sample contained in a cell. It generates a green light beam collimated and coherent with a wavelength of 532.5 nm.

- Cell holder is formed by a circular groove that allows the light beam to enter and hit the sample in glass cell and then the scattered light to get to the detector. The cell holder is filled with toluene which presents the same refractive index of the glass cell, so the laser refraction at interface glass-air is avoided.

- Thermostat that keeps the fixed temperature in a narrow range (i.e. $25.0 \pm 0.05^\circ\text{C}$) and allows us to set it.

-Optical fiber that guides the scattered light to the detector.

-Detector (PMT-120_OP/B) that is connected to the optical fiber and, by means of a goniometer and a rotating arm, can collect the scattered light at different angles. In any case, the detection device and the laser source must be aligned toward the geometrical center of the sample cell. The detector transforms the light beam that hits the sample into a electric current, whose intensity is proportional to the intensity of scattered radiation. The intensity of the scattered light must be within a specific range for the detector to successfully measure it. If too much light is detected, then the detector will become saturated. To overcome this, an attenuator is used to reduce the intensity of the laser source and hence reduce the intensity of scattering. For samples that do not scatter much light, such as very small particles or samples of low concentration, the amount of the scattered light must be increased. In this situation the attenuator will allow more laser light through to the sample. On the other hand, for samples that scatter more light, such as large particles or samples at higher concentration, the intensity of scattered light must be decreased.

- Correlator (Flex 02-101D) that collects the intensity of scattered light coming from the detector and builds the intensity autocorrelation function. This correlator information is then passed to a computer where a detailed program for data processing will allow us to obtain diffusion coefficient of particles in the analyzed sample.

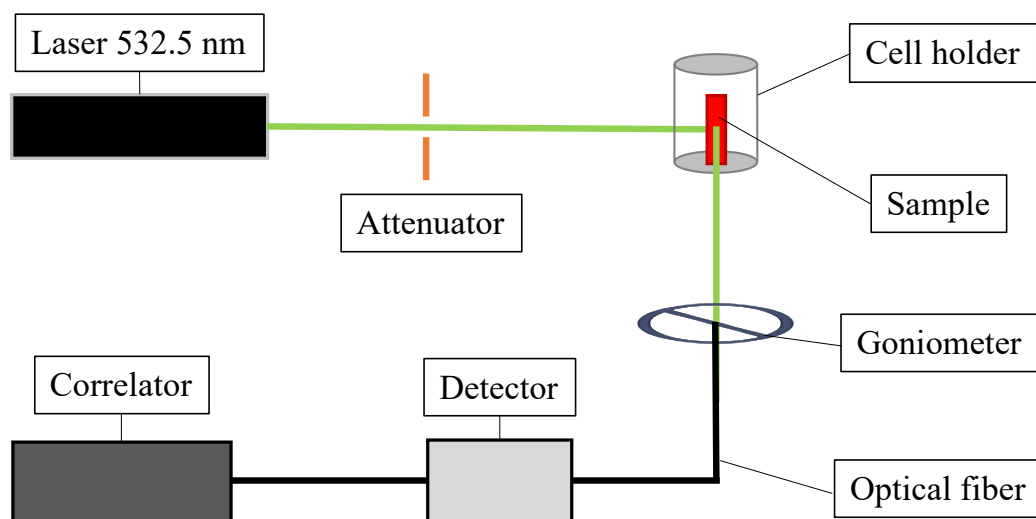


Figure 11. Schematic representation of a DLS instrument

4. Contact angle

The topic of spreading plays an important role in many industrial processes, such as oil recovery, lubrication, liquid coating, printing, and spray quenching. The measurement of the contact angle is a key point in the determination of important parameters, such as the surface energy of a solid [11]. There are two different approaches for contact angle measurements: the static and the dynamic contact angles [12]. The former approach consists of placing a droplet on a horizontal surface and the three-phase boundary is not moving. The latter approach is used when the three-phase boundary is moving and so the dynamic parameters are measured considering a reference. Furthermore, there is a classification on the type of contact angle measurement based on the indirect force methods and direct optical methods. In the present work, in order to evaluate the wettability of tested solutions, static contact angles and direct optical method are employed.

In three-phase system, three different interfacial energies exist from the pairwise combination between the phases, Fig. 6:

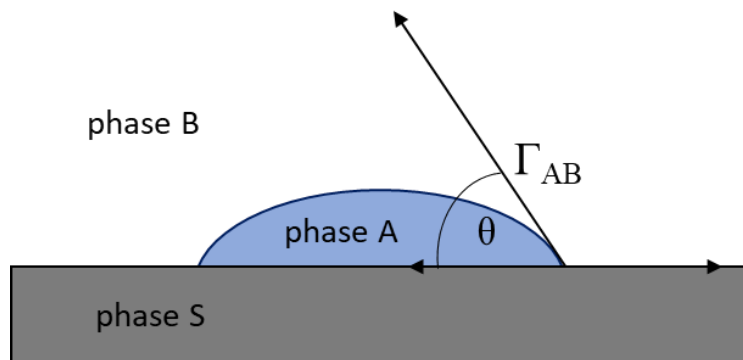


Figure 12. Schematic drawing of a solid-liquid-liquid arrangement of a droplet of a secondary fluid “A” residing on a flat surface of the solid “S” surrounded by a bulk liquid “B”.

The contact angle θ is determined from these quantities by the Young:

$$\Gamma_{SB} - \Gamma_{SA} - \Gamma_{AB} \cos \theta = 0 \quad \text{Equation 50}$$

Converting this balance leads to:

$$\cos \theta = \frac{\Gamma_{SB} - \Gamma_{SA}}{\Gamma_{AB}} \quad \text{Equation 51}$$

The Young equation is only valid for an ideal solid surface that is defined as rigid, smooth, chemically homogenous, insoluble and non-reactive [13].

Drop shape analysis (DSA) is a method to evaluate the contact angle from a side-view image of a sessile droplet [14]. As first step, a droplet is placed on a solid surface and an image is acquired. The drop will assume a spherical shape. Then, the software recognizes the border of the drop from the solid surface base line and thanks to the projection of the ideal sphere, the contact angle can be obtained.

4.1. Contact angle instrument

In order to verify the wetting ability of the surfactant mixtures, contact angle measurements were carried out using the OCA 15EC system (DataPhysics, Filderstadt, Germany) and the drop shape was analyzed with the SCA20 software (DataPhysics).

The instrument in Fig. 13 consists in [15]:



Figure131

. Contact angle instrument OCA 15EC model by DataPhysics.

-Sample table which can slide freely in X- and Y-direction and the Z-direction is adjusted with a handle wheel.

- one electronic syringe modules to dose the droplet.
- optical lens which allow to focus and zoom the interested are.
- USB 3 camera for the imagines.

For each measurement, a sample droplet of 3 μL was placed on a solid support. Silicon wafers {1.1.1} in three different states of surface activation (native, hydrophilic and hydrophobic) were used as supports.

5. Derivation of thermodynamic equations

In Chapter 4 we consider two mixed systems composed by Rha-SLES and mRha-CTAC. The trends of cmc of each system were interpreted with two theoretical models of mixed micellization proposed by Clint for ideal mixing and Holland and Rubingh for regular solutions respectively [16,17]. In this section we report the detailed derivation of Eq. 6 in 4.1.3.3. paragraph for Rha-SLES mixture which is applied also for mRha-CTAC mixture. Firstly, we consider the binary system water-Rha at a surfactant concentration exceeding cmc_{Rha} . According to the pseudo-phase separation model, the chemical potential of Rha monomers in the aqueous pseudo-phase (whose concentration is assumed to be equal to cmc_{Rha}) is the same as that in the micellar pseudo-phase:

$$\mu_{Rha}^{aq} = \mu_{rha}^{mic} \quad \text{Equation 52}$$

$$\mu_{Rha}^0 + RT \ln cmc_{Rha} = \mu_{Rha}^* \quad \text{Equation 53}$$

where μ_{Rha}^0 is the infinite dilution-chemical potential of Rha in the aqueous medium and μ_{Rha}^* is the surfactant chemical potential in the micelle composed only by Rha.

Following the same considerations, for the binary system water-SLES one obtains:

$$\mu_{SLES}^0 + RT \ln cmc_{SLES} = \mu_{SLES}^* \quad \text{Equation 54}$$

where μ_{SLES}^0 is the infinite dilution-chemical potential of SLES in the aqueous medium and μ_{SLES}^* is the surfactant chemical potential in the micelle composed only by SLES.

We consider now the ternary system water-Rha-SLES at a total surfactant concentration exceeding the cmc . The two surfactants partition between the aqueous and the micellar pseudo-phases. In equilibrium conditions the following relations hold:

$$\begin{cases} \mu_{Rha}^0 + RT \ln(X_{Rha} cmc) = \mu_{Rha}^* + RT \ln(\gamma_{Rha} Y_{Rha}) \\ \mu_{SLES}^0 + RT \ln(X_{SLES} cmc) = \mu_{SLES}^* + RT \ln(\gamma_{SLES} Y_{SLES}) \end{cases} \quad \text{Equation 55}$$

In Eq. 55 we have assumed that the aqueous pseudo-phase is dilute enough to be considered ideal; moreover, the reference chemical potentials are the same as in Eqs. 53 and 54.

Eq. 55 can be re-arranged as:

$$\begin{cases} \frac{\mu_{Rha}^0 - \mu_{Rha}^*}{RT} = \ln \frac{\gamma_{Rha} Y_{Rha}}{X_{Rha} cmc} \\ \frac{\mu_{SLES}^0 - \mu_{SLES}^*}{RT} = \ln \frac{\gamma_{SLES} Y_{SLES}}{X_{SLES} cmc} \end{cases} \quad \text{Equation 56}$$

In the same way, Eqs. 53 and 54 can be re-arranged as:

$$\begin{cases} \frac{\mu_{Rha}^0 - \mu_{Rha}^*}{RT} = \ln \frac{1}{cmc_{Rha}} \\ \frac{\mu_{SLES}^0 - \mu_{SLES}^*}{RT} = \ln \frac{1}{cmc_{SLES}} \end{cases} \quad \text{Equation 57}$$

Comparison between Eqs. 56 and 57 leads to:

$$\begin{cases} \ln \frac{1}{cmc_{Rha}} = \ln \frac{\gamma_{Rha} Y_{Rha}}{X_{Rha} cmc} \\ \ln \frac{1}{cmc_{SLES}} = \ln \frac{\gamma_{SLES} Y_{SLES}}{X_{SLES} cmc} \end{cases} \quad \text{Equation 58}$$

$$\begin{cases} Y_{Rha} = \frac{X_{Rha} cmc}{\gamma_{Rha} cmc_{Rha}} \\ Y_{SLES} = \frac{X_{SLES} cmc}{\gamma_{SLES} cmc_{SLES}} \end{cases} \quad \text{Equation 59}$$

Since $Y_{Rha} + Y_{SLES} = 1$, one obtains:

$$\frac{X_{Rha} cmc}{\gamma_{Rha} cmc_{Rha}} + \frac{X_{SLES} cmc}{\gamma_{SLES} cmc_{SLES}} = 1 \quad \text{Equation 60}$$

$$\frac{1}{cmc} = \frac{X_{Rha}}{\gamma_{Rha} cmc_{Rha}} + \frac{X_{SLES}}{\gamma_{SLES} cmc_{SLES}} \quad \text{Equation 61}$$

Eq. 61 is Eq. 6 reported in 4.1.3.3 paragraph.

Eq. 59 can be rewritten as:

$$\begin{cases} \ln \frac{1}{cmc_{Rha}} = \ln \frac{Y_{Rha}}{X_{Rha} cmc} + \ln \gamma_{Rha} \\ \ln \frac{1}{cmc_{SLES}} = \ln \frac{Y_{SLES}}{X_{SLES} cmc} + \ln \gamma_{SLES} \end{cases} \quad \text{Equation 62}$$

According to the regular solution model,

$$\begin{cases} \gamma_{Rha} = \exp[\beta Y_{SLES}^2] \\ \gamma_{SLES} = \exp[\beta Y_{Rha}^2] \end{cases} \quad \text{Equation 63}$$

and Eq. 62 becomes:

$$\begin{cases} \ln \frac{1}{cm_{CRha}} = \ln \frac{Y_{Rha}}{X_{Rha} cmc} + \beta Y_{SLES}^2 \\ \ln \frac{1}{cm_{CSLES}} = \ln \frac{Y_{SLES}}{X_{SLES} cmc} + \beta Y_{Rha}^2 \end{cases} \quad \text{Equation 64}$$

Deriving the parameter β from Eq. 64 we obtain:

$$\begin{cases} \beta = \frac{\ln \frac{X_{Rha} cmc}{Y_{Rha} cmc Rha}}{Y_{SLES}^2} \\ \beta = \frac{\ln \frac{X_{SLES} cmc}{Y_{SLES} cmc SLES}}{Y_{Rha}^2} \end{cases} \quad \text{Equation 65}$$

The first relation of Eq. 65 is Eq. 11 reported in 4.1.3.3. paragraph. By considering that the RHS of the equations reported as Eq. 64 must be equal, we obtain:

$$\frac{\ln \frac{X_{Rha} cmc}{Y_{Rha} cmc Rha}}{Y_{SLES}^2} = \frac{\ln \frac{X_{SLES} cmc}{Y_{SLES} cmc SLES}}{Y_{Rha}^2} \quad \text{Equation 66}$$

Eq. 64 coincides with Eq. 10 reported in 4.1.3.3. paragraph.

If the mixed micelles behave as an ideal mixture ($\beta = 0$), Eq. 64 becomes:

$$\begin{cases} \frac{1}{cm_{CRha}} = \frac{Y_{Rha}}{X_{Rha} cmc} \\ \frac{1}{cm_{CSLES}} = \frac{Y_{SLES}}{X_{SLES} cmc} \end{cases} \quad \text{Equation 67}$$

which can be rearranged as:

$$\begin{cases} cmc = \frac{Y_{Rha} cmc Rha}{X_{Rha}} \\ cmc = \frac{Y_{SLES} cmc SLES}{X_{SLES}} \end{cases} \quad \text{Equation 68}$$

Consequently:

$$\frac{Y_{Rha} cmc Rha}{X_{Rha}} = \frac{Y_{SLES} cmc SLES}{X_{SLES}} \quad \text{Equation 69}$$

which, considering that $Y_{SLES} = 1 - Y_{Rha}$, leads to:

$$Y_{Rha} = \frac{X_{Rha}^{cmCSLES}}{X_{SLESCmCRha} + X_{Rha}^{cmCSLES}}$$

Equation 70

Eq. 70 is reported in the main text of **4.1.3.3.** paragraph as Eq. 11.

References

- [1] Hiemenz, P.C., 1987, Surface tension and contact angle: application to pure substance; in Undergraduate Chemistry, a series of textbooks, vol.4, 287-346, J.J. Lagowski, New York and Basel: Marcel Dekker, INC.
- [2] Evans D.F. and Wennerstrom H., 1999, Surface chemistry and monolayers, in The colloidal domain: where physics, chemistry, biology, and technology meet – 2nd ed, 49-98, New York: Wiley-VCH.
- [3] Mitropoulos A.Ch., What is a surface excess?, Journal of Engineering Science and Technology, review 1 , 2008, 1-3.
- [4] Weil J.A.; Bolton J.R; Wertz J.E.: Electron Paramagnetic Resonance, Elementary Theory and Practical Applications. Wiley-Interscience, New York (1994).
- [5] <http://www.bruker-biospin.com/ew.html>
- [6] Berne B.J.; Pecora R.: Dynamic Light Scattering: with applications to chemistry, biology, and physics. Courier Dover Publications, 2nd edition, New York (2000)
- [7] Fennell Evans D.; Wennerström H.: The Colloidal Domain. Wiley VCH Publishers, New York (1994)
- [8] Pusey P.N.: In Neutrons, X-Ray and Light: Scattering methods applied to soft condensed matter; Lindener, P.Zmeb, T.: Eds. Elsevier: Amsterdam, pp 203-220 (2002)
- [9] Brown W.: Scattering methods: a brief introduction. Lecture notes; Uppsala University, Sweden (1994)
- [10] Brehm G.A.; Bloomfield V.A.: Analysis of polydispersity in polymer solutions by inelastic laser light scattering. Macromolecules, 8(5), 663-665 (1975).
- [11] Chau T. T., “A review of techniques for measurement of contact angles and their applicability on mineral surfaces,” Miner. Eng., vol. 22, no. 3, pp. 213–219, 2009.
- [12] Hoorfar M. & Neumann A. W., “Axisymmetric Drop Shape Analysis (Adsa) For the determination of Surface Tension and Contact Angle,” *J. Adhes.*, 2004, 80, 727–743.

[13] Bikerman J. J., “A Method of Measuring Contact Angles,” *Ind. Eng. Chem. - Anal. Ed.*, vol. 13, no. 6, pp. 443–444, 1941.

[14] KRÜSS, “Drop Shape Analysis,” 2015. [Online]. Available: <http://www.kruss.de/services/education-theory/glossary/drop-shape-analysis/>. [Accessed: 04-Jan-2018].

[15] <https://www.dataphysics-instruments.com/products/oca/>

[16] Clint J.H., Micellization of mixed nonionic surface active agents, *J. Chem. Soc., Faraday Trans.*, 1975, 1, 71, 1327–1334, <http://dx.doi.org/10.1039/F19757101327>.

[17] Holland P. M.; Rubingh D. N., Nonideal multicomponent mixed micelle model, *J. Phys. Chem.*, 1983, 87, 1984–1990. <https://doi.org/10.1021/j100234a030>

Il candidato Rodolfo Esposito ringrazia il Programma Operativo Complementare Ricerca e Innovazione 2014–2020, Azione I.1 “Dottorati Innovativi con caratterizzazione Industriale” per aver finanziato il seguente progetto di Dottorato per il XXXV Ciclo.

La borsa di dottorato è stata finanziata con le risorse del
Programma Operativo Complementare Ricerca e Innovazione 2014-2020,
Azione I.1 “Dottorati Innovativi con caratterizzazione industriale”



UNIONE EUROPEA
Fondo Sociale Europeo



*Ministero dell'Università
e della Ricerca*

POC
RICERCA E INNOVAZIONE
2 0 1 4 - 2 0 2 0